Extraterrestrial Physics - The Sun and Heliosphere

Lecture Notes

Robert F. Wimmer-Schweingruber
Christian-Albrechts-Universität zu Kiel
Institut für Experimentelle und Angewandte Physik
Abt. Extraterrestrik
Leibnizstrasse 11, D-24118 Kiel

May 20, 2019

Contents

Chapter 1

Introduction

Chapter 2

Single Particle Motion in a Magnetized Plasma

2.1 Introduction and Repetition

In this section, we consider the motion of a particle in a magnetic field. There is more to this easy-sounding problem than meets the eye and a lot of interesting phenomena can be understood based on the equation of motion for a particle of mass m and charge q (expressed in units of the elementary charge, e),

$$\frac{\mathrm{d}\vec{p}}{\mathrm{d}t} = q\left(\vec{E} + \vec{v}\times\vec{B}\right), \tag{2.1}$$

where $\vec{p} = \gamma\, m\, \vec{v}$ is the relativistic particle momentum, and

$$\gamma \doteq \frac{1}{\sqrt{1 - v^2\,/\,c^2}}. \tag{2.2}$$

The particle's total energy is given by $U = m\gamma c^2$, its kinetic energy is $T = (\gamma - 1)mc^2$. If the electric field vanishes everywhere at all times, $\vec{E} = 0$, then the induction equation implies that $\vec{B}$ remains constant in time, $\dot{\vec{B}} = 0$. In this case, we can compute the scalar product of the equation of motion with momentum $\vec{p}$,

$$\frac{\mathrm{d}\vec{p}}{\mathrm{d}t}\cdot\vec{p} = q\left(\vec{v}\times\vec{B}\right)\cdot\vec{p} = 0, \quad \text{where} \quad \frac{\mathrm{d}\vec{p}}{\mathrm{d}t}\vec{p} = \frac{1}{2}\frac{\mathrm{d}p^2}{\mathrm{d}t} \tag{2.3}$$

because velocity $\vec{v}$ is parallel to momentum, $\vec{p}$. This tells us that the magnitude of the momentum is conserved in a magnetic field, $\mathrm{d}|\vec{p}|\,/\,\mathrm{d}t = 0$, and hence that total kinetic energy U as well as the Lorentz factor are conserved quantities as well. This is nothing else than the well-known fact that a magnetic field performs no work. Expanding momentum in the equation of motion

allows us to find the acceleration acting on the particle

$$\frac{\mathrm{d}\vec{v}}{\mathrm{d}t} = \frac{q}{m\,\gamma}\left(\vec{v}\times\vec{B}\right). \tag{2.4}$$

We now define a new vector quantity, $\vec{\Omega}$,

$$\vec{\Omega} \doteq \frac{-q}{m\,\gamma}\vec{B} \tag{2.5}$$

which allows us to rewrite the previous equation 2.4

$$\frac{\mathrm{d}\vec{v}}{\mathrm{d}t} = \vec{\Omega}\times\vec{v}. \tag{2.6}$$

$\vec{\Omega}$ is called the gyro frequency, in the non-relativistic limit, $v^2\,/\,c^2 \ll 1$, it tends towards the cyclotron frequency.

Exercise 2.1 *Check that the units of* Ω *are correct.*

Next we divide the motion of the particle into a part that is parallel to the magnetic field and a part perpendicular to it, as sketched in Fig.2.1. Defining

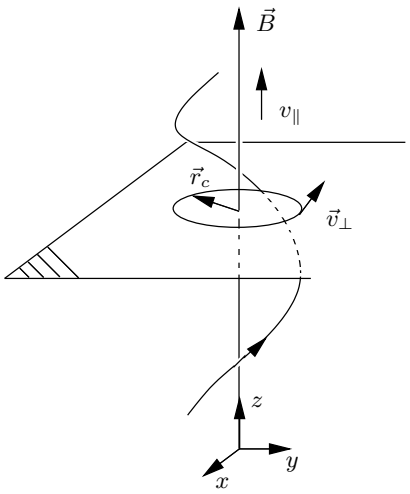

Figure 2.1: The particles motion can be visualized as a superposition of a circular motion perpendicular to $\vec{B}$ and a linear motion along $\vec{B}$.

the z component of our coordinate system to point along $\vec{B}$, we can now rewrite eq. 2.6 in components

$$\begin{aligned}
\dot{v}_x &= \Omega_y\,v_z - \Omega_z\,v_y = -\Omega_z\,v_y,\\
\dot{v}_y &= \Omega_z\,v_x - \Omega_x\,v_z = \Omega_z\,v_x, \qquad (2.7)\\
\dot{v}_z &= \Omega_x\,v_y - \Omega_y\,v_x = 0.
\end{aligned}$$

(2.8)

Because $\vec{\Omega}$ points along $\vec{B}$, $\Omega_x = \Omega_y = 0$, implying that $\dot{v}_z = 0$, i. e. a uniform motion along z. Hence we may consider the motion to be a superposition of a linear motion along $\vec{B}$ and a circular motion which can be described by

$$\vec{v}_\perp = \vec{\Omega} \times \vec{r}_c, \tag{2.9}$$

where $\vec{r}_c$ is the position vector of the particle as seen from the field line it is circling or from an imaginary point that lies at the center of the circle and moves along the magnetic field at a speed $v_\parallel$. This center is called the guiding center, r_c is the gyro radius, in the non-relativistic case it reduces to the Larmor radius. It can be found using eq. 2.22 and taking the vector product of eq. 2.9 with $\vec{\Omega}$, $\vec{v}_\perp \times \vec{\Omega}$,

$$\vec{r}_c \;=\; -\frac{q}{m\gamma}\frac{\vec{v}\times\vec{B}}{\Omega^2} \;=\; \frac{m\,\gamma}{q}\frac{\vec{B}\;\times\;\vec{v}}{B^2} \;=\; \frac{1}{q}\frac{\vec{B}\;\times\;\vec{p}}{B^2}. \tag{2.10}$$

Evaluating r_c for the field configuration studied here, we find that

$$r_c \;=\; |\vec{r}_c| \;=\; \frac{1}{q\,B^2}\left(B_z^2\,p_y^2 \;+\; B_z^2\,p_x^2\right)^{1/2} \;=\; \frac{|p_\perp|}{q\,B} \;=\; \frac{p\sin\alpha}{q\,B}, \tag{2.11}$$

where the angle α defined by $\tan\alpha = p_\perp/p_\parallel$ is the pitch angle. For a circular motion (i. e., $\alpha = \pi/2$) we have $r_c = p/(qB)$. The quantity

$$c\,B\,r_c = \frac{p\,c}{q} \tag{2.12}$$

is called **magnetic rigidity** and has units Volts, as is readily verified.

Exercise 2.2 *Convert between energy and rigidity for electrons, protons, and alpha particles and plot the results between 10* keV *and 10* GeV*.*

Exercise 2.3 *Determine the gyro radius for solar wind protons ($v_{\rm th} \approx 40$* km/s*) in an ambient interplanetary magnetic field of 5 nT (this is a typical value at 1 AU).*

2.2 Guiding-Center Motion

Now let us consider the situation where the magnetic field is not uniform, but varies slowly on a large spatial scale L,

$$\frac{1}{L} \sim \left|\frac{1}{B}\frac{\partial\,B_i}{\partial x_j}\right|, \tag{2.13}$$

i. e. $1/L$ is about equal to the largest of the quantities $|(1/B)(\partial B_i/\partial x_j)|$. In the following, we will assume that L is always much larger than the distance travelled by the particle during one gyration period $\tau = 2\pi/\Omega$,

$$L \gg v\tau \gg r_c. \tag{2.14}$$

This implies that the magnetic field does not change appreciably within the gyroradius and that we may use its value at the guiding center for further computations and that our results will be accurate to within $\pm(r_c/L)^2$ or $\pm(v\tau/L)^2$. Given the position $\vec{x}$ of the particle, the position of the guiding center is

$$\vec{x}_G = \vec{x} - \vec{r}_c, \tag{2.15}$$

and the velocity of the guiding center is

$$\begin{aligned} \vec{v}_G &= \frac{\mathrm{d}\vec{x}}{\mathrm{d}t} - \frac{\mathrm{d}\vec{r}_c}{\mathrm{d}t} = \vec{v} - \frac{\mathrm{d}}{\mathrm{d}t}\left(\frac{\vec{B}\times\vec{p}}{q\,B^2}\right), \\ &= \vec{v} + \frac{1}{q}\left[\frac{\mathrm{d}\vec{p}}{\mathrm{d}t}\times\frac{\vec{B}}{B^2} + \vec{p}\times\frac{\mathrm{d}}{\mathrm{d}t}\left(\frac{\vec{B}}{B^2}\right)\right], \end{aligned} \tag{2.16}$$

where we have inserted the expression for the gyroradius, eq. 2.10. Because there is no electric field, we know that $\partial B/\partial t = 0$ and hence,

$$\frac{\mathrm{d}}{\mathrm{d}t}\left(\frac{\vec{B}}{B^2}\right) = \frac{\partial}{\partial t}\frac{\vec{B}}{B^2} + \left(\vec{v}\cdot\vec{\nabla}\right)\frac{\vec{B}}{B^2} = \left(\vec{v}\cdot\vec{\nabla}\right)\frac{\vec{B}}{B^2}. \tag{2.17}$$

The derivative, $\mathrm{d}/\mathrm{d}t = \partial/\partial t + \vec{v}\cdot\vec{\nabla}$ is called the **substantial derivative** and needs to be introduced here.

Consider a parcel of a fluid which is moving in space. Let it be at a point $\vec{x}_1$ at a time t_0 and have speed $\vec{v}_1$. At a later time, t_2 it is at $\vec{x}_2$ with speed $\vec{v}_2$. Let us now consider a quantity in the fluid, e.g., its density, ρ. It will have changed between the two times and locations:

$$\frac{\mathrm{d}\rho}{\mathrm{d}t} \doteq \lim_{t_2\longrightarrow t_1}\frac{\rho_2-\rho_1}{t_2-t_1}. \tag{2.18}$$

This derivative is the substantial derivative and describes the change of a quantity along the movement of the fluid parcel.

Density $\rho_1 = \rho_1(x_1, y_1, z_1, t_1)$ changes to $\rho_2 = \rho_2(x_2, y_2, z_2, t_2)$ and we can now expand ρ_2 into a series

$$\rho_2 = \rho_1 + \left(\frac{\partial\rho}{\partial x}\right)(x_2-x_1) + \left(\frac{\partial\rho}{\partial y}\right)(y_2-y_1) + \left(\frac{\partial\rho}{\partial z}\right)(z_2-z_1) + \frac{\partial\rho}{\partial t}(t_2-t_1).$$

We divide this by $(t_2 - t_1)$ and insert in eq. 2.18 to obtain

$$\begin{aligned} \frac{\mathrm{d}\rho}{\mathrm{d}t} = \lim_{t_2\longrightarrow t_1}\left(\frac{\rho_2-\rho_1}{t_2-t_1}\right) &= \lim_{t_2\longrightarrow t_1}\left[\frac{\partial\rho}{\partial x}\frac{x_2-x_1}{t_2-t_1} + \frac{\partial\rho}{\partial y}\frac{y_2-y_1}{t_2-t_1} + \frac{\partial\rho}{\partial z}\frac{z_2-z_1}{t_2-t_1} + \frac{\partial\rho}{\partial t}\right] \\ &= \left(\frac{\partial\rho}{\partial x}\right)v_x + \left(\frac{\partial\rho}{\partial y}\right)v_y + \left(\frac{\partial\rho}{\partial z}\right)v_z + \frac{\partial\rho}{\partial t}, \\ \frac{\mathrm{d}\rho}{\mathrm{d}t} &= \left(\frac{\partial}{\partial t} + v_x\frac{\partial}{\partial x} + v_y\frac{\partial}{\partial y} + v_z\frac{\partial}{\partial z}\right)\rho. \end{aligned} \tag{2.19}$$

Thus we have defined the substantial derivative as

$$\frac{\mathrm{d}}{\mathrm{d}t} \doteq \frac{\partial}{\partial t} + v_x \frac{\partial}{\partial x} + v_y \frac{\partial}{\partial y} + v_z \frac{\partial}{\partial z} = \frac{\partial}{\partial t} + \left(\vec{v} \cdot \vec{\nabla}\right) \tag{2.20}$$

It consists of a **temporal derivative**, $(\partial/\partial t)$, and a **convective derivative** $\vec{v} \cdot \vec{\nabla}$.

We now return to the motion of the guiding center and insert the equation of motion for $\mathrm{d}\vec{p}/\mathrm{d}t$ in eq. 2.16, to obtain,

$$\vec{v}_G = \vec{v} + \frac{1}{q}\left[q\left(\vec{v} \times \vec{B}\right) \times \frac{\vec{B}}{B^2} \; + \; \vec{p} \times \left(\vec{v} \cdot \vec{\nabla}\right) \frac{\vec{B}}{B^2}\right]. \tag{2.21}$$

Now

$$\left(\vec{v} \times \vec{B}\right) \times \vec{B} = -\vec{B} \times \left(\vec{v} \times \vec{B}\right) = -\left[\vec{v}\left(\vec{B} \cdot \vec{B}\right) - \vec{B}\left(\vec{B} \cdot \vec{v}\right)\right]. \tag{2.22}$$

The second term in the square brackets is just the projection of $\vec{v}$ onto $\vec{B}$ multiplied by B^2,

$$\vec{v}_{\parallel} = \frac{\vec{B}\left(\vec{v} \cdot \vec{B}\right)}{B^2}, \text{ moreover, } \vec{v}_{\perp} = \vec{v} - \vec{v}_{\parallel}. \tag{2.23}$$

and hence eq. 2.22 is just $-v_{\perp}B^2$. Inserting, we have

$$\vec{v}_{\mathrm{G}} = \vec{v}_{\parallel} + \vec{p} \times \left(\vec{v} \cdot \vec{\nabla}\right) \frac{\vec{B}}{qB^2}, \tag{2.24}$$

which tells us that the guiding center exhibits no transverse motion if $\vec{B}$ is uniform.

So far, we have computed the instantaneous motion of the guiding center. Very often however, it is more convenient to know the "smoothed" motion of the guiding center, neglecting all the small changes that may occur over the course of one gyration. This is done by averaging $\vec{v}_{\mathrm{G}}$ over one gyroperiod τ,

$$\vec{V}_{\mathrm{G}\perp} \doteq \langle \vec{v}_{\mathrm{G}\perp} \rangle_{\tau} \doteq \frac{1}{\tau} \int_0^{\tau} \mathrm{d}t \vec{v}_{\mathrm{G}\perp}. \tag{2.25}$$

Thus we are faced with the problem of evaluating

$$\vec{V}_{G\perp} = \frac{1}{q} \left\langle \left[\vec{p} \times \left((\vec{v} \cdot \vec{\nabla}) \frac{\vec{B}}{B^2}\right)\right] \right\rangle_{\tau} \tag{2.26}$$

using zero-order quantities for $\vec{p}$, $\vec{v}$, $\vec{B}$, B^2, i. e. evaluating these quantities at the guiding center. Then we can take the guiding center as the origin of our

coordinate system, just as sketched in Fig. 2.1. Thus $B_x = B_y = 0$ and we have

$$\frac{v_x}{v} = \frac{p_x}{p} = -\sin\alpha\sin\Omega t, \tag{2.27}$$
$$\frac{v_y}{v} = \frac{p_y}{p} = -\sin\alpha\cos\Omega t, \tag{2.28}$$
$$\frac{v_z}{v} = \frac{p_z}{p} = \cos\alpha. \tag{2.29}$$

Again, just to rub the point in, v_z is constant and is independent of the magnetic field magnitude (independent of Ω). Hence, we write only the x and y components of the averaged guiding center motion,

$$V_{x\mathrm{G}} = \frac{1}{q}\left\langle p_y v_i \frac{\partial}{\partial x_i}\frac{B_z}{B^2} - p_z v_i \frac{\partial}{\partial x_i}\frac{B_y}{B^2}\right\rangle_\tau, \tag{2.30}$$
$$V_{y\mathrm{G}} = \frac{1}{q}\left\langle p_z v_i \frac{\partial}{\partial x_i}\frac{B_x}{B^2} - p_x v_i \frac{\partial}{\partial x_i}\frac{B_z}{B^2}\right\rangle_\tau, \tag{2.31}$$

where the repeated indices, i, imply the Einstein summation convention. In order to compute these quantities, we need to know the gyroperiod-averaged products of $v_i p_j$,

$$\langle v_i\, p_j\rangle_\tau = \frac{1}{\tau}\int_0^\tau \mathrm{d}t\, vp\sin^2\alpha\sin(\Omega t)\cos(\Omega t) = 0, \text{ for } i \neq j \tag{2.32}$$
$$\langle v_i\, p_j\rangle_\tau = \frac{1}{\tau}\int_0^\tau \mathrm{d}t\, vp\sin^2\alpha\sin^2(\Omega t) = \frac{1}{2}vp\sin^2\alpha, \text{ for } i = j = x \tag{2.33}$$
$$\langle v_i\, p_j\rangle_\tau = \frac{1}{\tau}\int_0^\tau \mathrm{d}t\, vp\sin^2\alpha\cos^2(\Omega t) = \frac{1}{2}vp\sin^2\alpha, \text{ for } i = j = y \tag{2.34}$$
$$\langle v_z\, p_z\rangle_\tau = \frac{1}{\tau}\int_0^\tau \mathrm{d}t\, vp\cos^2\alpha = \frac{1}{2}vp\cos^2\alpha, \tag{2.35}$$
$$\tag{2.36}$$

and evaluate the derivatives (remembering that $B_x = B_y = 0$)

$$\begin{aligned}
\frac{\partial}{\partial z}\frac{B_x}{B^2} &= \frac{1}{B^4}\left((\frac{\partial}{\partial z}B_x)B^2 - B_x\frac{\partial}{\partial z}B^2\right), \\
&= \frac{1}{B^2}\frac{\partial}{\partial z}B_x, \\
&= \frac{1}{B^3}\left(B_x\frac{\partial}{\partial x} + B_y\frac{\partial}{\partial y} + B_z\frac{\partial}{\partial z}\right)B_x = \frac{1}{B^3}\left(\vec{B}\cdot\vec{\nabla}\right)B_x, \quad (2.37) \\
\frac{\partial}{\partial z}\frac{B_y}{B^2} &= \frac{1}{B^4}\left((\frac{\partial}{\partial z}B_y)B^2 - B_y\frac{\partial}{\partial z}B^2\right), \\
&= \frac{1}{B^2}\frac{\partial}{\partial z}B_y, \\
&= \frac{1}{B^3}\left(B_x\frac{\partial}{\partial x} + B_y\frac{\partial}{\partial y} + B_z\frac{\partial}{\partial z}\right)B_y = \frac{1}{B^3}\left(\vec{B}\cdot\vec{\nabla}\right)B_y, \quad (2.38) \\
\frac{\partial}{\partial x_i}\frac{B_z}{B^2} &= \frac{1}{B^4}\left((\frac{\partial}{\partial x_i}B_z)B^2 - B_z\frac{\partial}{\partial x_i}B^2\right) \text{ where, } B = B_z \\
&= \frac{1}{B^4}\left((\frac{\partial}{\partial x_i}B)B^2 - B2B\frac{\partial}{\partial x_i}B\right), \\
&= -\frac{1}{B^2}\frac{\partial}{\partial x_i}B. \quad (2.39)
\end{aligned}$$

Now we can evaluate the gyroperiod-averaged guding-center motion in x and y,

$$\begin{aligned}
V_{x\mathrm{G}} &= \frac{1}{q}\left\langle p_y\left(v_x\frac{\partial}{\partial_x} + v_y\frac{\partial}{\partial_y} + v_z\frac{\partial}{\partial_z}\right)\frac{B_z}{B^2} - p_z\left(v_x\frac{\partial}{\partial_x} + v_y\frac{\partial}{\partial_y} + v_z\frac{\partial}{\partial_z}\right)\frac{B_y}{B^2}\right\rangle_\tau, \\
V_{y\mathrm{G}} &= \frac{1}{q}\left\langle p_z\left(v_x\frac{\partial}{\partial_x} + v_y\frac{\partial}{\partial_y} + v_z\frac{\partial}{\partial_z}\right)\frac{B_x}{B^2} - p_x\left(v_x\frac{\partial}{\partial_x} + v_y\frac{\partial}{\partial_y} + v_z\frac{\partial}{\partial_z}\right)\frac{B_z}{B^2}\right\rangle_\tau,
\end{aligned}$$

Inserting the previously found expressions for the gyroperiod-averaged products pv and partial derivatives, we find

$$\begin{aligned}
V_{x\mathrm{G}} &= \frac{pv}{qB^2}\left[\frac{1}{2}\sin^2\alpha\left(\frac{\partial}{\partial y}B_z\right) - \cos^2\alpha\frac{\partial}{\partial z}B_y\right], \\
V_{y\mathrm{G}} &= -\frac{pv}{qB^2}\left[\frac{1}{2}\sin^2\alpha\left(\frac{\partial}{\partial x}B_z\right) - \cos^2\alpha\frac{\partial}{\partial z}B_x\right].
\end{aligned}$$

Next we symmetrize these equations with the aim of writing them more concisely as a vector equation. We can achieve this aim by noting that the x and y components of the magnetic field vanish and so any quantity that is multiplied by them may be added to the equations above with no adverse effects.

Together with eqs. 2.37 to 2.39 we find

$$\begin{aligned} V_{x\mathrm{G}} &= \frac{pv}{q}\left[\frac{1}{2}\sin^2\alpha\frac{1}{B^3}\left(B_y\frac{\partial}{\partial z}B - B_z\frac{\partial}{\partial y}B\right) + \right. \\ &\quad \frac{\cos^2\alpha}{B^4}\left\{B_y\left(B_x\frac{\partial}{\partial_x} + B_y\frac{\partial}{\partial_y} + B_z\frac{\partial}{\partial_z}\right)B_z - \right. \\ &\quad \left.\left. B_z\left(B_x\frac{\partial}{\partial_x} + B_y\frac{\partial}{\partial_y} + B_z\frac{\partial}{\partial_z}\right)B_y\right\}\right], \\ V_{y\mathrm{G}} &= \frac{pv}{q}\left[\frac{1}{2}\sin^2\alpha\frac{1}{B^3}\left(B_z\frac{\partial}{\partial x}B - B_x\frac{\partial}{\partial z}B\right) + \right. \\ &\quad \frac{\cos^2\alpha}{B^4}\left\{B_z\left(B_x\frac{\partial}{\partial_x} + B_y\frac{\partial}{\partial_y} + B_z\frac{\partial}{\partial_z}\right)B_x - \right. \\ &\quad \left.\left. B_x\left(B_x\frac{\partial}{\partial_x} + B_y\frac{\partial}{\partial_y} + B_z\frac{\partial}{\partial_z}\right)B_z\right\}\right]. \end{aligned}$$

These lengthy expressions can now be compactly written as a vector equation which gives us the perpendicular motion of the guiding center in a given non-uniform magnetic field,

$$\vec{V}_{\mathrm{G}\perp} = \frac{pv}{qB}\left[\frac{1}{2}\sin^2\alpha\frac{\vec{B}\times\vec{\nabla}B}{B^2} + \cos^2\alpha\frac{\vec{B}\times\left[\left(\vec{B}\cdot\vec{\nabla}\right)\vec{B}\right]}{B^3}\right]. \tag{2.40}$$

It is important to remember that this equation is not valid for all non-uniform field configurations. It was derived under the explicit assumptions that we may evaluate all quantities at the guiding center and do not need to know them at the particle's exact location. This expression is correct up to second-order terms in r_c/L or in $v\tau/L$ and no more. It is not a general expression such as the equation of motion, eq. 2.1.

2.3 Some Drifts

While eq. 2.40 is not as general an expression as the equation of motion of a particle, it tells us a lot about the motion of the guiding center in a weakly non-uniform field. The first term in the square brackets of eq. 2.40 describes the influence of the transverse gradient of the magnetic field strength, the second results from the curvature of the field lines. The first term can be brought into a possibly more familiar form by inserting the explicit expression for the gyroradius (eq. 2.11) and using $v_\perp = v\sin\alpha$. Then we have the usual expression for the gradient drift,

$$\vec{V}_{\mathrm{G}\perp\nabla} = \frac{1}{2}r_c v_\perp\frac{\vec{B}\times\vec{\nabla}B}{B^2}. \tag{2.41}$$

This describes a drift perpendicular to $\vec{B} \times \vec{\nabla} B$, i. e. perpendicular to both $\vec{B}$ and $\vec{\nabla} B$. It points in opposite directions for positively and negatively charged particles because the charge enters as an odd power in these expressions (obvious in eq. 2.40, hidden in r_c in eq. 2.41). An often cited special case of this drift is of great importance for the modulation of cosmic rays. Consider a greatly simplified heliospheric current sheet as sketched in Fig. 2.2. The particles

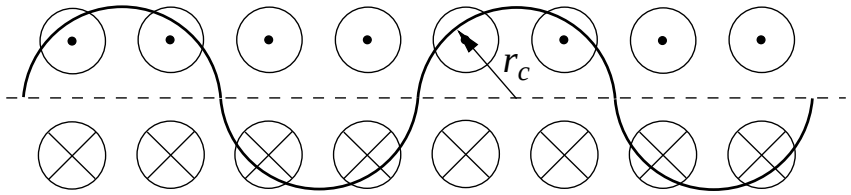

Figure 2.2: $\vec{\nabla} B$ drift in a very much simplified heliospheric current sheet (dashed line) configuration.

will drift along the current sheet, positively charged particles in one diection, negatively charged particles in the other. This may explain the differences in the fluxes of GCR protons (and, in a limited fashion, electrons) between even and odd solar activity cycles. However, even in this sketch, and even more so in reality, our assumption that the gyroradius is much smaller than the scale length of the non-uniformities of the field is flagrantly violated.

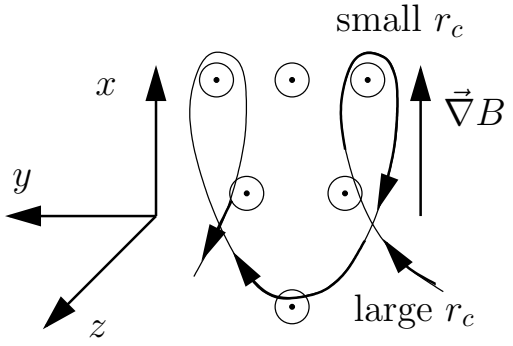

Figure 2.3: The motion of an ion in a non-uniform magnetic field exhibits a drift perpendicular to $\vec{B}$ and $\vec{\nabla} B$.

We can also understand this gradient drift from a more physical point of view. Consider the situation sketched in Fig 2.3 in which a magnetic field has a gradient in the x direction. The radii of curvature decrease along the gradient, they are large in the weak-field region but small where the field is strong. Therefore, a particle's orbit can not close anymore and, as we will see, a drift must set in. To simplify matters, we have chosen $\vec{\nabla} B$ parallel to x and perpendicular to z. The force acting on the ion in the x direction is

$$\dot{p}_x = q(\vec{v} \times \vec{B})_x = q(\vec{v} \times (\vec{B}_0 + \delta x \frac{\partial B_z}{\partial x})) \tag{2.42}$$

where $\delta x = r_c \cos \Omega t$. Averaged over an orbit and using eq. 2.28, we then have

$$\dot{p}_x = q \left\langle (v_y \delta x) \right\rangle \frac{\partial B_z}{\partial x} = -q r_c v \sin \alpha \left\langle \cos^2 \Omega t \right\rangle \frac{\partial B_z}{\partial x}. \tag{2.43}$$

The time average of $\cos^2 \Omega t$ over one oscillation period is just $1/2$, and so, using eq. 2.11 and $v_\perp = v \sin\alpha$ we have for the orbit-averaged force in x direction

$$\langle F_x \rangle = -\frac{1}{2} q \frac{p_\perp v_\perp}{qB} \frac{\partial B_z}{\partial x} = -\frac{m\gamma v_\perp^2}{2B} \frac{\partial B_z}{\partial x} = -\mu \frac{\partial B_z}{\partial x}, \quad \text{where} \quad \mu \doteq \frac{m\gamma v_\perp^2}{2B} \tag{2.44}$$

is the **magnetic moment** of the spiraling particle. Thus, we have a force acting on the particle in the direction away from the stronger magnetic field! This force must be balanced as a magnetic field can not perform work and the balancing force comes just from the drift. Let us assume that there is a drift in the y direction at a speed v_D. Then there is an additional force,

$$\vec{F}_D = q(\vec{v}_D \times \vec{B}), \tag{2.45}$$

which balances the gradient force discussed above. Equating the two forces yields the drift velocity, $\vec{v}_D$,

$$-\mu \vec{\nabla} B - q(\vec{v}_D \times \vec{B}) = 0 \implies \vec{v}_D = \frac{\mu}{q} \frac{\vec{B} \times \vec{\nabla} B}{B^2} = \pm \frac{1}{2} v_\perp r_c \frac{\vec{B} \times \vec{\nabla} B}{B^2}, \tag{2.46}$$

where we have used the vector identity, eq. 2.22, and the fact that $\vec{v}_D \perp \vec{B}$. As we can see from eq. 2.46, drift velocity depends on the sign of the charge.

Let us now consider the second term in the square brackets in eq. 2.40. It can be rewritten using $v_\parallel = v \cos\alpha$. Then we have

$$\vec{V}_{\mathrm{G}\parallel\mathrm{curv}} = \frac{\gamma m v_\parallel^2}{qB^4} \left[\vec{B} \times \left\{ \left(\vec{B} \cdot \vec{\nabla} \right) \vec{B} \right\} \right], \tag{2.47}$$

which again may be more familiar. Remembering that $(\vec{B} \cdot \vec{\nabla})\vec{B}$ is the change of $\vec{B}$ along $\vec{B}$ we see that the drift is perpendicular to the plane containing the surface spanned by the curved field line and points in opposite directions for oppositely charged particles.

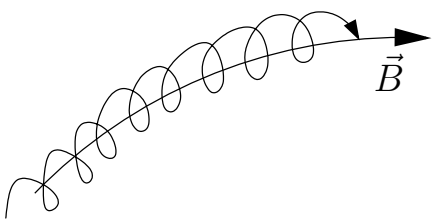

Figure 2.4: The motion of an ion in a curved magnetic field.

In order to familiarize ourselves with single-particle motion in a plasma, let us again consider this drift in some more detail. As an ion sprials along a curved magnetic field, it feels a centrifugal force

$$\vec{F}_{\mathrm{cf}} = \frac{m\gamma v_\parallel^2}{R_{\mathrm{curv}}} \frac{\vec{R}_{\mathrm{curv}}}{R_{\mathrm{curv}}} \tag{2.48}$$

which points radially outwards. According to the general law for drift velocities, this results in a drift,

$$\vec{v}_{\mathrm{curv}} = \frac{1}{q} \frac{\vec{F}_{\mathrm{cf}} \times \vec{B}}{B^2} = \frac{m\gamma v_\parallel^2}{qB^2} \frac{\vec{R}_{\mathrm{curv}} \times \vec{B}}{R_{\mathrm{curv}}^2}, \tag{2.49}$$

which is the well-know expression for curvature drift (e.g., *Chen*, 1984). The drift velocity is perpendicular to the magnetic field, $\vec{B}$, and the curvature radius, $\vec{R}_{\rm curv}$, as expected.

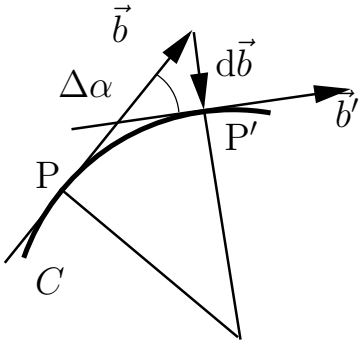

Figure 2.5: Definition of curvature and curvature radius.

The connection between eq. 2.49 and eq. 2.47 is easily seen by considering the definition of curvature, as sketched in Fig. 2.5. The curvature, κ, of a curve, C, is defined as the change of the angle spanned by the tangents to two points on the curve as the points are moved arbitrarily close together,

$$\kappa \doteq \lim_{P \longrightarrow P'} \frac{\Delta\alpha}{\Delta s} = \frac{\mathrm{d}\alpha}{\mathrm{d}s}. \tag{2.50}$$

The change in the direction of the magnetic field, $\vec{b}' - \vec{b}$ is just $\Delta\alpha$, and this change points opposite to the radius of curvature. With $\vec{b} = \vec{B}/B$ we have, from differential geometry,

$$\frac{\mathrm{d}\vec{b}}{\mathrm{d}s} = -\frac{\vec{R}_{\rm curv}}{R^2_{\rm curv}} \tag{2.51}$$

Now the derivative along the curve, $\mathrm{d}/\mathrm{d}s$ is just that, the derivative along the curve, $(\vec{b}\cdot\vec{\nabla})\vec{b}$! Hence,

$$(\vec{b}\cdot\vec{\nabla})\vec{b} = -\frac{\vec{R}_{\rm curv}}{R^2_{\rm curv}} \tag{2.52}$$

from which eq. 2.47 follows readily.

2.4 Adiabatic Invariants

Consider the motion of a particle which can be described by a parameter λ. λ may change slowly under the influence of external forces, this is called adiabatic change. Slowly means that λ changes only by a small amount during a period T of the motion

$$\frac{\mathrm{d}\lambda}{\mathrm{d}t} \ll \frac{\lambda}{T}; \tag{2.53}$$

for $\mathrm{d}\lambda/\mathrm{d}t = 0$ the motion is strictly periodic and has a fixed energy, E. If λ changes slowly, so does E as some function of λ. This dependence of E on λ can be expressed by the constancy of some combination, I, of E and λ. This quantity, I, remains constant even for slow changes of the system. It is called an adiabatic invariant; a formal derivation can be found using the Hamiltonian formalism (see, e. g. , *Landau* and *Lifschitz*, 1981, vol. I),

$$I \doteq \frac{1}{T}\oint p\mathrm{d}q, \tag{2.54}$$

where the contour is over a complete period of the motion, T, and p and q are conjugate canonical coordinates. I can be considered as the area enclosed by the orbit of the system in phase space (p, q).

In the following we will give adiabatic invariants for the motion of the guiding center in a weakly non-uniform field. There are three adiabatic invariants for this motion, the first is due to the gyromotion of the particle around the guiding center (Fig. 2.6). The second comes from a longer time scale, the bounce time scale sketched in Fig. 2.8 when there is such a scale. The third is due to the curvature drift and the time scale is the time it takes the particle to move once around the configuration, e. g. , the Earth's magnetic field, as sketched in Figs. 2.9 and 2.10. Adiabatic invariants can be found by considering quantities that would be conserved if the system were not changing at all, as we will see in the following three examples.

Let us consider the adiabatic invariant for the motion of a particle in a weakly non-uniform magnetic field sketched in Fig. 2.6. The particle gyrates

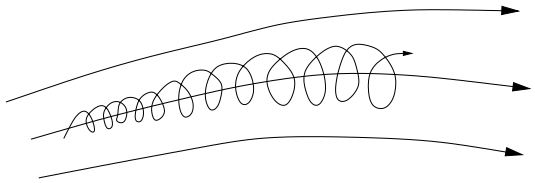

Figure 2.6: Motion of a particle in a weakly non-uniform magnetic field.

around its guiding center; in a uniform field, the angular momentum of the particle would be a conserved quantity, and we insert it in place of the generalized momentum into eq. 2.54,

$$I_1 = \frac{1}{2\pi} \oint p \sin\alpha r_c \mathrm{d}\varphi = \frac{(p \sin\alpha)^2}{q\,B} = \frac{p_\perp^2}{q\,B} = \frac{(m\gamma v_\perp)^2}{q\,B} = \frac{m\gamma}{q} 2\,|\vec{\mu}|, \qquad (2.55)$$

where we have inserted the expression for the gyroradius and $\vec{\mu}$ is the magnetic moment of the particle gyrating around the guiding-center field line. In this case, I is often called the first adiabatic invariant. It itself is a conserved quantity of the motion of the particle in the non-uniform field.

This conservation has important consequences. Consider a particle approaching a magnetic mirror, sketched in Fig. 2.7. Then the conservation of the first adiabatic invariant will often lead to a reflection of the particle. This is easily seen. Because there is no electric field, the kinetic energy of the particle is conserved and composed of two parts, the parallel and perpendicular terms: $E_{\mathrm{kin}} = 1/2mv_\parallel^2 + 1/2mv_\perp^2 = \mathrm{const}$. The second term is equal to μB. Because μ is conserved even with increasing B, the first term needs to change appropriately to ensure energy conservation. This is achieved by converting all kinetic energy into gyration energy. When this happens, the particle does not

propagate parallel to the field anymore, but the guiding center stands still for a brief moment, before the motion is reversed and the guiding center moves back along its previous trajectory, resulting in a net change of linear momentum, $\Delta p = 2p$. The strength of the field in the mirror as well as the pitch angle of the particle determine whether a partice will be reflected at the mirror or transmitted. Which particles are reflected? Let us consider a region where

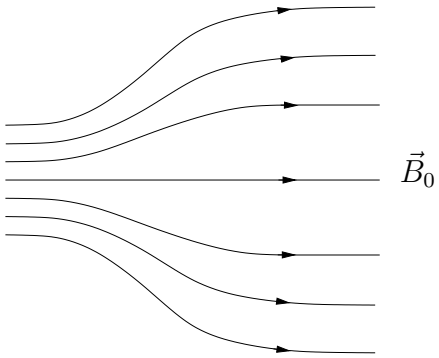

Figure 2.7: Magnetic mirror.

the magnetic field strength is constant, $\vec{B} = \vec{B}_0$, and the region in the mirror where the particle has no forward momentum anymore, $\vec{B} = \vec{B}_1$. Because of the invariance of μ we have

$$\frac{1}{2}m\frac{v_{\perp 0}^2}{B_0} = \frac{1}{2}m\frac{v_{\perp 1}^2}{B_1} \tag{2.56}$$

and because of conservation of kinetic energy

$$v_{\perp 1}^2 = v_{\perp 0}^2 + v_{\parallel 0}^2 = v_0^2. \tag{2.57}$$

We rewrite eq. 2.56 and insert eq. 2.57

$$\begin{aligned} \frac{1}{2}m\frac{v_{\perp 0}^2}{B_0} &= \frac{1}{2}m\frac{v_{\perp 1}^2}{B_1}, \\ \frac{B_0}{B_1} &= \frac{v_{\perp 0}^2}{v_{\perp 1}^2}, \\ &= \frac{v_{\perp 0}^2}{v_0^2}, \\ &= \sin^2\alpha. \end{aligned} \tag{2.58}$$

If we could measure the pitch angles of all particles in the region where $\vec{B} = \vec{B}_0$, then those would be reflected by the mirror which have a pitch angle $\alpha > \alpha_m$, for which

$$\sin^2\alpha_m = \frac{B_0}{B_m}. \tag{2.59}$$

The previous expressions for the adiabatic invariant can also be written differently by keeping the gyro-radius at the expense of $p_\perp$,

$$I_1 = \frac{1}{2\pi}\oint p\sin\alpha r_c \mathrm{d}\phi = \frac{q}{2\pi}\oint Br_c^2 \mathrm{d}\phi = qBr_c^2, \tag{2.60}$$

which shows that we may consider the conservation of the fist adiabatic invariant as equivalent to the conservation of the magnetic flux through the particle's orbit.

Writing this in full relativistic glory, we have for the canonical perpendicular momentum of the charged particle

$$\vec{P}_\perp = \vec{p}_\perp + q\vec{A} \tag{2.61}$$

where $\vec{p}_\perp$ is the relativistic three-momentum perpendicular to $\vec{B}$, and $\vec{A}$ is the magnetic potential $\vec{B} = \vec{\nabla}\times\vec{A}$. In this formulation

$$I_1 = \oint_C \vec{P}_\perp\cdot\mathrm{d}\vec{l} = \oint_C \vec{p}_\perp\cdot\mathrm{d}\vec{l} + q\oint_C \vec{A}\cdot\mathrm{d}\vec{l} = \oint_C \gamma m\vec{v}_\perp\cdot\mathrm{d}\vec{l} + q\int_S \vec{B}\cdot\mathrm{d}\vec{S} \tag{2.62}$$

where we have used Stokes' theorem and S is the circular area enclosed within the curve C along which the contour integral is performed. Thus we have

$$I_1 = 2\pi r_c\gamma m v_\perp + q\int_S \vec{B}\cdot\mathrm{d}\vec{S} \tag{2.63}$$

wich covers the area enclosed by the circular motion of the particle with gyro-radius r_c.

If we now define $\mathrm{d}\vec{l}$ to point in the same direction as $\vec{v}_\perp$ and remember that the Lorentz force needs to point inwards to keep the particle on its circular motion, we see that $\vec{B}$ and $\mathrm{d}\vec{S}$ need to point in opposite directions for $\mathrm{d}\vec{S}$ and $\mathrm{d}\vec{l}$ to be a right-handed system. So the second term in eq. 2.63 is negative and

$$I_1 = 2\pi r_c\gamma m v_\perp - qB\pi r_c^2. \tag{2.64}$$

With $\Omega = v_\perp/r$ we also obtain

$$I_1 = 2\pi r_c^2\gamma m\Omega - qB\pi r_c^2. \tag{2.65}$$

Inserting $\Omega = qB/m\gamma$ (eq. 2.5)

$$I_1 = 2\pi r_c^2 qB - qB\pi r_c^2 = qB\pi r_c^2, \tag{2.66}$$

in other words, the first adiabatic invariant is the flux through the particle's orbital circle (*Jackson*, 1962).

If the magnetic field in the mirror changes with a frequency ω, then when ω approaches Ω, the induced electric field will be in phase with the particles

and accelerate them, In this case, the concept of adiabatic invariants breaks down, our assumption that changes are slow compared with typical time scales of the system is no longer valid. An example of this violation is the heating of a plasma by cyclotron waves such as in an electron cyclotron resonance ion source (ECRIS) or with ion-cyclotron waves in the solar corona.

Next let us consider the motion of the guiding center in a situation similar to that sketched in Fig. 2.8. The particle bounces back and forth between two

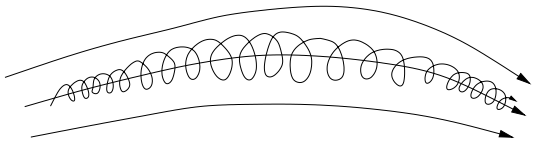

Figure 2.8: Field configuration leading to the conservation of the second adiabatic invariant. The particle (guiding center) bounces back and forth between two magnetic mirrors.

magnetic mirrors which only move slowly. Neglecting drifts, we can consider the motion of the guiding center only in a scalar magnetic field/potential – in this picture the kinetic energy of the guiding center is converted to potential energy when the particle is at rest at a position l_m along the field line, where l measures the length along a field line. Then the relevant canonical momentum of the guiding center is $P_{\mathrm{G}\parallel} = m\gamma V_{\mathrm{G}\parallel}$ and the spatial coordinate is the length along the field line, $\mathrm{d}l$. Hence

$$I_2 = \oint P_{\mathrm{G}\parallel}\mathrm{d}l = m\gamma \oint V_{\mathrm{G}\parallel}\mathrm{d}l. \tag{2.67}$$

This quantity is called the second adiabatic invariant and is conserved during bounce motion. (The Lorentz factor, γ may be taken infront of the integral because v^2 is not changed. In the absence of electric fields, time-constant magnetic fields perform no work.)

If the mirrors approach and retract fom each other at a frequency ω which approaches Ω_{bounce} then, of course, our assumption of slow changes breaks down and the second adiabatic invariant is not conserved. This situation arises in the process of transit-time pumping or transit-time damping (see Sec. 12.2).

The derivation of the third adiabatic invariant is somewhat more complicated. Consider particles bouncing back and forth between two mirrors in a nearly axially symmetric field configuration such as that sketched in Fig. 2.9. The bounce period T can be computed using

$$T_b = 2\int_{l_m}^{l_m^*} \frac{\mathrm{d}l}{V_{\mathrm{G}\parallel}} = \frac{2}{v}\int_{l_m}^{l_m^*} \frac{\mathrm{d}l}{\langle\cos\alpha\rangle_\tau}, \tag{2.68}$$

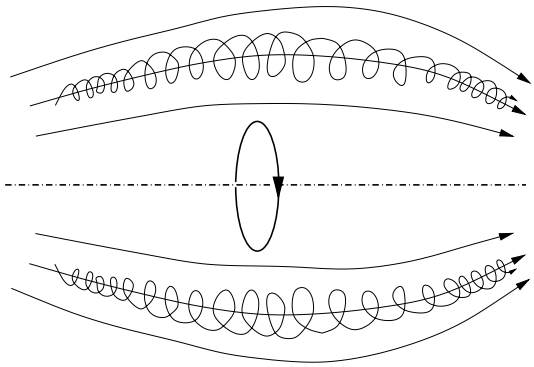

Figure 2.9: Field configuration leading to the conservation of the third adiabatic invariant. Note that it is not completely symmetric about the "symmetry" axis (dash-dotted line), but nearly so. The bounce period between two mirrors, T_b, is much shorter than the time required for the particle to move around the symmetry axis.

where $\langle \cos\alpha \rangle_\tau$, the gyroperiod-averaged pitch-angle cosine, is itself a function of l. l_m and l_m^* denote the two mirror points. We know, from our previous considerations of the motion in a magnetic mirror, that

$$\sin^2\alpha = \frac{B}{B(l_m)}, \tag{2.69}$$

and hence

$$T_b = \frac{2}{v}\int_{l_m}^{l_m^*} \frac{\mathrm{d}l}{\sqrt{1-\frac{B(l)}{B(l_m)}}}. \tag{2.70}$$

From Hamiltonian mechanics we know that when the Hamiltonian is independent of a certain coordinate q_k or component thereof, then the conjugate momentum is a conserved quantity because

$$\frac{\mathrm{d}p_k}{\mathrm{d}t} = -\frac{\partial \mathbf{H}}{\partial q_k} \quad (=0 \quad \text{in this case}). \tag{2.71}$$

An axially symmetric field configuration is independent of the azimuth angle φ and hence P_φ, the momentum along the azimuthal direction, is a conserved quantity. In a configuration that is only nearly axially symmetric

$$I_3 = \frac{1}{T_b}\int_0^{2\pi} \mathrm{d}\varphi P_{\mathrm{G}\varphi} \tag{2.72}$$

is a conserved quantity and is, of course, called the third adiabatic invariant. $P_{\mathrm{G}\varphi}$ can easily be derived using the Hamiltonian formalism by $P_{\mathrm{G}\varphi} = \partial\mathcal{L}/\partial\dot{\varphi}$.

In order to do so we need to find the Lagrangian, $\mathcal{L}$ of a particle in an electromagnetic field. The problem is that in the relativistic limit this is no longer simply $\mathcal{L} = E_{\rm kin} - E_{\rm pot}$, but the Lagrangian needs to be derived differently. We use the fact that

$$p_x = \frac{\partial \mathcal{L}}{\partial \dot{x}} = m\gamma\dot{x}. \tag{2.73}$$

This equation can be integrated to obtain the Lagrangian of a free particle

$$\begin{aligned}
\mathcal{L} &= m\int \gamma(\dot{x})\dot{x}\mathrm{d}\dot{x}, \\
&= m\int \frac{\dot{x}}{\sqrt{1-(\dot{x}/c)^2}}\mathrm{d}\dot{x}, \\
&= m\int \frac{c\dot{x}'}{\sqrt{1-\dot{x}'^2}}c\mathrm{d}\dot{x}', \quad \text{where} \quad \dot{x} = c\dot{x}' \\
&= -mc^2\sqrt{1-\dot{x}'^2} + X(\dot{y},\dot{z}),
\end{aligned} \tag{2.74}$$

where the integration constant $X(\dot{y},\dot{z})$ is an arbitrary function of $\dot{y}$ and $\dot{z}$ only. Because it is arbitrary we may choose it to also be convenient and thus choose $X(\dot{y},\dot{z}) = 0$. Using the same procedure for the y and z components of the momentum we find the Lagrangian for a free particle as

$$\mathcal{L} = -mc^2/\gamma. \tag{2.75}$$

For an interacting particle we need to subtract the potential energy, $V(\vec{x},\dot{\vec{x}},t)$ to obtain

$$\mathcal{L} = -mc^2/\gamma - V(\vec{x},\dot{\vec{x}},t). \tag{2.76}$$

The Lagrangian of a charged particle in a given field configuration is thus given by

$$\mathcal{L} = q\left(\vec{A}\cdot\vec{v} - \phi\right) - mc^2\sqrt{1-v^2/c^2}, \tag{2.77}$$

where $\vec{A}$ is the vector potential ($\vec{B} = \vec{\nabla}\times\vec{A}$) and ϕ is the scalar potential ($\vec{E} = \partial_t\vec{A} - \nabla\phi$). In an axially symmetric (cylindrically symmetric) configuration, we have

$$\mathcal{L} = q\left(A_r\dot{r} + A_\varphi r\dot{\varphi} + A_z\dot{z} - \phi\right) - mc^2\sqrt{1-(\dot{r}^2 + r^2\dot{\varphi}^2 + \dot{z}^2)/c^2}. \tag{2.78}$$

Now we know from Hamiltonian mechanics the general relation that

$$P_{\mathrm{G}\varphi} = \frac{\partial \mathcal{L}}{\partial \dot{\varphi}} = qA_\varphi r + \gamma m r^2\dot{\varphi}. \tag{2.79}$$

Since this is a conserved quantity in the symmetric case, we may evaluate it at any convenient location, e. g., at the time t_0 when $\dot{\varphi}(t_0) = 0$. Then we have

$$\frac{1}{2\pi}I_3 = qr_0A_\varphi = q\frac{1}{2\pi}\oint \mathrm{d}\vec{s}\vec{A}, \tag{2.80}$$

where $\mathrm{d}\vec{s} = r\mathrm{d}\varphi\vec{e}_\varphi$ and the contour integral is along a circle with radius r_0. This is true because $\vec{A}$ is independent of φ. Using Stoke's theorem and $\vec{B} = \vec{\nabla} \times \vec{A}$ we see that

$$q\frac{1}{2\pi}\oint \mathrm{d}\vec{s}\vec{A} = q\frac{1}{2\pi}\int \mathrm{d}\vec{\sigma}\vec{B} = q\frac{1}{2\pi}\Phi, \tag{2.81}$$

where Φ is the magnetic flux through the circle described by the guiding center around the "symmetry axis". Φ will remain constant during the time needed for the particle to drift around the whole field configuration. Or, in other words, the particle will move in such a way as to conserve the flux, Φ, enclosed in its orbit. This is shown in Fig. 2.10.

The importance of the third adiabatic invariant is not as large as that of the two first ones because it is only conserved on very long time scales. In the Earth's magnetosphere hydromagnetic waves often destroy this nice property because they are in phase with some particles and can accelerate their drift motion. Nevertheless, it lies at the heart of the so-called ring current in the magnetosphere.

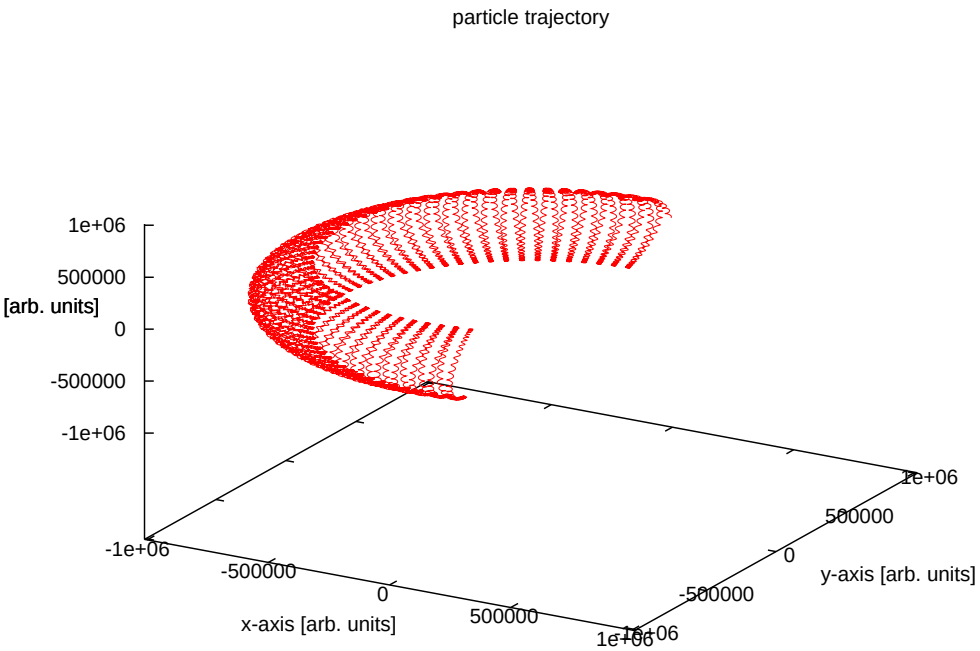

Figure 2.10: Motion of a proton in a dipolar magnetic field. The bounce motions due to the magnetic mirror force and the equatorial drift can both be seen. Because the drift along the equator depends on the sign of the particle's charge, it results in a current along the magnetic equator, the so-called ring current.

Obviously, adiabatic invariants aren't always going to be conserved. Whether or not depends strongly on the temporal and spatial scales of field variations. If the time scale of variations is large compared to the largest of the scales discussed above, the drift time scale, then all three adiabatic invariants will be conserved. If the field changes faster than the time needed for surrounding the Earth once but slower than the time required for one bounce, then the third adiabatic invariant is not going to be conserved, but the other two may well still be. If the system changes quicker than the bounce period but more slowly than a gyro period, then neither the third nor the second adiabatic invariants will be conserved, but the first will still be. Finally, in a system which changes faster than the gyroperiod, the concept of adiabatic invariants does not apply, nor will the guiding-center approximation.

Similar considerations hold true for spatial variations, as can be seen by transforming them into the time domain. If the system changes on spatial scales, L, smaller than the characteristic radius, r_a, of the motion related to the adiabatic invariant, then the latter will not be conserved. As an example let us consider the case in which $L/r_c < 1$. Using the definition of the gyro radius, eq. 2.9, we have (neglecting parallel motion)

$$v_\perp = \Omega r_c. \tag{2.82}$$

Dividing both sides by the spatial scale of the change (i.e., the gradient length of the change) we see that

$$\omega = \frac{v_\perp}{L} = \Omega \frac{r_c}{L} > \Omega, \tag{2.83}$$

i.e., that the system changes faster than the gyroperiod, and, hence, the first adiabatic is no more conserved. Similar considerations can be made for the other two adiabatic invariants.

2.5 Mean Free Paths

Formally, every mean free path can be expressed as the inverse of the product of the number density, n, of scattering centers and their scattering cross section, σ,

$$\lambda = \frac{1}{n\sigma}. \tag{2.84}$$

The difficulty lies not in this simple equation, but in the definition of what scatters and, sometimes, in the derivation of the scattering cross section. For neutral particles, this is relatively simple. The scattering occurs between neutral particles whose density, n_n, is well defined. Their scattering cross section, $\sigma_n \approx 10^{-19}\mathrm{m}^2$, is an empirical number which includes several complicated processes such as resonances in the electron shells, etc. The crucial point here

is that neutral particle interactions are short ranged, and we consider their collisions just like those of billard balls.

In the case of charged particles in a fully ionized plasma, the situation is more complicated. The long range of the Coulomb force means that particles will scatter even when they are separated by distances much larger than their atomic (ionic) sizes, and that they tend to scatter by smaller angles. Furthermore, in a dense plasma, a given particle will be shielded by the other plasma particles from a particle that potentially would scatter with it. This is accounted for by introducing the Debye sphere within which the Coulomb potential of the charge is considerer to be confined. However, this does not mean that we can now use $\sigma = \pi\lambda_D^2$ as scattering cross section. Particles with higher energies can penetrate deeper into the exponential Debye-shielded potential than low-energy particles. Nevertheless, they will still have a larger probability of scattering by a small angle than by a large angle. See Sec. 8.2.2 for a more detailed treatment.

To calculate the Coulomb scattering cross section, σ_C, for an electron to scatter on an ion, we make use of the following simplifying assumptions. The force felt by the electron at its closest approach to the ion is approximately

$$F_C = -\frac{e^2}{4\pi\varepsilon_0 d_c^2}, \tag{2.85}$$

where d_c is the impact parameter. The electron feels this force for a time $\tau \approx d_c/v_e$, where v_e is the electron's speed. Thus, the change in momentum, $|\Delta(m_e v_e)|$, is approximately

$$|\Delta(m_e v_e)| \approx |F_c \tau| = \frac{e^2}{4\pi\varepsilon_0 v_e d_c}. \tag{2.86}$$

We now consider the change in momentum for a large deflection angle, $\gamma \approx 90°$. It is then of the same order as the particle's momentum itself, i.e., $|\Delta(m_e \cdot v_e)| \approx m_e v_e$. We can insert this very rough approximation into eq. 2.86 to obtain an estimate for the impact parameter, d_c,

$$d_c \approx \frac{e^2}{4\pi\varepsilon_0 m_e v_e^2} \tag{2.87}$$

which leads directly to the scattering cross section

$$\sigma_c = \pi d_c^2 \approx \frac{e^4}{16\pi\varepsilon_0^2 m_e^2 \langle v_e \rangle^4} \tag{2.88}$$

where we have replaced the electron speed with the electron populations average speed, $\langle v_e \rangle$.

The collision frequency between electrons and ions is then simply

$$\nu_{ei} = n_e \sigma_c \langle v_e \rangle \approx \frac{n_e e^4}{16\pi\varepsilon_0^2 m_e^2 \langle v_e \rangle^3}. \tag{2.89}$$

Using the expression for the average thermal energy of an electron, $k_B T_e = \frac{1}{2} m_e \langle v_e \rangle^2$, and using the expression for the plasma frequency, $\omega_e = \sqrt{(n_e e^2)/m_e \varepsilon_0)}$, we can rewrite the collision frequency with macroscopic quantities,

$$\nu_{ei} \approx \frac{\sqrt{2}\omega_{pe}^4}{64\pi n_e} \left(\frac{k_B T_e}{m_e} \right)^{-3/2}. \tag{2.90}$$

The mean free path of electrons in a plasma is given by

$$\lambda_e = \frac{\langle v_e \rangle}{\nu_{ei}} = \frac{1}{n_e \sigma_c}. \tag{2.91}$$

Using the Debye-length, $\lambda_D \doteq \sqrt{\varepsilon_0 / n_e e^2} \sqrt{k_B T_e}$, and eq. 2.88 we find that

$$\lambda_e = 64\pi n_e \lambda_D^4. \tag{2.92}$$

The number of electrons within a Debye-sphere is

$$N = n_e \frac{4\pi}{3} \lambda_D^3 \doteq \frac{1}{3}\Lambda \quad \Longrightarrow \quad \Lambda = n_e 4\pi \lambda_D^3 \tag{2.93}$$

where Λ is within a factor 4π the so-called plasma parameter. It is the exponential of the so-called Coulomb logarithm, $\ln \Lambda$. Thus

$$\lambda_e \approx 16 \Lambda \lambda_D, \tag{2.94}$$

which implies that the electron mean free path is significantly longer than a Debye radius.

Let us illustrate these points by considering the interplanetary medium. At one astronomical unit (1 AU) from the Sun, we have mean electron densities of roughly 5 per cm^3 at a temperature of 100'000 K, we have a mean Debye radius of about 10 m. Then, the mean free path at 1 AU is about (eq. 2.92),

$$\lambda_e = 64\pi \ \cdot 5 \times 10^6 \times 10^4 \approx 200 \times 5 \times 10^{10} = 10^{13} \text{m} \tag{2.95}$$

which is considerably longer than the distance from Sun to Earth (1 AU $\approx 1.5 \cdot 10^{11}$m) and nearly the size of the heliosphere. Nevertheless, we do measure effects of Coulomb collisions in the solar wind (see next chapter).

There is a peculiar point to be mentioned here. The solar wind can be successfully modelled with MHD methods. The theory of MHD requires that the mean free path of the fluid particles be considerably shorter than the dimensions of the system. Where's the problem? Well, as we just saw, the mean free path is much larger than a typical scale of the system (the heliosphere), and so the assumptions made by MHD should be violated. Nevertheless, it works remarkably well. How come? The point here is that there are other "collisions" which act to equilibrate the particle distributions, thus driving the system into a state in which it can be described as a magnetized fluid. The "collisions" are events where a particle interacts resonantly with one of the many kinds of waves which are ubiquitous in the solar system plasma.

2.6 Pitch-Angle Scattering as a Example of Wave-Particle Interactions

As an example of a particle scattering off a wave, we consider the important phenomenon of pitch-angle scattering. As already mentioned in the discussion of Fig. 2.1, a particle's velocity can be split into a part parallel and a part perpendicular to the ambient magnetic field, $\vec{B}_0$. When a wave passes a particle, the latter sees the wave at a Doppler-shifted frequency. When this lies in the range of the particle's gyro-frequency, the particle can sense the wave's electromagnetic field and can resonantly interact with it. The condition for such a gyro-resonance between wave and particle is

$$\omega - \vec{k}_{\|} \cdot \vec{V}_{\|} = n\Omega, \tag{2.96}$$

where ω and $\vec{k}$ are the wave frequency and wave vector. n is an integer, $= 0, \pm 1, \pm 2, \ldots$, and the case $n = 0$ is called Landau resonance. When condition 2.96 is satisfied, particle and wave can exchange energy and momentum. Figure 2.11 shows the force felt by the particle. Its motion and the wave's magnetic field, $\vec{B}_\omega$, lead to a Lorentz force which can increase or decrease the particle's parallel and perpendicular velocity components depending on the phase of the wave relative to the particle's motion. The situation shown in Fig. 2.11a would lead to a decrease in pitch angle and increase in $v_{\|}$. If the phase between the wave's $\vec{B}_\omega$ and the particle's motion were shifted by π, $\vec{B}_\omega$ would point downwards, an the Lorentz force would point in the opposite direction. Figure 2.11b shows the ineraction with the parallel motion of the particle. The Lorentz force acts to slow down the gyration of the particle. Again, if the relative phase between particle and wave were shifted by π, the opposite force would be felt by the particle and it would be accelerated in its gyration. Obviously, such wave-particle interaction can change the particles momentum and energy. Because the pitch angle is given by the ratio of perpendicular to parallel speeds, it too, can be changed in such an interaction. Resonant wave-particle interactions only occur on a short time scale, small in comparison with the particle's gyroperiod. This means that the first adiatic invariant, the magnetic moment, $\vec{\mu}$, is not conserved. Thus, in the inertial frame, the particle's energy is not conserved. However, it is conserved in the rest frame of the wave. This can be seen by the following argument (see, e.g., *Tsurutani* and *Lakhina*, 1997, which we have closely followed.). Let us assume that the particle gains a quantum of energy $\Delta E = \hbar\omega$ where ω is the wave frequency. Then its parallel momentum will increase by

$$m\Delta V_{\|} = \hbar k_{\|} = \frac{k_{\|}}{\omega}\Delta E. \tag{2.97}$$

As the energy gain is likely to be small, we can write it as

$$\Delta E = m(V_{\|}\Delta V_{\|} + V_{\perp}\Delta V_{\perp}). \tag{2.98}$$

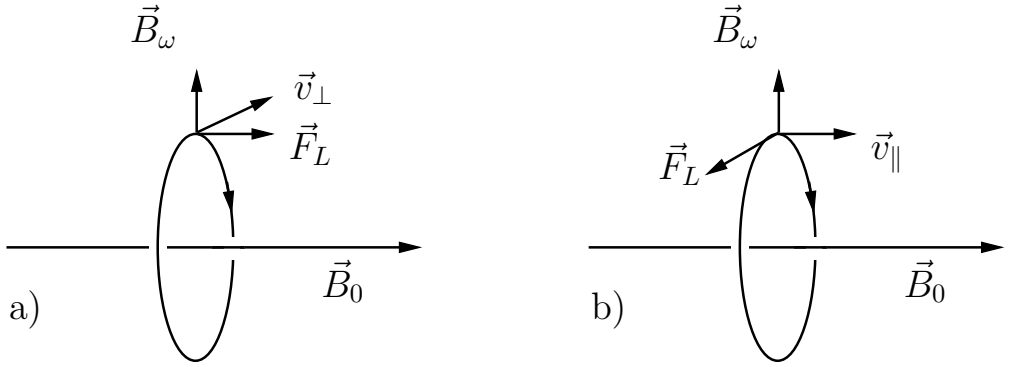

Figure 2.11: Interaction between a positively charged ion and a wave. a) shows the interaction with the $\vec{v}_\perp$ velocity component, and b) shows the interaction with the $\vec{v}_\parallel$ component. The Lorentz force due to the particles motion and the wave field, $\vec{B}_\omega$, can change the particles momentum (and pitch angle). After *Tsurutani* and *Lakhina* (1997).

Inverting eq. 2.97 for ΔE we obtain

$$\Delta E = \frac{m\omega}{k_\parallel}\Delta V_\parallel = mV_{\rm ph}\Delta V_\parallel, \tag{2.99}$$

where $V_{\rm ph}$ is the wave phase speed. Subtracting eq. 2.99 from eq. 2.98 and integrating (using the substitution $\Delta V \longrightarrow {\rm d}V$) we have

$$\frac{1}{2}mV_\perp^2 + \frac{1}{2}m\left(V_\parallel - V_{\rm ph}\right)^2 = \text{const.} \tag{2.100}$$

which shows that the particle's energy is conserved in the wave frame (because the integrand has to vanish). If the wave transfers an energy $\Delta E = \hbar\omega$ to the particle, the particle's parallel energy is increased and the wave phase speed is decreased accordingly.

Similar considerations can be made for particles scattering with the electric component of resonant electromagnetic or electrostatic waves. This is illustrated in Fig. 2.12.

Scattering off waves appears to be much more frequent in the heliosphere than Coulomb scattering. We will investigate wave-particle interactions in some more detail in the following chapter on the solar wind. Heating of particle distributions by ion-cyclotron waves appears to be a significant energy source to heat and accelerate the solar wind.

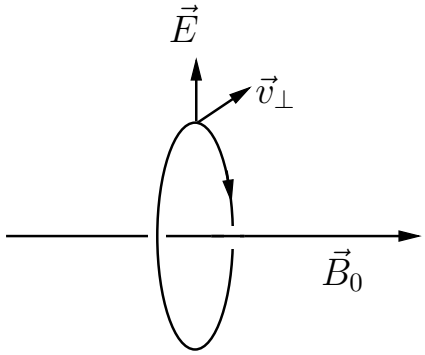

Figure 2.12: Interaction between a positively charged ion and the electric component of a resonant electromagnetic or electrostatic wave. After *Tsurutani* and *Lakhina* (1997).

Chapter 3

Waves in Plasmas

3.1 Introduction

The strength of the Coulomb force as well as its long range entail that plasmas are highly sensitive to perturbations. The individual particles (electrons and ions) which constitute a plasma are constantly moving due to their thermal motion. This combination can give rise to an incredible richness in organized behavior of the plasma which we call collective behavior or, in some cases, waves. Despite this sensitivity, a plasma does not exhibit random waves. Two conditions must be met by a disturbance to generate waves:

- The disturbance must be a solution of the equations of the plasma. If I disturb a plasma at an extremely high frequency, nothing will happen. Similarly, no waves will be generated if I move it very slowly. Only a limited and discrete number of modes will be able to exist in a plasma.

- What is a wave? We will speak of a wave only when its amplitude exceeds that of the always-present thermal fluctuations. This tells us that the disturbance needs to be large enough to affect the plasma more than the thermal fluctuations.

We will begin this chapter with a discussion of waves in a unmagnetized plasma and *etc., as we see what happens* For most of this chapter we will assume that disturbances are large, i.e., that they can lead to waves and that the wave amplitudes are larger than the thermal fluctuations. This can also be reworded as assuming a cold plasma. Nevertheless, we will also assume that the waves and disturbances are small enough that we can treat them linearly, that is that we can treat disturbances as a superposition of plane waves. A plane wave can be written in the form using its Fourier components,

$$\vec{A}(\vec{k},\omega)\exp(i\vec{k}\cdot\vec{x}-i\omega t). \tag{3.1}$$

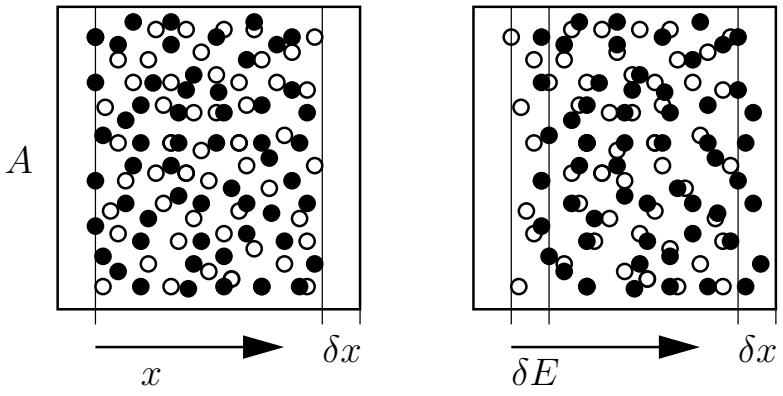

Figure 3.1: The displacement of the electrons by a distance δx results in a restoring electric field δE which acts on the the electrons and pulls them back. If there is insufficient friction (e.g., by collisions), the electrons will overshoot, and plasma oscillations set in.

This allows us to recall the definitions of the phase velocity, $\vec{v}_{\rm ph}$ and group velocity, $\vec{v}_{\rm gr}$ of the wave,

$$\vec{v}_{\rm ph} = \omega\vec{k}/k^2, \tag{3.2}$$
$$\vec{v}_{\rm gr} = \partial\omega/\partial\vec{k}, \tag{3.3}$$

where the phase velocity points parallel to the wave vector and thus in the same direction as the wave propagates. The group velocity does not necessarily point in the same direction but in the direction in which energy is transported by the wave.

We will largely follow the three books by *Baumjohann* and *Treumann* (1997), *Chen* (1984), and *Goedbloed* and *Poedts* (2004).

3.2 Waves in an Unmagnetized Plasma

Consider a charge-neutral plasma which is confined in a volume $V = A{\cdot}x$ where A is the cross section and x some length perpendicular to it (see Fig. 3.1). Because ions are much heavier than electrons, they are often considered to be immobile. Consider now a sudden displacement of all electrons in the plasma by a distance δx which is fast enough that the ions can't follow them. This displacement will set up a restoring electric field, δE, which points from ions to electrons and exerts a force $F = -e\delta E$ on every electron. Of course the ions also feel this force, but in the other direction. Because they are much heavier, the acceleration felt by them is much smaller. Thus, the electrons will be forced back to conserve charge neutrality. If their motion is not damped,

e.g., by collisions, they will overshoot and the situation will be reversed, with the electric field pulling them back in the other direction. This sets up plasma oscillations at a frequency known as the plasma frequency. Let us consider the magnitude of the electric field. It is given by Poisson's equation

$$\vec{\nabla} \cdot \vec{E} = \rho/\varepsilon_0 = (e/\varepsilon_0)(Zn_i - n_e), \tag{3.4}$$

where ρ is the charge density, and we have introduced the ion and electron number densities, n_i, and n_e, respectively. In this one-dimensional case, we may write

$$\partial E/\partial x = (e/\varepsilon_0)\,(Zn_i - n_e) \;\longrightarrow\; \partial E = (e/\varepsilon_0)\,(Zn_i - n_e)\,\partial x \;\longrightarrow\; \delta E = (e/\varepsilon_0)\,(Zn_i - n_e)\delta x. \tag{3.5}$$

The equation of motion for an electron is then

$$m_e \frac{\partial^2 \delta x}{\partial t^2} = -(e^2/\varepsilon_0)\;(Zn_i - n_e)\delta x. \tag{3.6}$$

But this is exactly the equation for a harmonic oscillator, the force is proportional to the displacement, and we immediately see that we need to expect a harmonic oscillation with frequency

$$\omega_{\rm pe} = \pm\sqrt{\frac{ne^2}{m_e\varepsilon_0}}, \tag{3.7}$$

where n is the undisturbed number density of electrons.

We will now rederive this result in a different and somewhat more precise manner to illustrate an important method, in which we make use of the smallness of perturbations by linearizing the fluid equations of the plasma. The electron continuity equation is

$$\frac{\partial n_e}{\partial t} + \vec{\nabla} \cdot (n_e \vec{v}_e) = 0, \tag{3.8}$$

and the equation of motion (or momentum conservation) is

$$m_e n_e \left(\frac{\partial \vec{v}_e}{\partial t} + \left(\vec{v}_e \cdot \vec{\nabla} \right) \vec{v}_e \right) = -e n_e \vec{E}. \tag{3.9}$$

Together with Poisson's equation, eq. 3.4, these equations describe the unmagnetized plasma we are studying. Next, we split the quantities which appear in these equations into an equilibrium part indexed with a subscript 0, i.e., n_0, E_0, and v_0, and a perturbed part indexed with a subsript 1, i.e.,

$$n = n_0 + n_1, \qquad \vec{v}_e = \vec{v}_0 + \vec{v}_1, \qquad \vec{E} = \vec{E}_0 + \vec{E}_1. \tag{3.10}$$

By definition, the time average of the perturbed values vanishes, and the time average of the original quantities is just n_0, $\vec{v}_0$, and $\vec{E}_0$. The equilibrium values are stationary and homogeneous (i.e., without oscillations), so

$$\begin{aligned} \vec{\nabla} n_0 &= \vec{v}_0 = \vec{E}_0 = 0, && (3.11)\\ \frac{\partial n_0}{\partial t} &= \frac{\partial \vec{v}_0}{\partial t} = \frac{\partial \vec{E}_0}{\partial t} = 0. && (3.12) \end{aligned}$$

We now rewrite the momentum conservation equation (eq. of motion, eq. 3.9) in these quantities and make use of the relations 3.11 and 3.12:

$$\begin{aligned} m_e n_e \left(\frac{\partial \vec{v}_e}{\partial t} + \left(\vec{v}_e \cdot \vec{\nabla} \right) \vec{v}_e \right) &= -e n_e \vec{E}, \\ m_e \left(\frac{\partial (\vec{v}_0 + \vec{v}_1)}{\partial t} + \left((\vec{v}_0 + \vec{v}_1) \cdot \vec{\nabla} \right) (\vec{v}_0 + \vec{v}_1) \right) &= -e(\vec{E}_0 + \vec{E}_1), \\ m_e \left(\frac{\partial \vec{v}_1}{\partial t} + \left(\vec{v}_1 \cdot \vec{\nabla} \right) \vec{v}_1 \right) &= -e\vec{E}_1, \\ m_e \left(\frac{\partial \vec{v}_1}{\partial t} + 0 \right) &= -e\vec{E}_1, && (3.13) \end{aligned}$$

where in the last step we have neglected the quadratic term. In other words, we have *linearized* the equation of motion in the perturbed quantities.
We linearize the continuity equation in a similar manner,

$$\begin{aligned} \frac{\partial n_e}{\partial t} + \vec{\nabla} \cdot (n_e \vec{v}_e) &= 0, \\ \frac{\partial (n_0 + n_1)}{\partial t} + \vec{\nabla} \cdot ((n_0 + n_1)(\vec{v}_0 + \vec{v}_1)) &= 0, \\ \frac{\partial n_1}{\partial t} + \vec{\nabla} \cdot (n_0 \vec{v}_0 + n_0 \vec{v}_1 + n_1 \vec{v}_0 + n_1 \vec{v}_1) &= 0, \\ \frac{\partial n_1}{\partial t} + (\vec{\nabla} n_0)\vec{v}_0 + (n_0 \vec{\nabla}) \cdot \vec{v}_0 + \ldots + (\vec{\nabla} n_1)\vec{v}_1 + n_1 (\vec{\nabla} \cdot \vec{v}_1) &= 0, \\ \frac{\partial n_1}{\partial t} + n_0 (\vec{\nabla} \cdot \vec{v}_1) + \vec{v}_1 \cdot (\vec{\nabla} n_0) &= 0, \\ \frac{\partial n_1}{\partial t} + n_0 (\vec{\nabla} \cdot \vec{v}_1) &= 0. && (3.14) \end{aligned}$$

In equilibrium, we have $n_{0i} = n_{0e} = n_0$, and because the ions don't move, we also have $n_{i1} = 0$, so Poisson's equation is now

$$\varepsilon_0 \vec{\nabla} \cdot \vec{E}_1 = -e n_1. \qquad (3.15)$$

In a next step, we decompose the oscillating quantities into their Fourier

components, similar to eq. 3.1,

$$\vec{v}_1 = v_1 \exp\left(i(\vec{k}\cdot\vec{x}-\omega t)\right)\hat{x}, \tag{3.16}$$

$$n_1 = n_1 \exp\left(i(\vec{k}\cdot\vec{x}-\omega t)\right), \tag{3.17}$$

$$\vec{E}_1 = E_1 \exp\left(i(\vec{k}\cdot\vec{x}-\omega t)\right)\hat{x}. \tag{3.18}$$

In this notation the time derivative can always be replaced by $-i\omega$, and the gradient by $i\vec{k}$,

$$\frac{\partial}{\partial t} \longrightarrow -i\omega, \quad \vec{\nabla} \longrightarrow i\vec{k}, \tag{3.19}$$

and equations 3.13 to 3.15 then become

$$-im_e\omega v_1 = -eE_1, \tag{3.20}$$

$$-i\omega n_1 = -n_0 ikv_1, \tag{3.21}$$

$$ik\varepsilon_0 E_1 = -en_1. \tag{3.22}$$

We solve eq. 3.22 for E_1, insert in eq. 3.20, in which we replace n_1 using eq. 3.21 to obtain

$$-im_e\omega v_1 = -e\frac{-e}{ik\varepsilon_0}\cdot\frac{-n_0 ikv_1}{-i\omega} = -i\frac{n_0e^2}{\varepsilon_0\omega}v_1. \tag{3.23}$$

We are now nearly at the end inasmuch as we have found an equation for ω. Afterall, we are interested in the situation where v_1 does not vanish, and, hence, we can divide eq. 3.23 by v_1 to obtain the same expression as eq. 3.7 for the plasma frequency,

$$\omega_{\rm pe} = \pm\sqrt{\frac{n_0e^2}{m_e\varepsilon_0}}. \tag{3.24}$$

Note that plasma oscillations do not propagate, the group velocity, $\vec{v}_{\rm gr} = \partial\omega/\partial\vec{k}$ vanishes because the plasma frequency does not depend on the wave vector, $\vec{k}$. The phase velocity, $\vec{v}_{\rm ph} = \omega\vec{k}/k^2$, changes with every oscillation because the wave vector, $\vec{k}$ points in opposite directions every half oscillation.

This situation is not entirely realistic. When they are displaced, some of the electrons can propagate further into the unperturbed plasma because of their higher thermal velocity. Thus, a pressure gradient,

$$\vec{\nabla}p_e = \gamma k_B T_e\vec{\nabla}n_e = 3k_BT_e\vec{\nabla}(n_0+n_1) = 3k_BT_e\frac{\partial n_1}{\partial x}\hat{x}, \tag{3.25}$$

will build up, which will influence the motion of the other electrons. In other words, this pressure gradient needs to be included in the equation of motion for the electrons. Already linearized, this now reads

$$m_en_0\frac{\partial v_1}{\partial t} = -en_0E_1 - 3k_BT_e\frac{\partial n_1}{\partial x}. \tag{3.26}$$

Again we write the fluctuating quantities in their Fourier components and transform this partial differential equation to an analytic equation,

$$-im_e\omega n_0 v_1 = -en_0 E_1 - 3k_B T_e ikn_1. \tag{3.27}$$

Now Poisson's equation and the continuity equation are both not altered by the introduction of this additional pressure term, so E_1 and n_1 are still given by eqs. 3.22 and 3.21, and so we end up with

$$\begin{aligned} -im_e\omega n_0 v_1 &= \left\{ en_0 \left(\frac{-e}{ik\varepsilon_0} \right) + 3k_B T_e ik \right\} \frac{n_0 ik}{i\omega} v_1, \\ \omega^2 v_1 &= \left(\frac{n_0 e^2}{\varepsilon_0 m_e} + \frac{3k_B T_e}{m} k^2 \right) v_1, \\ \omega &= \pm\sqrt{\omega_{\rm pe}^2 + \frac{3}{2}k^2 v_{\rm th}^2}, \end{aligned} \tag{3.28}$$

where $v_{\rm th}^2 = 2k_B T_e/m$. These oscillations now propagate and are called Langmuir waves. These waves only occur because of the finite temperature of the electrons.

3.3 Waves in Magnetized Plasmas

Of course, there are many more phenomena in unmagnetized plasmas than the two just treated, plasma oscillations and Langmuir waves. Nevertheless, we must go on and begin studying wave phenomena in magnetized plasmas. After all, the heliospheric plasma is magnetized. Again we will restrict ourselves to a subset of the rich phenomenology and consider only MHD waves. We will closely follow *Goedbloed* and *Poedts* (2004).

But before we begin with MHD equations, we will illustrate the procedure once more, this time with ordinary sound waves. The equations of gas dynamics (which are also included in MHD) are:

$$\frac{\partial \rho}{\partial t} + \vec{\nabla} \cdot (\rho \vec{v}) = 0, \tag{3.29}$$

$$\rho \left(\frac{\partial \vec{v}}{\partial t} + \vec{v} \cdot \vec{\nabla} \vec{v} \right) + \vec{\nabla} p = 0, \tag{3.30}$$

$$\frac{\partial p}{\partial t} + \vec{v} \cdot \vec{\nabla} p + \gamma p \vec{\nabla} \cdot \vec{v} = 0, \tag{3.31}$$

where ρ is mass density, p pressure, and $\gamma = c_p/c_v$ is the ratio of specific heats. We now need to linearize these equations about a time independent, infinite, and homogeneous background. This implies that $\partial/\partial t = 0$ and $\vec{\nabla}\cdot = 0$ for these

background quantitites, indexed by 0, while we write the small perturbations with an index 1. Thus, we recover the linearized equations of gas dynamics,

$$\left(\frac{\partial}{\partial t} + \vec{v}_0 \cdot \vec{\nabla}\right) \vec{v}_1 + \rho_0 \vec{\nabla} \cdot \vec{v}_1 = 0, \tag{3.32}$$

$$\rho_0 \left(\frac{\partial}{\partial t} + \vec{v}_0 \cdot \vec{\nabla}\right) \vec{v}_1 + \vec{\nabla} p_1 = 0, \tag{3.33}$$

$$\left(\frac{\partial}{\partial t} + \vec{v}_0 \cdot \vec{\nabla}\right) p_1 + \gamma p_0 \vec{\nabla} \cdot \vec{v}_1 = 0. \tag{3.34}$$

We wish to find an equation for $\vec{v}_1$, i.e., the perturbation in velocity, as this will give us the expression for wave propagation, as it did in the preceding section. The first in these equations is decoupled from the other two and we can disregard it for the time being. We can solve the other two by first applying the operator $\partial/\partial t + \vec{v}_0 \cdot \vec{\nabla}$ to the first (eq. 3.33 and the operator $\vec{\nabla}$ to the second (eq. 3.34). With the latter, we can eliminate p_1 from the former, and we obtain

$$\left(\frac{\partial}{\partial t} + \vec{v}_0 \cdot \vec{\nabla}\right)^2 \vec{v}_1 - \frac{\gamma p_0}{\rho_0} \vec{\nabla}\vec{\nabla} \cdot \vec{v}_1 = 0. \tag{3.35}$$

The factor $\gamma p_0/\rho_0$ infront of the second term has dimensions of speed squared, it is in fact nothing else but the square of the speed of sound, $c_s = \sqrt{\gamma p_0/\rho_0}$. Again, we write the fluctuating quantity, here $\vec{v}_1$ as a superposition of plane waves,

$$\vec{v}_1(\vec{r}, t) = \sum_{\vec{k}} \hat{\vec{v}}_{\vec{k}} e^{i(\vec{k}\cdot\vec{r} - \omega t)}. \tag{3.36}$$

Inserting in the wave equation, eq. 3.35, we can replace all derivatives by the corresponding algebraic factors, and we obtain

$$\left\{\left(\omega + \vec{k} \cdot \vec{v}_0\right)^2 \mathbf{I} - c_s^2 \vec{k}\vec{k}\right\} \cdot \vec{v}_1 = 0. \tag{3.37}$$

Let us transform into a frame of reference comoving with the gas (i.e., $\vec{v}_0 = 0$). Then we find that, in this simple system, there is no preferred direction. So now we can assume that the waves will propagate, e.g., in the z direction, $\vec{k} = k\hat{\vec{z}}$. In this case, eqs. 3.37 reduce to the following set of equations,

$$\begin{aligned} \omega^2 \hat{v}_x &= 0, \\ \omega^2 \hat{v}_y &= 0, \\ (\omega^2 - k^2 c^2)\hat{v}_z &= 0, \end{aligned} \tag{3.38}$$

which have the physically relevant solutions

$$\omega = \pm kc; \quad \text{where} \quad \hat{v}_x = \hat{v}_y = 0, \quad \text{and} \quad \hat{v}_z \quad \text{is arbitrary.} \tag{3.39}$$

These two solutions represent plane sound waves travelling to the right (+) and to the left (−). They are compressible because $\vec{\nabla}\cdot\vec{v}_1 \neq 0$ and longitudinal because $\vec{v}_1 \parallel \vec{k}$. The other solutions $\omega^2 = 0$ for arbitrary $\hat{v}_x$ and $\hat{v}_y$ and $\hat{v}_z = 0$ are not interesting from a physics point of view as they only describe time-independent incompressible transverse translations.

We will now proceed to derive three kinds of MHD waves, Alfvén waves, and the fast and slow magnetosonic waves from the equations of MHD in the same way as shown above. The equations of MHD are given by

$$\frac{\partial\rho}{\partial t} + \vec{\nabla}\cdot(\rho\vec{v}) = 0, \tag{3.40}$$

$$\rho\left(\frac{\partial\vec{v}}{\partial t} + \vec{v}\cdot\vec{\nabla}\vec{v}\right) + \vec{\nabla}p - \frac{1}{\mu_0}\left(\vec{\nabla}\times\vec{B}\right)\times\vec{B} = 0, \tag{3.41}$$

$$\frac{\partial e}{\partial t} + \vec{v}\cdot\vec{\nabla}e + (\gamma-1)e\vec{\nabla}\cdot\vec{v} = 0, \tag{3.42}$$

$$\frac{\partial\vec{B}}{\partial t} - \vec{\nabla}\times\left(\vec{v}\times\vec{B}\right) = 0, \quad \vec{\nabla}\cdot\vec{B} = 0, \tag{3.43}$$

where $e = e_0 = p_0/((\gamma-1)\rho_0)$ is the internal energy of the plasma. We will linearize these equations shortly, but before that, we rewrite the terms with vector products according to

$$-\left(\vec{\nabla}\times\vec{B}\right)\times\vec{B} = \left(\vec{\nabla}\vec{B}\right)\cdot\vec{B} - \vec{B}\cdot\vec{\nabla}\vec{B}, \tag{3.44}$$

$$-\vec{\nabla}\times\left(\vec{v}\times\vec{B}\right) = -\vec{B}\cdot\vec{\nabla}\vec{v} + \vec{B}\vec{\nabla}\cdot\vec{v} + \vec{v}\cdot\vec{\nabla}\vec{B}, \tag{3.45}$$

which leads to the following set of equations:

$$\frac{\partial\rho}{\partial t} + \vec{\nabla}\cdot(\rho\vec{v}) = 0, \tag{3.46}$$

$$\rho\left(\frac{\partial\vec{v}}{\partial t} + \vec{v}\cdot\vec{\nabla}\vec{v}\right) + (\gamma-1)\vec{\nabla}(\rho e) + \frac{1}{\mu_0}\left(\vec{\nabla}\vec{B}\right)\cdot\vec{B} - \frac{1}{\mu_0}\vec{B}\cdot\vec{\nabla}\vec{B} = 0, \tag{3.47}$$

$$\frac{\partial e}{\partial t} + \vec{v}\cdot\vec{\nabla}e + (\gamma-1)e\vec{\nabla}\cdot\vec{v} = 0, \tag{3.48}$$

$$\frac{\partial\vec{B}}{\partial t} - \vec{B}\cdot\vec{\nabla}\vec{v} + \vec{B}\vec{\nabla}\cdot\vec{v} + \vec{v}\cdot\vec{\nabla}\vec{B} = 0, \tag{3.49}$$

and, of course, $\vec{\nabla}\cdot\vec{B} = 0$. We now linearize these equations with the same assumption as above, namely that ρ_0, $\vec{B}_0$, and e_0 are constants, i.e., constant in time and homogeneous in space. Thus, their time derivatives and gradients

vanish. In this fashion, we obtain

$$\frac{\partial \rho_1}{\partial t} + \rho_0 \vec{\nabla} \cdot \vec{v}_1 = 0, \tag{3.50}$$

$$\rho_0 \frac{\partial \vec{v}_1}{\partial t} + (\gamma - 1)\left(e_0 \vec{\nabla}\rho_1 + \rho_0 \vec{\nabla} e_1\right) + \frac{1}{\mu_0}(\vec{\nabla}\vec{B}_1)\cdot\vec{B}_0 - \frac{1}{\mu_0}\vec{B}_0 \cdot \vec{\nabla}\vec{B}_1 = 0, \tag{3.51}$$

$$\frac{\partial e_1}{\partial t} + (\gamma - 1) e_0 \vec{\nabla} \cdot \vec{v}_1 = 0, \tag{3.52}$$

$$\frac{\partial \vec{B}_1}{\partial t} - \vec{B}_0 \vec{\nabla} \cdot \vec{v}_1 + \vec{B}_0 \cdot \vec{\nabla} \cdot \vec{v}_1 = 0, \tag{3.53}$$

To reduce the amount of writing, we introduce the notation

$$\vec{b} \doteq \frac{\vec{B}_0}{\sqrt{\mu_0 \rho_0}}. \tag{3.54}$$

With all of this now prepared, we wish to derive a wave equation using the momentum conservation equation, eq. 3.51. We take an extra time derivative to obtain

$$\frac{\partial^2 \vec{v}_1}{\partial t^2} + (\gamma - 1)\left(e_0/\rho_0 \vec{\nabla}\frac{\partial \rho_1}{\partial t} + \vec{\nabla}\frac{\partial e_1}{\partial t}\right) + \frac{\partial}{\partial t}(\vec{\nabla}\vec{B}_1)\cdot\vec{b} - \frac{\partial}{\partial t}\vec{b}\cdot\vec{\nabla}\vec{B}_1 = 0. \tag{3.55}$$

We now wish to replace all other fluctuating quantities except v_1 with expressions involving v_1. We can achieve this by applying the operator $\vec{\nabla}$ to eqs. 3.50, 3.52, and 3.53. We then insert the resulting expressions for the other fluctuating quantities in eq. 3.55 to obtain

$$\frac{\partial^2 \vec{v}_1}{\partial t^2} - \left\{(\vec{b}\cdot\vec{\nabla})^2 \mathbf{I} + (b^2 + c^2)\vec{\nabla}\vec{\nabla} - \vec{b}\cdot\vec{\nabla}(\vec{\nabla}\vec{b} + \vec{b}\vec{\nabla})\right\}\cdot\vec{v}_1 = 0. \tag{3.56}$$

For vanishing magnetic field, $\vec{b} = 0$, we recover the quation for the sound wave, eq. 3.37, as we would expect to happen. Again inserting the plane wave solutions, we get the algebraic eigenvalue equation,

$$\left\{\left[\omega^2 - (\vec{k}\cdot\vec{b})^2\right]\mathbf{I} - (b^2 + c^2)\vec{k}\vec{k} + \vec{k}\cdot\vec{b}(\vec{k}\vec{b} + \vec{b}\vec{k})\right\}\cdot\vec{v}_1 = 0. \tag{3.57}$$

As opposed to the case of pure sound waves, where there was no preferred direction, we now do have one, i.e., the direction of the magnetic field, which we define to be the z direction. We can now decompose eq. 3.57 into its components,

$$\begin{pmatrix} \omega^2 - k_\perp^2(b^2 + c^2) - k_\parallel^2 b^2 & 0 & -k_\perp k_\parallel c^2 \\ 0 & \omega^2 - k_\parallel^2 b^2 & 0 \\ -k_\perp k_\parallel c^2 & 0 & \omega^2 - k_\parallel^2 c^2 \end{pmatrix} \begin{pmatrix} \hat{v}_x \\ \hat{v}_y \\ \hat{v}_z \end{pmatrix} = 0. \tag{3.58}$$

This eigenvalue equation has a solution if the determinant of the matrix on the left-hand side vanishes. Nevertheless, we can already see one solution. The central matrix element will occur as a common multiplicative factor in the determinant. It describes a wave which propagates parallel to the field with a frequency

$$\omega = \pm\omega_A = \pm k_\parallel v_A \doteq \pm k_\parallel \sqrt{\frac{B_0^2}{\mu_0 \rho_0}}. \tag{3.59}$$

We have retrieved the famous Alfvén waves. They propagate to the right (along the direction in which $\vec{B}_0$ is pointing, i.e., positive) or to the left (negative sign, pointing opposite to $\vec{B}_0$). The velocity perturbation points in the $\pm y$ direction, as does the magnetic perturbation, the wave is a transverse wave. The electric field points in the $\pm x$ direction. The group velocity, $v_{\rm gr} = \partial\omega/\partial k = v_A$, points along the wave vector, and is constant. Thus, Alfvén waves show no dispersion. They are transverse oscillations of the magnetic field. A small velocity perturbation $\vec{v}_1$, perpendicular to $\vec{B}_0$ results in a tension force on the field line which acts to restore the velocity perturbation. Because there is no damping term, it will overshoot and the field line oscillates about $\vec{B}_0$ in a frame comoving with the wave.

The determinant of eq. 3.58 is easily calculated to be

$$\det = (\omega^2 - k_\parallel^2 b^2)\left[\omega^4 - k^2(b^2 + c^2)\omega^2 + k_\parallel^2 k^2 b^2 c^2\right] = 0, \tag{3.60}$$

where $k^2 = k_\parallel^2 + k_{perp}^2$. There are two other solutions to the dispersion relation, eq. 3.58 which fall out of eq. 3.60. The solution to the other (non-Alfvénic) factor of the determinant is given by

$$\omega_{\rm ms}^2 = \frac{k^2}{2}\left\{(v_A^2 + c^2) \pm \left[(v_A^2 - c^2)^2 + 4v_A^2 c^2 \frac{k_\perp^2}{k^2}\right]^{1/2}\right\}. \tag{3.61}$$

These oscillations are two magnetosonic waves, the fast (positive sign infront of the square bracket) and slow modes.

3.4 The General Dispersion Relation

The relationship between wave frequency and wave vector is called a dispersion relation. It differs for the various different waves present in a plasma. It is rather tedious to derive them all from similar considerations as we just used. A plasma allows for many different waves, and this can get rather involved. Moreover, one is then never sure that one has found all possible waves in the plasma under investigation. In the following, we will derive the most general dispersion relation for a magnetized plasma. This can, in principle then be solved, and will yield all possible waves for a given description of the plasma.

We do this by first deriving the general wave equation, and then deriving the general dispersion relation. We will closely follow *Baumjohann* and *Treumann* (1997).

3.4.1 The general wave equation

Consider a plasma which is subjected to some time- and spatially varying external currents and charge distributions, $\vec{j}_{\rm ex}$ and $\rho_{\rm ex}$. It will be goverend by some selfconsistent currents and charge densities, $\vec{j}$ and ρ, and electric and magnetic fields which will transport the information about the disturbances. This system is goverend by Maxwell's equations:

$$\vec{\nabla} \times \vec{B} = \varepsilon_0 \mu_0 \frac{\partial \vec{E}}{\partial t} + \mu_0 \left(\vec{j} + \vec{j}_{\rm ex} \right), \tag{3.62}$$

$$\vec{\nabla} \times \vec{E} = -\frac{\partial \vec{B}}{\partial t}, \tag{3.63}$$

$$\vec{\nabla} \cdot \vec{B} = 0, \tag{3.64}$$

$$\vec{\nabla} \cdot \vec{E} = \frac{1}{\varepsilon_0} \left(\rho + \rho_{\rm ex} \right). \tag{3.65}$$

As usual, we can derive the wave equation by taking the time derivative of the first equation,

$$\partial_t \left(\vec{\nabla} \times \vec{B} \right) = \varepsilon_0 \mu_0 \frac{\partial^2 \vec{E}}{\partial t^2} + \mu_0 \left(\partial_t \vec{j} + \partial_t \vec{j}_{\rm ex} \right),$$

and substituting $\partial_t \vec{B}$ with eq. 3.63. Using $\vec{\nabla} \times \vec{\nabla} \times \ldots = \vec{\nabla}(\vec{\nabla} \cdot \ldots) - \Delta \ldots$ ("rot rot = grad div - Laplace"), we obtain

$$\Delta \vec{E} - \vec{\nabla}(\vec{\nabla} \cdot \vec{E}) - \varepsilon_0 \mu_0 \frac{\partial^2 \vec{E}}{\partial t^2} = \mu_0 \left(\partial_t \vec{j} + \partial_t \vec{j}_{\rm ex} \right). \tag{3.66}$$

The selfconsistent current reacts to the electric fields according to Ohm's law,

$$\vec{j}(\vec{x}, t) = \int \mathrm{d}^3 x' \int_{-\infty}^{t} \mathrm{d}t' \sigma(\vec{x}, \vec{x}', t, t') \cdot \vec{E}(\vec{x}', t'). \tag{3.67}$$

The time integral expreses causality - the entire history of the plasma contributes to the exact behaviour of the current. In fact, even this complicated expression is a linearized version which is valid for small perturbations in the fields. The quantity σ is the conductivity tensor of the plasma, and eq. 3.67 closes the above system of equations if σ is known. One can determine σ if one knows the plasma, i.e., if one has a plasma model which allows one to derive an expression for σ. In other words, the plasma model determines the

conductivity tensor, and then we can derive the full spectrum of waves allowed in that plasma.

Let us now assume that the plasma responds linearly to perturbations in the fields or external currents or charge densities. In that case the conductivity tensor depends only on the relative positions and timing, i.e., $\sigma(\vec{x}-\vec{x}_0, t-t_0)$. Writing

$$\vec{E} = \vec{E}_0 + \delta\vec{E}, \quad \text{where} \quad \vec{E}_0 = 0$$

we then have

$$\Delta\delta\vec{E} - \vec{\nabla}(\vec{\nabla}\cdot\delta\vec{E}) - \varepsilon_0\mu_0\frac{\partial^2\delta\vec{E}}{\partial t^2} = \mu_0\partial_t\vec{j}. \tag{3.68}$$

The left-hand side describes the purely electromagnetic response of the plasma to the fluctuating current density on the right-hand side. The left-hand side (response) is independent of the medium! The influence and response of the medium is fully described by the right-hand side, by the fluctuating current density which itself responds to the fluctuating field according to Ohm's law,

$$\vec{j}(\vec{x},t) = \int \mathrm{d}^3x' \int_{-\infty}^{t} \mathrm{d}t\sigma(\vec{x}-\vec{x}', t-t')\cdot\delta\vec{E}. \tag{3.69}$$

Eq. 3.68 is the general wave equation. It is supplemented by Ohm's law (eq. 3.69) which requires a detailed model of the plasma so it can be calculated.

3.4.2 The general dispersion relation

We now derive the general dispersion relation. We again write the field fluctuations as a superposition of plane waves

$$\delta\vec{E}(\omega,\vec{k}) = \delta\vec{E}_0(\omega,\vec{k})\exp(i\vec{k}\cdot\vec{x} - i\omega t).$$

As usual, this will transfom the left-hand side of the wave equation into an algebraic equation. What about the right-hand side? The convolution theorem states that the Fourier transform of this convolution integral can be replaced by the product of the Fourier transforms of the two individual factors, σ and $\delta\vec{E}$. This simplifies the equation considerably, because it separates σ from $\delta\vec{E}$ (in Fourier space). Thus, we can separate the fluctuating field to obtain

$$\left[\left(k^2 - \frac{\omega^2}{c^2}\right)\mathbf{1} - \vec{k}\vec{k} - i\omega\mu_0\sigma(\omega,\vec{k})\right]\cdot\delta\vec{E}_0(\omega,\vec{k}) = 0. \tag{3.70}$$

This is already close to the dispersion relation. To be valid for all fluctuating fields, the determinant of the square brackets must vanish. The fields and conductivity tensor satisfy

$$\delta\vec{E}^*(\vec{k},\omega) = \delta\vec{E}(-\vec{k},-\omega), \tag{3.71}$$

$$\sigma^*(\vec{k},\omega) = \sigma(-\vec{k},-\omega), \tag{3.72}$$

assuring real (non-imaginary) field amplitudes. The dispersion relation is then

$$\mathrm{Det}\left[\left(k^2-\frac{\omega^2}{c^2}\right)\mathbf{1}-\vec{k}\vec{k}-i\omega\mu_0\sigma(\omega,\vec{k})\right]=0. \tag{3.73}$$

It is often written with the dielectric tensor, ϵ, with which

$$\delta\vec{j}(\omega,\vec{k})=-i\omega\varepsilon_0\left[\epsilon(\omega,\vec{k})-\mathbf{1}\right]\cdot\delta\vec{E}(\omega,\vec{k}).$$

Thus, we also have

$$\epsilon(\omega,\vec{k})=\mathbf{1}+\frac{i}{\omega\varepsilon_0}\sigma(\omega,\vec{k}). \tag{3.74}$$

With this, we can write the general dispersion relation in the customary form,

$$\mathrm{Det}\left[\frac{k^2c^2}{\omega^2}\left(\frac{\vec{k}\vec{k}}{k^2}-\mathbf{1}\right)+\epsilon(\omega,\vec{k})\right]=0. \tag{3.75}$$

This is the general dispersion relation for any active medium such as a plasma. The solutions to this equation describe the (linear) waves present in the medium. Their frequency is $\omega=\omega(\vec{k})$. There are not infinitely many solutions, but rather, this is an eigenvalue problem and has a finite number of solutions. Their exact behaviour depends on the model used to describe the plasma via its dielectric tensor ϵ.

3.4.3 Application: Cold Electron Plasma Waves

As an application of the procedure just outlined, we derive the dispersion relation for a cold magnetized plasma with a constant background field, $\vec{B}_0$. This means that only a linear term $\delta\vec{v}\times\vec{B}_0$ in the Lorentz force needs to be retained. We can rewrite this term using the electron gyrofrequency, eq. 2.9, $\vec{\omega}_{ge}=e\vec{B}_0/m_e$, and obtain the system of equations of motion for the electrons,

$$\begin{aligned}\frac{\mathrm{d}\delta\vec{v}_\parallel}{\mathrm{d}t} &= -\frac{e}{m_e}\delta\vec{E}_\parallel,\\ \frac{\mathrm{d}\delta\vec{v}_\perp}{\mathrm{d}t} &= -\frac{e}{m_e}\delta\vec{E}_\perp+\vec{\omega}_{ge}\times\delta\vec{v}_\perp.\end{aligned}$$

We differentiate the second equation with respect to time, using the vector relation $\vec{a}\times(\vec{b}\times\vec{c})=\vec{b}(\vec{a}\cdot\vec{c})-\vec{c}(\vec{a}\cdot\vec{b})$,

$$\partial_t^2\delta\vec{v}_\perp+\omega_{ge}^2\delta\vec{v}_\perp=-\frac{e}{m_e}\left(\partial_t\delta\vec{E}+\vec{\omega}_{ge}\times\delta\vec{E}_\perp\right).$$

This is an oscillator equation, as we will see shortly. What we want to do now is obtain an expression for the conductivity tensor, $\sigma(\omega,\vec{k})$. Since we have,

by assumption, a cold plasma, there are no pressure gradients working on the plasma. The ensemble of electrons all move at exactly the same speed caused by the electric field, and the current density, defined by this motion is

$$\delta\vec{j} = -en_0\delta\vec{v} = \sigma \cdot \delta\vec{E}.$$

Inserting a plane wave Ansatz for the electric field, and a similar oscillatory Ansatz for the velocity fluctuations, we obtain

$$-\omega^2\delta\vec{v}_\perp + \omega_\perp^2\delta\vec{v}_\geq = -\frac{e}{m_e}\left(-i\omega\delta\vec{E}_\perp + \vec{\omega}_{ge}\times\delta\vec{E}_\perp\right),$$

which we can solve for $\delta\vec{v}_\perp$,

$$\delta\vec{v}_\perp = -\frac{e}{m_e}\frac{1}{\omega_{ge}^2-\omega^2}\left(-i\omega\delta\vec{E}_\perp + \vec{\omega}_{ge}\times\delta\vec{E}_\perp\right) = -\frac{1}{en_0}\sigma\cdot\delta\vec{E}_\perp. \tag{3.76}$$

After a little bit of maths, and using the expression for the electron plasma frequency,

$$\omega_{pe} = \sqrt{\frac{ne^2}{m\varepsilon_0}},$$

we obtain an expression for the conductivity tensor,

$$\sigma(\omega) = \varepsilon_0\omega_{pe}^2\begin{bmatrix} \frac{i\omega}{\omega^2-\omega_{ge}^2} & \frac{\omega_{ge}}{\omega^2-\omega_{ge}^2} & 0 \\ \frac{-\omega_{ge}}{\omega^2-\omega_{ge}^2} & \frac{i\omega}{\omega^2-\omega_{ge}^2} & 0 \\ 0 & 0 & \frac{i}{\omega} \end{bmatrix}, \tag{3.77}$$

where the last line is due to the motion of the electrons parallel to the magnetic field (which is unaffectied by it). In other words, the conductivity tensor is independent of the wave vector and depends only on the wave frequency. It is now straightforward to derive the dielectric tensor, ϵ, of the cold plasma according to eq. 3.74.

$$\epsilon_{\text{cold}}(\omega) = \begin{bmatrix} 1+\frac{i\omega_{pe}^2}{\omega_{ge}^2-\omega^2} & -\frac{i\omega_{ge}}{\omega}\frac{\omega_{pe}^2}{\omega_{ge}^2-\omega^2} & 0 \\ \frac{i\omega_{ge}}{\omega}\frac{\omega_{pe}^2}{\omega_{ge}^2-\omega^2} & 1+\frac{\omega_{pe}^2}{\omega_{ge}^2-\omega^2} & 0 \\ 0 & 0 & 1-\frac{\omega_{pe}^2}{\omega^2} \end{bmatrix}, \tag{3.78}$$

which can be inserted into eq.3.75 to give the cold electron dispersion relation

$$\text{Det}\left[\underbrace{\frac{k^2c^2}{\omega^2}\left(\mathbf{1}-\frac{\vec{k}\vec{k}}{k^2}\right)}_{\text{electromagnetic}} + \underbrace{\epsilon_{\text{cold}}(\omega)}_{\text{plasma}}\right] = 0. \tag{3.79}$$

Because the wave vector does not appear in the dielectric tensor, we find that the only electrostatic variations in the cold electron plasma are pure oscillations which do not propagate, just as we found the plasma oillations in the plasma with frequency $\omega = \omega_{pe}$. The only propagating waves are electromagnetic in nature.

3.5 Landau Damping

Sofar, we have studied cold plasmas in which the thermal distribution of the ions and electrons did not play an appreciable role. This is a valid approximation if the electrons and ions are much slower than the phase velocities, ω_{pe}/k, of plasma waves in the plasma. But what happens if the wave vector, k, is large? Then the phase velocity can become arbitrarily small, even smaller than the thermal velocity of the particles constituting the plasama. At this point we will need to investigate the detailed behavior of the ions and electrons and a more complex physical picture of the plasma will emerge. The waves will couple to the particle's velocity distribution functions which in turn will influence the electromagnetic fields pervading the plasma.

Because the physics and mathematics of such a situation are already complicated enough, we will restrict ourselves to an unmagnetized plasma, i.e., $\vec{B}_0 = 0$. A cold unmagnetized plasma allows for two kinds of waves, electromagnetic and electrostatic. Electromagnetic waves propagate at essentially the speed of light, and are not going to be affected in any measurable way by the thermal properties of the plasma, but the electrostatic ones certainly will. Electrostatic plasma oscillations do not propagate and at their high frequencies ions will remain essentially at rest due to their large inertia.

To describe the physics properly, we need to consider the velocity distribuion function (VDF) of the electrons, $f(\vec{v}, \vec{x}, t)$. Its temporal behavior is governed by the Vlasov equation

$$\frac{\partial f}{\partial t} + \vec{v} \cdot \vec{\nabla} f - \frac{e}{m} \vec{E} \cdot \vec{\nabla}_v f = 0. \tag{3.80}$$

The electric field will be governed by Poisson's equation,

$$\begin{aligned} \vec{\nabla} \cdot \vec{E} &= \frac{\rho}{\varepsilon_0} = \frac{\rho_i - \rho_e}{\varepsilon_0} = e \frac{n_i - n_e}{\varepsilon_0} \\ &= \frac{e}{\varepsilon_0} \left(\int \mathrm{d}^3 v f_i(\vec{x}, \vec{v}, t) - \int \mathrm{d}^3 v f_e(\vec{x}, \vec{v}, t) \right) \end{aligned} \tag{3.81}$$

We again proceed by introducing unperturbed background quantities, $f_0, \vec{E}_0, \vec{B}_0$, and perturbations thereon, $f_1, \vec{E}_1, \vec{B}_1$. Since we have already assumed an unmagnetized plasma, we have $\vec{B}_0 = 0$. A macroscopic electric field would drive

currents until it vanishes, so we may assume $\vec{E}_0 = 0$. f_0 will satisfy the zeroth-order Vlasov equation, leaving the first-order Vlasov equation,

$$\frac{\partial f_1}{\partial t} + \vec{v} \cdot \vec{\nabla} f_1 - \frac{e}{m} \vec{E}_1 \cdot \vec{\nabla}_v f_0 = 0. \tag{3.82}$$

Again, we assume that we can Fourier decompose f_1,

$$f_1 \propto \exp\left(i\vec{k} \cdot \vec{x} - i\omega t\right). \tag{3.83}$$

We now define the x-direction to be along the electric field (i.e., $E_y = E_z = 0$). Inserting in eq. 3.82, we have

$$-i\omega f_1 + ikv_x f_1 = \frac{e}{m} E_x \frac{\partial f_0}{\partial v_x}, \quad \text{thus,} \tag{3.84}$$

$$f_1 = \frac{ieE_x}{m} \frac{\partial f_0/\partial v_x}{\omega - kv_x}. \tag{3.85}$$

With these considerations, Poisson's equation (eq. 3.81) turns into

$$ik\varepsilon_0 E_x = -e \int \mathrm{d}^3 v f_1, \tag{3.86}$$

because the ions are not affected by the high-frequency fluctuations. Moreover, the zero-order electron VDF is not affected by them either, by definition. Inserting the expression for f_1 (eq. 3.85) we readily obtain

$$1 = -\frac{e^2}{k\varepsilon_0 m} \int \mathrm{d}^3 v \frac{\partial f_0/\partial v_x}{\omega - kv_x}. \tag{3.87}$$

We can perform the two integrals perpendicular to the x-direction, and will obtain

$$1 = -\frac{e^2}{k\varepsilon_0 m} \int \mathrm{d}v_x \frac{\partial \hat{f}_0/\partial v_x}{\omega - kv_x}, \tag{3.88}$$

where $\hat{f}_0$ is the VDF integrated over the y and z velocity direction. In other words, we now have reduced the 3-d problem to one in one dimension. Obviously, the integral is singular at $\omega = kv_x$, which tells us that something is going on when particles have the speed $v_x \approx \omega/k$, i.e., when they are in resonance with the phase velocity of the wave, i.e., with the wave. These particles will interact strongly with the wave because they will feel the associated electric field very strongly. Particles traveling much faster or slower will feel a strongly oscillating field, these oscillations will tend to cancel out. In other words, only the particles with velocities in the x-direction which are close to the phase velocity of the wave (by definition in the x-direction) will interact with it. This is the physical origin of the singularity in the integrand. It is telling us that something is going on here, and that we need to be careful how we treat it!

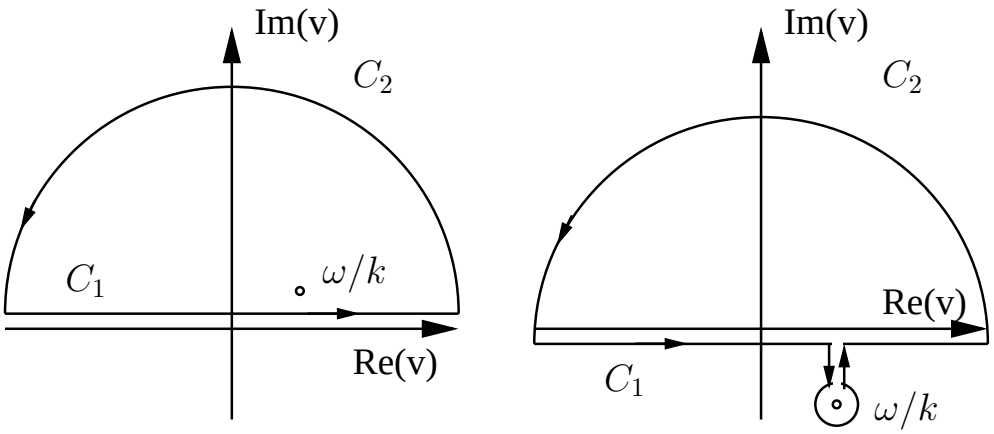

Figure 3.2: Contours for the integration in eq. 3.89 for an unstable wave (left), and a damped wave (right).

We can normalize eq. 3.88 by factoring out $n_0 = \int \mathrm{d}^3 v f_0$ and defining $\hat{f}_0$ as the normalized VDF. We then have the dispersion relation

$$1 = \frac{\omega_p^2}{k^2} \int \frac{\partial \hat{f}_0 / \partial v_x}{v_x - \omega/k}. \tag{3.89}$$

This resonance condition was noticed by Landau in 1946 who was the first who treated this case correctly. At this resonance, the particles and the waves can exchange momentum and energy. This interaction is 'collisionless', i.e., there are no collisions between particles associated with this interaction. For a Maxwellian VDF, $\hat{f}_0$, this exchange of energy and momentum results in a damping of the wave, this is called Landau damping. Landau showed how to treat this problem using the Laplace transform, but this treatment is somewhat obscure to physicists, who are more used to the Fourier transform. So let us do it the 'complicated' way, and inspect the physical significance of this process.

Actually, the singularity does not lie exactly on the integration contour. In fact, waves are normally damped or they grow (by some instability process), which means that their Fourier decomposition also has an imaginary component. Therefore, since v is always real, the denominator in eq. 3.89 does not vanish. Nevertheless, their pole does contribute to the physics by modifying the plasma wave dispersion function.

This integral needs to be performed as a contour integral, see Fig. 3.2. For the case of weak damping and large phase velocity, the pole lies near (and below) the real axis and we can approximate the integral by a sum of the real Cauchy principal value plus $2\pi i$ times half the residue of the pole,

$$1 = \frac{\omega_p^2}{k^2} \left[P \int_{-\infty}^{\infty} \frac{\partial \hat{f}_0 / \partial v}{v - (\omega/k)} \mathrm{d}v + i\pi \left. \frac{\partial \hat{f}_0}{\partial v} \right|_{v=\omega/k} \right]. \tag{3.90}$$

This is evaluated by integrating along the real axis

Chapter 4

The Solar Wind

4.1 Introduction

The idea that the Sun may be emitting streams of charged particles dates back to the end of the 19th century. For instance *Fitzgerald*[1], in 1892 and 1900, and *Lodge* in 1900, suggested that magnetic storms on the Earth were caused by "a torrent or flying cloud of charged atoms or ions"; that aurorae were caused by the "cathode ray constituents . . . as they graze past the polar regions"; that comet tails could not be accounted for by solar electromagnetic radiation pressure (for the simple fact that one can see stars shining through them), but could be accounted for by particle radiation emanating from sunspots "like a comet's tail" with an "average velocity [of] about 300 miles per second"; and finally that "there seems to be some evidence from auroras and magnetic storms that the earth has a minute tail like that of a comet directed away from the Sun" (all quoted from *Dessler* (1967)). Similar ideas were put forward and later substantiated experimentally in the laboratory and in an expedition by *Birkeland* in 1896. Figure 4.1 shows Birkeland in his laboratory observing the effects of a beam of charged particles on a terrella. *Birkeland* (1908, 1913) published the results of the 1902 – 1903 Norwegian Auroral Expedition, which, together with work by *Chapman* (1918; 1919), made these ideas more popular. Note that Birkeland in fact suggested a continuous solar wind (*Dessler*, 1967). The idea that it was solar corpuscular radiation that caused geomagnetic activity was soon deeply entrenched in the minds of geomagneticians which is witnessed by Bartels definition of the K_p index (*Bartels*, 1949): The K_p index is "designed to measure the varying intensity of solar particle radiation by its geomagnetic effects".

Viewed in this historic light, the postulation by *Biermann* (1951, 1953, 1957) of a continuous solar wind causing cometary tails to be deflected from the flight path towards the radial direction away from the Sun has the virtue

[1] Yes, the Lorentz-Fitzgerald contraction Fitzgerald

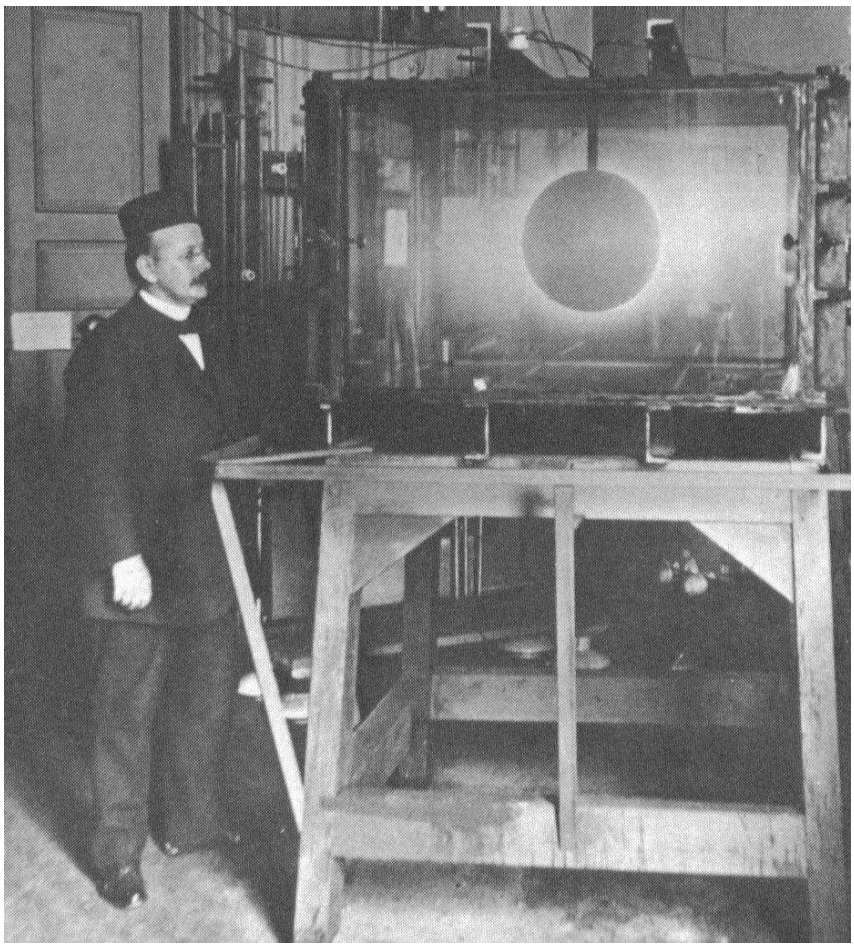

Figure 4.1: Birkeland observing a terrella in his laboratory. Source unknown.

of bringing up these ideas from the past and of emphasizing that the solar wind is continuous. These ideas and the first in situ measurements of the solar wind in the early 1960s by a series of Russian (Luna 2, Luna 3, and Venus 3) (*Gringauz et al.*, 1960; *Gringauz*, 1961; *Gringauz et al.*, 1967) and American (Explorer 10, Mariner 2, and Imp 1) (*Bonetti et al.*, 1963; *Scherb*, 1964; *Snyder* and *Neugebauer*, 1964; *Neugebauer* and *Snyder*, 1966, 1967; *Ness et al.*, 1964) space probes and satellites have intrigued us modern people for a long time. As a carrier of solar material the solar wind constantly supplies us with a sample of the solar composition, and thus of "the stuff we're made of". Some of the questions that arose early in the course of its investigation still remain unresolved. They may be reduced to two fundamental questions:

- How is the solar wind accelerated out of the solar gravitational potential?
- What is the mechanism of coronal heating?

Answers to these two questions are very likely to be related but are still lacking. Nevertheless, we will review some of the ideas which have shaped over the course of the last fourty years in this chapter.

4.1.1 Electron-Driven Solar Wind

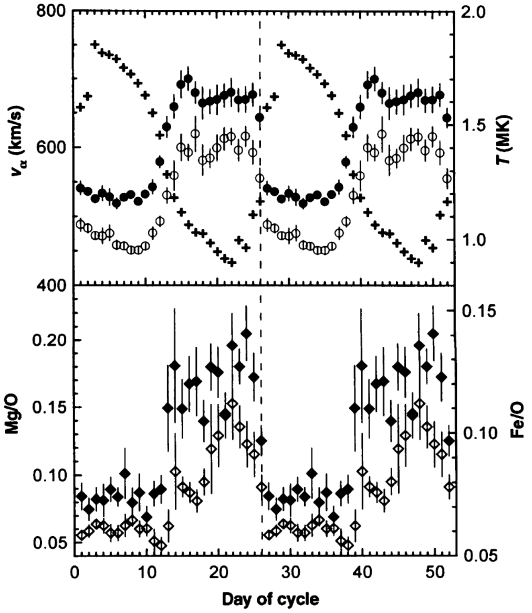

Figure 4.2: Ulysses measurements of recurring high-speed and slow wind streams show distinct compositional differences in both ionization temperature (top) and FIP (bottom). From *Geiss et al.* (1995*b*). Legend: + iα-particle speed, open (filled) circles show freeze-in temeperature of carbon (oxygen), open (filled) diamonds the Mg/O (Fe/O) element abundance ratio.

The first model to explain the supersonic solar wind proposed by Parker *Parker* (1958)has already been treated in the introductory lecture and need not be repeated here. The expansion of an isothermal corona results in the supersonic solar wind. However, the model has several shortcomings. First, the slow wind should originate in cool coronal regions according to this model. However, from measurements of the charge states of solar wind ions, we know that it comes from hot regions. On the other hand, the fast solar wind, which should come from hot coronal regions according to the Parker model, originates in cool coronal holes. Second, the corona is not isothermal. Third, the density profiles observed with SOHO/UVCS show such rapid decrease with radius that the solar wind must be accelerated much faster than assumed in this simple model. Parker knew (and knows) about these shortcomings and concluded that some sort of energy source must be available in the corona to further accelerate the solar wind.

The solar wind is accelerated to speeds typically ranging from 300 km/s to 750 km/s and occasionally to > 2000 km/s by processes still not understood. In normal conditions, it consists of two types, a fast ($v \gtrsim 600$ km/s) wind and a slow wind. The fast wind originates in coronal holes, regions of unipolar open magnetic field lines. The source of the slow wind is not known and hotly debated. Three classes of scenarios have been proposed. A first class places the origin of the slow solar wind at the boundaries of coronal holes,

where the field lines from the open coronal hole reconnect with closed loops from the streamer belt, thus releasing highly fractionated plasma into the solar wind. A second class posits the edges of active regions as the source of the slow wind. Systematic outflows at such boundaries have indeed been observed (*Sakao et al.*, 2007*a*). The third class is based on a topological argument that requires every coronal hole on the Sun to be linked to all other coronal holes of the same magnetic polarity (*Antiochos et al.*, 2011). The 'channels' which are needed to connect the holes have been named 'S-web' and would then be the source of the slow wind.
The twin problem of heating the corona and accelerating the solar wind is as old as it still is controversial. Two classes of models have been proposed to solve this problem in a self-consistent manner. In one class of models, the wind is accelerated and the corona heated by waves generated by footpoint motions of magnetic flux tubes. Indeed, Alfvén waves are known to have enough energy to heat the corona and accelerate the solar wind (*De Pontieu et al.*, 2007). The other class is based on the observation that all open flux tubes on the Sun root in the vicinity of closed loops, the 'magnetic carpet' (*Title* and *Schrijver*, 1998). When an open field line reconnects with one of the evolving but still closed loops, it funnels the material of that loop into the solar wind. *Cranmer* (2010) summarizes the key properties of these two classes.
The composition of the solar wind is an important diagnostic tool for the orgin of the solar wind which has a composition which differs systematically from that of the photosphere. Elements with low first ionization potential (FIP) are more enriched relative to oxygen in the slow wind than in the fast wind (see Fig. 4.2). This has been known for a long time (**?***Geiss et al.*, 1995*a*,*b*) and average properties of both solar wind types have been studied extensively (e.g., *von Steiger et al.*, 2000). The fast wind appears to be relatively uniform in its properties while the slow wind is much more variable. There are various theories to explain the FIP ordering, all rely on some mechanism to separate neutral atoms from charged ions (see *Hénoux*, 1998, for a review.). The FIP effect is explained in more detail in Sec. 4.5.3. The fast and slow wind are not only fractionated in different ways, but also have different charge-state composition (see Fig. 4.2). This has an important and badly understood consequence. Charge-state composition is determined in the corona, while the element-fractionating FIP-process occurs in the chromosphere. Thus this compositional link hints at an intimate connecion between corona and chromosphere.

4.2 Sources of the Solar Wind

4.2.1 Coronal Holes as the Source of the Fast Wind

The fast solar wind is known to originate in coronal holes (*Krieger et al.*, 1973; *Nolte et al.*, 1976), regions of open magnetic fields with low electron

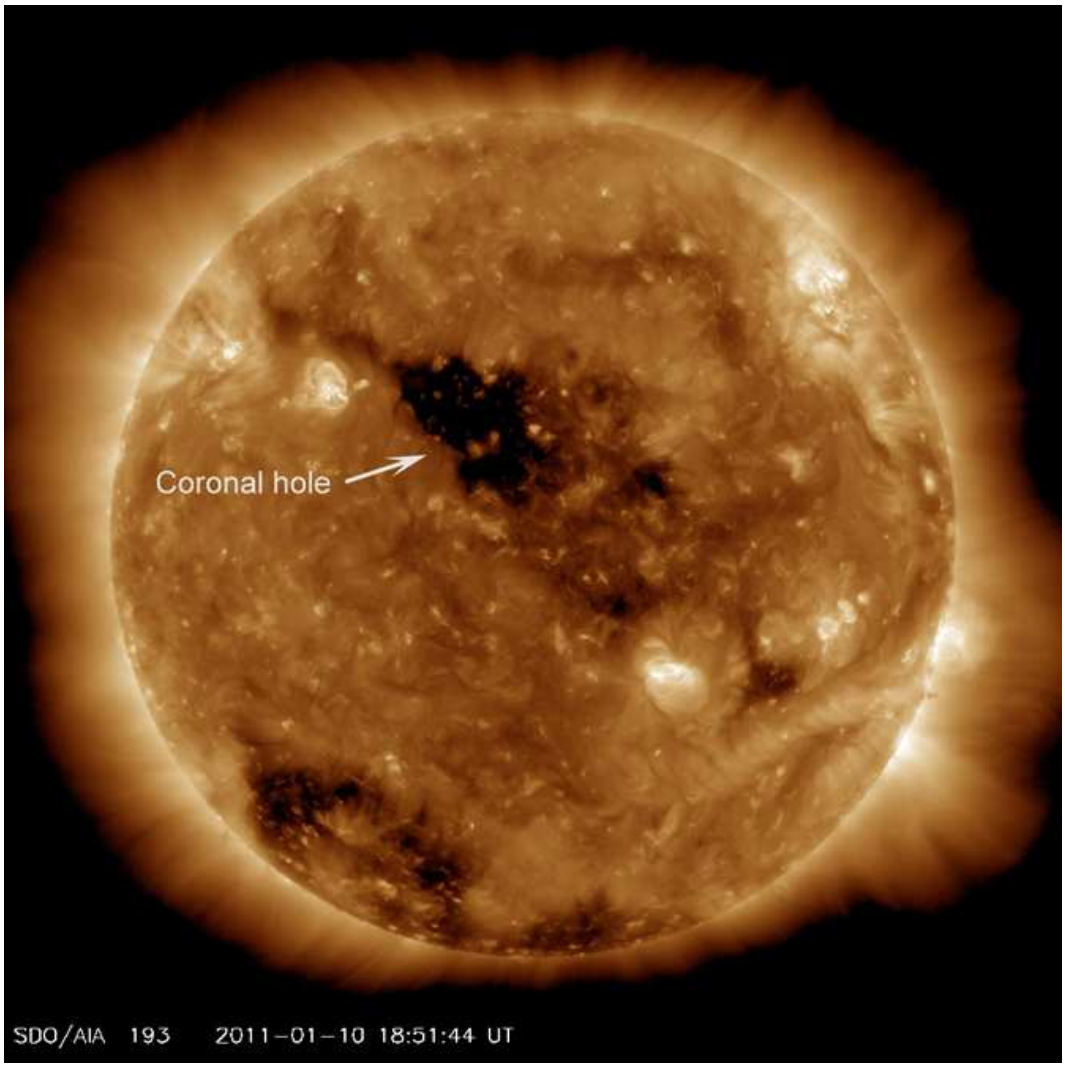

Figure 4.3: Solar Dynamics Observatory (SDO) extreme UV (EUV) image of the full Sun showing a coronal hole. Credit NASA

density, easily visible as dark (underexposed) regions in white-light, X-ray, and extreme ultraviolet images. An example is shown in Fig. 4.3. As shown by *Krieger et al.* (1973), the size of the coronal hole is well correlated with the speed of the solar wind emanating from the hole. Those authors took the observations that the y-intercept of the fitted linear relation exceeds the speed of the solar wind as proof that the slow wind can not originate in small coronal holes. However, that work was performed on data from only three recurrences of the same coronal hole, and, interestingly, it has not been repeated since.

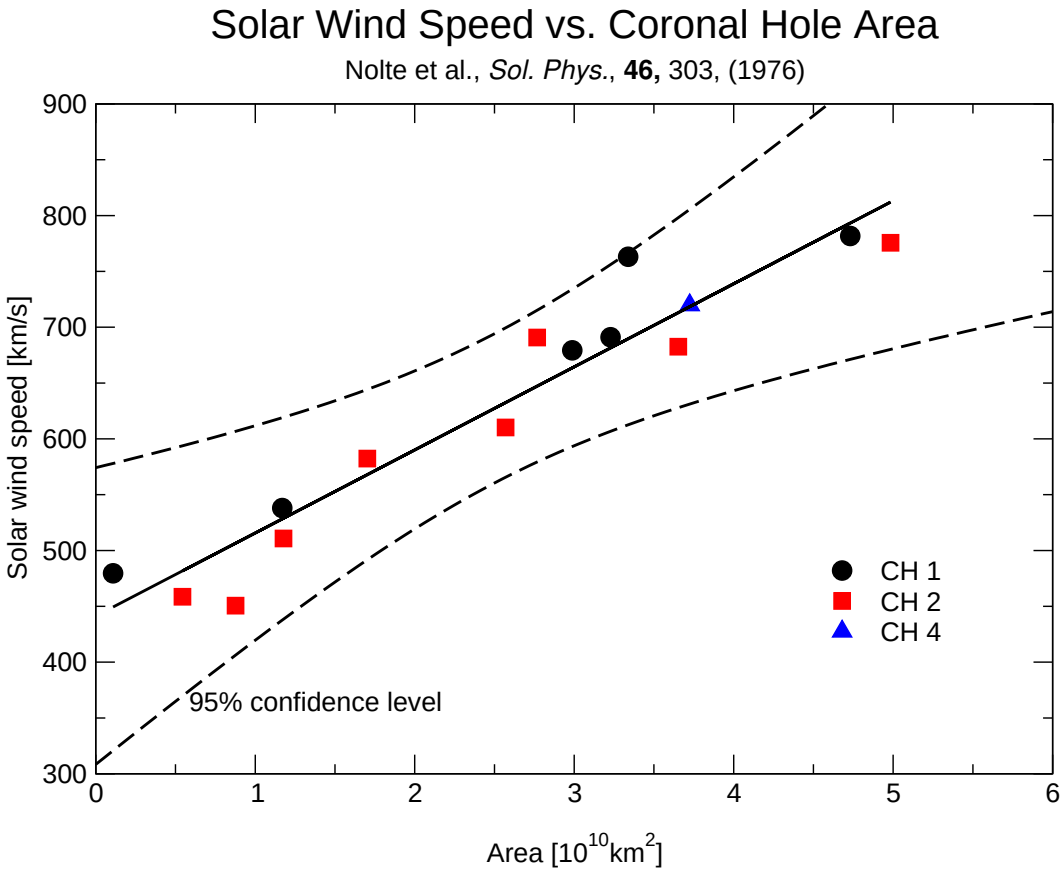

Figure 4.4: Solar wind speed vs. coronal hole size. After *Krieger et al.* (1973).

Today, we believe that it is the superradial expansion factor that determines fast solar wind speed (*Wang* and *Sheeley*, 2006). These authors compared solar wind speed with superradial expansion factors derived from the potential field source surface model and found them to be well explained by a conservation of mass and energy along a flux tube, $\rho v/B = \rho_0 v_0/B_0$, and $F_w/B = F_{w_0}/B_0$ where ρ is density, v speed, B magnetic field strength, and F_w wind energy flux density, the index zero refers to these quantities at the coronal base. With $F_w \approx (\rho/2)v^3$, this means that solar wind speed is completely determined by the original energy given to the proton at the coronal

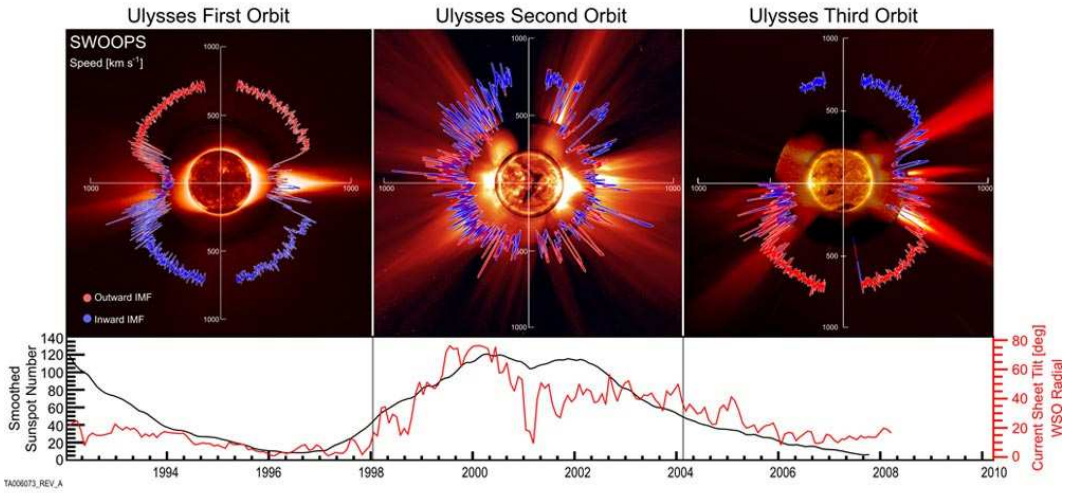

Figure 4.5: 3-dimensional structure of the heliosphere as measured by Ulysses. From *McComas et al.* (2008).

base, $v \approx \sqrt{(2F_{w_0})/(\rho_0 v_0)}$. Because $\rho_0 v_0$ increases with increasing superradial expansion, wind speed decreases with it. This is a simplified argument following the more general solar wind scaling law of *Schwadron* and *McComas* (2003) but neglecting radiative and gravitational losses.

4.2.2 The Streamer Belt as the Source of the Slow Wind

The origin of the slow solar wind is believed to lie in the vicinity of helmet streamers and/or coronal hole boundaries. Using SOHO/SUMER data, *Madjarska et al.* (2004) observed a 4-5 times higher reconnection rate along the edges of a coronal hole than on the quiescent Sun. These reconnection events were visible as bidirectional jets expelling solar material at speeds up to 150 km/s. They interpreted their results as support for the findings of *Wang et al.* (1998) that the edges of coronal holes are a source of the slow solar wind. However, the latter authors also found that the streamers themselves were sources of the slow solar wind, i.e., that this kind of wind has multiple sources, the blobs emanating from the cusps of streamers, probably by footpoint-interchange reconnection, and the edges of neighboring coronal holes. These findings, based on remote-sensing observations by SOHO instruments, are consistent with the findings of *Neugebauer et al.* (1998); *Burton et al.* (1999) and *Ko et al.* (2006*a*) who found that the slow wind maps back to streamers. On the other hand, *Posner et al.* (2001) identified the boundaries of coronal holes as the source region for stream interfaces which they found to be rotational discontinuities.

Figure 4.5 shows the association of the slow wind with the streamer belt.

The left-hand panel shows Ulysses measurements of solar wind speed around solar activity minimum. The slow wind is concentrated along the equatorial regions while the fast wind comes from the poles. At this stage of solar activity, streamers are concentrated along the heliomagnetic equator, as can be seen in the inset SOHO/LASCO image. The bright regions to the left and the right of the Sun are coronal streamers. As LASCO images in white light, this implies an enhanced electron density, as is the case for coronal streamers. The fast wind emanates from coronal holes which are located in the polar regions and exhibit equatorward extensions at solar activity minimum. These polar coronal holes can be seen in the EIT image that is inset in the left-hand panel of Fig. 4.5. The right-hand panel shows the situation around solar activity maximumen the solar corona is structured much more unevenly. Streamers emanate at all angles - a consequence of the large tilt of the solar magnetic dipole as it turns from one polarity to the other. ast and slow wind are seen at all latitudes.

4.2.3 Active Regions

Whether active regions on the Sun contribute to the solar wind is a highly controversial issue. Active regions appear as bright regions in EIT images. As EIT measures in the extreme UV, this corresponds to a hot plasma which is confined by closed magnetic fields. Because of these closed field lines, we would not expect any solar wind to be able to escape. Nevertheless, images especially from the Hinode and SDO missions do show what appear to be open field lines and outflows emanating from them (see elow). However, it is not clear whether they are truly open or whether we simply do not see their continuation because they have a low density. Brightness in UV images goes with density squared, as all collisionally excited emission.

Recently,*Sakao et al.* (2007*b*) have used the new X-Ray Telescope (XRT) on JAXA's Hinode spacecraft to measure outflows from what appears to be the interface region between an active region and a coronal hole boundary. Figure 4.6 shows their observations. The left-hand panel shows an overview of the active region, the white bar indicates the position at which the X-ray CCDs were positioned. The middle panel gives a time-distance plot of brightness enhancements measured by the CCDs in the time from February 22, 11:33:34 UT to February 22, 17:40 T. The brightness patterns appear to move upward at a speed of up to 100 km/s, which is better seen in the rightmost panel, an expanded view of the region between the two bright lines in the middle panel. The dotted white line represents west-to-east motion at a speed of 140 km/s. This may indicate the outflow of solar material into interplanetary space.

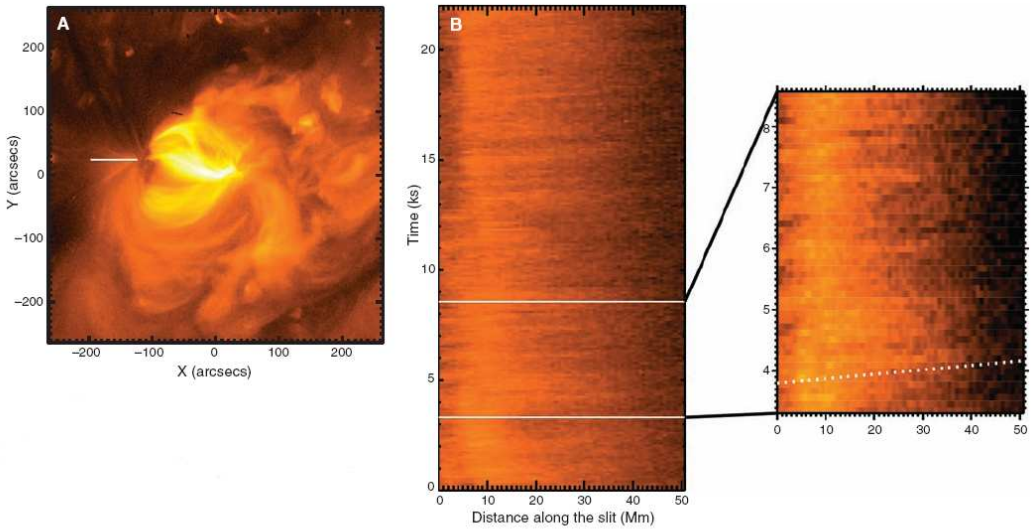

Figure 4.6: Hinode/XRT observations of outflow from the edge of an active region. The white bar in panel A shows the position of the CCD which were kept there for three days. The middle panel shows the east-west-moving brightness patterns during a subset of 22'000 s. The region between the two white lines has been expanded in the rightmost panel, C. The dotted white line corresponds to a speed of 14 km/s. From *Sakao et al.* (2007*b*).

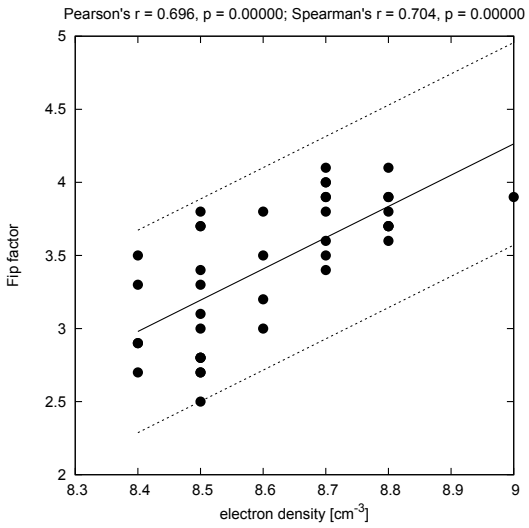

Figure 4.7: FIP fractionation factor as a function of coronal electron density at the edges of the active region studied by *Brooks* and *Warren*. The solid line shows the linear fit discussed in the text, dashed lines show 95% confidence interval. Data from Table 1 of *Brooks* and *Warren* (2011).

Several authors have investigated the link between corona and heliosphere. *Ko et al.* (2006*b*) observed a coronal hole at the boundary of an active region with UVCS aboard SOHO and compared the measured elemental composition (mainly) of the active region with that measured in-situ by SWICS on ACE. Because UVCS measures mainly on the solar limb, but SWICS measures plasma originiating from close to disk center, UVCS and SWICS did not measure the same material as such. However, those authors stress that the active region and coronal hole did not evolve much in the 7 days covered by that campaign. Therefore, they concluded, the similarities in the evolution of elemental and charge-state composition at the solar site and measured in the solar wind were highly suggestive that active regions are one of the sources of the slow solar wind. Since then, e.g., *Sakao et al.* (2007*a*) and *Harra et al.* (2008) have directly observed outflows from the edges of active regions with speeds which could reach above 100 km/s using XRT and EIS on Hinode, respectively. The latter authors interpreted their observations as an expansion of loops that lie over the active region, which may either reconnect with neighboring large-scale loops or are likely to open to the interplanetary space, and thus to contribte to the solar wind. Indeed, newer observations of active region outflows with EIS (*Brooks* and *Warren*, 2011) tend to confirm this idea by showing a FIP fractionation pattern that is comparable to that of the slow solar wind. Fig. 4.7 shows their measurement of the FIP fractionation factor as a function of (measured) electron density. The solid line is a linear fit (regression coefficient $r \approx 0.7$, see header), the dashed lines show the 95% confidence level interval. The probability of randomly distributed points to produce such a fit is vanishingly small ($p < 10^{-6}$). Some of the questions that arise from these observations are the physical cause for this corellation, whether it could survive out to 1 AU, and whether it could be measured in-situ.

4.2.4 Observations at 1 AU

The overall properties of the solar wind at 1 AU are easily summarized. During solar minimum, a two-stream structure is often seen (as shown in Fig. 4.8), in which high-speed streams alternate with slow solar wind. The fast streams have values of typically $v_{\rm p} \approx 700$ km/s, $n_{\rm p} \approx 3$ cm^{-3}, and $T_{\rm kinp} \approx 2{\times}10^5$ K. The slow wind is much more variable, but the average properties are $v_{\rm p} \approx 400$ km/s, $n_{\rm p} \approx 10$ cm^{-3}, and $T_{\rm kinp} \approx 4 \times 10^4$ K. He/H abundance ratios are typically around 5% and 4% in the fast and slow wind, respectively, but He/H ranges from nearly 0% up to 30% in the slow wind. Interestingly, the flux, $n_{\rm p} \times v_{\rm p}$ is similar (only a factor 2 different) for fast and slow wind, $\approx 2 \times 10^8 {\rm cm}^{-2}{\rm s}^{-1}$ and $\approx 4 \times 10^8 {\rm cm}^{-2}{\rm s}^{-1}$, respectively. It does not make much sense to give average values of the magnetic field, as this depends much on compression, speed, etc. However, as the discussion in Sec. **??** showed, the radial component of the magnetic field should follow a $1/r^2$ law. At one AU it is measured to lie around 3 nT for both fast and slow solar wind.

Already early measurements had shown that the solar wind needs to be divided into at least two classes, fast and slow wind. The fast wind emanates from coronal holes (see Section 4.2.1) and, as Ulysses has shown has a nearly radial speed of typically about 750 km/s. Its composition is near photospheric, whether it is enriched in ow-FIP elements is still under debate. Ionic charge-states indicate its origin in cool coronal holes, typically between 1 and 1.2 MK. The kinetic temperature of the fast wind , however, hotter than that of the slow wind. In the ecliptic, the fast solar wind is often not as fast as mentioned above. This is likely due to the interaction of the original fast stream with adjacent slow wind streams. This is likely to happen already very close to the Sun within 0.3 AU, as can be seen from Fig. 4.2.4, discussed below. At high latitudes, the fast wind is very steady, both in composition and in velocity. Fluctuations are generally small and correlated with fluctuations in the magnetic field, indicating the presence of Alfvén waves, as discussed in Chapter 7 and shown in Fig. 7.6.

The slow wind is much more variable in its properties than the fast wind. This is already seen in the slow-wind periods in Fig. 4.8. Density, temperature, speed, composition, and magnetic field rarely settle down to the relatively constant values attained in high-speed streams. Ionic charge-state composition indicates a hotter original plasma,but the kinetic temperature is normally much cooler than that of high-speed streams. As ionic charge states freeze in roughly at the location where their expansion time becomes small compared to the ionization/recombination time, this probably implies an expansion geometry in which the slow wind is very rapidly accelerated or in which coronal densities rapidly decrease. The large variability points to an intermittent origin of the slow wind - and that is just about as much as we know about its origin - as discussed above.

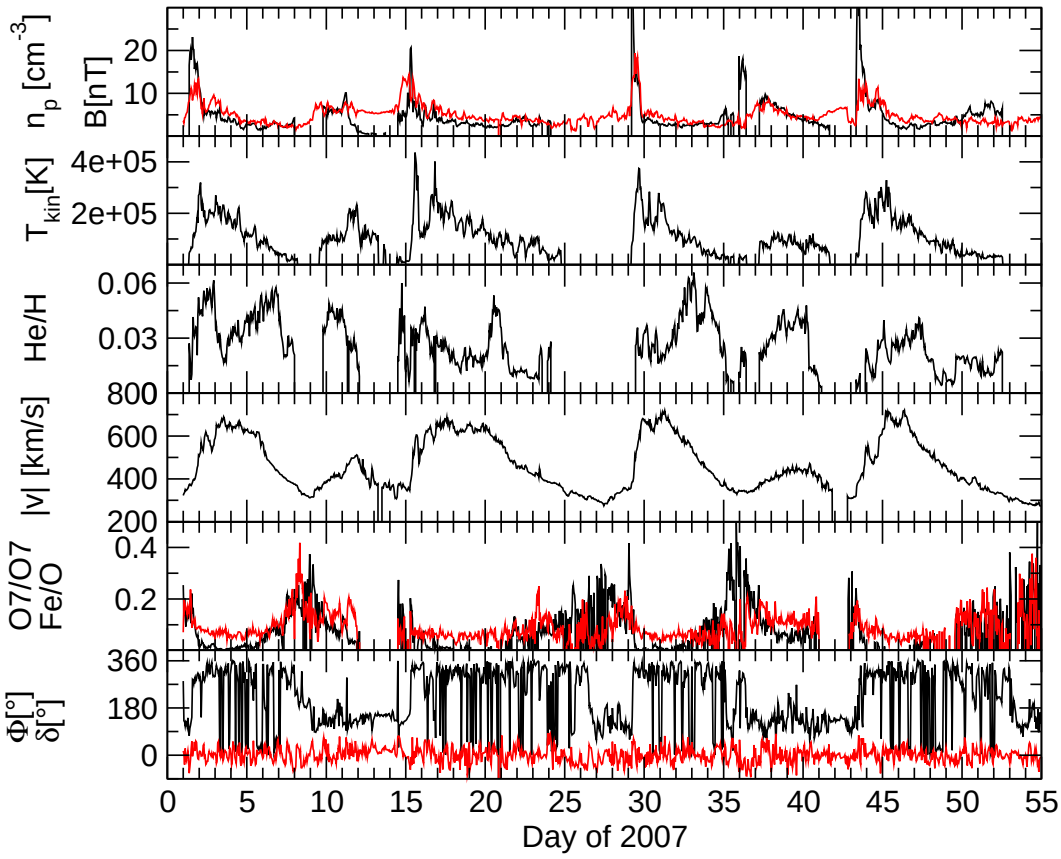

Figure 4.8: Solar wind data from the Advanced Composition Explorer (ACE). From top to bottom: proton number density (black) and magnetic field strength (red), proton kinetic temperature, He/H abundance ratio, proton speed, O^{7+}/O^{6+} charge-state ratio (black) and Fe/O elemental abundance ratio (red), magnetic field azimuth (black) and elevation (red) angles.

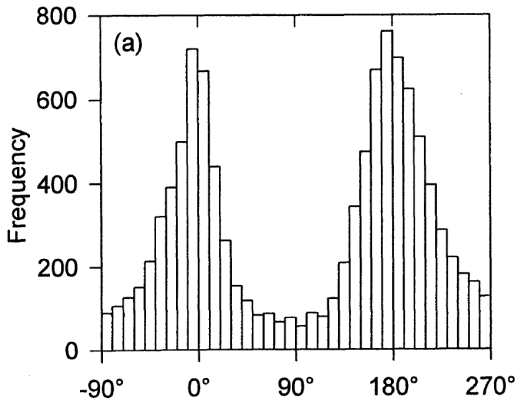

Figure 4.9: Measured magnetic field angles minus the predicted Parker field angle. The two peaks around 0° and 180° show overall agreement with the Parker model. From *Forsyth et al.* (1996).

We see in Fig. 4.8 the solar wind speed and the magnetic field angles. Do they agree with Parker's prediction? Indeed, as Fig. 4.9 shows, they do reasonably well, but with a remarkable spread. This is due to the presence of Alfvén waves and other structures in the solar wind which are discussed in Chapter 7.

Measurements often use the so-called **RTN system** which is defined in the following manner and in Fig. 4.10.

One AU data can be obtained from the ACE Science Center:
`http://www.srl.caltech.edu/ACE/ASC/`.

Data from all (US) space missions can be obtained from:
`http://cdaweb.gsfc.nasa.gov/`.

The solar wind streams and their magnetic field observed at one AU have already undergone substantial processing on their way from the Sun to 1 AU. As fast wind catches up with slower wind, they begin to interact and, ultimately, coalesce. From observations by the Heliospheric Imager (HI) on STEREO (*Eyles et al.*, 2009), we know that this processing must be quite extensive. Figure 4.2.4 shows a large number of individual streams in the vicinity of the Sun (small elongations) while only a few survive out to one AU or beyond.

4.3 Solar Wind Acceleration and Heating

Figure 4.12 shows a compilation of many measured coronal density profiles. They all fall off faster than a simple $1/r^2$ profile that would be expected if the corona were static. To conserve flux, there must be some coronal expansion driving a solar wind. Near the Sun, the density profiles are best fit by the

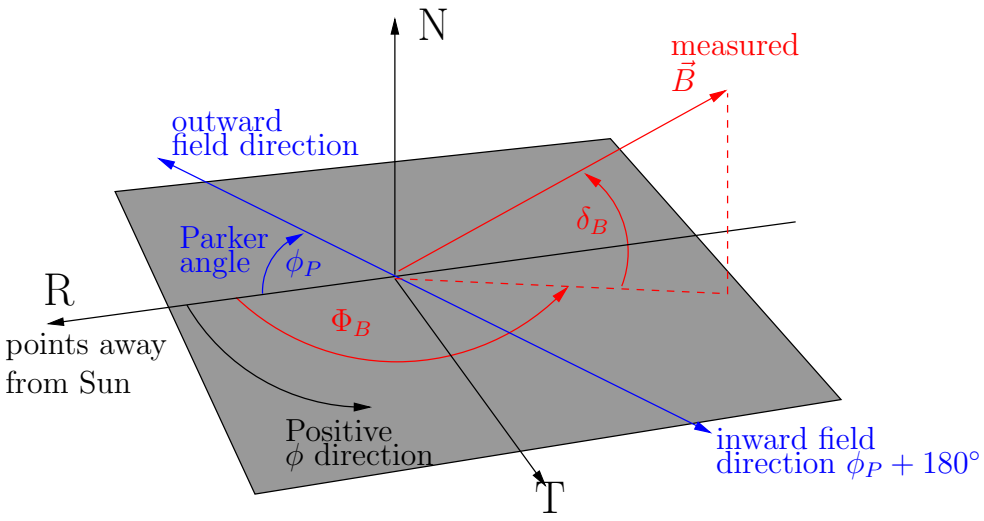

Figure 4.10: Definition of the RTN coordinate system. The R direction points radially outwards, away from the Sun. The RT plane is inclined to the solar equator at the same angle as the spacecraft heliographic latitude. N stands perpendicular to this plane and in the half space in which $\vec{\Omega}$, the solar rotation angular velocity, points. T completes the right-handed system (and generally points tangentially). The measured magnetic field vector (red) is given by its magnitude B, and the two angles ϕ_B and δ_B. Often co-latitude, ϑ_B is used instead of δ_B.

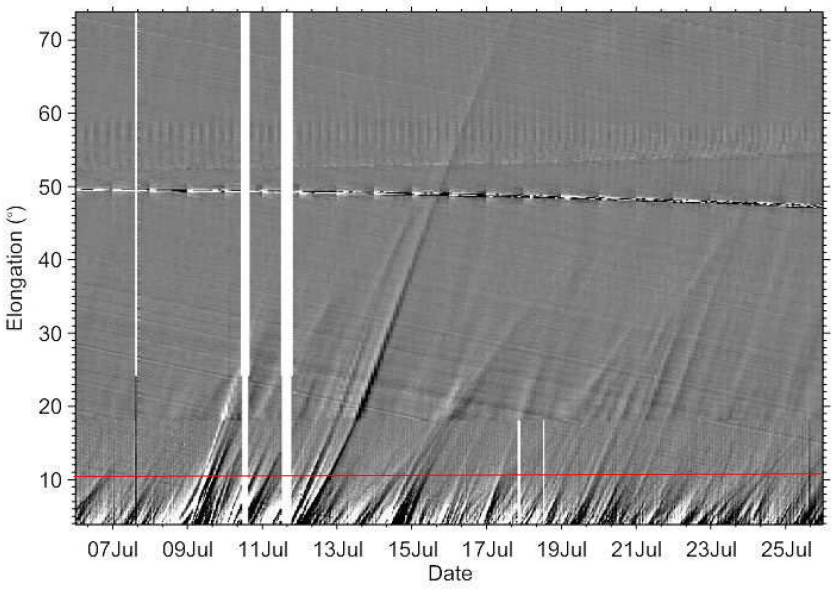

Figure 4.11: A height-time plot of small scale solar wind structures in the solar wind, as measured by the Heliospheric Imager on STEREO. While there are many individual streams in the solar vicinity, they are washed out by the time they reach one AU.

following empirical expression (*Aschwanden*, 2005):

$$n_e(r) = 10^{14}\left[2.99\left(\frac{r}{r_\odot}\right)^{-16} + 1.55\left(\frac{r}{r_\odot}\right)^{-6} + 0.036\left(\frac{r}{r_\odot}\right)^{-1.5}\right]\mathrm{m}^{-3} \quad (4.1)$$

while far from the Sun IPS measurements give

$$n_e(r) = 7.2\cdot 10^{11}\left(\frac{r}{r_\odot}\right)^{-2}\mathrm{m}^{-3} \quad \text{for} \quad r \gg r_\odot. \quad (4.2)$$

Because $v(r)n(r) \propto 1/r^2$ because of flux conservation, we immediately see that the solar wind must be accelerated to high speeds already close to the Sun. At one astronomical unit, we have a solar wind number density of about 5 particles per cm^{-3}. With an average solar wind speed of 400 km/s, we have a flux of $2\cdot 10^{12}\mathrm{m}^{-2}$. The flux must increase as $1/r^2$ as we approach the Sun because mass is conserved. Thus, the speed profile can be estimated by extrapolating solar wind flux to the heliocentric distance in question and inverting nv for v. This shows that solar wind speed must increase very fast in the corona.

4.3.1 Wave-Particle Interaction

We have already encountered the concept of wave-particle interaction in the previous chapter, section 2.6. Here we introduce the basic concepts and that of

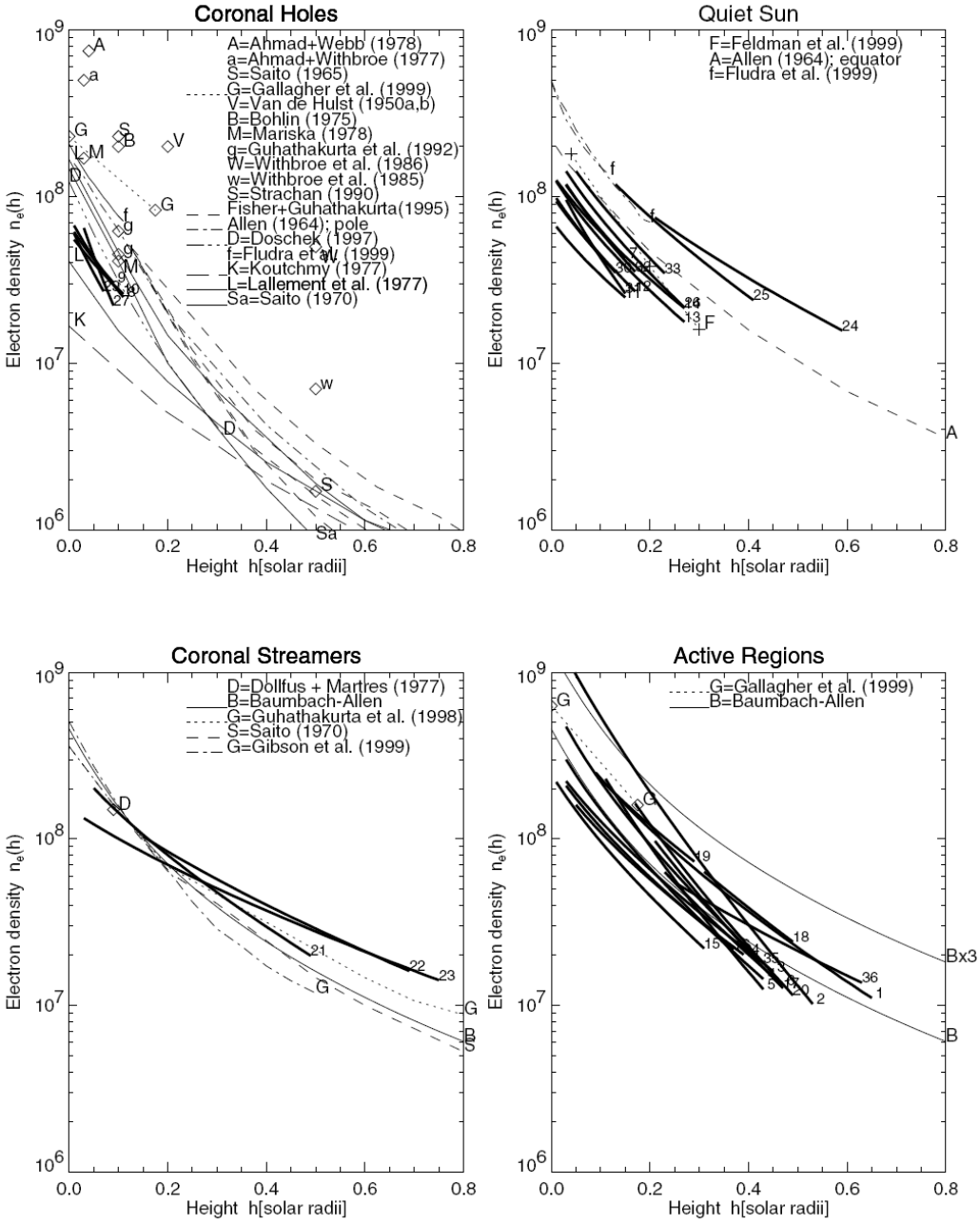

Figure 4.12: A compilation of coronal density profiles. From *Aschwanden* (2005).

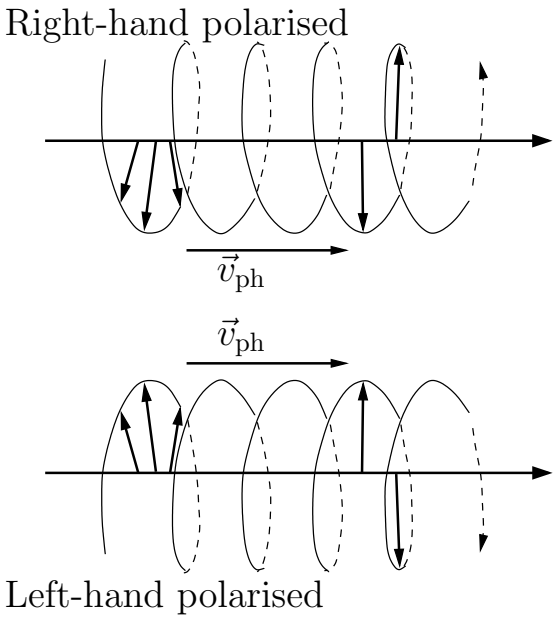

Figure 4.13: Right- and left-hand circularly polarized electromagnetic waves propagating towards the right. The sense of polarisation is measured from the source of the waves, i. e., in the sense of their propagation.

Landau damping. Figure 4.13 shows two circularly polarized electromagnetic waves propagating to the right at their phase velocity $v_{\rm ph}$. There are two conflicting conventions to define the polarization of a wave, here we use the convention that we use the sens of polarisation as seen from the source or in the direction of wave proagation. In that convention, ions will gyrate left-handedly, and electrons right-handedly. As we saw in the previous chapter, particles gyrate around the ambient magnetic field and propagate along it. While most particles will never notice an electromagnetic field because it passes it too fast or too slowly to notice, it is intuitively clear that if a particle moves at the "right" speed, it will feel the wave's electromagnetic field. As the particle and wave move at their relative speeds, the wave appears Doppler shifted in the particle frame of reference. If the wave frequency is the same as the particle gyro frequency, then particle and wave are in resonance and the particle strongly feels the wave's electromagnetic field. More precisely, the condition for such a cyclotron resonce is written as

$$\omega - \vec{k}_{\|} \cdot \vec{V}_{\|} = n\Omega \tag{4.3}$$

where ω and $\vec{k}$ are the wave frequency and wave vector, $\vec{V}$ and Ω are the particle veloctiy and gyroperiod. n is an integer, $n = 0, \pm 1, \pm 2, \ldots$ The case $n = 0$ describes the situation where the particle velocity is close to the wave phase speed, $\vec{V} \approx \vec{v}_{\rm ph} = \frac{\omega}{k}$. The treatment here is performed in the non-relativistic

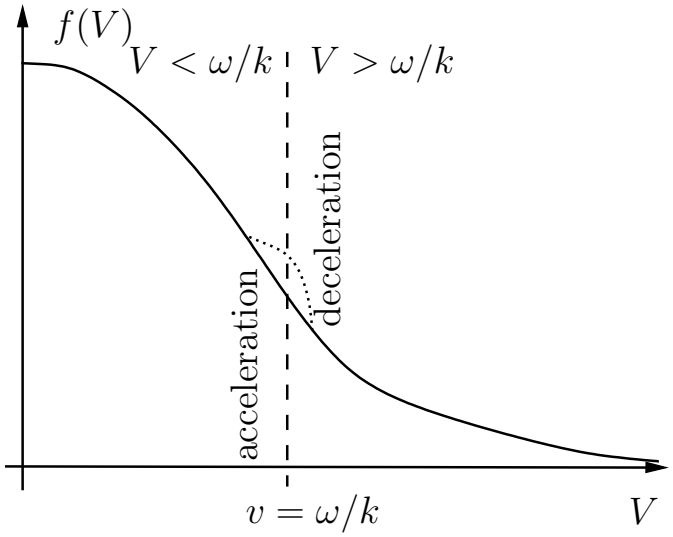

Figure 4.14: The physics of Landau damping.

approximation because the solar wind and the waves in it only propagate at low speeds compared to e speed of light.

4.3.2 Landau Damping

In the case where $n = 0$ the wave and the particle move in unison and the particle feels the electromagnetic field of the wave which changes its momentum until the particle is no more in resonance with the wave. Thus, the particle and wave exchange momentum (and energy). If the wave moves slightly faster than the particle, it will transfer momentum (and energy) to the particle and vice-versa. This situation is called Landau damping. Obiously, for parallel motion, ions will be able to resonate with left-hand polarized waves and electrons with right-hand polarized waves. To understand this, let us consider a wave propagating across a thermalized plasma with a Maxwellian velocity distribution function, $f_0(\vec{V})$. Then those particles will be able to resonate with the wave which have velocities $V = \omega/k$ because they will be moving at the same speed as the wave. Obviously, those particles which move slightly faster than the wave will feel the opposite force from those moving just slightly more slowly. We can consider the wave as a particle with energy $\hbar\omega$ and momentum $\hbar k$. Interactions between particles and waves can the be treated as elastic collisions between particles; particles slower than the wave will be accelerated, particles faster than the wave will be decelerated as they will impart part of the momentum to the wave. Fig. 4.15 shows the popular view of Landau damping as 'surfing the waves' in analogy with a surfer ahead of a wave. Only if he is about the speed of the wave can he surf it. If he is simply floating on his

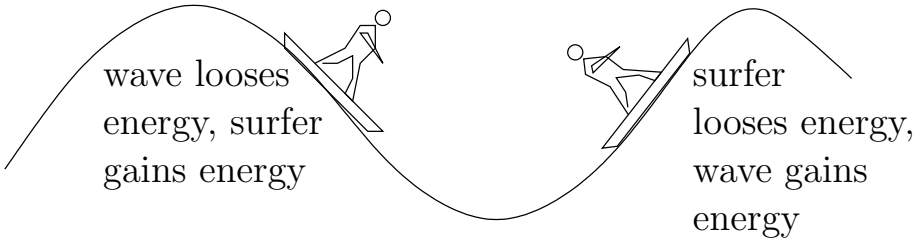

Figure 4.15: Physically intuitive, although not entirely correct, picture for Landau damping. In the situation athe left, the surfer gains energy from the wave, at the right, he looses energy to the wave. In the particle picture, particles which are marginally slower than the phase velocity of the wave will gain energy from the wave, particles that are slightly faster will loose energy.

board he will only be moved up and down by the waves, if he is much faster than the waves, their effect will average out.

Inspite of its elastic, and thus dissipationless nature, this kind of interaction is called Landau damping. The damping occurs because for a normal particle population there are more particles that are slower than the wave than are faster. Thus, the wave tends to loose energy when it passes through such a particle population. This distorts the particle velocity distribution function as indicated by the dotted line in Fig. 4.14.

Consider a distribution $f(V)$ of particles encountering waves with a phase speed ω/k. The change in velocity which a particle experiences is small and independent of this transformation and we have the total change of particle energy as

$$\Delta E = m \int_{-\infty}^{\infty} \mathrm{d}V \; V \left\langle \Delta V \right\rangle \;\; f(V) \tag{4.4}$$

where $\langle \Delta V \rangle$ is the velocity change averaged over one wavelength or wave oscillation. Let us transform into the rest frame of the wave by subtracting the phase speed from the particle speeds, $V' = V - \omega/k$. Then the above equation is transformed to

$$\Delta E = m \int_{-\infty}^{\infty} \mathrm{d}V' \; (V' + \omega/k) \left\langle \Delta V \right\rangle \;\; f(V' + \omega/k) \tag{4.5}$$

We can now expand $f(V)$ around $V' = 0$, i.e., $V = \omega/k$, and obtain

$$\Delta E = m \int_{-\infty}^{\infty} \mathrm{d}V' \; (V' + \omega/k) \left\langle \Delta V \right\rangle \;\; \left[f\left(\frac{\omega}{k}\right) + \frac{\omega}{k} \left. \frac{\partial f}{\partial V} \right|_{V'=\omega/k} \right]. \tag{4.6}$$

Let us assume that the particle is accelerated. Then, in the rest frame of the wave it will soon feel a retarding force which slows it down until it is slower

than the phase speed again. Then it is accelerated again, etc. Thus, we can consider this particle trapped in a harmonic oscillator in which the energy gain has to be an odd function of V' (otherwise it would not oscillate). The particle population will receive a net gain in energy if there are more particles which are slower than the waves phase speed, i.e., the population will experience a net energy gain if

$$\Delta E > 0 \quad \text{if} \quad \left.\frac{\partial f}{\partial V}\right|_{V'=\omega/k} < 0, \tag{4.7}$$

i.e., if the local slope is negative at the phase speed. In equilibrium, the energy transferred from the wave to the particles equals the loss of energy to the wave,

$$\frac{\Delta E}{t} = -\frac{\Delta \mathrm{d}E_{\mathrm{wave}}}{\mathrm{d}t}. \tag{4.8}$$

The average rate of energy loss to the wave is given by the half product of the waves oscillating electric field with its conjugate complex (the "square" of the electrc field),

$$E_{\mathrm{wave}} = \varepsilon_0 \delta E(t) \cdot \delta E^*/2. \tag{4.9}$$

In this product, only the real part of the exponent survives, and the wave experiences damping,

$$\frac{\Delta E}{t} = -\frac{\Delta \mathrm{d}E_{\mathrm{wave}}}{\mathrm{d}t} \propto \gamma E_{\mathrm{wave}}(0) \tag{4.10}$$

where the damping factor γ again depends on e sign of the derivative of the particle velocity distribution function at $V\prime = \omega/k$. Usually, this will be negative, and so gamma will be negative as well. However, in cases where the dictrbution function exhibits a positive slope, the wave will gain energy from the particles, possibly leading to the grow of instabilities. Such a situation can occur when a beam of accelerated particles impinges on a low-energy particle population. We will investigate Landau damping in more detail in Chapter 8.

4.3.3 Ion-Cyclotron Resonance

Let us next consider the case $n = 1$ of eq. 4.3 in which we have

$$\omega - k_{\|} V_{\|} = \Omega. \tag{4.11}$$

As long as ω and Ω (the wave and particle frequency and gyro frequency) are known, the resonance condition can be calculated. For parallel propagation we have

$$V_{\|} = \frac{\omega - \Omega}{k_{\|}}. \tag{4.12}$$

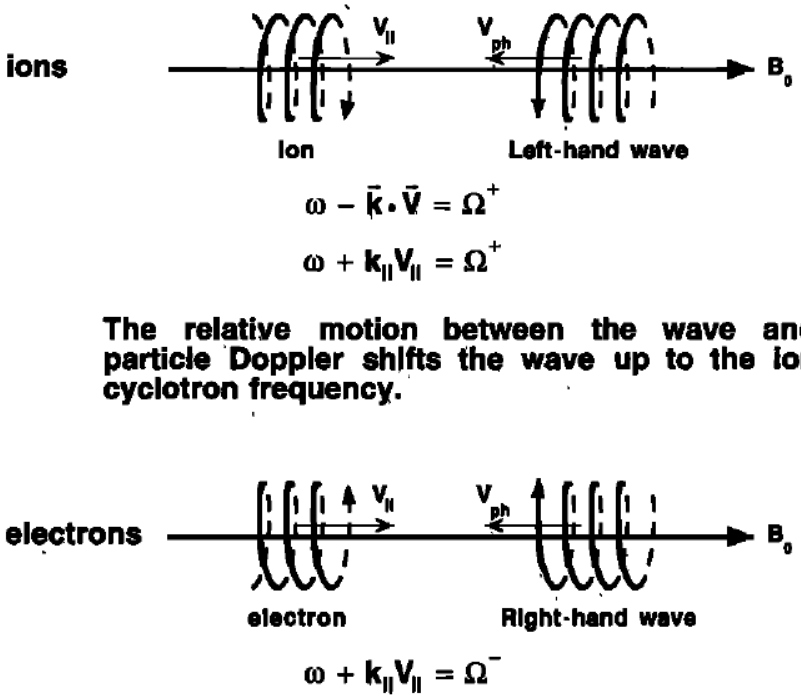

Figure 4.16: Normal first-order cyclotorn resonance between charged particles and circularly polarized electromagnetic waves.

The parallel kinetic energy of such particles can be written as

$$E_{\parallel,\mathrm{res}} = \frac{1}{2} m V_{\parallel,\mathrm{res}}^2 = \frac{1}{2} m \frac{(\omega - \Omega)^2}{k_\parallel^2} = \frac{1}{2} m V_{\mathrm{ph}}^2 \left(1 - \frac{\Omega}{\omega}\right)^2 , \tag{4.13}$$

where $V_{\mathrm{ph}} = \omega / k_\parallel$ is the parallel phase speed of the wave. If the waves are at frequecies which are much less than the cyclotron frequency of the particle, their phase speed can be aproximated by the Alfven speed, $v_a = \sqrt{B^2/(2\mu_0 \rho)}$, where ρ is the ambient plasma mass density.

In Fig. 4.13 (from *Tsurutani* and *Lakhina* (1997)) we see two waves, one left-hand circularly polarized (top) and one right-hand circularly polarized (bottom). At low frequency (compared to the ion gyro frequency) the left-hand polarized waves are ordinary Alfvén waves, at high frequencies they are ion-cyclotron waves. As long as the plasma frequeny is larger than the electron gyro frequency, $\Omega_{\mathrm{pe}} > \Omega^-$, left-hand polarized waves can at frequencies exist up to the ion gyro frequency. Right-hand waves can exist up to the electron gyro frequency. This is because left-hand waves normally resonate with ions and right-hand waves normally resonate with electrons.

For resonance to occur, wave and partile normally have to approach each other. Figure 4.16 shows the normal situation. Because waves and particles

approach each other, $\vec{k} \cdot \vec{V}$ is negative and the ensuing Doppler shift shifts the slow wave oscillation up to the fast particle gyro frequency.

There is the possibility that the particle is faster than the wave and catches up with it. In this case, ions will interact with right-hand polarized waves and electrons with left-hand waves because they see the waves "from in behind". This situation is called anomalous resonance. It appears in regions upstream of a shock where shock-accelerated particles escape from the shock and generate right-hand polarized waves.

We have already seen in chapter 2 that ions can be heated by wave-particle interactions when they resonantly feel an outward-pointing Lorentz or electric force which increases their pitch angle.

4.3.4 Proton-Driven Solar Wind

Investigations with the UltraViolet Coronal Spectrometer (UVCS) on SOHO have revolutionized our understanding of the acceleration of the solar wind. Fig. 4.17 shows a compilation of various studies with UVCS. These observations can not be understood without a massive heating by waves or turbulence.

4.3.5 Wave-Driven Solar Wind

We have already seen in chapter 2 that particles can interact with waves and can be heated/accelerated by them. Given the dynamic nature of the corona, one can easily imagine ways to tap into this energy reservoir to heat the corona and accelerate the solar wind.

Let us consider a coronal wave field which consists of many waves (*Aschwanden*, 2005). Each of them can be described by a wave vector $\vec{k}$ and has an energy $\hbar\omega$. The number of waves or wave packets in a given energy range, $W(\vec{k})/\hbar\omega$, is given by $N(\vec{k}, t)$. This is also called the occupation number of photons in the energy range $W(\vec{k})$ in $\vec{k}$ space. Its evolution with time will be given by an equation of the following form

$$\frac{\partial N(\vec{k},t)}{\partial t} + \vec{v}_g(\vec{k})\frac{\partial N(\vec{k},t)}{\partial \vec{r}} = \Gamma\left(\vec{k}, f(\vec{p})\right) N(\vec{k}) - \Gamma_{\rm coll}(\vec{k}) N(\vec{k}), \qquad (4.14)$$

where $\vec{v}_g = \partial\omega(\vec{k})/\partial\vec{k}$ is the group velocity. The left-hand side of eq. 4.14 is easily recognized as a continuity equation for the occupation number, $N(\vec{k})$. If it were conserved, the right-hand side would have to vanish and we would recover a 'normal' continuity equation. However, wave occupation number is not conserved, it can grow or it can decrease. The growth rate is given by $\Gamma\left(\vec{k}, f(\vec{p})\right)$ and is determined by many (often non-linear) processes. For instance, waves may be generated by footpoint motions in the photosphere which excite the field lines which thread through the corona. These modes

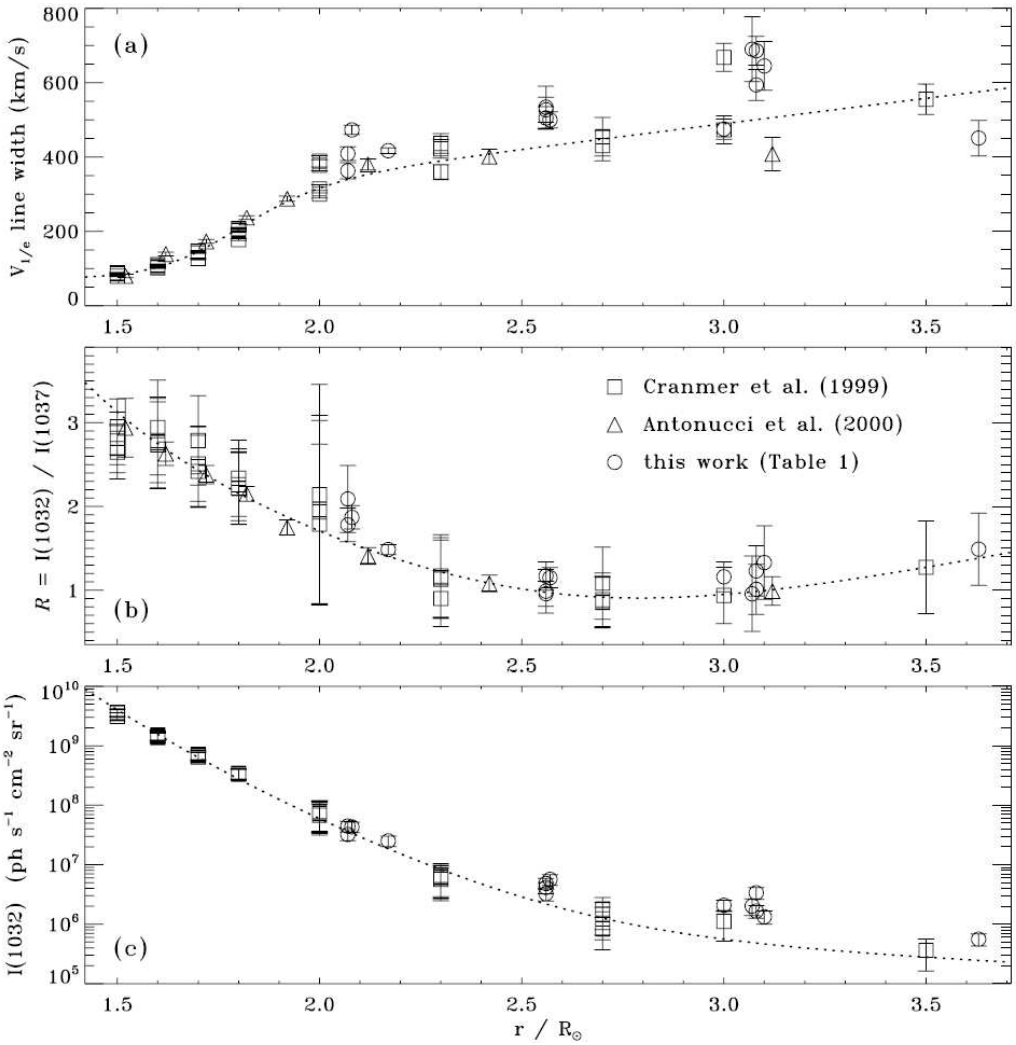

Figure 4.17: Collected UVCS polar coronal hole measurements of (a) O VI line widths $V_{1/e}$, (b) ratio of O VI λ1032Åto O VI λ1037Åintensities, and (c) O VI λ1032Ålineintegrated intensities, with symbols specifying the sources of the data (see labels for references). Error bars denote $\pm\sigma$ observational uncertainties. Also shown are the parameterized fits given by *Cranmer et al.* (1999) (dotted lines). From *Cranmer et al.* (2008).

can then cascade to higher wave numbers through a process called turbulent cascade which is described in more detail in chapter 7. This growth rate is multiplied with the occupation number, in other words, the source of waves is proportional to the growth rate and the already existing occupation number. Waves can also be 'lost' and this is described by the sink term, $\Gamma_{\rm coll}(\vec{k})N(\vec{k})$, where $\Gamma_{\rm coll}(\vec{k})$ is the wave damping rate due to cillisions.

But there is a quantity in this equation which is still undetermined, $f(\vec{p})$. That is the particle momentum distribution function or phase space density, i.e., the number of particles in a given volume of phase space, $(\vec{r},\vec{k})$. It too is goverened by a similar equation,

$$\frac{\partial f(\vec{p})}{\partial t}+\vec{v}(\vec{p})\frac{\partial f(\vec{p})}{\partial r} = \frac{\partial}{\partial p_j}\left\{\mathbf{D}_{ij}\left(N(\vec{k})\right)\frac{\partial f(\vec{p})}{\partial p_i}\right\}+\left(\frac{\partial f(\vec{p})}{\partial t}\right)_{\rm source}+\left(\frac{\partial f(\vec{p})}{\partial t}\right)_{\rm loss}. \tag{4.15}$$

Again the left-hand side looks like a continuity equation and the right-hand side gives sources and sinks. The first term on the right-hand side in curly braces cntains the diffusion tensor, $\mathbf{D}_{ij}\left(N(\vec{k})\right)$, which depends on the occupation number of waves in energy range $W(\vec{k})$. The two other terms are source and loss terms out of a given volume in phase space.

The two equations, eq. 4.14 and eq. 4.15 are coupled to each other via $f(\vec{p})$ in eq. 4.14 and $\mathbf{D}_{ij}\left(N(\vec{k})\right)$ in eq. 4.15. This system of partial differential equations needs to be solved self-consistently so that the particle phase space density can influence the wave spectrum and vice versa. Obviously, this is non-trivial, however, first such models have been developed and applied to the heating and acceleration of the solar wind.

It does not end here, however. The solar wind is described by the equations of mass, momentum, and energy conservation along its motion through the corona These equations can be expressed as moments of the Boltzmann equation (basically, eq. 4.15, but augmented with a force term). Appendix A4 of my lecture notes 'Physik VI - Teil II' goes through the detailed derivation. As you may recall, some kind of closure relation needs to be used to end the otherwise infinite set of equations.

Thus, a full, self-consistent model for the acceleration of the solar wind needs to incorporate all of the above equations. *Cranmer et al.* (2007) have developed such a model in one dimension and in steady state. They compute the properties of the plasma along a one-dimensional magnetic flux tube and the evolution of accoustic and Afvén waves from the photosphere through the chromosphere and corona into the heliosphere. It is driven by an empirically derived spectrum of accoustic waves which drive shocks heating the chromosphere and transition regions. It includes heating by Alfvén waves which are partially reflected at some coronal boundary and the are dissipated by a MHD turbulent cascade. Finally, acceleration of the solar wind by gradients of gas pressure, accoustic wave pressure, and Alfvén-wave pressure is calculatated.

4.3.6 Superradial Expansion

Figure 4.18 shows the superradial expansion of two model coronal holes. The high pressure in the coronal holes compared to that in the streamer belt deflects the magnetic field lines equatorwards, resulting in this superradial expansion (i.e., the field strength decreases faster than $1/r^2$. This also leads to a density profile similar to the one given in eq. 4.1. The superradial expansion is often fitted by the following function

$$f(r) = 1 + (f_{max} - 1) \left\{ \frac{1 - \exp[(R_\odot - r)/\sigma_1]}{1 + \exp[(R_1 - r)/\sigma_1]} \right\}, \tag{4.16}$$

where f_{max} and R_1 are empirical numbers. *Cranmer et al.* (2008) quote values of $f_{max} = 6.5$ and $R_1 = 1.5R_\odot$.

4.3.7 Outflow speeds from coronal holes

4.4 Mircroscopic Source of the Solar Wind

The measurements shown in Fig. 4.20 indicate a highly structured plasma flow in the corona which also results in highly sheared flows. Nevertheless, the flow pattern is quasi steady, possibly signifying large-scale circulation in the corona.

4.5 Composition of the Solar Wind

4.5.1 Overview and Basic Assumptions

- **Stratification.** The idea that the solar corona may be gravitationally stratified, i. e. that the He/H ratio decreases with increasing height in the solar atmosphere, allows an interpretation of the observed low helium to hydrogen ratio in wind from coronal streamers *Borrini et al.* (1981); *Gosling et al.* (1981) and the constant higher ratio in fast streams from coronal holes *Bame et al.* (1977). This may signify that the slow wind from coronal streamers originates in very high layers of the corona *Borrini et al.* (1981); *Gosling et al.* (1981); *Feldman et al.* (1981), while fast streams stem from lower layers *Bame et al.* (1977). If this idea is correct, we should observe *less* heavy ions in wind from streamers than in the surrounding solar wind and in fast streams.

- **Frictional coupling** Theoretical studies of the conditions for acceleration of heavy ions out of the solar atmosphere **?***Bürgi* and *Geiss* (1986) reveal the importance of "Coulomb friction". The heavier ions are "pulled" out of the solar atmosphere by the lighter electron-proton plasma. In this concept He is at a disadvantage with respect to the heavy

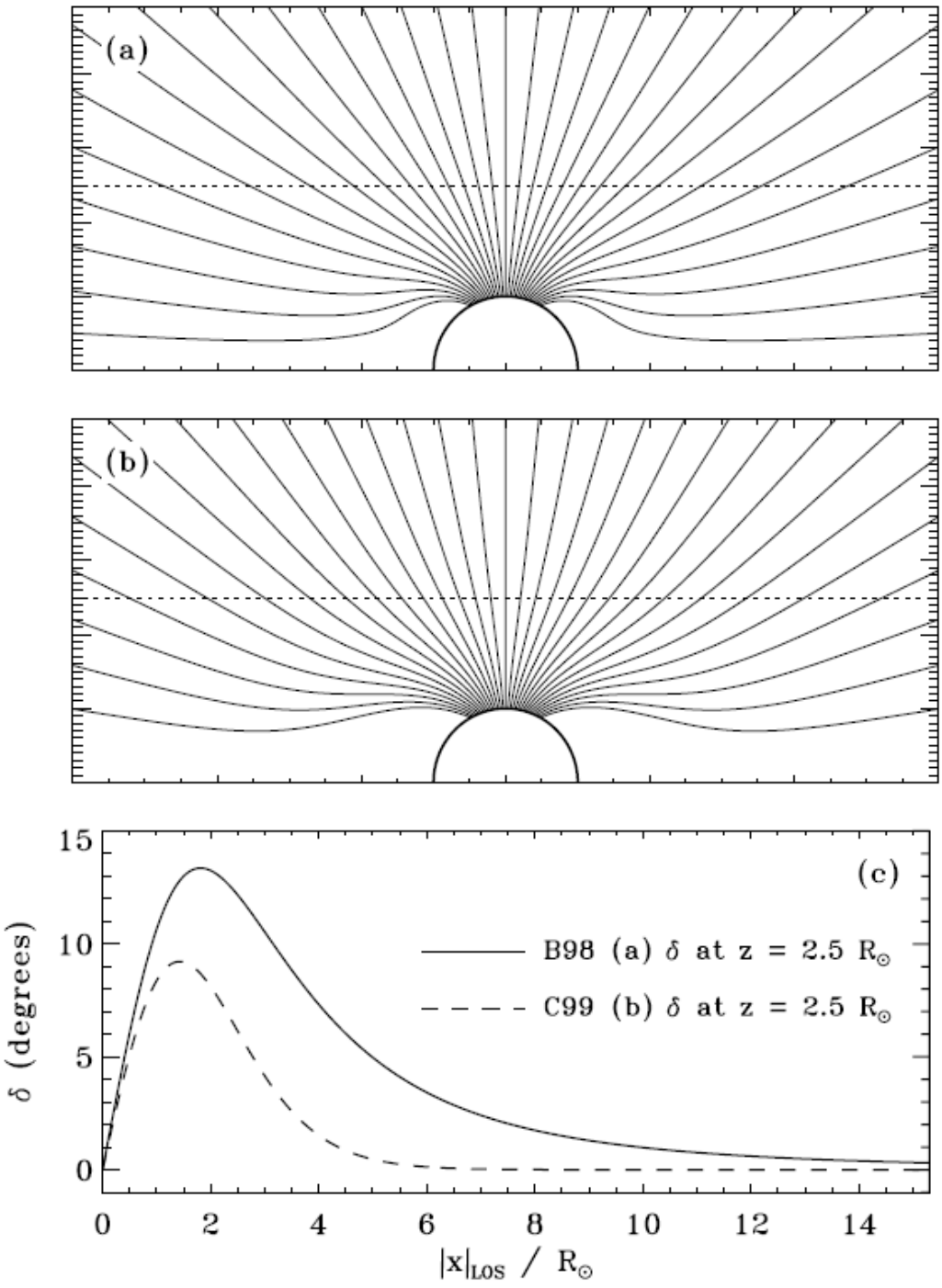

Figure 4.18: Magnetic field lines in the plane of the sky for (a) the B98 (Banaszkiewicz et al. 1998) model, and (b) the C99 (Cranmer et al. 1999) model that used the Kopp & Holzer (1976) flux-tube area function. The dotted horizontal line denotes the position of the LOS along which various quantities are plotted in (c). In (c), the superradial angle δ is given as a function of $|x|$ (it is the same in the foreground and background halves of the LOS) for the two models shown above (see labels). From *Cranmer et al.* (2008).

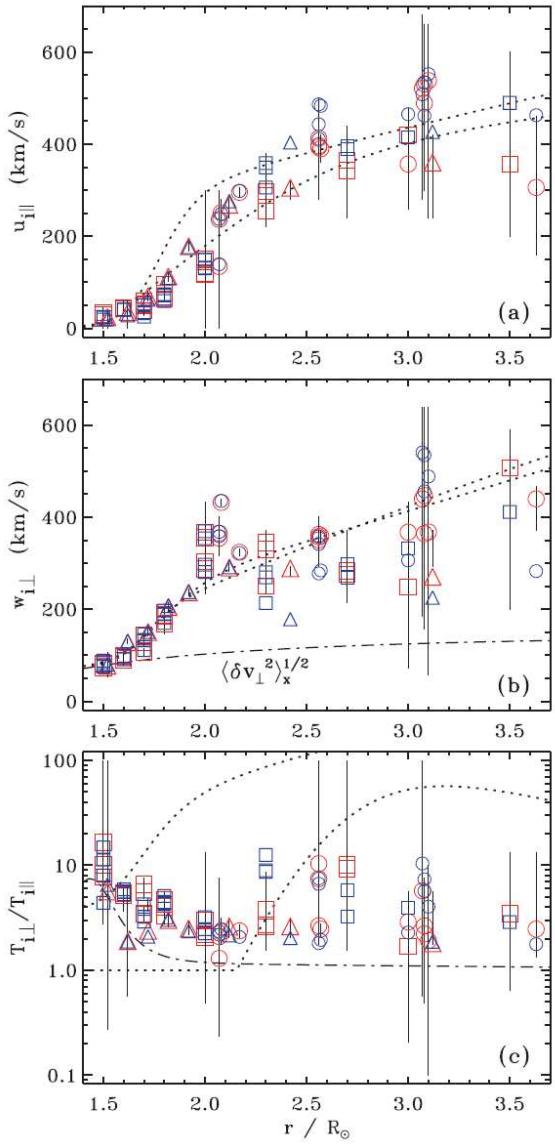

Figure 4.19: (a) Derived outflow speeds, (b) perpendicular most probable speeds, and (c) kinetic anisotropy ratios for model R (red points) and model C (blue points). Symbols show the weighted means of the reduced probability distributions, with styles the same as in Fig. 1. Vertical bars show the full range of parameter space with reduced probabilities greater than $P_{1\sigma}$ (for model R). Also shown are empirical models B1 and B2 from *Cranmer et al.* (1999) (dotted lines) andAlfvén wave quantities $\langle \delta v_\perp^2 \rangle^{1/2}$ in (b) and A_{eff} in (c), derived from the model of Cranmer et al. (2007) (dot-dashed lines). From *Cranmer et al.* (2008).

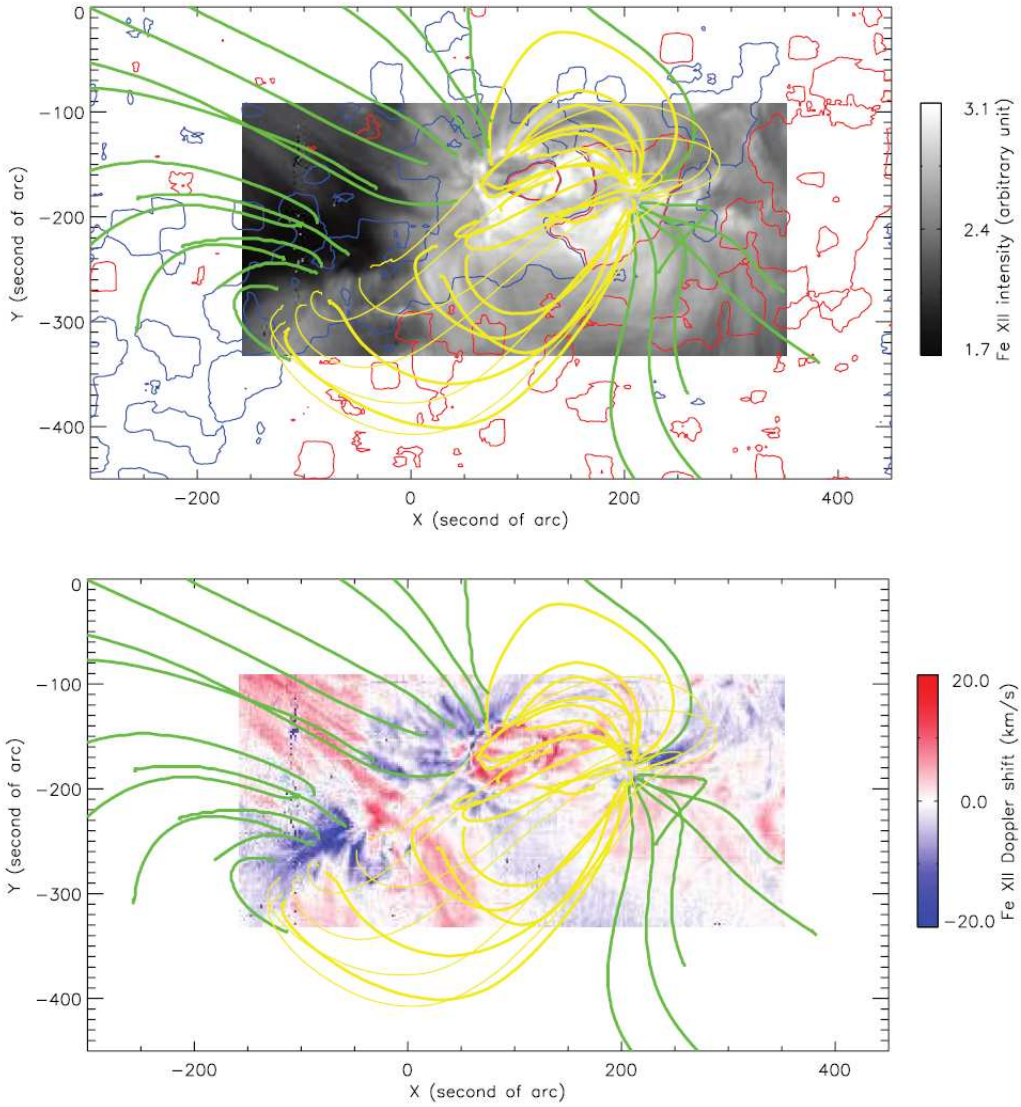

Figure 4.20: Green and yellow lines show open and closed magnetic fields, respectively. Top panel: red and blue contours show regions of opposite magnetic polarity, grey shades show Fe XII radiance in arbitrary units. Bottom panel: red and blue color shades show Doppler shift of the corresponding Fe XII line. Field lines start and end in regions of predominantly red or blue shift, i.e., the footpoints of magnetic field lines are asociated with either up or downflows. From *Marsch et al.* (2008).

ions inasmuch as these will always be accelerated out as long as He is, but not vice versa. One may determine minimum flux factors (minimum proton flux) which need to be satisfied for all ions heavier than hydrogen to be pulled out of the solar gravitational field **?**. This mechanism again might explain the observed low α/p ratios observed in wind from coronal streamers *Borrini et al.* (1981); *Gosling et al.* (1981); *Feldman et al.* (1981). If this is the correct explanation, then we expect to observe a lower He/O ratio, i. e. *more* heavy ions, in wind from streamers than in the ambient solar wind or fast streams.

- **The FIP effect** A comparison of the abundances of elements in the solar wind or in olar energetic particles (SEPs) with their photospheric abundances shows a remarkable pattern (**?**). Elements with low first ionization potential (FIP) appear to be enriched with respect to elements with a high FIP. Often, elemental abundances are compared to that of oxygen as a normalization. The ratio $[X/O]/[X/O]_{\rm photo}$ where X/O is the abundance of an element relative to that of O is often used as an indicator of the strength of this FIP effect. It differs for fast and slow wind, the FIP effet is stronger in the slow wind than in the fast wind. There is considerable discussion about the ordering quantity. Is it FIP or the first ionization time (FIT)? The latter would be physically more intuitive, however, it is not an atomic quantity, but depends on conditions in corona and chromosphere. Thereore, FIP is normally used, but with the understanding that FIT may be the physically relevant parameter. The FIP effect is also observed in coronae of other stars (*Brinkman et al.*, 2001; *Drake et al.*, 2001). On some occasions it appears to *deplete* low-FIP elements (*Audard et al.*, 2003), a feature which is not explained by most models for the FIP effect. One exception is that by *Laming* (2004) which builds on the ponderomotive force acting on ions when they are heated by a turbulent wave field. This field is a result of the turbulent cascade which sets in when upward propagating waves are reflected at the chromosphere-corona interface and ineract with the upward propagating waves. The strength of the FIP effect is determined by the wave power only. This model is especially promising because it closely resembles the wave-driven models for the solar wind acceleration (see section 4.3.5) and could probably be included in such in a self-consistent manner. The cause of the FIP fractionation of galactic cosmic rays (GCR) could lie in a similar effect for stellar winds or in a volatile - condensible fractionation into dust grains which are then accelerated, see *Klecker et al.* (2001) and references therein for a review of GCR abundances.

While several other processes are of importance for acceleration and heating in the solar atmosphere, it is the two processes mentioned above, together with the FIP effect (First Ionization Potential), that we believe are responsible

for the separation of different elements. While the physics of the FIP fractionation process have been well studied **?***Vauclair* and *Meyer* (1985); **?**, and abundant experimental evidence has been found *Hovestadt et al.* (1973); **?**); *Cook et al.* (1984); *Geiss* and *Bochsler* (1985); *Breneman* and *Stone* (1985), the relative importance of stratification and friction has not yet been established experimentally. Earlier studies revealing significantly lower α/p ratios in wind from coronal streamers *Borrini et al.* (1981); *Gosling et al.* (1981); *Feldman et al.* (1981) could not distinguish between the two processes. The importance of the FIP effect has not been investigated for coronal streamers as such *Meyer* (1993),

4.5.2 Inefficient Coulomb Drag

Describe in more detail, use **?**.

4.5.3 The FIP Effect

Use *Hénoux* (1998) and *Laming* (2004)
Describe in more detail

4.5.4 Gravitational Settling

Describe in more detail

Chapter 5

Dust in the Solar System

Apart from photons, magnetic field, ions, and electrons, dust particles of all sizes also contribute to the interplanetary medium. They originate from asteroids, comets, and interstellar space. First hints at their existence can be found in reports by Cassini (1683 and 1693!) about his observations of the zodiacal light. His pupil, Noccolo Fatio de Duiliiers, gave the first correct interpretation of these observations in 1684.

Unfortunately, observations of the zodiacal light are rare in our modern ages because of the increasing amount of light pollution. Zodiacal light is invisible from the vicinity of large agglomerations because scattered light from them is more intense than the faint zodiacal light. From a modern point of view, the first observations of zodiacal lights from the vicinity of Paris and Geneva seem all the more remarkable. Additional historical accounts can be found in *Fechtig et al.* (2001).

Today we interpret the light from the F-corona as photospheric light which is reflected towards the observer by interplanetary dust particles (IDPs, cf. Fig. 5.1 which shows a photograph of an IDP). The light scattered at IDPs is mainly unpolarised (only 17% - 19%, *Fechtig et al.* (2001)) and the photospheric Fraunhofer lines are well visible in the spectrum of the F corona because of the slow stochastic motions (and resulting low speeds) of IDPs.

5.1 The Motion of a Particle in a Central Potential

In preparation of the following sections, we collect the relevant concepts to describe the motion of a particle in a central potantial, e.g., a gravitational potential, as is the case for dust particles in the gravitational well of the Sun. We closely follow *Landau* and *Lifschitz* (1981), vol. I. Given a central potential $U(r)$ which depends only on the distance from the origin (heliocentric distance

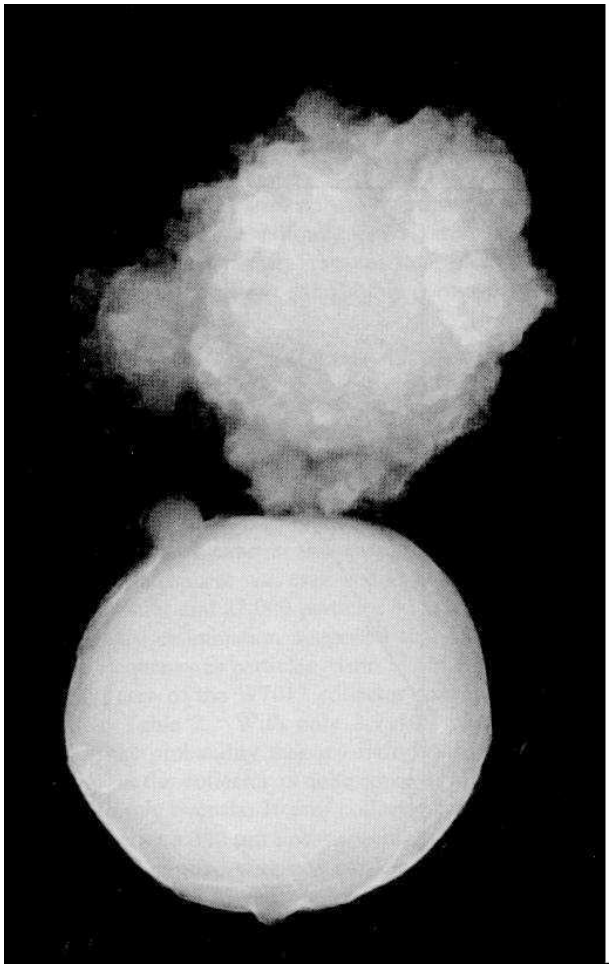

Figure 5.1: Interplanetary dust particles. Photo courtesy Max-Planck-Institute for nuclear physics, Heidelberg.

in our case), the force acting on a particle is given by

$$\vec{F} = -\frac{-\partial U(r)}{\partial \vec{r}} = -\frac{\mathrm{d}U}{\mathrm{d}r}\frac{\vec{r}}{r} \tag{5.1}$$

and also only depends on r and points along $\vec{r}$ (or antiparallel to $\vec{r}$). The angular momentum,

$$\vec{L} = \vec{r} \times \vec{p} \tag{5.2}$$

is a conserved quantity. Obviously, this conservation also means that the motion of the particle is constrained to a plane perpendicular to the angular momentum direction. Therefore, this motion can be described by two coordinates only, a radial distance from the origin of the central force, r, and the angle φ which describes the particles motion in polar coordinates. We will always keep distinct the vectorial quantity angular momentum, $\vec{L}$ and the scalar

Lagrangian, L,

$$L = \frac{m}{2}\left((\dot{r})^2 + r^2\dot{\varphi}^2\right) - U(r). \tag{5.3}$$

The conservation of angular momentum can easily be seen as a consequence of the Lagrange equation,

$$\frac{\mathrm{d}}{\mathrm{d}t}\frac{\partial L}{\partial \dot{q}_i} = \frac{\partial L}{\partial q_i} = 0. \tag{5.4}$$

This shows that the generalized momentum, $p_i = (\partial L)/(\partial \dot{q}_i)$, is a conserved quantity in the system described by this Lagrangian. In our case, the generalized momentum is just angular momentum,

$$p_\varphi = mr^2\dot{\varphi} = \vec{L}|z = |\vec{L}|. \tag{5.5}$$

It is easiest to solve the problem of the motion in a central field by now considering the conservation laws for energy and angular momentum. The energy of the particle is given by

$$E = E_{\mathrm{kin}} + E_{\mathrm{pot}} = \frac{m}{2}v^2 + U(r) = \frac{m}{2}\left((\dot{r})^2 + r^2\dot{\varphi}^2\right) + U(r) = \frac{m\dot{r}^2}{2} + \frac{\vec{L}^2}{2mr^2} + U(r). \tag{5.6}$$

This can easily be solved for $\dot{r}$,

$$\dot{r} = \frac{\mathrm{d}r}{\mathrm{d}t} = \sqrt{\frac{2}{m}\left\{E - U(r)\right\} - \frac{\vec{L}^2}{m^2r^2}}. \tag{5.7}$$

This in turn can be integrated to obtain t,

$$t = \int \frac{\mathrm{d}r}{\sqrt{\frac{2}{m}\left\{E - U(r)\right\} - \frac{\vec{L}^2}{m^2r^2}}} + \text{const.} \tag{5.8}$$

Using eq. 5.5 to write

$$\mathrm{d}\varphi = \frac{|\vec{L}|}{mr^2}\mathrm{d}t$$

and expressing $\mathrm{d}t$ by this expression in eq. 5.7, we obtain the equation which describes the φ coordinate,

$$\varphi = \int \frac{\frac{|\vec{L}|}{r^2}\mathrm{d}r}{\sqrt{2m\left\{E - U(r)\right\} - \frac{\vec{L}^2}{r^2}}} + \text{const.} \tag{5.9}$$

Equations 5.8 and 5.9 are the general solution of the problem. The second equation describes the orbit of the particle, the first is an implicit equation for the temporal evolution.

5.1.1 The Kepler Problem

We can now insert an appropriate expression for $U(r)$ to obtain the equations for a particles motion in the solar system (in the central potential of the Sun, neglecting the effects of planets and three-body collisions). In this case,

$$U(r) = -\frac{GM}{r}, \tag{5.10}$$

where $G = 6.67408(31) \times 10^{11}\mathrm{m}^3\mathrm{kg}^1\mathrm{s}^2$ is the gravitational constant and $M = (1.988550.00025) \times 10^{30}$ kg is the solar mass. Eq. 5.3 tells us that we can describe the radial motion of the particle as a motion in an effective potential,

$$U_{\mathrm{eff}} = U(r) + \frac{|\vec{L}|^2}{2mr^2}. \tag{5.11}$$

The second term is called the centrifugal potential. The values of r at which

$$U(r) + \frac{|\vec{L}|^2}{2mr^2} = E$$

determine the limits of the radial motion. That is the distances, r, at which $\dot{r} = 0$. Note that this does not mean that the particle no longer moves. At these locations, the azimuthal velocity component $r\dot{\varphi}$ is generally non-zero.

It is clear that the effective potential goes to infinity for very small heliocentric distances, has a global minimum

$$U_{\mathrm{eff}}|_{\mathrm{min}} = -\frac{G^2M^2m}{2|\vec{L}|^2} \quad \text{at} \quad r = \frac{|\vec{L}|^2}{GMm}.$$

for larger heliocentric distances, the effective potential approaches zero again from negative values. This shows that orbits with negative energy, E, are necessarily bound, and orbits with positive energy are unbound.

We obtain the shape of the orbit by inserting $U = -GM/r$ into eq. 5.9. Integration yields

$$\varphi = \arccos \frac{\frac{|\vec{L}|}{r} - \frac{mGM}{|\vec{L}|}}{\sqrt{2mE + \frac{G^2M^2m^2}{|\vec{L}|^2}}} + \mathrm{const.} \tag{5.12}$$

The integration constant is determined by the choice of the reference direction for the angle φ which we choose such that is vanishes. Introducing the quantities

$$p \doteq \frac{|\vec{L}|^2}{gMm} \quad \text{and} \quad e = \sqrt{1 + \frac{2E|\vec{L}|^2}{mG^2M^2}} \tag{5.13}$$

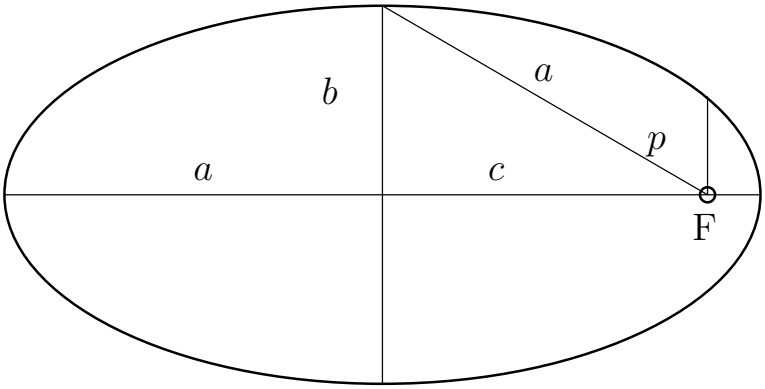

Figure 5.2: An ellipse and its relevant quantities.

we can simplify eq. 5.12 considerably and obtain the equation for the orbit of the particle,

$$\frac{p}{r} = 1 + e\cos\varphi, \tag{5.14}$$

where p is the so-called parameter (not the impact parameter), and e is the eccentricity of the orbit. In the coordinate system chosen here (by the choice of setting the integration constant to zero), $\varphi = 0$ at the perihelion, i.e., where the particle is closest to the Sun. Note that this equation (eq. 5.16) can also be obtained simply by simplifying eq. 5.12 and then inserting the definitions eq. 5.13 which are motivated below.

It is obvious from the definition of eccentricity above (eq. 5.13) that for $E < 0$ $e < 1$, i.e., the orbit is elliptical. For $E > 0$ $e > 1$, in other words, unbound orbits are hyperbolae.

For an ellipse, as shown in Fig. 5.2 we have from analytical geometry that the linear eccentricity, c, is

$$c^2 = a^2 - b^2$$

where a and b are the semi-major and semi-minor axes, respectively. Eccentricity, e, is then $e = c/a$, and the paramter is $p = b^2/a$.

With these definitions we find

$$\begin{aligned} c^2 &= a^2 - b^2, \\ b^2 &= a^2 - c^2 = a^2 - \frac{c^2 a^2}{a^2} = a^2 \cdot (1 - e^2), \\ p &= \frac{b^2}{a} = a(1 - e^2), \\ a &= \frac{p}{1 - e^2}, \\ b &= a\sqrt{1 - e^2} = \frac{p}{\sqrt{1 - e^2}}, \\ a &= \frac{p}{1 - e^2} = \frac{|\vec{L}|^2}{GMm} \frac{1}{1 - 1 + \frac{2E|\vec{L}|^2}{G^2 M^2 m}}, \\ &= \frac{|\vec{L}|^2}{GMm} \frac{G^2 M^2 m}{2E|\vec{L}|^2} = \frac{GM}{2E}. \end{aligned} \tag{5.15}$$

The aphelion and perihelion can be determined by setting the effective potential equal to the energy of the orbit,

$$\begin{aligned} U_{\text{eff}} &= -\frac{GM}{r} + \frac{|\vec{L}|^2}{2mr^2} = E, \\ 0 &= Er^2 + GMr - \frac{|\vec{L}|^2}{2m}, \\ r_{\text{min,max}} &= \frac{-GM \pm \sqrt{G^2 M^2 + \frac{4E|\vec{L}|^2}{2m}}}{2E}, \\ r_{\text{min,max}} &= \frac{-GM \pm GMe}{2E} = a \pm ae, \end{aligned} \tag{5.16}$$

where we have used that the semi-major axis $a = |\frac{GM}{2E}|$, as shown in eqs. 5.15.

5.2 Sources of Dust

5.2.1 Asteroids and Comets

Small dust particles with sizes on the order of the wavelength of light experience another force apart from gravitation.The IDP feels the the pressure exerted by the incoming light which results in a reduction of the "felt" central force, gravitation.

$$G\,M \longrightarrow (1 - \beta) G\,M.$$

The pressure force exerted by light on an unmoving particle is given by

$$F_r = \frac{S\,A}{c}, \tag{5.17}$$

where $S = (1/\mu_0)\vec{E} \times \vec{B}$ is the Poynting flux, A the cross section (roughly the cross sectional area), and c the speed of light.

Exercise 5.1 *Check the units in eq. 5.17!*

If a meteor hits an asteroid and produces fine-grained dust which may escape the weak gravitational potential of the asteroid, or if a dust particle leaves a comet, it will have roughly the same velocity as its parent body up to some ejection or thermal velocity (which is normally small compared to the orbital velocity of asteroids and comets), but will experience a reduced gravitation which will lead to a change in its orbit. Depending on the eccentricity of the orbit of the parent body, this may force the dust particle onto an unbound hyperbolic orbit and it will leave the solar system.

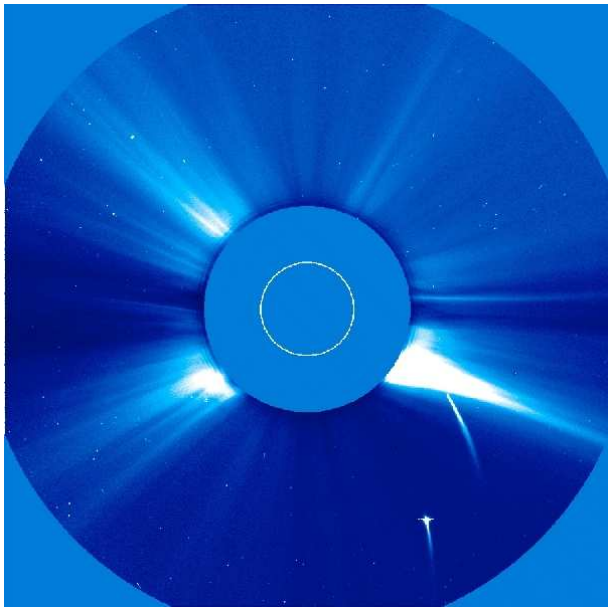

Figure 5.3: Two sungrazing comets heading towards the Sun. They disappear before exiting from the other side, indicating that they evaporate in the solar corona. From `http://sohowww.nascom.nasa.gov/`.)

Let us consider the extreme case of a dust particle leaving one of the countless SOHO-comets near perihelion. Two examples are shown in Fig. 5.3 (from `http://sohowww.nascom.nasa.gov/`). These comets fly on highly eccentric orbits and come very close to the Sun where most of them evaporate. In nearly all of those cases the escaping dust particle will leave the solar system. Its orbit can be parametrised by the angle ϕ

$$R = \frac{a(1-e)}{1+e\,\cos\phi}. \qquad (5.18)$$

For an elliptic (or parabolic) orbit we have

$$v^2(R_p) = \frac{G\,M}{a}\frac{1-e}{1+e}, \qquad (5.19)$$

which is now changed because of $\beta \neq 0$

$$\begin{aligned} \frac{v^2}{2} - (1-\beta)\frac{G\,M}{R} &= \frac{E}{m}, \\ \frac{G\,M}{2\,a}\frac{1+e}{1-e} - (1-\beta)\frac{G\,M}{a(1-e)}\,(1+e\,\cos\phi) &= \frac{E}{m}, \\ \frac{1+e}{2} - (1-\beta)\,(1+e\,\cos\phi) &= \frac{E/m}{G\,M}a(1-e). \end{aligned} \qquad (5.20)$$

For a bound orbit the orbital energy E/m needs to be negative, which gives an upper limit on β,

$$\begin{aligned} \frac{1+e}{2} - (1-\beta)(1+e\,\cos\phi) &\leq 0 \\ \frac{e-1}{2} + \beta\,(1+e\,\cos\phi) - e\,\cos\phi &\leq 0 \\ \beta &\leq \left(\frac{1-e}{2} + e\,\cos\phi\right)(1+e\,\cos\phi)^{-1} \end{aligned} \tag{5.21}$$

The orbits of SOHO comets are highly elliptic, $e \approx 1$ and hence nearly all emitted dust particles are unbound. Other parent bodies have different eccentricities and, hence, the dust particles emitted by them will also have different orbital properties. Figure 5.4 shows the values of β for which particles remain on stable orbits in dependence of their initial eccentricity and for the orbital angle ϕ at which they left their parent body.

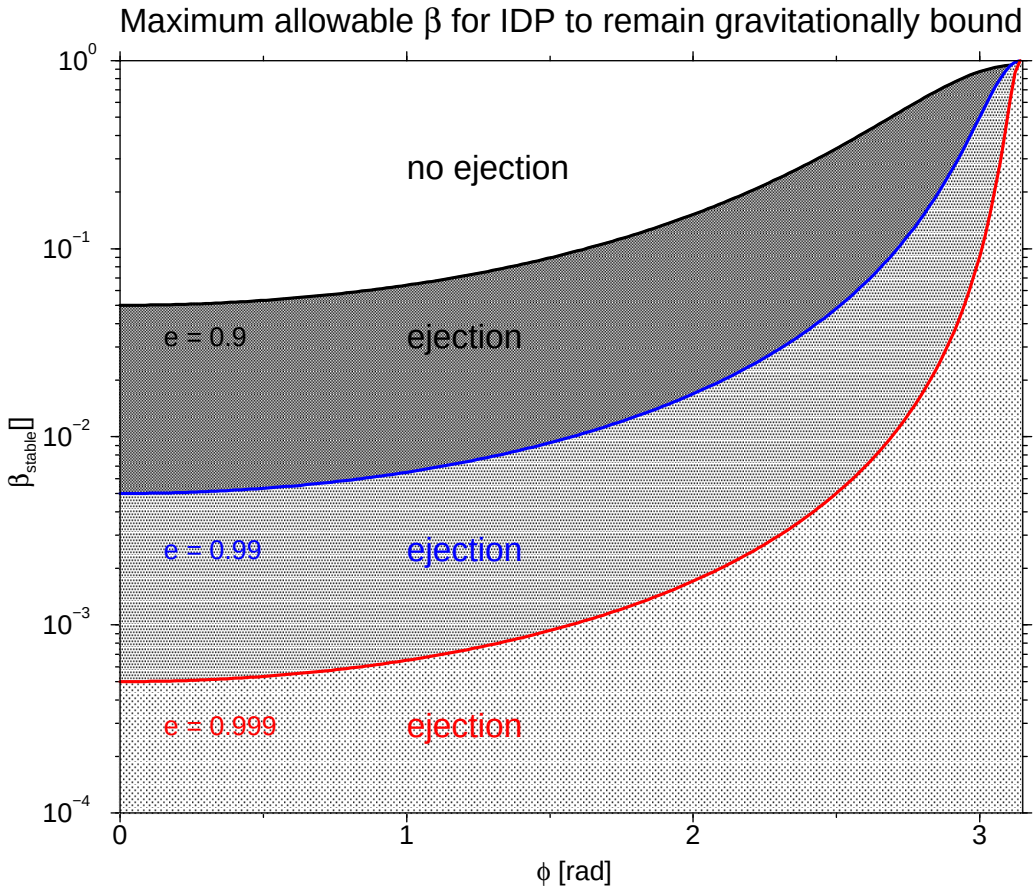

Figure 5.4: Maximum values for β for a particle to remain on a stable bound orbit if it leaves the parent body at orbital angle ϕ.

5.2.2 Interstellar Dust

The interstellar medium contains dust and gas in various proportions which is often given as the so-called gas to dust mass ratio, $R_{\rm g/d}$, which gives the ratio of mass in the gas phase to the mass locked up in dust. First indications of dust in the interstellar medium came from the absorption and reddening of light from cepheids which originally had led to large corrections in the size of the known universe. After Eddington had explained the basic structure of interstellar absorption lines, it was Trümpler in 1930 who explained interstellar absorption and reddening as a consequence of dust in the interstellar medium. Dust grains absorb light from stars which are at high temperatures and emit it at a much lower temperature, thus leading to absorbtion and reddening.

The local interstellar cloud also contains dust and the curently best estimates for $R_{\rm g/d} = 149 - 217$ assuming solar abundances (*Slavin* and *Frisch*, 2008). This ratio is obtained using the "missing mass" hypothesis in which one assumes that the elements not visible in absorption spectra against nearby stars must be in grains. This is the case for most refractory (non-volatile) elements. These calculations take into account the line spectra of nearby stars, of the warm inerstellar gas and from the cloud wall.

Interestingly, in-situ measurements with the Ulysses and other dust and gas detectors give the interstellar $R_{\rm g/d} = 116 - 127$ (*Ref missing!*). This value is an upper limit, as the smallest dust particles do not enter the solar system because of photon pressure and particle charging (see below). This discrepancy is not understood.

Interstellar dust that enters the solar system is or was measured with the dust detector on Ulysses, Cassini, Galileo, and Helios between 0.3 AU and 5 AU. Measured radii of these particles range from 0.05 μm to above 1 μm. Measurements show that grains of different sizes show different dynamic properties as a consequence of gravitational focussing, solar radiation pressure, and electromagnetic interaction with the time-varying interplanetary magnetc field.

Interstellar dust enters the heliosphere from the same direction as interstellar neutral atoms - or so it was believed based on measurements with Ulysses and other spaceraft up to a few years ago. Recent measurements reported by *Krüger et al.* (2007) show that this is not anymore the case in the past few years. A systematic shift in direction appears to have taken place which is not understood. Is it due to effects in the heliosheath, in the LIC or inside the heliosphere? Fig. 5.6 shows the situation.

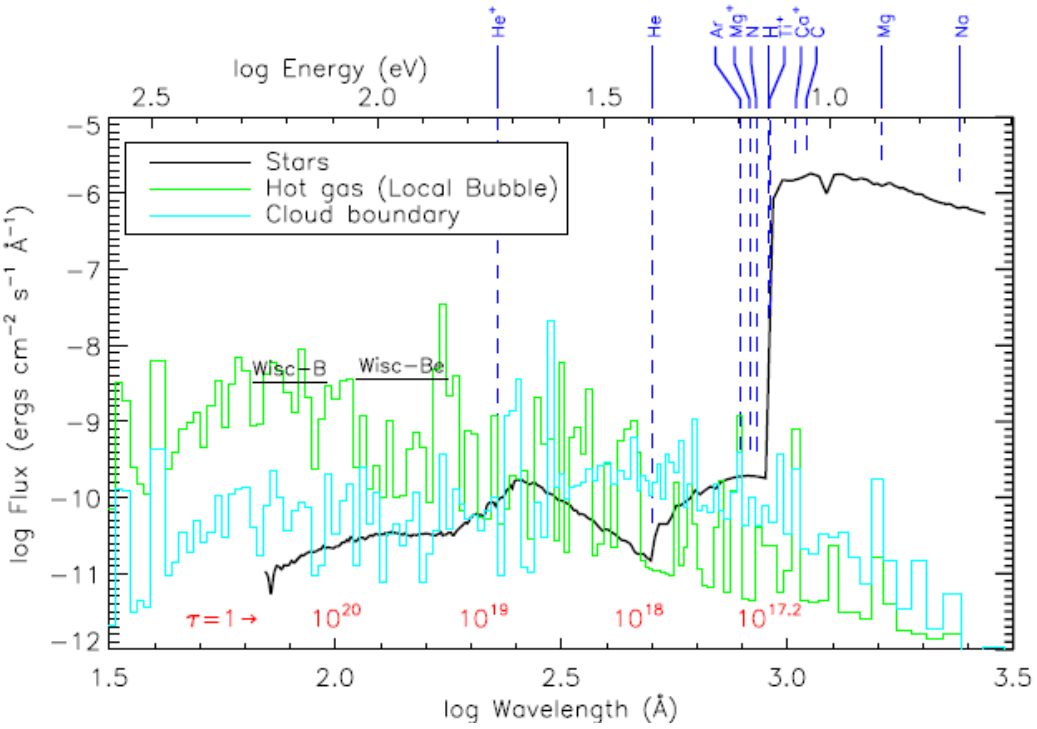

Figure 5.5: Background interstellar radiation field responsible for ionizing the LIC. The black line is the FUV/EUV flux from stars, the green line is a model spectrum for the diffuse emission from hot gas and the cyan line is the modeled emission from the evaporative boundary of the cloud. The ionization edges for several important ions are shown in dark blue. The wavelength at which the cloud is optically thick for several different column densities is indicated in red. From *Slavin* and *Frisch* (2008).

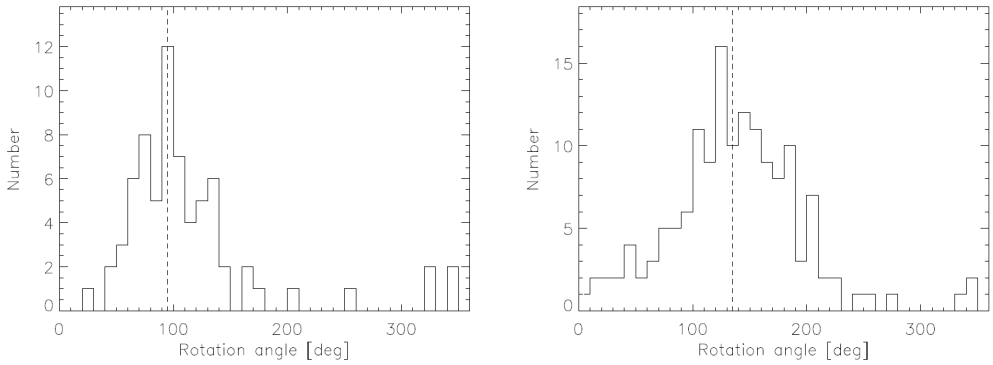

Figure 5.6: Distribution of measured impact directions (i.e. spacecraft rotation angle at dust particle impact) of interstellar impactors for two time intervals. Left: 1 January 1997 to 31 December 1999; right: 1 January 2003 to 31 December 2005. In the earlier time interval the maximum of the distribution is at a rotation angle of 95° very close to the value expected from the interstellar helium flow. In the second interval the maximum is at 135°. From *Krüger et al.* (2007).

5.3 Forces Acting on Dust Particles and Implications for Dust Dynamics

5.3.1 Gravitation

To first order, IDPs move on Keplerian orbits throughout the solar system. They can only change their orbits by collisions or three-body encounters. The energy of their orbit is given by

$$\frac{E}{m} = \frac{v^2}{2} - \frac{G\,M}{R} = \frac{G\,M}{2\,a - R_p}, \tag{5.22}$$

where a is the semi-major axis and $R_p = a(1-e)$ is the orbits perihelion.

Exercise 5.2 *Prove eq. 5.22.*

5.3.2 Mie-Scattering

As already mentioned in section 5.2.1, small IDPs experience a reduced gravitation because light pressure acts as an additional force. Here, we show how to calculate the scattering of light off small sperical particles by summarizing so-called Mie-scattering. We begin by approximating the incoming light waves by plane waves and then allowing them to scatter off a sphere of arbitrary size:

- Describe light as a plane wave

$$\vec{E} = \vec{E}_0 \exp(i\vec{k}\cdot\vec{x} - i\,\omega\,t),$$

and

$$\vec{B} = \vec{B}_0 \exp(i\vec{k} \cdot \vec{x} - i\,\omega\,t).$$

The wave vector $\vec{k}$ can be a complex quantity $\vec{k} = \vec{k}' + i\,\vec{k}''$.

- Because of $\vec{E} \perp \vec{B}$ we have $\vec{k} \cdot \vec{k} = \omega^2 \varepsilon \mu$.
- Properties of the material are all concealed in the index of refraction $N = n + i\,k = c\sqrt{\varepsilon\mu}$
- Expand the plane waves in spherical functions (because we are considering scattering by a sphere).
- This leads to some lengthy expressions which I do not reproduce here...
- These expressions then lead to the exact scattered and absorbed fields and the three cross sections $C_{\rm scat}$, $C_{\rm abs}$, and $C_{\rm ext}$.
- $Q_{\rm scat}$, $C_{\rm abs}$, and $Q_{\rm ext}$ give the efficiency of scattering and extinction, $Q = C/A$, where A is the geometric cross sectional area of the spherical IDP.
- The resulting expressions contain Bessel functions. Their recursion relations are then used to derive some remarkably simple recursion relations for $Q_{\rm scat}$, $Q_{\rm abs}$ und $Q_{\rm abs}$ which allow very efficient calculations of these quantities.

$Q_{\rm scat}(\lambda)$, $C_{\rm abs}(\lambda)$, and $Q_{\rm ext}(\lambda)$ can be calculated for a sphere of radius s in this fashion. *Bohren* and *Huffman* (1983) give an efficient algorithm as well as a FORTRAN code for the numerical computation of these cross-sections. Fig. 5.7 shows the behavior of $Q_{\rm scat}(\lambda)$ in a representation which also includes the size of the particles by choosing $2\pi s/\lambda$ as the independent variable, where λ is the wave length of the light wave considered.

5.3.3 Light Pressure

The pressure exerted by the light and experienced by the particle is composed of two parts, the absorbed light and the momentum transfer after the scattering of light. The expression for the light pressure cross section, $Q_{\rm pr}$, is then

$$Q_{\rm pr} \doteq Q_{\rm abs} + Q_{\rm scat}\,(1 - \langle\cos\theta\rangle)\,. \tag{5.23}$$

The parenthesis contains an expectation value for the cosine of the scattering angle which also needs to be obtained from Mie theory. Hower, we can also understand the expression without complicated calculations. If the body is a perfect absorber, it will not scatter any light at all, and so $Q_{\rm scat} = 0$. Therefore, $Q_{\rm pr} = Q_{\rm abs}$, a black body is a perfect "forward scatterer". If the body scatters isotropically, then the expectation value for the cosine vanishes and we have

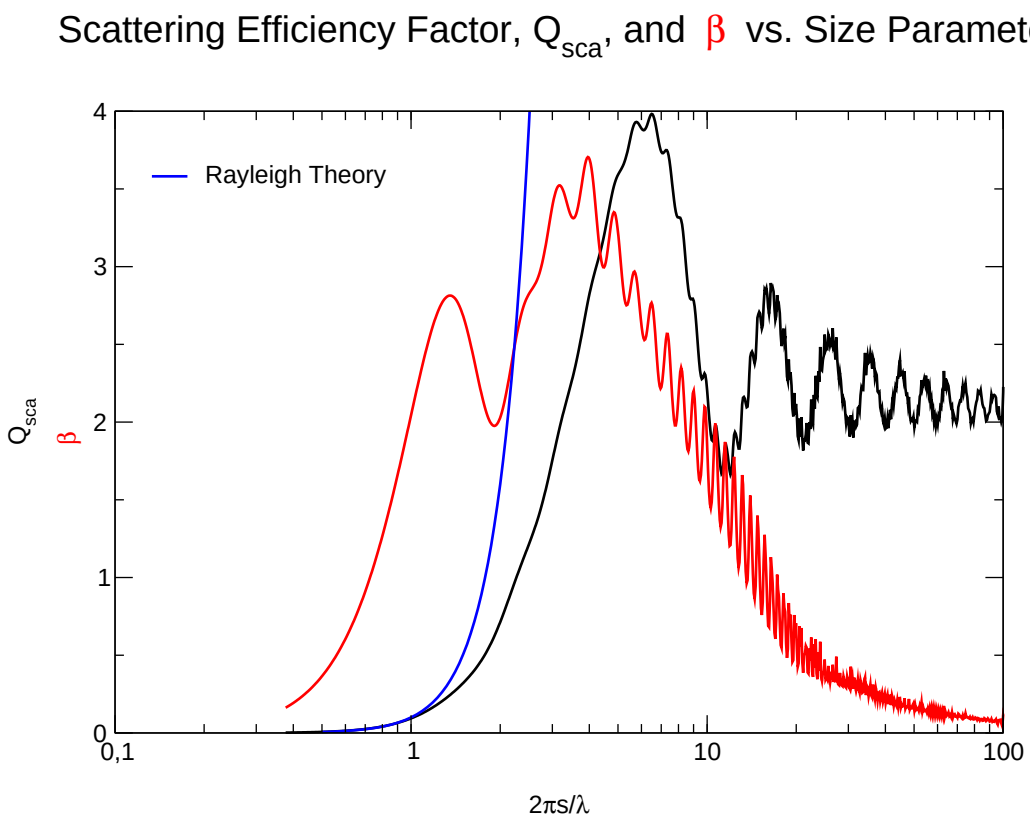

Figure 5.7: Scattering efficiency $Q_{\rm scat}(\lambda)$ for spheres with radius s.

$Q_{\rm pr} = Q_{\rm abs} + Q_{\rm scat}$. If the body scatters backwards, like a plane mirror, and does so perfectly, then for every photon it scatters, it will receive twice the momentum, and we have $Q_{\rm pr} = Q_{\rm abs} + 2Q_{\rm scat}$.

Often the so-called Rayleigh-Gans theory is used for very small particles. It is valid for $|N-1| \ll 1$ and $k\,s\,|N-1| \ll 1$. In this case, one can use a simple analytic expression for $Q_{\rm scat}$,

$$Q_{\rm scat} = \frac{128\pi^4\,s^4}{3\lambda^4}\left(\frac{N^2-1}{N^2+2}\right)^2 . \tag{5.24}$$

This expression is often used when discussing radiation pressure on small particles. However, this is rather problematic because the refractive index, N, can be a strong function of wave-length and is often not smaller than unity, as is shown in Fig. 5.8. Therefore, Rayleigh-Gans theory should only be used if one knows exactly what one is doing. It should never be used to derive size distributions of IDPs from the zodiacal light.

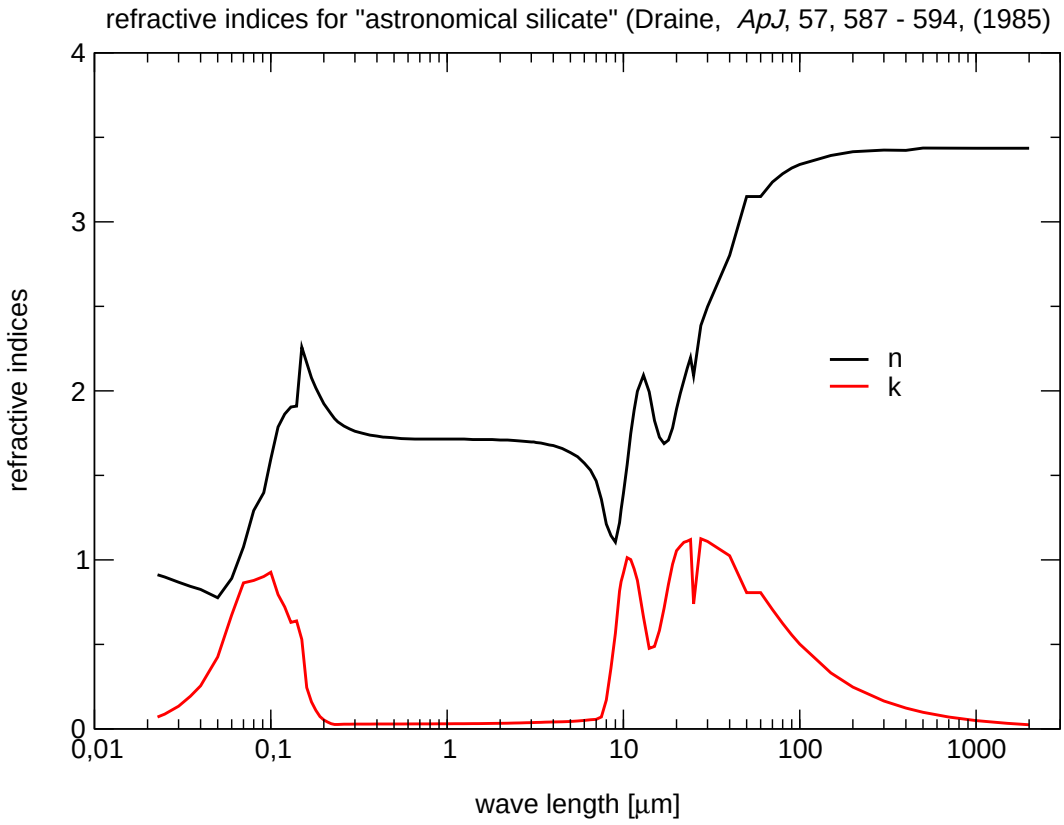

Figure 5.8: Refractive index for astronomical silicate After *Draine* (1985).

5.3.4 Light - The Poynting-Robertson Effect

In the following we derive how to calculate β. Light is scattered by a particle and exerts a pressure force on it. For the case of a sphere, this can be calculated exactly using Mie-theory. Let us repeat some results of scattering theory. Figure 5.9 shows the relevant quantities. The light which is scattered into solid angle $\sin\theta \mathrm{d}\theta \mathrm{d}\phi$ around direction (θ, ϕ) must have entered the system along a tube whose radius is just the impact parameter, b. The cross-sectional area of this tube is just the cross section $C_\lambda(\theta, \phi)$ for direction (θ, ϕ) and wavelength λ. The amount of scattered light at wavelength λ can be obtained by integrating over θ and ϕ, thus defining the total cross section $C_{\mathrm{scat}}(\lambda)$. Similarly, we can define a cross section, C_{abs}, for absorption. Then the cross section for extinction, C_{ext} is also defined, $C_{\mathrm{ext}} \doteq C_{\mathrm{scat}} + C_{\mathrm{abs}}$. Thus, extinction is not the same as absorbtion! A very nice and simple example can be shown using a transparent dish filled with milk and one with black ink which are placed on a projector. Both will cast the same shadow on the screen but one (milk) will appear bright with scattered light whereas the dish filled with ink will remain dark, also when looked at directly.

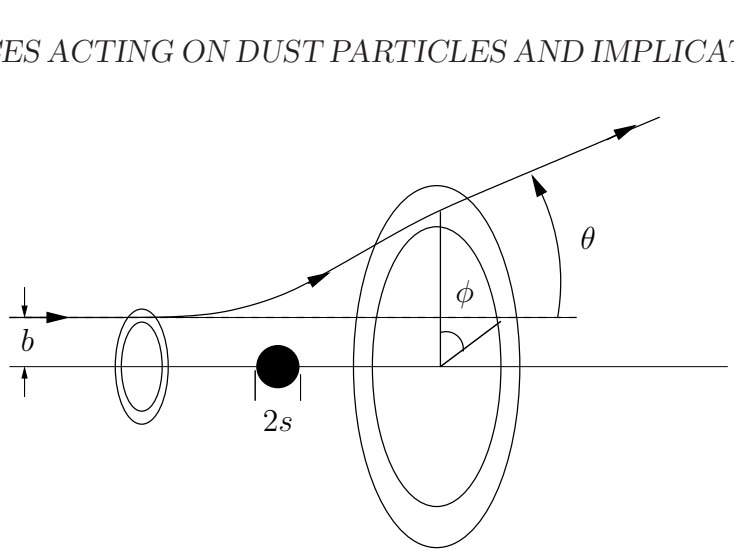

Figure 5.9: Scattering geometry

To derive the effective β, i.e., the pressure force on the particle normalized to the gravity force, $Q_{\rm pr}$ must be integrated over the solar spectrum.

$$\langle Q_{\rm pr}\rangle = \int_0^\infty d\lambda\, Q_{\rm pr}\, F_\odot(\lambda) \tag{5.25}$$

The quantity β is defined by

$$\beta \doteq \frac{F_r}{F_G}. \tag{5.26}$$

Thus, we divide the pressure force

$$F_r = S_0 \left(\frac{R_0}{R}\right)^2 \frac{\pi\, s^2}{c} \langle Q_{\rm pr}\rangle \tag{5.27}$$

by the gravitation force

$$F_G = \frac{4\pi}{3}\rho s^3 \frac{GM_\odot}{R^2}. \tag{5.28}$$

As expected, the ratio of the two forces is independent of heliocentric distance,

$$\beta = \frac{F_r}{F_G} = \frac{3}{4}\frac{S_0\, R_0^2}{c\, G\, M_\odot}\frac{1}{\rho\, s}\ \langle Q_{\rm pr}\rangle = 5.74\cdot 10^{-4}\frac{\langle Q_{\rm pr}\rangle}{\rho s} \tag{5.29}$$

Howver, there is a complicated dependence on the size of the particles. For large IDPs, the pressure force efficiency,$Q_{\rm pr}$, is constant and β must decrease as $1/s$, were s is the particle radius. For small particles the dependence is more complicated, Fig. 5.10 shows β for spheres of radius s composed of astronomical silicate. Obviously, there can not be any silicate-IDPs in the solar system with radii between $0.05 < s < 0.8$ μm. These would leave the solar system as so-called β-meteoroids. Indeed, such particles have been measured, they are dust

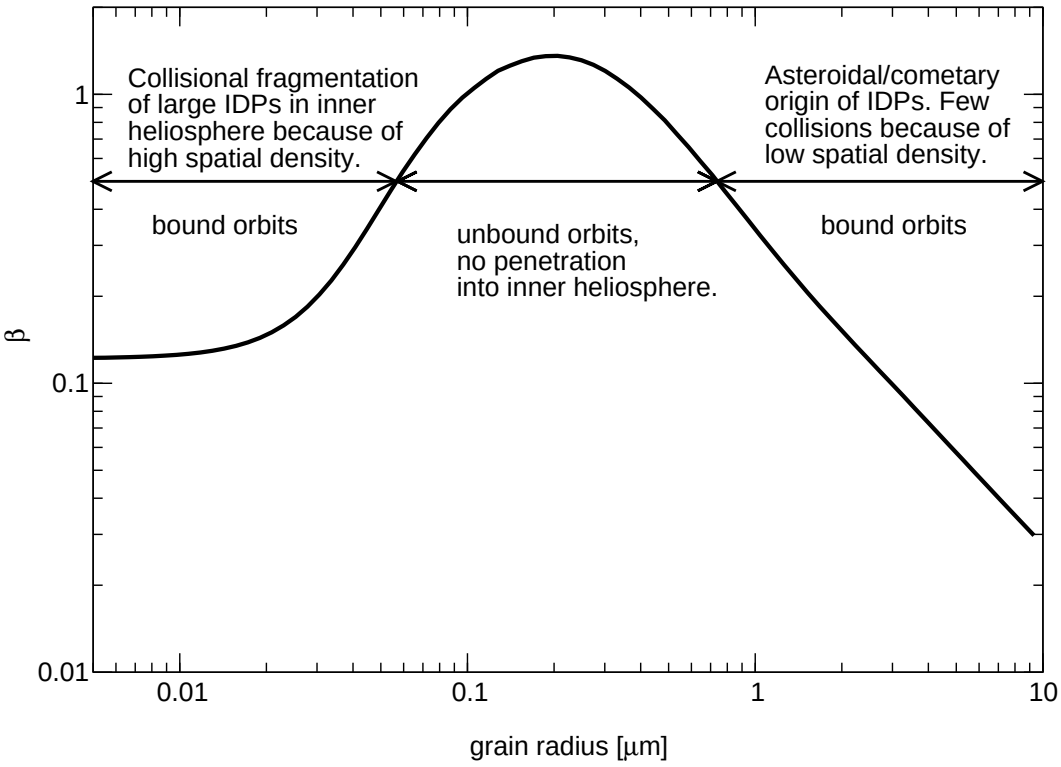

Figure 5.10: β for spheres of astronomical silicate with radius s.

particles which have been freshly created and are leaving the solar system on hyperbolic trajectories.

Our discussion of the dynamics of IDPs in the solar system is only half finished. The interaction of small particles with the solar photon field does not only result in a reduction of the experienced gravitation, but also leads to a slowing down of the IDPs, as we will see shortly.

Consider a particle on its orbit around the Sun (Fig. 5.11). Let its heliocentric distance be R, its velocity $\vec{v}$. The Poynting flux incident on the particle is $S' = S_0(1 - \dot{\vec{R}}/c)$, where $\dot{\vec{R}} = \vec{v} \cdot \vec{S}/|S|$ is the radial velocity component of the particle. The expression in parenthesis, $(1 - \dot{\vec{R}}/c)$, is a consequence of the Doppler effect. According to eq. 5.17, the pressure force exerted on the particle is then given by

$$F_{\mathrm{r}\,r} = \frac{S' A \langle Q_{\mathrm{pr}} \rangle}{c} \frac{\vec{S}}{|\vec{S}|}. \tag{5.30}$$

The non-radial motion of the particle leads to a additional non-radial component of the pressure force. This can be understood in two different, but equivalent ways. On one hand, the non-radial velocity component means that

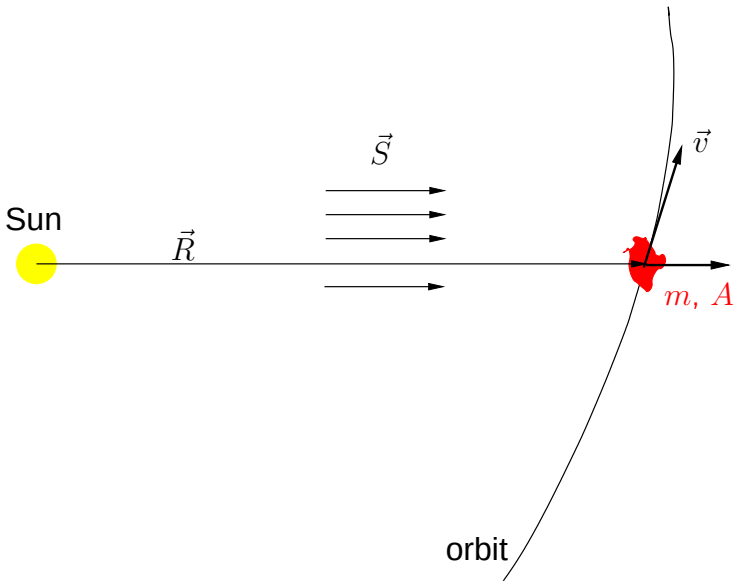

Figure 5.11: Sketch illustrating the dynamics of an IDP in the solar photon field.

the solar radiation does not only hit the particle from the side, but also slightly from infront (from the direction into which the particle is moving). This aberation by tha angle $\vec{v}_\perp/c$ leads to a pressure force

$$F_{\mathrm{r}\perp} = -\frac{S' A \langle Q_{\mathrm{pr}} \rangle}{c^2} \vec{v}. \tag{5.31}$$

It the absorbed energy, $S' A \langle Q_{\mathrm{pr}} \rangle$ is emitted isotropically in the rest frame of the particle (see Fig. 5.12), then no additional force is exerted on the particle. The other explanation is a little more complicated. In the rest frame of the Sun, the particle is moving and the frequency of the emitted light is Doppler-shifted. This leads to a loss of momentum by the particle which corresponds exactly to the force due to aberration discussed above. Thus, apart from gravitation, the net force experienced by the particle is given by

$$m\dot{\vec{v}} = \frac{S' A \langle Q_{\mathrm{pr}} \rangle}{c} \frac{\vec{S}}{|\vec{S}|} - \frac{S' A \langle Q_{\mathrm{pr}} \rangle}{c^2} \vec{v}. \tag{5.32}$$

The first expression is the radial force, the second results in a slowing down of the particle. The second term is often called Poynting-Robertson deceleration. It leads to a decrease of the semi-major axis of the orbit with a time constant of

$$\tau_{\mathrm{PR}} = \frac{s^2}{4Q_{\mathrm{pr}}} \frac{mc^2}{S_0 r_0^2 A} \tag{5.33}$$

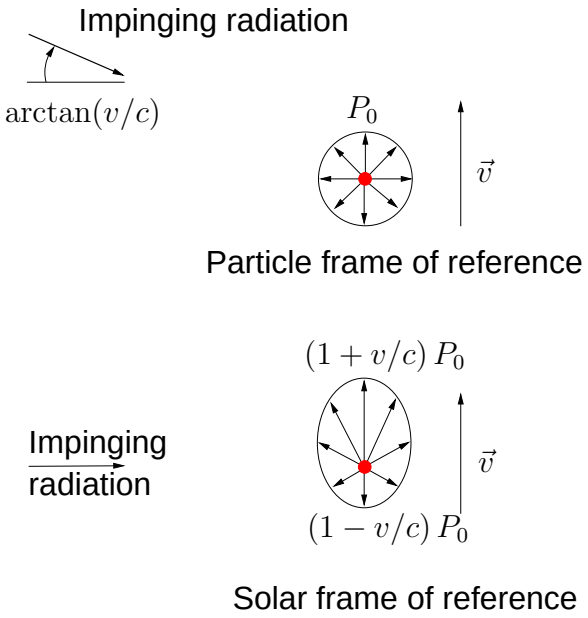

Figure 5.12: The Poynting-Robertson effect.

according to *Burns et al.* (1979). After inserting the relevant quantities, this can be simplified into the mnemonically simple expression

$$\tau_{\rm PR} = 400\frac{R^2}{\beta} \text{ in years,} \tag{5.34}$$

where R is measured in astronomical units, AU. We can now easily calculate the time which a particle will remain in a radial interval $[R, R + \mathrm{d}R]$

$$\mathrm{d}\tau_{\rm PR} = 800\frac{R}{\beta(s)}\mathrm{d}R. \tag{5.35}$$

Again, this is only half the story. Let us consider what happens to a dust particle on its way from the asteroid belt to the inner heliosphere. For large IDPs, $s \geq 1\mu$m, we have, according to Fig. 5.10, $\beta(s) \sim 0.2/s$. Now the solar wind and UV flux impinging on the particle will knock atoms out of the IDP matrix. This process is commonly called sputtering. It leads to a reduction of the size of the IDP. We know the approximate sputtering rate from investigations of noble gases in lunar soil grains, from which on finds an average sputtering rate at 1 AU of approximately $\mathcal{S}_0 \approx 1$ Å per year (*Borg et al.*, 1980). According to eq. 5.35, a μm IDP released at 2 AU will reach 1 AU after about 50'000 years. However, in the mean time, its size will have decreased - not by 50'000 Å, but somewhat less because the sputtering rate at 2 AU is four times less than at 1 AU. However, we can easily take this into ccount and derive the time dependence of the particles size. The change in

radius is proportional to the time spent in the sputtering environment and to the sputtering flux.

$$\mathrm{d}s = -\mathrm{d}t\mathcal{S}_0 \left(\frac{R_0}{R}\right)^2 \tag{5.36}$$

We divide this equation by $\mathrm{d}R$ and obtain

$$\begin{aligned}
\frac{\mathrm{d}s}{\mathrm{d}R} &= -\frac{\mathrm{d}\tau}{\mathrm{d}R}\mathcal{S}_0 \left(\frac{R_0}{R}\right)^2, \\
&= 800\frac{R}{\beta(s)}\mathcal{S}_0 \left(\frac{R_0}{R}\right)^2, \\
&= 800\frac{\mathcal{S}_0\, s}{0.2}R_0^2 R^{-1}, \\
\frac{\mathrm{d}s}{s} &= 0.4\frac{\mathrm{d}R}{R},
\end{aligned} \tag{5.37}$$

where the numerical constant in the last step is obtained by evaluating all the units. The sign disappears after the first line because $\mathrm{d}R$ is negative in our case. The IDP spirals towards the Sun, thus reducing R with time. We can now integrate this expression,

$$\begin{aligned}
\ln s &= 0.4 \ln R + C, \\
s(R) &= s_0\, R^{0.4}
\end{aligned} \tag{5.38}$$

where the integration constant was used to normalize to the original size of the particle. Thus, our IDP has shrunk by some 30% on its way from 2 AU to Earth.

5.3.5 Charging of Dust

IDPs experience further forces which are due to the electric charge they acquire when exposed to the solar wind and solar UV flux. Several processes lead to charging of the IDP:

- Absorption of solar wind ions and electrons is the most obvious process. The charge of the IDP makes it attractive or repulsive for electrons or ions. The absorption cross section for electrons and ions is not equal. It is easy to show that the absorption cross section for a solar wind particle with mass, m_j, speed u, and charge Z_j, $\sigma_j(U)$ for an IDP with radius s and surface potential U is given by

$$\sigma_j(u) = \pi s^2 \left(1 - \frac{2\, Z_j\, e\, U}{m_j u^2}\right). \tag{5.39}$$

  Because electrons have a negative charge ($Z_\mathrm{e} = -1$) and a mass which is approximately 1840 times less than that of a proton, the expression

in parenthesis for positive surface potential is much larger for electrons than for protons. Therefore, one would expect that a positive charge of an IDP would rapidly be cancelled by an inflow of electrons. On the other hand, a negative charge would be much more stable. Because of their much larger mass, ions don't feel the small surface potential of the IDP and therefore pass by it without noticing. The rule of thumb is that ions have roughly 1 keV/amu of energy (corresponding to 440 km/s solar wind speed), whereas electrons at the same solar wind speed have nearly 2000 times less energy. Thus, the solar wind will tend to charge IDPs negatively.

- The emission of secondary electrons when the IDP is hit by primary ions or electrons will tend to reduce the effect just discussed in the previous bullet. It is easier to eject electrons from an IDP (as from any surface) than an ion, and so it is more probable to charge the ion positively with this process. The efficiency of secondary electron emission (number of emitted electrons per incident electron) depends strongly on the incident energy and is given, e.g., by *Mukai et al.* (2001).

$$\delta_y(E) = \frac{\delta_M}{e^2} \left(\frac{E}{E_M}\right) \exp\left[-2\left(\frac{E}{E_M}\right)^{1/2}\right], \tag{5.40}$$

  where $\delta_M$is a numerical value between 1 and 10. The efficiency maximizes at $E \sim E_M$, where $\sim$ 100eV $< E_M <\sim$ 1000eV. The kinetic energy of solar wind electrons is considerably lower, but energetic electrons can easily reach these values.

- When a photon with energy greater than the work function of the IDP material hits the IDP, photoemission of (mainly) electrons occurs. The resulting current out of the surface is

$$I = 4\pi s^2 \left(\frac{R_0}{R}\right)^2 \int_{h\nu=\epsilon_{\rm work}+\epsilon_{\rm min}}^{\infty} {\rm d}(h\nu)\, \frac{F_\odot(\lambda)}{h\nu} Q_{\rm abs} Y \cdot \int_{\epsilon_{\rm min}}^{\epsilon_{\rm max}} {\rm d}\epsilon f(\epsilon), \tag{5.41}$$

  where $\epsilon_{\rm max} = h\nu - \epsilon_{\rm work}$ and $\epsilon_{\rm min} = 0$ for negatively charged and $\epsilon_{\rm min} = eU$ for positively charged IDPs.

- At very high temperatures above 1000 K, the thermionic effect can contribute to charging IDPs. At such temperatures, some electrons in the solid matrix of the IDP have enough kinetic energy to surmount the work function and leave the particle. This effect is only important in the close vicinity of the Sun where the particles can get hot enough.

The processes disussed above all contribute to the charging of IDPs in interplanetary space. They all rely on emission of low-energy charge carriers.

In general, IDPs charge to a low positive voltage which implies that more electrons are emitted than ions. Because the solar wind consists of a low-energy thermal population of electrons, the IDP can not charge to high voltages, the low-energy eletrons feel the IDP potential and can not escape. Moreover, there are not enough high-energy electrons to contribute significantly to IDP charging. Thus, the charge of IDPs establishes itself at a relatively low value of few Volts, 5 V are a typical value which is often used.

The charge on the IDPs also influences their dynamics. The interplanetary magnetic field which is convected by them by the solar wind leads to a Lorentz force which can move the particles out of the plane of their motions. Because the IMF is organized in inward and outward pointing sectors (see Physik VI, Teil II, Extraterrestrische Physik), this deflection alternates between South- and Northward pointing. As the sectors are never of exactly the same duration, this leads to net long-term diffusion out of the ecliptic plane. Because the magnetic field is larger in the vicinity of the Sun, this effect is more important there than at large heliocentric distances.

The charge on an IDP is easily estimated from the surface potential.

$$q = 4\,\pi\,\varepsilon\,s\,U \tag{5.42}$$

With this, it is easy to estimate the Lorentz force acting on the particle. At about 2.5 AU, in the asteroid belt, the magnetic field is already nearly perpendicular to the solar wind and the Lorentz force is then simply

$$F_{\mathrm{L}} \approx q\,u_{\mathrm{SW}}\,B = 4\,\pi\,\varepsilon\,s\,U\,u_{\mathrm{SW}}\,B \approx 10^{-17}\mathrm{N} \tag{5.43}$$

This is a small force compared to gravitation, $F_{\mathrm{G}} = GM_{\odot}4\pi\rho s^3/(3r^2) \approx 10^{-14}$ N, and is therefore often neglected. However, this is the only influence, apart from three-body collisions, which can move an IDP out of the ecliptic plane. Therefore, it is an important force for the dynamics of IDPs. On the other hand, its small influence has been shown by *Sekanina* (2000), who investigated the tails of sun-grazing comets (the SOHO comets) and who found no deviation from the expected trajectories based on gravitation and Poynting-Robertson effect.

5.4 Measurements of IDPs

Auer (2001) gives a summary of common *in-situ* measurement methods for interplanetary dust. Figure 5.13 (after *Auer* (2001)) gives a summary.

- The spatial distribution and density of IDP can be inferred from the intensity of the zodiacal light by inversion. This is only possible within a certain size (and mass) interval of IDPs. This method requires that the instrumental stray light is suppressed below about 1% of the zodiacal

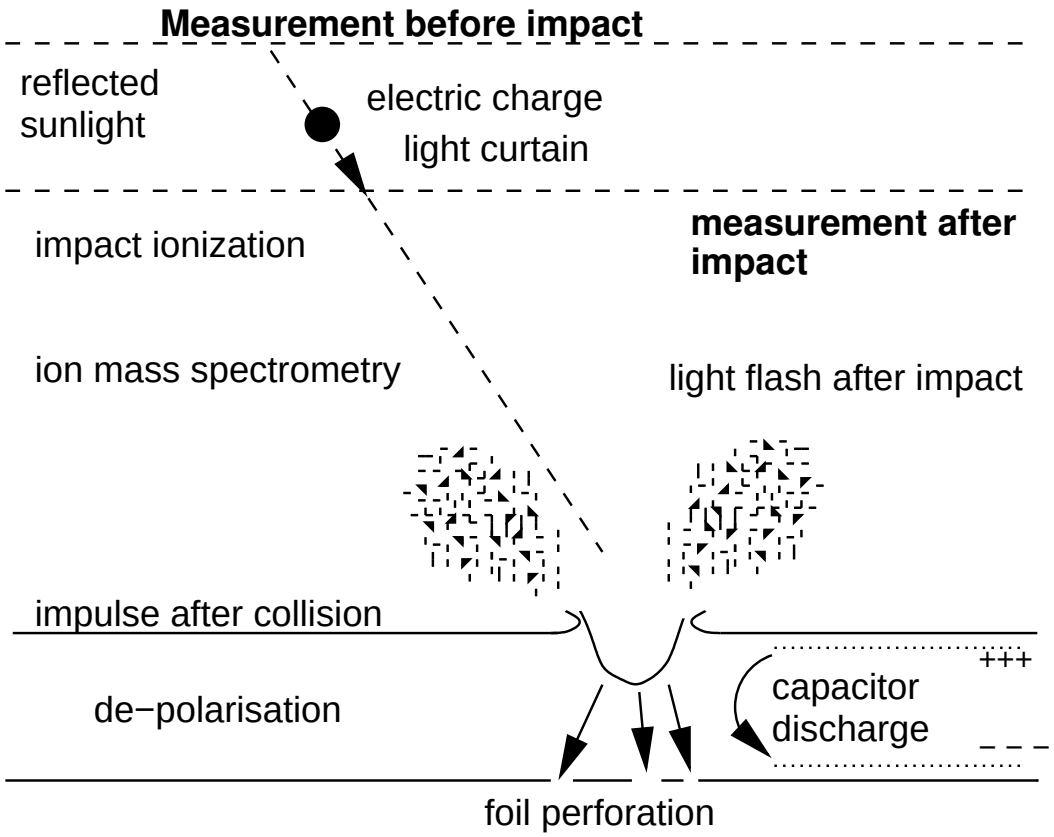

Figure 5.13: Various measurement methods for IDPs. After *Auer* (2001).

light, normally about 15 orders of magnitude are achieved. Moreover, the thermal emission of the spacecraft must be taken into account or suppressed in the infrared part of the spectrum.

- Imaging telescopes can detect light reflected by individual IDPs and can measure the projection of the velocity of IDPs. With some assumptions about the size of the IDPs, about geometry and stability of the particles, some inferences about their radial velocity component can be made.

- Particles in the immediate vicinity of the instrument can be detected with a so-called light curtain. It illuminates a small area of e.g., 0.01 m^2 with a width of approx. 4mm (for the Rosetta dust experiment). Once it triggers, two additional light curtains are immediately turned on and the reflected light is focused and the particle time of flight and intensity of the light are measured to derive speed and size of the particle.

- If a charged particle passes close by an electric conductor, it can induce a voltage pulse. Using multiple crossed wire meshes, the velocity vector

and charge of an IDP can be determined. By applying a retarding or accelerating voltage to some of these meshes the mass of the particle can be determined.

- Some detectors use the light flash that is produced when the IDP hits a surface to determine the flux of particles. With high time resolution electronics, the flash of the crater material can also be resolved. As it depends on the speed of the incident particle, this gives a measure of the IDP speed.

- The material that is heated in the impact is partially ionized and can hit other walls of the sensor where it can lead to further ionization. This impact ionization is very sensitive even for very small projectile masses. On the other hand, the instruments require very careful calibration and modeling, and different fractions of the IDP can be ionized, depending on its composition.

- The ionized material can also be measured in a time-of-flight mass spectrometer. Careful choice of the voltages applied to the focusing grids and electrodes even allows elementally and isotopically resolved composition measurements on individual dust particles.

- When IDPs hit a thin foil, they can perforate it. They loose some energy and, depending on their mass and kinetic energy, can be totally destroyed.

- The fragments after perforation can be measured with a second foil. Some instruments use pressurized vessels and particles are measured by sudden drops in pressure.

- Alternatively, the discharge of a capacitor can be used which signals passage of an IDP. The dielectric between the electrodes can turn conductive due to the high pressures and temperatures during passage of an IDP. In evacuated capacitors, the impact-ionized material of the IDP can lead to a voltage spike which can also be measured.

- The impact of an IDP onto a suitable polarised material leads to its permanent de-polarization which can be measured optically.

- *Add STEREO SWAVES measurements!*

Chapter 6

Interstellar Pickup Ions in the Heliosphere

6.1 Introduction

The solar wind which fills interplanetary space carries with it a certain momentum and an embedded magnetic field. At some point on its way from the Sun, the solar wind ram pressure equals the pressure in the interstellar medium, resulting in a stagnation surface, the boundary between solar system plasma and the local interstellar medium (LISM) – the heliopause. There is some observational evidence for the heliopause. Both Voyager spacecraft have detected some unusual radio emissions in the outer heliosphere during two intervals, one in 1983-84 (*Kurth et al.*, 1984), the other in 1992-93 (*Gurnett et al.*, 1993). In both cases, the radio emission occurred about 400 days after a period of intense solar activity which both produced the largest Forbush decreases ever observed. Such Forbush decreases are strong (10%) decreases in the counting rate of neutron monitors which are the consequences of strong shocks propagating outward from the Sun into the outer heliosphere. These large-scale disturbances reduce the flux of galactic cosmic rays in the inner heliosphere, which, in turn, decreases the count rates in neutron monitors. The outward propagating shocks and disturbances eventually interact with the heliopause and produce characteristic radio emission. Figure 6.1 schematically illustrates the situation as it is believed to have taken place during the two periods when Voyager I and II both measured the unusual radio emission from the boundary of the heliosphere. In the inner heliosphere, electron density, n_e, decreases as $1/r^2$. The plasma frequency, f_p is defined as

$$f_p = \sqrt{\frac{e^2 n_e}{\varepsilon_0 m_e}},$$

and therefore decreases linearly with increasing heliocentric distance. At 1 AU, $f_p \sim 20$ kHz, and thus at 100 AU, $f_p \sim 200$ Hz, which lies significantly below

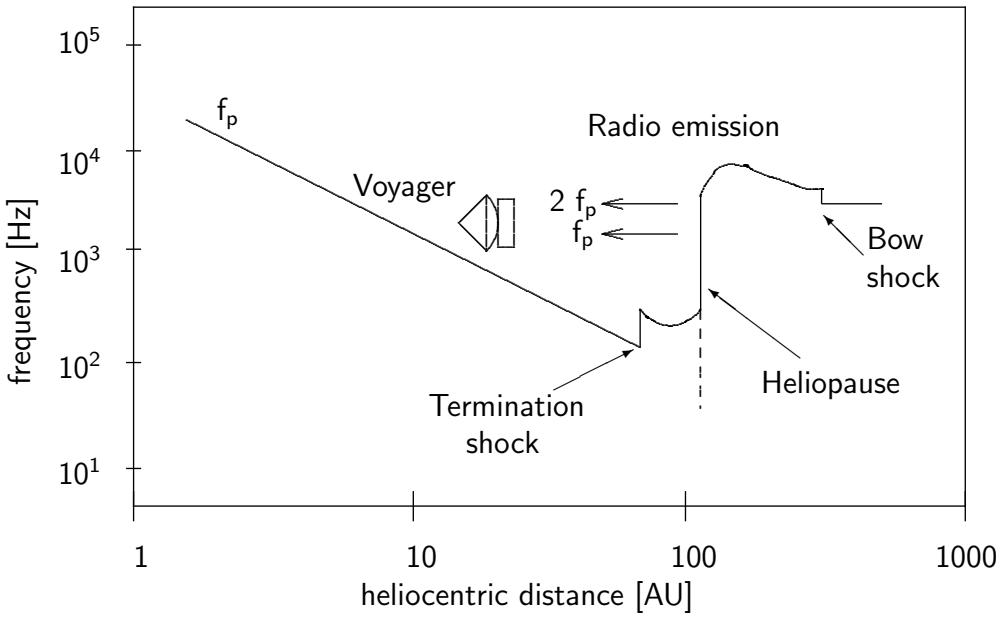

Figure 6.1: Plasma frequency as a function of heliocentric distance. In the solar wind, f_p decreases with distance. As the solar wind turns subsonic at the termination shock, f_p increases by a factor < 2. It increases again at the heliopause to the value representative of the density needed for pressure balance with the interstellar medium. Adapted from *Gurnett et al.* (1993)

the observed 2 - 3 kHz radio emission. Therefore, the emitting region must have a higher density. The region beyond the termination shock is probably not that much denser than within, because the termination shock is most probably rather weak (*Cummings* and *Stone*, 1996). However, even a strong shock would not suffice to allow for sufficiently high densities to account for the high frequencies. Since the heliopause is the locus of pressure balance between the interstellar medium and the (now subsonic) solar wind, we may expect significantly higher densities at that location. Estimates for the electron density in the interstellar medium range from 0.6 cm^{-3} to 1 cm^{-3}, resulting in a plasma frequency, $f_p \sim 2.2 - 2.8$ kHz. This strongly supports the view that the radio emission originated at the heliopause. Depending on the assumptions made for the propagation speed of the shocks, the distance to the heliopause can be calculated from the time difference between Forbush decrease and the measurement of the radio emission. *Gurnett et al.* (1993) arrive at a heliocentric distance of the heliopause between 110 and 160 AU.

Interstellar gas that enters the heliosphere as neutral atoms is ionized inside, and swept back outward by the solar wind. The distribution functions resulting from this process are highly non-Maxwellian and result in a net heating of the plasma filling the heliosphere. As a result, the originally strongly

supersonic solar wind flow turns into a subsonic flow at a point somewhere within the heliopause, the termination shock. Estimates for the distance to the termination shock range from 80 - 100 AU, beyond the current position of the upstream Voyager spacecraft. A simple calculation for pressure equilibrium would demand

$$\rho(r_s)v_{\rm sw}^2 = \rho_0 \left(\frac{r_0}{r_s}\right) v_{\rm sw}^2 = P_\infty, \tag{6.1}$$

where P_∞ is the pressure in the interstellar medium. Obviously, r_s can be obtained from this equation. A more realistic calculation was presented by *Parker* (1963) who imposed the Rankine-Hugoniot relations at the shock and demanded that $P \longrightarrow P_\infty (r \longrightarrow \infty)$. Equation 6.1 is slightly modified,

$$P_\infty = \rho_0 \left(\frac{r_0}{r_s}\right) v_{\rm sw}^2 \left\{ \frac{2}{\gamma+1} \left[\frac{(\gamma+1)^2}{4\gamma}\right]^{\frac{\gamma}{\gamma-1}} \right\}, \tag{6.2}$$

where $\gamma = 5/3$ is the ratio of specific heats for an ideal mono-atomic gas. The expression in curly braces evaluates to 0.88 which lies near unity. The uncertainties due to insufficient knowledge of P_∞ (both the kinetic and the magnetic component), as well as the questionable validity of the assumption of a strong hydrodynamical shock introduce uncertainties which are larger than the deviation from unity. Depending on the values inserted in equation 6.2, shock locations in the range between 70 and 140 AU can be obtained.

However, there is an intriguing derivation of the shock location, as well as of its strength that has been proposed by *Cummings* and *Stone* (1996). They used energy spectra of the anomalous component of cosmic rays (ACRs) measured with instruments aboard the Voyager spacecraft to determine several important heliospheric parameters. Using energy spectra of different elements with different masses and ionization properties, as well as their radial dependence, they succeeded in deriving a value of $80.8(-3.0, +2.4)$ AU for the heliocentric distance of the termination shock.

The existence of a bowshock of the heliosphere in the interstellar medium, analogous to the Earth's bowshock, is an object of debate. Its existence depends strongly on the strength of the magnetic field in the LISM.

The heliosphere itself is structured by the solar wind, and, with increasing heliocentric distance, the mass loading by interstellar pick-up ions. In the inner heliosphere, the interactions between solar wind streams of different speeds set up interaction regions. During solar activity minimum conditions, these interaction regions form recurrent patterns, corotating interaction regions, CIRs. As a fast solar wind stream catches up with slow solar wind, pressure builds up at the stream interface. The pressure wave propagates forward into the slow wind, and, symmetrically, another wave propagates backward into the high-speed stream. Eventually, the two waves steepen into a forward and a reverse shock which bound the CIR. The identity of the two

solar wind streams is not lost, but their kinetic properties are altered completely (*Wimmer-Schweingruber et al.*, 1997, 1999). The interaction of the fast and slow streams and the shocks generate substantial amounts of turbulence. Suprathermal particles, i. e. particles which are sufficiently removed from the core of the velocity distribution functions of the solar wind, are readily accelerated in these turbulent regions and in turn generate waves that can serve as scattering centers for other particles. Recent results of *Gloeckler et al.* (1994) have shown that these particles are not accelerated at the shocks themselves, but rather in the turbulent regions. *Schwadron et al.* (1996) have identified the acceleration process as transit-time damping. The pre-accelerated particles are then efficiently injected into shock acceleration at the bounding shocks, more efficiently at the reverse shock because they are already more energetic there.

The heliosphere is an important modulator of galactic cosmic rays at the Earths orbit. Only the more energetic particles can diffuse inward against the magnetic turbulence present in the heliosphere, and against more formidable barriers presented to the cosmic rays, such as the large-scale magnetic structures associated with coronal mass ejections or, to a lesser extent, corotating interaction regions. Both these objects merge at larger heliocentric distances to form merged interaction regions. The modulation of the GCR is thus strongly dependent on the phase of the 22-year solar cycle, GCR fluxes being higher during solar activity minimum than during maximum. The modulation of the GCR is an excellent test for our understanding of the role of scattering in turbulent plasmas. An extensive review of the heliosphere is given by *Suess* (1990).

6.2 The Model of Vasyliunas and Siscoe

6.2.1 Neutral Particle Trajectories

We will describe the dynamics of interstellar neutral particles entering the heliosphere at a velocity v_∞. We will follow the work of *Fahr* (1968); *Semar* (1970) and *Blum* and *Fahr* (1970). Its orbit will be completely determined by its impact parameter p_0 and by v_∞ except for symmetry around the axis pointing towards the entering neutral flow. Thus the problem is intrinsically a two-dimensional one, and the orbit can be described by two coordinates, distance from the scattering center (the Sun) and an angle ϑ which is measured relative to the axis pointing towards the entering neutral flow. In the center of mass coordinate system, an unbound Keplerian orbit can be described by

$$r = \frac{p}{1 + e\cos\varphi}, \tag{6.3}$$

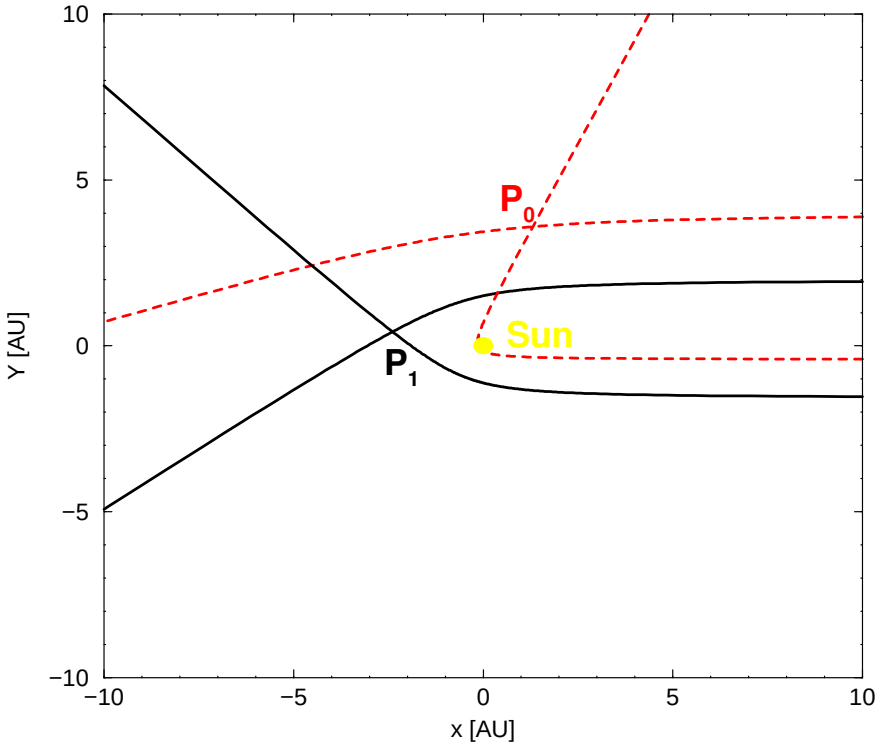

Figure 6.2: Two pairs of orbits intersecting in points $P_0(r_0, \vartheta_0)$ and $P_1(r_1, \vartheta_1)$. Both orbits are completely determined by their impact parameters p_{01}, p_{02} and by v_∞.

where p is the parameter (not the impact parameter) and e is eccentricity. In terms of more physical parameters,

$$r = \frac{\beta p_0^2}{1 + \beta c \cos\varphi} \tag{6.4}$$

with impact parameter p_0 and semi-major axis β,

$$\beta \doteq \frac{v_\infty^2}{GM}, \tag{6.5}$$

$$c^2 = p_0^2 + \frac{1}{\beta^2}. \tag{6.6}$$

In this coordinate system $\varphi = 0$ at perihelion, $r_{\min} = 1/\beta(e-1)$. It is more convenient to transform into a system with origin in the upwind direction, i. e. to transform to an angle ϑ according to $\varphi = \varphi_0 - \vartheta$, where φ_0 is the angle towards the incoming flow. Then, using the identity $\cos\varphi = \cos(\varphi_0 - \vartheta) = \cos\varphi_0 \cos\vartheta + \sin\varphi_0 \sin\vartheta$ we have the convenient formulation of eq. 6.4

$$r = \frac{\beta p_0^2}{1 + \beta p_0 \sin\vartheta - \cos\vartheta}. \tag{6.7}$$

Each point in the (r, ϑ)-plane is reached by two orbits corresponding to two impact parameters, p_{01}, p_{02}. They can be found by solving eq. 6.7 for p_0,

$$p_{0\,1,2} = \frac{r}{2}\sin\vartheta \pm \left[(\frac{r}{2}\sin\vartheta)^2 - (1-\mu)\frac{GM}{v_\infty^2} r(1-\cos\vartheta)\right]^{1/2}. \qquad (6.8)$$

μ is a parameter that accounts for the reduction in the gravitational force due to photon pressure. It is approximately unity for hydrogen, and smaller for other atoms. The velocity in P is always along the trajectory and its magnitude is

$$v(r) = \sqrt{v_\infty^2 + v(r)^2_{\rm escape}} = v_\infty\sqrt{1+\frac{2}{\beta r}}. \qquad (6.9)$$

Ignoring ionization processes, the flux of neutral particles along a trajectory

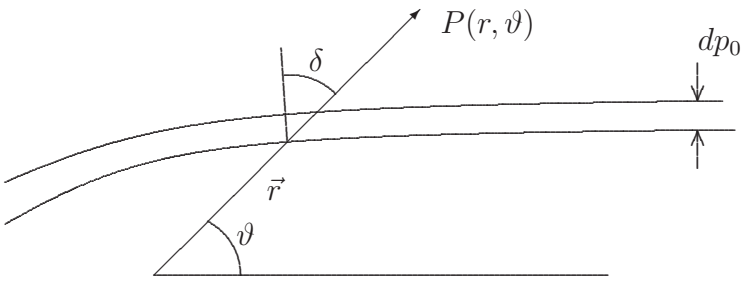

Figure 6.3: Definition of δ and dp_0.

is constant. This can be written as a continuity equation along a neutral flux tube of diameter dp_0

$$n_\infty v_\infty p_0 dp_0 = N(r,\vartheta)v(r) r\sin\vartheta dr\cos\delta, \qquad (6.10)$$

where δ and dp_0 are defined in Fig. 6.3. As is shown in Fig. 6.4,

$$\cos\delta = \frac{r d\vartheta}{\sqrt{dr^2 + (rd\vartheta)^2}} = \frac{r}{\sqrt{r^2 + (\frac{dr}{d\vartheta})^2}}. \qquad (6.11)$$

It is easier to evaluate the derivatives in the φ coordinate system, and then to transform into the ϑ system again,

$$\cos\delta = \frac{p_0}{r\sqrt{1+\frac{2}{\beta r}}}. \qquad (6.12)$$

Solving eq. 6.10 for the neutral density at point $P(r,\vartheta)$ yields

$$N_0(r,\vartheta) = \frac{n_\infty}{\sin\vartheta}\frac{dp_0}{dr}. \qquad (6.13)$$

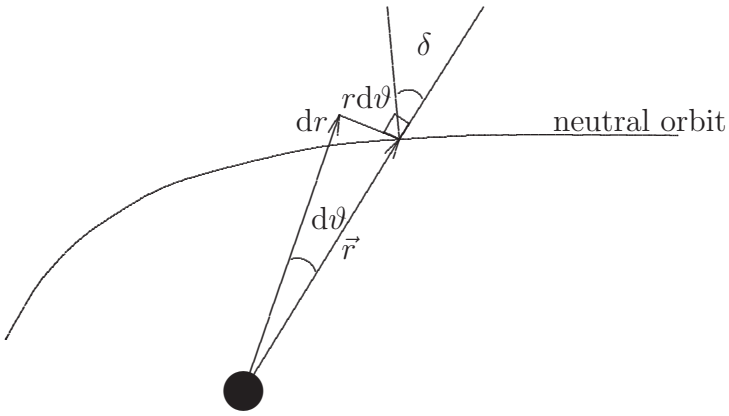

Figure 6.4: Geometry for eq. 6.11.

6.2.2 Neutral Particle Density

We have found the expression for the neutral density at a given point in the heliosphere under the assumption that there is no ionization. In order to derive the neutral density of ionizable atoms we need to include ionization processes. There are two main processes, photoionization which is the dominant process for He, C, and Ne, and ionization by resonant charge exchange which dominates for H. Both processes contribute in about equal amounts to the ionization of O and Ar. For N, no data on charge exchange are currently available. In this discussion, we will limit ourselves to ionization by these two processes, charge exchange (subscript $_{\mathrm{c-e}}$) and photo ionization (subscript $_p$).

The probability to ionize a neutral atom on an infinitesimal part of the trajectory, $d\vec{l}$ is

$$dp_i = \frac{d\vec{l}}{v(r)} \left(n_{\mathrm{sw}}(\vec{r}) \sigma_{\mathrm{c-e}}(|\vec{v}_{\mathrm{sw}}(\vec{r}) - \vec{v}(\vec{r})|) |\vec{v}_{\mathrm{sw}}(\vec{r}) - \vec{v}(\vec{r})| + \sigma_p \Phi_p \left(\frac{r_0}{r} \right)^2 \right). \tag{6.14}$$

The first term gives the time spent on $d\vec{l}$, while the terms in the large brackets give the total ionization rate $1/\tau$. In the following we will omit the arguments of $\sigma_{\mathrm{c-e}}$. $\sigma_{\mathrm{c-e}}$ is only a weak function of relative speed between 300 km/s and 800 km/s. In addition we define the encounter speed v_{rel},

$$v_{\mathrm{rel}} \doteq |\vec{v}_{\mathrm{sw}}(r, \vartheta) - \vec{v}(r)|. \tag{6.15}$$

In analogy with the optical depth, we integrate dp along the trajectory to obtain an extinction function $E(r, \vartheta)$ (*Semar*, 1970),

$$E(r, \vartheta) = \exp \left[- \int_{\infty}^{l(r)} \frac{d\vec{l}}{v(r)} \left(n_{\mathrm{sw}}(r, \vartheta) \sigma_{\mathrm{c-e}} v_{\mathrm{rel}} + \sigma_p \Phi_p \left(\frac{r_0}{r} \right)^2 \right) \right]. \tag{6.16}$$

From Fig. 6.3 we see that

$$dl = \sqrt{r^2 + \left(\frac{dr}{d\vartheta}\right)^2}\, d\vartheta. \tag{6.17}$$

Again taking the derivatives in the φ coordinate system, we find

$$\frac{dl}{d\varphi} = \frac{r^2}{p_0}\sqrt{1 + \frac{2}{\beta r}}. \tag{6.18}$$

We can now easily find the result for the case of a low density cloud and where the solar wind is not strongly influenced by pick-up ions. In that case, solar wind density drops as $1/r^2$, and $v_{\rm sw}$ remains constant. Assuming a speed independent charge-exchange cross section, we find that the ionization rate drops with $1/r^2$ and we can write the integral in eq. 6.16 as

$$\begin{aligned} I &= \int_{\infty}^{l(r,\vartheta)} \frac{dl}{v(r)} \left(\frac{r_0}{r}\right)^2 \frac{1}{\tau'}, \\ &= \frac{r_0^2}{\tau' v_\infty} \int_{\varphi_1}^{\varphi_2} d\varphi' \frac{\left(\frac{r^2}{p_0}\sqrt{1+\frac{2}{\beta r}}\right)}{\left(r^2\sqrt{1+\frac{2}{\beta r}}\right)}, \\ &= \frac{r_0^2 \vartheta}{\tau' v_\infty p_0}, \end{aligned} \tag{6.19}$$

because the integration over φ' is just ϑ. Thus, including the two trajectories intersecting in each point, we have, under the assumptions just mentioned, the density of interstellar neutral gas at a given point $P(r, \vartheta)$,

$$N(r,\vartheta) = \frac{n_\infty}{\sin\vartheta}\left[\frac{dp_{01}}{dr} e^{-\frac{r_0^2\vartheta}{\tau v_\infty p_{01}}} + \frac{dp_{02}}{dr} e^{-\frac{r_0^2(2\pi-\vartheta)}{\tau v_\infty p_{02}}}\right]. \tag{6.20}$$

6.2.3 The Flux of Pick-Up Ions

With these preparations the flux of pick-up ions at a point $P(r, \vartheta)$ is easily derived. As is shown in Figure 6.5 all that needs to be done is to integrate the number of ionized particles along the radius vector $\vec{r}$ to $P(r, \vartheta)$,

$$F_i(r,\vartheta) = \int_0^r dr' N(r',\vartheta) R_{\rm ionis}, \tag{6.21}$$

where

$$R_{\rm ionis} \doteq n_{\rm sw}\sigma_{\rm c-e} v_{\rm rel} + \Phi_{p0}\left(\frac{r_0}{r'}\right)^2 \sigma_p \tag{6.22}$$

is the ionization rate at a given point $P'(r', \vartheta')$. Under the assumption that

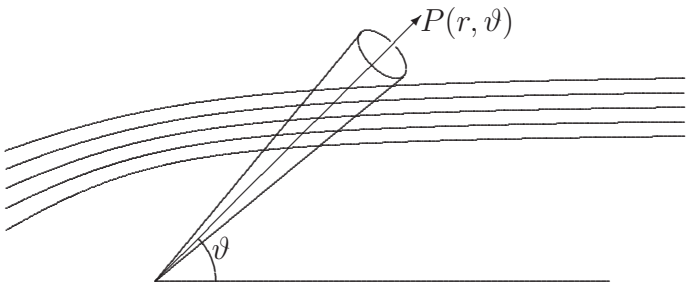

Figure 6.5: The flux of pick-up ions at a point $P(r,\vartheta)$ is the integral along the line vector $\vec{r}$ over the number of ionized particles at the intersection of $\vec{r}$ and the neutral trajectories.

the solar wind flux, $\Phi_{\rm sw} = n_{\rm sw} v_{\rm sw}$, decreases as $(r_0/r)^2$,

$$\begin{aligned} F_i(r,\vartheta) &= \frac{n_\infty}{\sin\vartheta}\int_0^r dr' R_{\rm ionis}\left[\frac{dp_{01}}{dr}e^{-\frac{r_0^2\vartheta}{\tau v_\infty p_{01}}} + \frac{dp_{02}}{dr}e^{-\frac{r_0^2(2\pi-\vartheta)}{\tau v_\infty p_{02}}}\right], \qquad (6.23)\\ &= \frac{n_\infty}{\sin\vartheta}\left(\frac{r_0}{r}\right)^2 R_{\rm ionis}(r_0)\left[\int_0^{\rm p01} dp'_{01}e^{-\frac{r_0^2\vartheta}{\tau v_\infty p'_{01}}} + \int_0^{\rm p02} dp'_{02}e^{-\frac{r_0^2(2\pi-\vartheta)}{\tau v_\infty p'_{02}}}\right], \end{aligned}$$

which is equivalent to the expression derived by **?**. This can readily be integrated. The integral is of the functional form

$$I = \int_0^u dx\ e^{-\beta/x}, \qquad (6.24)$$

where $\beta = r_0^2\ \vartheta/(\tau v_\infty)$ and $u = p_0$. Transforming $z = 1/x$ we easily find (eq. 3.351.4 in *Gradshteyn* and *Ryzhik*, 1980),

$$I = ue^{-\beta/u} + \beta\ {\rm Ei}(-\beta/u). \qquad (6.25)$$

The exponential integral, ${\rm Ei}(-x)$, with negative arguments is not easily handled numerically, and we use the functional relation

$${\rm Ei}(-\beta/u) = \int_{\beta/u}^\infty dt\ \frac{e^{-t}}{t} = -E_1(\beta/u) \qquad (6.26)$$

to obtain our final result,

$$\begin{aligned} F_i(r,\vartheta) &= \frac{n_\infty}{v_\infty}\frac{1}{\sin\vartheta}\frac{r_0^4}{r^2}R_{\rm ionis}^2\left[\vartheta\Psi\left(\frac{p_{01}}{\lambda\vartheta}\right)\right.\\ &\quad \left. + (2\pi-\vartheta)\,\Psi\left(\frac{p_{02}}{\lambda(2\pi-\vartheta)}\right)\right], \qquad (6.27) \end{aligned}$$

where

$$\Psi \doteq xe^{-1/x} - E_1\left(1/x\right). \tag{6.28}$$

This is the result originally derived by **?**. We have plotted $F_i(r, \vartheta)$ for $\vartheta = 0$ and for pick-up protons and neon using the ionization rates given by **?** in Figure 6.6. From it we read off that the flux of interstellar pick-up neon is

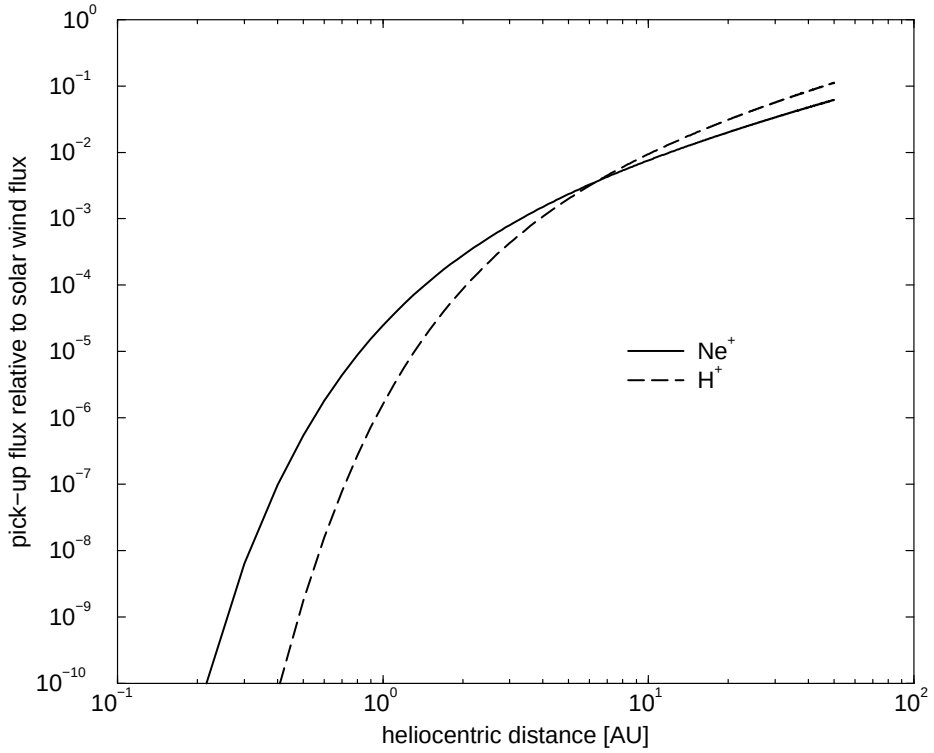

Figure 6.6: Flux of picked-up protons and neon relative to the solar wind flux versus heliocentric distance in the upwind direction ($\vartheta = 0$).

about 2.5 10^{-5} times the solar wind neon flux at 1 AU.

6.2.4 The Interaction of the Solar Wind With Pick-Up Ions

The preceding discussion has tacitly assumed that the newly created pick-up ions are so few in number that they have no effect on the solar wind. However, brief consideration of the numbers involved will easily convince us that this is not true. Present day values for n_∞ are in the range $0.05 - 0.25\text{cm}^{-3}$. Solar wind density at 1 AU is approximately 10 cm^{-3}. Thus, at 10 AU, solar wind density has already dropped to n_∞. Thus, apart from charge-exchange ionization, there must be some additional interaction between the solar wind

and the interstellar medium within the heliosphere. A newly created pick-up ion will gyrate around the interplanetary magnetic field and thus have a speed of between $-v_{\rm sw}$ and $v_{\rm sw}$ with respect to the solar wind. A Maxwellian distribution with this width would indeed be very hot. Due to the adiabatic expansion of the outwardly flowing solar wind, the pick-up ions are cooled and can thermalize with the solar wind. The resulting distribution function, f, is highly non-Maxwellian, but its effective temperature (defined as the second moment of f) is in any case considerably higher than that of the solar wind. We will derive it in Section 6.4.

The charge-exchange process is itself an additional source of interaction between the solar wind and the heliospheric interstellar matter. When an interstellar atom charge exchanges with a solar wind ion, the solar wind ion escapes as an energetic neutral atom (ENA) with approximately the speed of the solar wind, thus removing its momentum from the solar wind. Independent of the ionization process, photo ionization or charge-exchange ionization, the newly created pick-up ion needs to be accelerated to solar wind speed, thus mass-loading the solar wind. The net effect of these processes is to slow down the solar wind and to slow down the adiabatic cooling rate. At some point, the solar wind will then turn subsonic, leading to the formation of the termination shock.

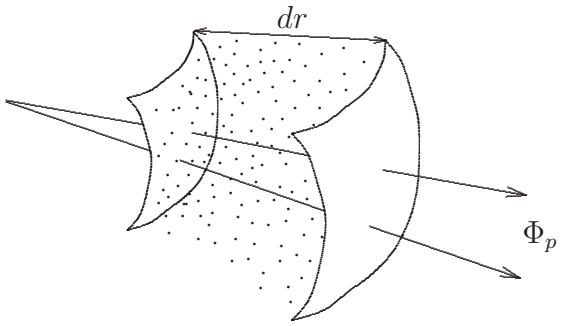

Figure 6.7: The photon flux decreases as $1/r^2$ and is additionally attenuated by the photoionization of neutral H.

Photoionization leads to a slight attenuation of the photon flux out of the heliosphere and the surrounding interstellar material. It is instructive to derive an analytic expression. Following the sketch in Figure 6.7 we can write down the following differential equation for the photon flux:

$$\frac{d\Phi_p(r)}{dr} = -\frac{2}{r}\Phi_p(r) - N(r)\Phi_p(r)\sigma_p. \tag{6.29}$$

This equation has the solution

$$\Phi_p(r) = \Phi_{p0}\left(\frac{r_0}{r}\right)^2 e^{-\sigma_p \int_0^r dr' N(r')}. \tag{6.30}$$

Because the density of interstellar neutral particles is reduced in the inner heliosphere, the actual attenuation is somewhat less strong. We can include the depletion of neutral particles in the inner heliosphere by inserting the expression for neutral density found in eq. 6.20. The integral is easily evaluated for the upwind direction, and, for large distances, we find that, in addition to its $1/r^2$ attenuation, the photon flux is additionally attenuated by a factor

$$f_{\rm atten} = e^{\sigma_p n_\infty \gamma} \left(\frac{r_0}{\tau v_\infty} \right)^{\frac{r_0^2}{\tau v_\infty} \sigma_p n_\infty} \left(\frac{r_0}{r} \right)^{\frac{r_0^2}{\tau v_\infty} \sigma_p n_\infty} e^{-\sigma_p n_\infty r}, \qquad (6.31)$$

where $\gamma = 0.57721\ldots$ is Euler's constant. The first two factors are very near to unity because of the smallness of the exponent, the two radial functions are only a weak additional attenuation. We have plotted this additional attenuation (eq. 6.31) in Figure 6.8. The fact that the additional attenuation can plotted on a linear scale shows that this correction is small. For N independent of r, the

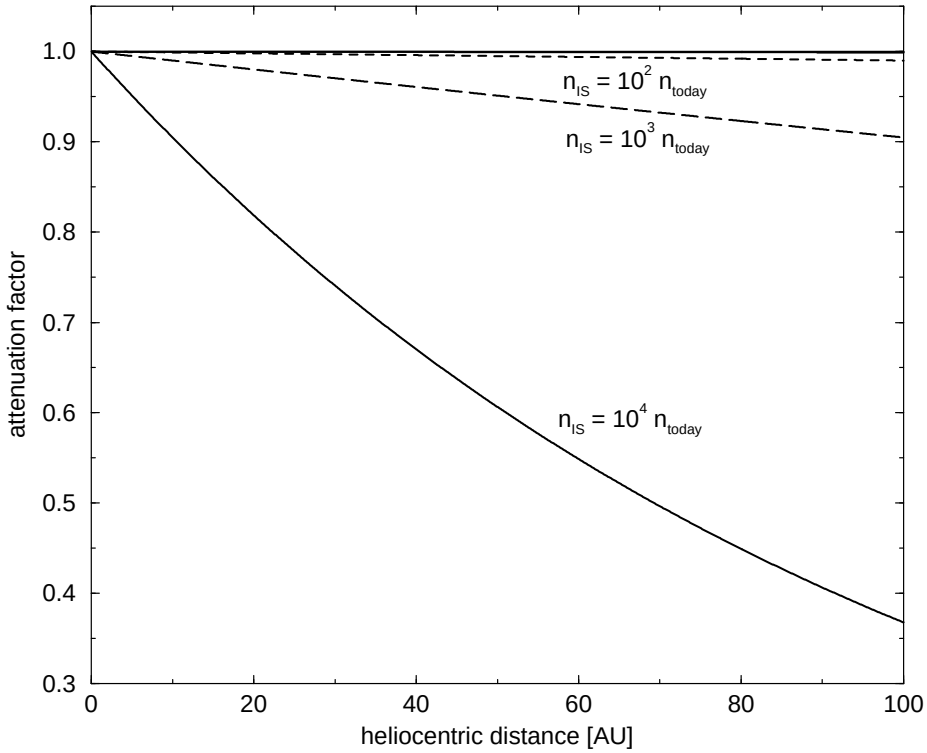

Figure 6.8: Additional attenuation of the $1/r^2$ photon flux due to ionization of interstellar neutrals. The overall effect is small.

exponent is of the form λr where $\lambda = N\sigma_p$ is the length scale. For $N = 0.1{\rm cm}^{-3}$ and $\sigma \sim 10^{-18}{\rm cm}^2$ λ turns out to be about half a parsec and this effect is not noticeable. However, for larger N, say $N = 1000{\rm cm}^{-3}$ as is the case in dense

molecular clouds, λ is on the order of about 10^2 AU. In other words, for almost all situations attenuation effects of the photon flux are unimportant for the ionization of the inflowing interstellar medium. Nevertheless, this discussion has prepared us for the following discussion.

Similar considerations can be made for the solar wind flux. However, for the ionization of interstellar atoms entering the heliosphere, we need to know the total flux of *ions* , $\Phi_i(r)$, not only of the solar wind, $\Phi_{\rm sw}(r)$. Since the charge-exchange process leaves the solar wind flux unchanged, we only need to consider photo ionization, but as a source of particles, not a loss of photons, as in eq. 6.29. Thus, we have the following equation for the ion flux,

$$\frac{d\Phi_i(r)}{dr} = -\frac{2}{r}\Phi_i(r) + N(r)\Phi_p(r)\sigma_p. \tag{6.32}$$

This equation is somewhat more complicated than eq. 6.29, since it contains $\Phi_p(r)$ as well as $\Phi_i(r)$. Its solution is

$$\Phi_i(r) = \Phi_{p0}\left(\frac{r_0}{r}\right)^2 \sigma_p \left[\int dr' N(r') e^{-\sigma_p \int dr'' N(r'')} + C\right], \tag{6.33}$$

where C is the integration constant that needs to be fixed such that $\Phi_i(r_0) = \Phi_{i0}$, i. e. ,

$$C = \frac{\Phi_{i0}}{\Phi_{p0}}\frac{1}{\sigma_p} - \int_0^{r_0} dr' N(r') e^{-\sigma_p \int_0^{r'} dr'' N(r'')}. \tag{6.34}$$

Inserting eq. 6.34 in eq. 6.33 we obtain the final expression for the solar wind flux,

$$\Phi_i(r) = \Phi_{i0}\left(\frac{r_0}{r}\right)^2 + \Phi_{p0}\left(\frac{r_0}{r}\right)^2 \sigma_p \int_{r_0}^{r} dr' N(r') e^{-\sigma_p \int dr'' N(r'')}, \tag{6.35}$$

Note that the charge-exchange cross section, $\sigma_{\rm c-e}$, does not enter in the discussion, since charge exchange leaves the flux of ions unchanged.

In order to determine the deceleration of the solar wind, the momentum flux, $\Phi_m(r,\vartheta)$ at a given point, $P(r,\vartheta)$, needs to be known. The momentum flux needs to obey the differential equation

$$\frac{d\Phi_m(r)}{dr} = -\frac{2}{r}\Phi_m(r) - m_p N(r)\Phi_i(r)\sigma_{\rm c-e} v_{\rm sw}(r), \tag{6.36}$$

where m_p is the proton mass and $v_{\rm sw}(r)$ is solar wind speed which is given by the ratio of momentum flux to particle flux,

$$v_{\rm sw}(r) = \frac{\Phi_m(r)}{\Phi_i(r) m_p}. \tag{6.37}$$

Inserting eq. 6.37 in eq. 6.36 we obtain a simpler equation for $\Phi_m(r,\vartheta)$,

$$\frac{d\Phi_m(r)}{dr} = -\frac{2}{r}\Phi_m(r) - N(r)\Phi_m(r)\sigma_{\rm c-e}, \tag{6.38}$$

which has the same type of solution as eq. 6.32,

$$\Phi_m(r) = \Phi_{m0} \left(\frac{r_0}{r}\right)^2 e^{-\sigma_{\mathrm{c-e}} \int_0^r dr' N(r')}. \tag{6.39}$$

Finally, we can write down the expression for solar wind speed, $v_{\mathrm{sw}}(r)$,

$$v_{\mathrm{sw}}(r) = \frac{\Phi_{m0} \left(\frac{r_0}{r}\right)^2 e^{-\sigma_{\mathrm{c-e}} \int_0^r dr' N(r')}}{m_p \left[\Phi_{i0} \left(\frac{r_0}{r}\right)^2 + \Phi_{p0} \left(\frac{r_0}{r}\right)^2 \sigma_p \int_{r_0}^r dr' N(r') e^{-\sigma_p \int dr'' N(r'')}\right]}. \tag{6.40}$$

In the case of small neutral densities we retrieve the usual result of constant solar wind speed. It is easier to see this by setting the cross sections equal to zero.

6.3 Measurements of Pickup Ions

Interstellar pick-up ions were first observed by *Möbius et al.* (1985), who measured interstellar He^+ at 1 AU. With launch of the Ulysses spacecraft with the SWICS instrument, a wealth of observations of pick-up ions has been made. Ions detected include H^+, He^+, C^+, N^+, O^+, and Ne^+ (*Möbius et al.*, 1985; *Gloeckler et al.*, 1993; *Geiss et al.*, 1994; **?**). In addition, inner-source pick-up ions have been measured.

Measurements of the distribution functions of pick-up ions have revealed interesting insights into transport phenomena in the heliosphere, for example long mean free paths for low-rigidity particles, i. e. pick-up ions (*Gloeckler et al.*, 1995). Published measurements of pick-up ion distribution functions with SWICS do not show the same shape of the distribution function as derived in eq. 6.46. The instrument field of view is not the same for all parts of the distribution function. This needs to be corrected using the so-called duty cycle which we define as the fraction of the distribution function that can be seen by the instrument compared to the full distribution function. It can be computed by integrating the distribution function $f(v)$ over the instrument viewing angles. For SWICS, this is achieved by first transforming the velocity distribution function into the spacecraft frame (a non-relativistic, i. e. Galilean transformation) and subsequently rotating from the spacecraft frame into the instrument frame. Then the distribution function needs to be integrated over the viewing angles and E/q acceptance of the instrument.

6.4 The Non-Thermal $f(v)_{\mathrm{pick-up}}$

The pick-up process and subsequent transport of the picked-up ions result in a non-thermal distribution function of pick-up ions. Nevertheless, the resulting

distribution function is surprisingly easy to derive. We follow **?** and investigate some of its consequences.

The picked up ions immediately begin to gyrate around the magnetic field that is swept along with the solar wind. It is often assumed that they then pitch-angle scatter on magnetic inhomogeneities and that they rapidly become isotropized. The measurements of *Gloeckler et al.* (1995) show that this simple picture is not quite correct, the picked-up ions do not easily scatter through 90°. For our purposes, this effect is unimportant and we will neglect it. It can be corrected with a simple Ansatz in the end. The isotropized pick-up distribution (a shell in velocity space) is convected outward with the solar wind and experiences adiabatic cooling. Thus, the radius of the shell will decrease with increasing heliocentric distance. Hence, the energy of a picked-up ion can give information about the distance where it was ionized. In the solar wind reference frame, the ion has kinetic energy $E_0 = 1/2\ mV_{\rm sw}^2\ (\propto kT)$. For an ideal gas we have for adiabatic expansion,

$$\begin{aligned} PV^\gamma &= nkTV^\gamma = \text{const.}, \\ &= \frac{\nu}{V} kTV^\gamma, \\ &= \nu kTV^{\gamma-1}, \end{aligned} \tag{6.41}$$

where ν is the number of particles and $\gamma = c_p/c_V$. Hence,

$$\begin{aligned} kTV^{\gamma-1} &= kTV^{\frac{2}{3}} \quad \text{for} \quad \gamma = 5/3, \\ kT &\propto V^{-\frac{2}{3}}, \\ kT &\propto r^{-\frac{4}{3}} \quad \text{and thus} \\ (kT)^{3/4}\, r &= \text{const.} \end{aligned} \tag{6.42}$$

Because $E = kT$, the inner energy of the gas $E^{3/4}r = \text{const.}$ Hence, a pick-up ion with energy $E \le E_{\rm sw}$ must have been ionized at a distance $(E/E_{\rm sw})^{3/4}r$. The shell shrinks with increasing distance from the ionization location. The outward flux of ions with thermal energies between E and $E_{\rm sw}$ through a shell with radius r must be equal to the integrated ionization rate between $(E/E_{\rm sw})^{4/3}r$ and r,

$$V_{\rm sw} \int_E^{E_{\rm sw}} dE' n(E') = \left(\frac{r_0}{r}\right)^2 \beta_{\rm ionis} \int_{(E/E_{\rm sw})^{3/4}r}^{r} dr' N(r'), \tag{6.43}$$

where $n(E)dE$ is the number density of particles with energy between E and $E + dE$, and $N(r)$ is the neutral density at r. Because a change in distance

can be expressed as a change in energy, we now take the energy derivative

$$\begin{aligned} -V_{\rm sw}n(E) &= -\left(\frac{r_0}{r}\right)^2 \beta_{\rm ionis} N\left(\left(\frac{E}{E_0}\right)^{\frac{3}{4}} r\right) r\frac{3}{4}\left(\frac{E}{E_{\rm sw}}\right)^{\frac{3}{4}-1}\frac{1}{E_{\rm sw}}, \\ V_{\rm sw}n(E) &= \left(\frac{r_0}{r}\right)^2 \beta_{\rm ionis}\frac{\frac{3}{4}r}{E_{\rm sw}} N\left(\left(\frac{E}{E_0}\right)^{\frac{3}{4}} r\right)\left(\frac{E}{E_{\rm sw}}\right)^{\frac{3}{4}-1}. \end{aligned} \tag{6.44}$$

We now need to transform from energy to velocity space to obtain $f(v)$. We have $\int dE' n(E') = \int d^3v' f(v')$, and hence

$$\begin{aligned} \int dv' mv' n(\frac{1}{2}mv'^2) &= \int_0^{2\pi} d\varphi \int_0^{\pi} d\vartheta \int dv' f(v') v'^2 \sin\vartheta, \\ \int dv' mv' n(\frac{1}{2}mv'^2) &= \int dv' f(v') 4\pi v'^2, \\ mv' n(\frac{1}{2}mv'^2) &= 4\pi v'^2 f(v'), \\ f(v) &= \frac{m}{4\pi v} n(\frac{1}{2}mv^2), \end{aligned} \tag{6.45}$$

for an isotropic distribution function. Combining equations 6.20 (neutral particle number density), 6.44 and 6.45, we can now easily find the velocity distribution function for pick-up ions. For the case where gravitation is balanced by photon pressure (which is generally assumed to be a good approximation for hydrogen), i. e. $\mu = 1$, we obtain

$$f(v) = \frac{3r_0^2}{8\pi V_{\rm sw}^4 r}\beta\left(\frac{v}{V_{\rm sw}}\right)^{-3/2} N\left(\left(\frac{v}{V_{\rm sw}}\right)^{3/2} r, \vartheta\right), v \le 1, \tag{6.46}$$

which is the expression obtained by **?** but corrected for a typographical error. We have plotted $f(v)$ for pick-up protons for various heliocentric radii for the upwind direction in Figure 6.9. The x-axis is the conventional $w \doteq v/v_{\rm sw}$. In this representation, freshly picked up ions are at $w = 1$, while lower w are indicative of ions which were ionized at a location nearer to the Sun. The influence of adiabatic cooling is evident, as is the strongly non-thermal nature of these distribution functions.

Because the pick-up distributions have such large contribution at large w, the contribution of pick-up ions to the total pressure is non negligible. We can easily compute the pressure in a pick-up distribution, it is the second moment of the distribution function,

$$\begin{aligned} p &= \int_0^{v_{\rm sw}} d^3\ vv^2 f(v) \\ &= \frac{3}{2} n_\infty v_{\rm sw}\beta\frac{r_0^2}{r}\int_0^1 dw\ w^{5/2} e^{-\frac{r_0^2\beta}{v_\infty}\frac{\theta}{\sin\theta}\frac{1}{r}w^{-3/2}}, \end{aligned} \tag{6.47}$$

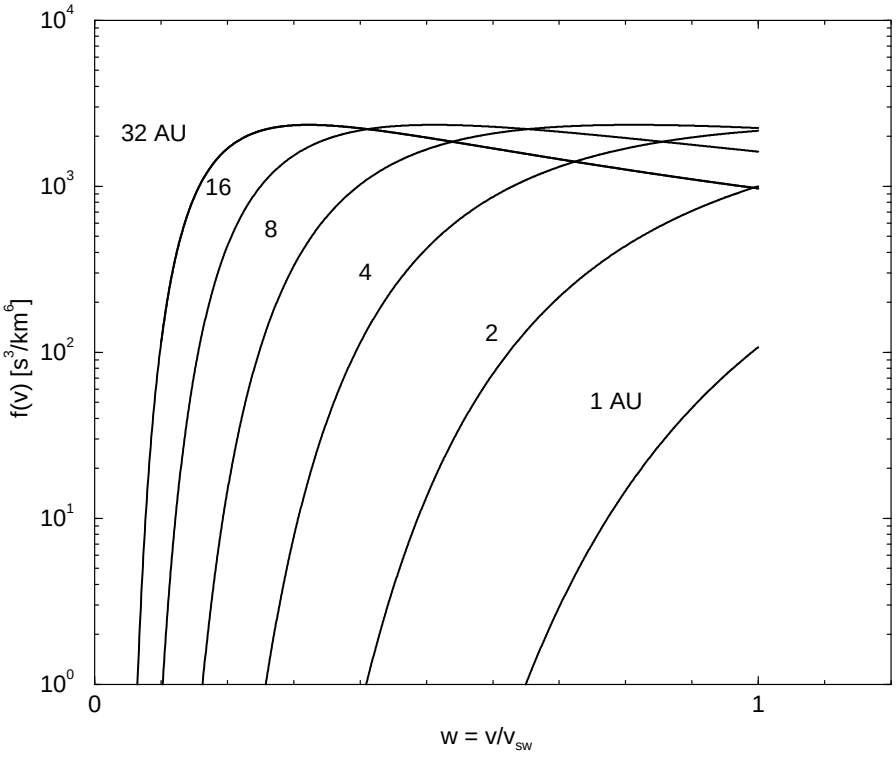

Figure 6.9: Pick-up proton velocity distribution functions for different heliocentric locations in the upwind direction.

where we have transformed v to w and to polar coordinates. Transforming $x = w^{-3/2}$, and using (*Gradshteyn* and *Ryzhik*, 1980, eq. 3.381.3)

$$\int_u^\infty dx\ x^{\nu-1}e^{-\mu x} = \mu^{-\nu}\Gamma(\nu, \mu u), \tag{6.48}$$

where $\Gamma(\nu, \mu u)$ is the incomplete Γ function, we obtain

$$p = m_p n_\infty v_{\rm sw}\beta\frac{r_0^2}{r}\left(\frac{r_0^2\beta}{v_\infty r}\frac{\theta}{\sin\theta}\right)^{7/3}\Gamma\left(-7/3, \frac{r_0^2\beta}{v_\infty r}\frac{\theta}{\sin\theta}\right). \tag{6.49}$$

We have plotted the pressure in pick-up protons versus heliocentric distance in Figure 6.10. For computational purposes, it is better to get rid of the negative first argument of the Γ function by iteratively using the functional relation

$$\Gamma(a+1, x) = a\Gamma(a, x) + x^a e^{-x}. \tag{6.50}$$

Pressure peaks at several astronomical units. The decrease beyond the max-

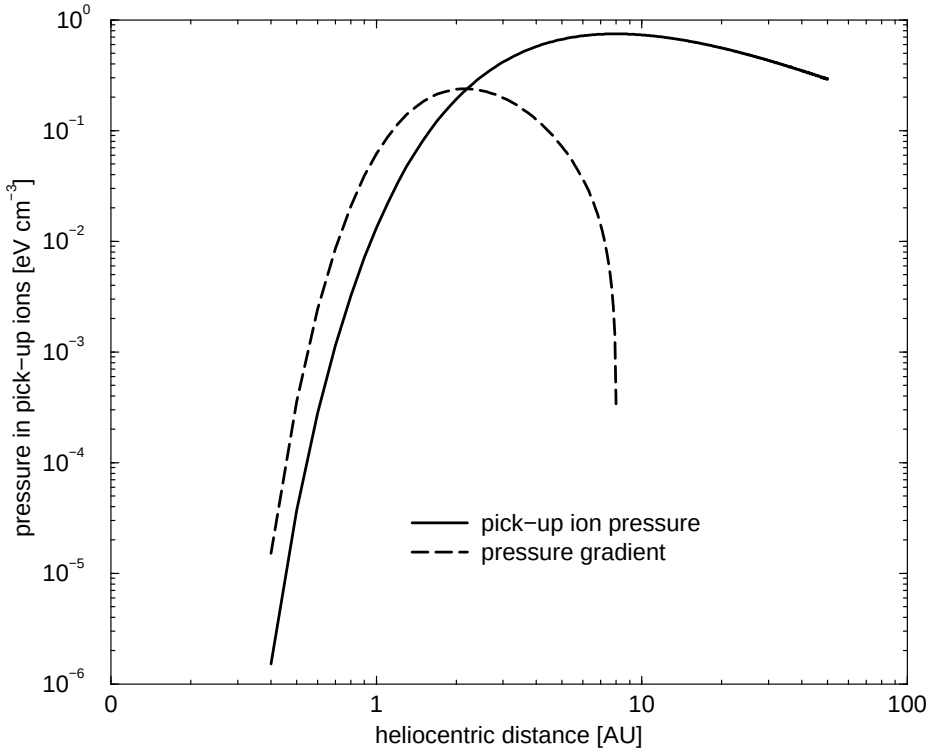

Figure 6.10: Pick-up proton pressure in the upwind direction versus heliocentric distance.

imum is not adiabatic initially, but drops much more slowly. However, the thermal pressure in the solar wind decreases adiabatically all the way from the

Sun except for some contribution by wave-heating or heating associated with compressional regions. *Burlaga et al.* (1994) have investigated five pressure-balanced structures in two merged interaction regions in the outer heliosphere at about 35 AU. They found that the changes in magnetic pressure were balanced by changes in the pick-up proton pressure. The observed thicknesses of discontinuities were several times larger than at one AU, even when expressed in units of the proton Larmor radius. However, expressed in units of *pick-up proton* Larmor radius, the thicknesses are the same at 35 AU as at 1 AU, further indicating the dominant role of pick-up ions in the outer heliosphere. *Richardson et al.* (1995) and *Gazis* (1995) have both looked for the slow-down of the solar wind that is expected as a consequence of the mass loading of the solar wind with pick-up ions. While *Richardson et al.* (1995) find a 7% decrease in the solar wind speeds observed at Voyager 2 if compared with those observed by IMP 8 at 1 AU, *Gazis* (1995) claims that only an upper limit can be given based on observations by the Pioneer Venus Orbiter, Imp 8, Voyager 2, and Pioneer 10. There are considerable difficulties involved when trying to measure the slow-down of the solar wind. The most important probably is the strongly time varying and spatially non homogeneous nature of the solar wind. *Wang et al.* (2000) have recently circumvented this difficulty by considering the average solar wind speeds observed at Ulysses and at Voyager 2 during the lign-up period between mid-1998 and mid-1999. They compared the measurements at Voyagers heliocentric distance (near 60 AU) with model predictions based on Ulysses measurements near 5 AU. Their simple, 1-dimensional MHD code agreed well with the average observations when they included a pick-up proton contribution to mass loading when considering a possible slow-down of the solar wind. Without inclusion of pick-up ions, the comparison was not as good. From their investigations, they inferred an interstellar neutral density of 0.05 cm^{-3}, leading to a $\sim 10\%$ decrease in solar wind speed. We can compare their observations to the simple model described in this chapter. For a present-day neutral density of $n_\infty = 0.1$ cm^{-3} we find a decrease of solar wind speed of nearly 15% near 60 AU. We did not perform the calculations for the case $n_\infty = 0.05$ cm^{-3}, obviously, the reduction in solar wind speed should be less than 15% and should be compatible with the $\sim 10\%$ inferred by *Wang et al.* (2000).

Figure 6.10 also shows the pick-up proton pressure gradient. This quantity plays an important role in the transport of particles in the heliosphere. It peaks around 2 AU. The seemingly larger slope at smaller r is due to the logarithmic scale of the plot.

6.5 Inner-Source Pickup Ions

In situ measurements of pickup ions (PUI) exhibit a component that has nearly thermalized with the solar wind. This implies an origin close to the Sun and is generally ascribed to interaction of the solar wind with interplanetary dust particles (IDPs).

Observations of singly-charged carbon ions in the outer heliosphere by the Solar Wind Ion Composition Spectrometer (SWICS) on Ulysses by *Geiss et al.* (1994) marked the discovery of an "inner source" of pickup ions (PUIs). The ions were believed to be due to the loss of the volatile elements C and O from interstellar dust particles between 2 - 3 astronomical units (AU). Subsequent work by *Gloeckler et al.* (2000), *Schwadron et al.* (2000), and *Schwadron* and *Geiss* (2000) identified an inner source of PUIs in the inner heliosphere, located between 10 - 50 solar radii from the Sun. The present paper deals with this latter "inner source" for heliospheric PUIs.

Normal heavy solar wind ions are multiply charged as a result of their interaction with hot electrons on their way from the solar surface through the corona into interplanetary space. Pickup ions are almost entirely singly charged and have a non-thermal velocity distribution functions. In this work we will consider only singly charged PUIs. Investigations of inner-source PUIs have lead to two remarkable discoveries. Their composition is to a good approximation solar, for instance, the Ne/Mg abundance ratio is about that of the average solar wind. Second, the flux of inner-source PUIs is amazingly high compared to the solar wind flux. Based on the flux of inner-source O^+, the neutralizing cross section per unit volume can be estimated to be $\Gamma \geq 1.3{\cdot}10^{-17}$ cm^{-1}, which is almost two orders of magnitude larger than other typical values (*Schwadron et al.*, 2000). The origin of inner-source PUIs has been attributed interplanetary dust particles (IDPs) which have been saturated with solar wind. In that view, dust particles trap and release solar wind particles (e, g. *Gloeckler et al.*, 2000). The net result is a neutralization of the solar wind.

? have proposed an alternative view in which inner-source pickup ions are created by a population of very small dust particles in which the solar wind is neutralized. It is capable of explaining the above mentioned observational puzzles, but at the cost of introducing a "new" population of very small dust particles.

Chapter 7

Turbulence

2014-04-09: Most (nearly all) corrections have been made. Remaining ones are questionable...

7.1 Hydrodynamic Turbulence

On the one hand, the subject of turbulence is common-day experience. We all know what coffee looks like when we poured some milk in it. It takes some time until the milk has finally spread throughout the whole cup or mug. We know smoke from fires first rises in a billowing manner but then splits up into more and more patches or whifs of smoke until it too, is evenly distributed. We also know it from the twinkling of stars in a clear night (and, as astronomers, are bothered by the bad seeing). Turbulence is an important agent in mixing fluids or air or even plasmas, which we shall all call fluids in this chapter. Turbulence occurs on nearly all length scales in nature. It limits the speed with which our body can supply our limbs with fresh blood, it determines the oxygen content of the upper layers of water bodies by turbulent (eddy) diffusion, it is key to the structure of the atmosphere. On Jupiter, turbulence results in the spectacular belts. Turbulence is an important factor in the convective motions inside the Earth's highly viscous mantle region and contributes to the heating of the solar chromosphere and maybe the corona. In the solar wind, turbulent motions are seen as variations in the radio signals from distant quasars in the interplanetary scintillation technique, similar flickering of radio souces is due to interstellar turbulence. It plays a crucial role in star and planet formation on the scale of molecular clouds. At even larger scales, in the early epoch following the Big Bang, turbulence likely resulted in chaotic spatial patterns of mass or energy concentrations which ultimately led to the formation of clusters of galaxies. Thus, turbulence spans length scales from below milimeters to billions of light years, or more than twentyfive orders of magnitude.

Obviously, such a ubiquitous phenomenon begs to be studied and understood. Unfortunately, it defies a rigorous description. An anecdote about

Figure 7.1: The air flow from the wing of this agricultural plane is made visible by a technique that uses colored smoke rising from the ground. The swirl at the wingtip traces the aircraft's wake vortex, which exerts a powerful influence on the flow field behind the plane. The vortex dissipates after some time, thereby driving turbulence via a turbulent cascade. Source: Wikipedia/NASA-Langley photo-ID EL-1996-00130.

Heisenberg recounts him answering the question, what he would ask God, should he meet him with the words "When I meet God, I am going to ask him two questions: Why relativity? And why turbulence? I really believe he will have an answer for the first." In other words, turbulence is not easy to understand once we leave the more cursory descriptions that we are familiar with.

Show why and that flows with equal Re have similar properties.

Given a fluid of density ρ, flowing at a speed V with typical length sale L, and viscosity μ, there is just one dimensionless number which can be formed with these quantities, the so-called **Reynolds number**, Re. It is defined by

$$\mathrm{Re} \doteq \frac{\rho V L}{\mu} = \frac{V L}{\nu} \tag{7.1}$$

Figure 7.2: The large-scale circulation can be seen very nicely in this image (from APOD). Obviously, total angular momentum is conserved.

fluid	μ Pa s
air	$18.27{\cdot}10^{-6}$
water	$1.{\cdot}10^{-3}$
blood	$3\text{-}4{\cdot}10^{-3}$
mercury	$1.5{\cdot}10^{-3}$
olive oil	0.08
corn syrup	1.4
honey	2'000 - 10'000
ketchup	50'000 - 100'000
peanut butter	250'000

Table 7.1: Approximate values for the dynamic viscosities of various fluids at roughly room temperature.

where μ and ν are the dynamic and kinematic viscosities of the fluid, respectively. The typical length scale could be, e.g., the diameter of a chimney or a pipe or a blood vessel. Some typical numbers for viscosity for various fluids are given in Table 7.1.

The nature of a flow is determined by its geometry, velocity, and the fluid's density and viscosity. Their combination into the Reynolds number is the governing quantity. Typically, flows with small Reynolds numbers are laminar and those with large Reynolds numbers are turbulent. At very low speeds, the flow is laminar, this is also true for highly viscous fluids such as honey or ketchup - have you ever tried to stir either fluid? At higher speeds, a transition from laminar to turbulent flow sets in until a fully-developed turbulent flow is established.

Consider the flow of a fluid through a pipe. For pipe flows, a Reynolds number greater than 4000 signals turbulent flow, values between 2100 and 4000 are transitional between laminar and fluid, values below that describe laminar flow. Consider various fluids flowing through a pipe of diameter 1cm. The typical length scale is thus set at 1cm. With the density of water and its viscosity, we see that flow speeds need to be kept below a few tens of cm/s for the flow to remain laminar, this is what we have in the water pipes leading to faucets. For drains, we have considerably larger diameters, typically several cm, and the flow turns turbulent. This is an important transition. We don't want deposits from the walls of the pipes to the faucets to be in our water, so we want laminar flows there, but we want deposits removed from drain pipes, hence we want turbulent flows there.

Exercise 7.1 *Go through similar considerations for blood in blood vessels and ketchup being squeezed out of a bottle.*

Redo completely: continuity eq. for incompressible fluids has $\vec{\nabla}\rho = 0$*, etc. see notes pp. 88 ff.*

This dependence of the flow type on the dimensionless Reynolds number is utilized to model flows over very large or very small bodies which can't easily be reproduced in a laboratory. For instance, scale models of commercial airliners can be tested at correspondingly higher wind speeds, models of ships or submarines can be tested with other fluids, etc.

Flows are described by the set of hydrodynamic equations consisting of the continuitiy equation, the momentum equations, and the energy equation. Depending on the viscosity of the fluid, the full Navier-Stokes equations need to be considered (for viscous fluids), or only the Euler equations (for inviscid fluids). Let us first consider an incompressible viscous Newtonian fluid[1]. Because it is incompressible, its density does not change, and hence the time derivative in the continuity equation vanishes. Hence,

$$\vec{\nabla} \cdot \vec{u} = \frac{\partial u_i(\vec{x})}{\partial x_i} = 0. \tag{7.2}$$

This can also be considered as an equation describing the conservation of mass. Correspondingly, the equation of motion is the equation that describes the conservation of momentum. For a fluid in steady state (stationary state) it can be written as[2]

$$u_j \frac{\partial u_i}{\partial x_j} = -\frac{1}{\rho}\frac{\partial p}{\partial x_i} + \nu \nabla^2 u_i. \tag{7.3}$$

Now multtply by ρ and take the divergence of both sides. Because the divergence of a gradient vanishes and ν and ρ are independent of $\vec{x}$, we have

$$\nabla^2 p = -\frac{\partial^2}{\partial x_i \partial x_j}(\rho u_i u_j) = -\frac{\partial^2}{\partial x_i \partial x_j}\tau_{ij}, \tag{7.4}$$

where we have made use of the fact that the divergence of an incompressible fluid vanishes. Basically, this expression tells us that changes in the pressure will move around the fluid, induce stresses, and, by the Newtonian approximation, alter the velocity field. Note that we have the structure of a Poisson equation with a source being given by the spatial variations of the stress tensor. It is a non-linear differential equation for the fluid velocity.

If we allow for a compressible fluid, several changes appear. The continuity equation is now

$$\frac{\partial \rho}{\partial t} = -\rho_0 \frac{\partial u_i}{\partial u_j} \tag{7.5}$$

[1]Fluids are called Newtonian if their stress tensors can be expressed in terms of gradients in their velocity field. Most "normal" liquids are Newtonian, as are most astrophysical (and heliophysical) plasmas. Blood, paint, aerosols, and emuslions are examples of non-Newtonian fluids.

[2]Note that all expressions involving the stress tensor disappear for a Newtonian fluid.

for a fluid at rest. Thus, spatial changes in velocity can alter the density of the fluid. For an isothermal fluid, we have the equation of motion

$$\frac{\partial \rho u_i}{\partial t} + \frac{\partial \tau_{ij}}{\partial x_j} = -\frac{\partial p}{\partial x_i} = -c_s^2 \frac{\partial \rho}{\partial x_i}, \tag{7.6}$$

which is reminiscent of a wave equation. Thus, we see that in incompressible fluids, fluctuations in density will lead to a redistribution of energy in the fluid via sound waves.

7.2 The Turbulent Cascade

Big whorls have smaller whorls
That feed on their velocity
And little whorls have lesser whorls
And so on to viscosity (in a molecular sense).
L. S. Richardson, (1922)

Explain what dissipation means

As elegantly summarized by Richardson, the idea of turbulence can be understood as a cascade of turbulent eddies beginning at the largest scale and ending at some scale where energy is dissipated. In fact, Richardson's idea of eddies feeding off eddies feeding off eddies ... and so on to viscosity (see Fig. 7.3) was picked up by *Kolmogorov* (1941) who extended this idea by two crucial assumptions.

So far, all considerations about turbulence have been incompressible[3] and basically adiabatic. No consideration sofar has been made about how energy is dissipated and injected into the fluid. However, the instabilities which are set up by finite viscosity and boundary conditions will ultimately lead to some form of dissipation which will tend to heat the fluid or increase its internal energy at the cost of systematic motions or of kinetic energy. This was also the state of affairs in turbulence studies until the late 1940s until Kolmogorov, Heisenberg and von Weizsäcker introduced some elegant and very modern ideas about self similarity into the field.

Obviously, the fluid does not move by itself and neither do its eddies just materialize out of nowhere. They are driven by other systematic motions of the fluid which in turn require energy to be stuck into the system. If this energy is not to build up in the system, it must be dissipated somewhere. The energy that is stuck ino the system will unfailingly lead to the formation of some large eddies (always cancelling out their angular momentum so as to conserve total angular momentum, see fig. 7.2). Because of the non-linear term $\vec{v} \cdot \vec{\nabla} \vec{v}$ in the governing Navier-Stokes equations, these large eddies will break

[3] or incomprehensible

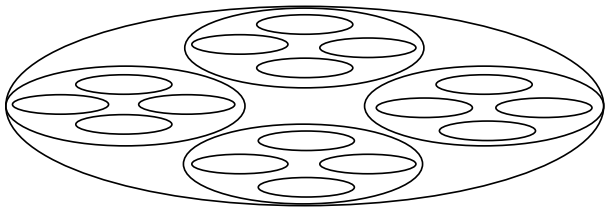

Figure 7.3: Large eddies feed smaller eddies which in turn feed smaller eddies, ... Note that the eddies are not space filling.

up into smaller ones of about half the scale length of the large addies. The rate of breaking up into smaller eddies is high, on the order of $\vec{v} \cdot \vec{\nabla} \approx \vec{k}\bar{v}$, i.e., a period of time which is comparable to the turnover time of an eddy. These smaller eddies again break up and feed smaller eddies, ... and so on to viscosity.

So let's stand back and consider what we have so far. We see that energy is being fed into the system at a length scale L and at a rate ϵ. The rate at which energy is being fed into the system must be matched by the rate at which energy is dissipated in a steady state system, so the energy dissipation rate is also ϵ. In other words, the energy cascade in a homogeneous and isotropic turbulent system in steady state must be determined by the rate at which energy is being fed into the system at the largest scale length, L. The fluid of density ρ which is organized at a scale length L is characterized by its kinematic viscosity $\nu = \mu/\rho$ where μ is its dynamic viscosity. Consider the units of energy dissipation and kinematic viscosity,

$$[\epsilon] = \frac{\text{energy}}{\text{time} \cdot \text{mass}} = \frac{\text{m}^2}{\text{s}^3} \quad \text{and} \quad [\nu] = \frac{\text{Pa} \cdot \text{s}}{[\text{density}]} = \frac{\text{kg m s m}^3}{(\text{m s})^2\text{kg}} = \frac{\text{m}^2}{\text{s}},$$

which is the specific energy dissipation rate of the system. With these two quantities, kinematic viscosity, ν, and specific energy dissipation rate, ϵ, there is exactly one length scale which can be established,

$$l_d = \left(\frac{\nu^3}{\epsilon}\right)^{1/4}, \tag{7.7}$$

which is called the Kolmogorov or dissipation scale. It is the scale at which energy is dissipated and hence we now have the largest scale, L and the smallest relevant scale, l_d, of the system. The typical time scale for dissipating the energy is similarly derived as

$$\tau_d = \left(\frac{\nu}{\epsilon}\right)^{1/2}, \tag{7.8}$$

and gives the characteristic time scale for the dissipation of energy by eddies of size l_d. Finally, a typical speed of the system at these smallest scales is given

by

$$v_d = (\nu\epsilon)^{1/4}, \quad \text{which is also } v_d = \frac{l_d}{\tau_d}. \tag{7.9}$$

So we have now found the length scale at which energy is dissipated, the Kolmogorov or dissipation scale, l_d, and we know the length scale at which energy is injected, L. These two scales normally differ by several orders of magnitude and the range inbetween is called the inertial range. Consider a cup of tea that is being stirred. Its diameter shall be 5cm, we assume the density of tea to be that of water for simplicity (no sugar and milk added). The tea is stirred such that the spoon circles the cup once every second. Then the rate at which energy is being stuck into the system can be approximated by the friction force on the spoon multiplied by the path length travelled per unit time, i.e., the spoons speed,

$$\epsilon \approx 6\pi\eta v^2 r \approx 6\pi\eta(2\pi R)^2 r \approx 5 \cdot 10^{-6}\text{W},$$

where we have assumed a spherical spoon of radius 1cm for simplicity. The dynamic viscosity, $\eta = \mu$ for tea (water) is approximately 10^{-6} m^2/s, and hence the dissipation length is on the order of

$$l_d \approx \left(\frac{10^{-18}}{5 \cdot 10^{-6}}\right)^{1/4} \approx 0.68\text{mm}.$$

The energy is dissipated at a scale slightly smaller than one milimeter. Note that the estimate of the energy input rate is very crude and likely to be too low which would lead to a smaller dissipation scale. The largest and smallest length scales here differ by two orders of magnitude.

The energy in a whorl or eddy can be described as follows[4]. Let the kinetic energy density with wave numbers between k and $k + \mathrm{d}k$ be $\rho I(k)\mathrm{d}k$. Then we have

$$\frac{\rho v^2}{2} = \frac{\rho}{2}\int I(k)\mathrm{d}k \tag{7.10}$$

for the total kinetic energy density. The velocity, v_k, of the eddies in the range $\mathrm{d}k \sim k$ of wave numbers is

$$v_k^2 = I(k)\mathrm{d}k \;\longrightarrow\; v_k^2 = I(k)k \tag{7.11}$$

Fig. 7.4 shows the general idea of the energy cascade from larger eddies to smaller ones. The wave number (roughly the inverse of the eddy size) increases from left to right. Now consider the energy in the range between $\sqrt{\delta}k$ and $k/\sqrt{\delta}$, where δ is some number $\delta \leq 1$, and we will let $\delta \longrightarrow 1$ in the end.

[4]We will be following the arguments given in *Kulsrud* (2005).

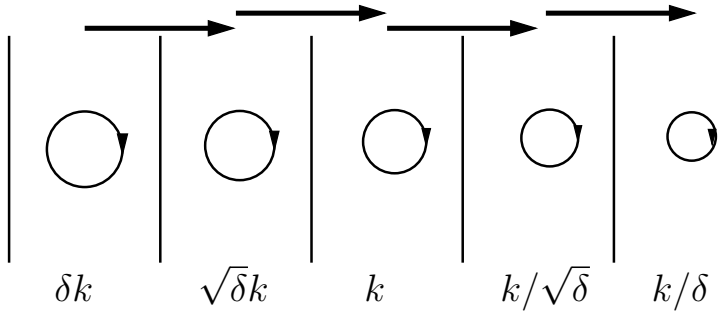

Figure 7.4: Energy transfer from one scale of eddies to the next smaller scale. For these considerations, $\delta \leq 1$.

Energy is transferred into this range from eddies in the range between $\delta^{3/2}k$ and $\sqrt{\delta}k$ at a rate given by the turnover rate of eddies of that larger size,

$$\text{turnover rate}(\delta k) = \delta k v_{\delta k}. \tag{7.12}$$

In the case of our coffee mug we have, for $\delta = 1$,

$$\text{turnover rate}(\delta k) = \frac{1}{R} \cdot \frac{2\pi R}{\tau} = 2\pi/\tau, \text{ i.e., } 2\pi \text{ per second.} \tag{7.13}$$

The smaller eddies which receive this energy will pass part of it on to the next smaller ones at their turnover rate kv_k. However, they will also loose some energy by viscous dissipation at a rate $k^2\nu$, where ν is the kinematic viscosity.

Let us again consider this viscous loss term in terms of the coffee mug.

$$k^2\nu \approx \frac{1}{R^2} \cdot 10^{-3} = \left(\frac{1}{0.025}\right)^2 \cdot 10^{-3} = \left(\frac{1}{2.5}\right)^2 \cdot 10^1 \approx 1.$$

We can easily see that this viscous dissipation will get more important as the size of the eddies decreases because it goes as with $k^2 \sim 1/R^2$.

We can now put together the energy balance equation for a step k in the cascade:

$$\frac{\partial(kI)}{\partial t} = (\delta k v_{\delta k})\,[\delta k I(\delta k)] - (k v_k)\,[kI(k)] - k^2\nu k I(k), \tag{7.14}$$

where the first term on the right is the energy input, the second is the energy being passed on to the next smaller scale (larger k) and the last term is the energy lost to dissipation (energy in the eddy times dissipation rate). Here we come to one of the crucial assumptions about the cascade made by *Kolmogorov* (1941). He argued that turbulence spectra appear to be universal in as much as they do not depend on the exact nature of the fluid in which they occur. Therefore, the spectrum should be independent of the viscosity of the fluid.

It should also be scale-invariant in the inertial range. We will see where the independence of viscosity comes in in a moment.

Next we insert $v_k^2 = I(k)k$ from eq. 7.11 and consider the first two terms on the right as part of a logarithmic derivative, $\mathrm{d}/\mathrm{d}\ln k$ with $\delta \longrightarrow 1$ (*Kulsrud*, 2005), to obtain[5]

$$\frac{\partial(kI)}{\partial t} = -\frac{\partial}{\partial \ln k}\left(k^{\frac{5}{2}} I^{\frac{3}{2}}\right) - k^3 \nu I. \tag{7.15}$$

For stationary turbulence, the left-hand side, and hence the right-hand side, vanish, thus reducing the partial differential equation to an ordinary differential equation. Now we want to solve for I, and introduce a new viable, y,

$$y \doteq k^{\frac{5}{2}} I^{\frac{3}{2}}. \tag{7.16}$$

Using

$$\frac{\partial y}{\partial \ln k} = \frac{\partial y}{\partial k}\frac{\partial k}{\partial \ln k} = \frac{\partial y}{\partial k} k \tag{7.17}$$

we obtain for eq. 7.15 in stationary form

$$\frac{\mathrm{d}y}{\mathrm{d}k} = -\nu k^{1/3} y^{2/3} \tag{7.18}$$

where we have cancelled a k. Eq. 7.18 can now be integrated

$$y^{1/3} = \left(k^{5/2} I^{3/2}\right)^{1/3} = C - \nu \frac{1}{4} k^{4/3}. \tag{7.19}$$

For large eddies with $k = k_0 = 2\pi/L$ and where v_0 is the turbulent velocity, the boundary condition is is given by

$$k_0 I(k_0) = v_0^2. \tag{7.20}$$

Because we can negelct the viscous term at large length scales, this determines the integration constant, $C = k_0^{1/3} v_0$. Note that at large scales we can neglect the viscous term which simplifies α. Inserting C into eq. 7.19 we can solve it for I

$$I = \frac{k_0^{2/3} v_0^2}{k^{5/3}}\left[1 - \left(\frac{k}{k_0}\right)^{4/3} \frac{k_0 \nu}{4 v_0}\right]^2 = \frac{k_0^{2/3} v_0^2}{k^{5/3}}\left[1 - \left(\frac{k}{k_0}\right)^{4/3} \frac{1}{4\mathrm{Re}}\right]^2. \tag{7.21}$$

The square bracket vanishes at some scale $k_{\max} = k_0(4\mathrm{Re})^{3/4}$ which is much smaller than the large scale k_0, namely by a factor $(4\mathrm{Re})^{3/4}$. All energy is

[5]The logarithmic derivative is defined by

$$\frac{d\mathrm{d}f}{\mathrm{d}\ln k} \doteq \lim_{\delta \longrightarrow 1} \frac{f(k) - f(\delta k)}{\delta}.$$

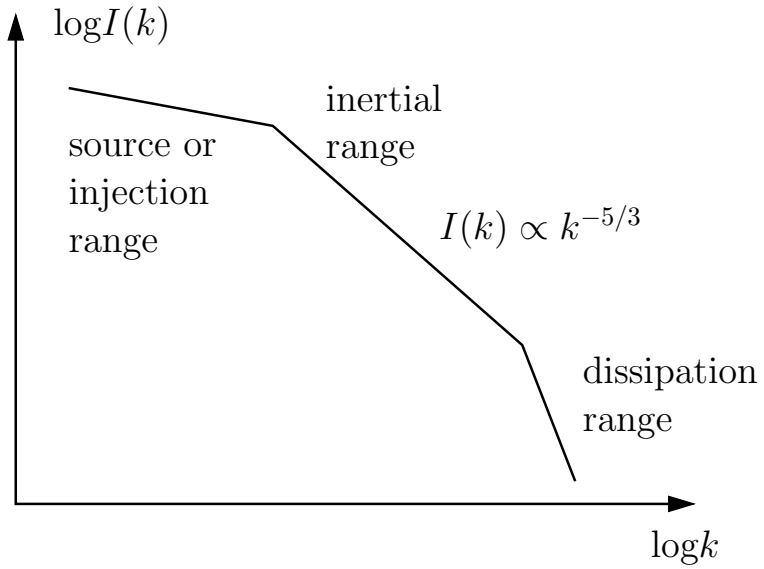

Figure 7.5: The spectral behavior of turbulence is different in the injection, intertial, and dissipation ranges. In the inertial range, turbulence is nearly always observed to exhibit a Kolmogorov spectrum, $I \propto k^{-5/3}$.

dissipated here. At larger scales, for $k \ll k_{\rm max}$, the square bracket is essentially unity, and we retrieve Kolmogorov's original result,

$$I = \frac{k_0^{2/3} v_0^2}{k^{5/3}}, \tag{7.22}$$

the well-known $k^{-5/3}$ power law. Interestingly, nearly all turbulence observed in nature shows this behavior! Well, actually it was this observation that led Kolmogorov (and later, but independently, Heisenberg and von Weizsäcker) to this result. Figure 7.5 summarizes the situation.

7.3 Magneto-Hydrodynamic Turbulence

The solar wind is an excellent and unique laboratory for turbulence in collisionless plasmas with one disadvantage - we normally have only single-point measurements of the occuring phenomena. Studies of the solar wind have shown a mixture of two competing models of turbulence in this supersonic flow.

On the one hand, the first observations of solar wind turbulence appeared to suggest turbulence driven by differential motions in solar wind streams. The accompanying instabilities driven by velocity shears produce long-wavelength Alfvén waves which cascade to shorter wave lengths until they can dissipate

by proton-cyclotron damping. This process results in a smoothing out of differential motions in the heliosphere and a heating of the solar wind plasma.

The other view popularized after the observations by *Belcher* and *Davis Jr.* (1971) of the highly correlated fluctuations between velocity and magnetic-field vectors, stated that the observed fluctuations were merely due to outward propagating Alfvén waves. *Belcher* and *Davis Jr.* observed that the purest Alfvén waves occured in high-speed streams and their trailing edges. Figure 7.6 shows their measurements of a high-speed stream with Mariner 5 in 1967. They

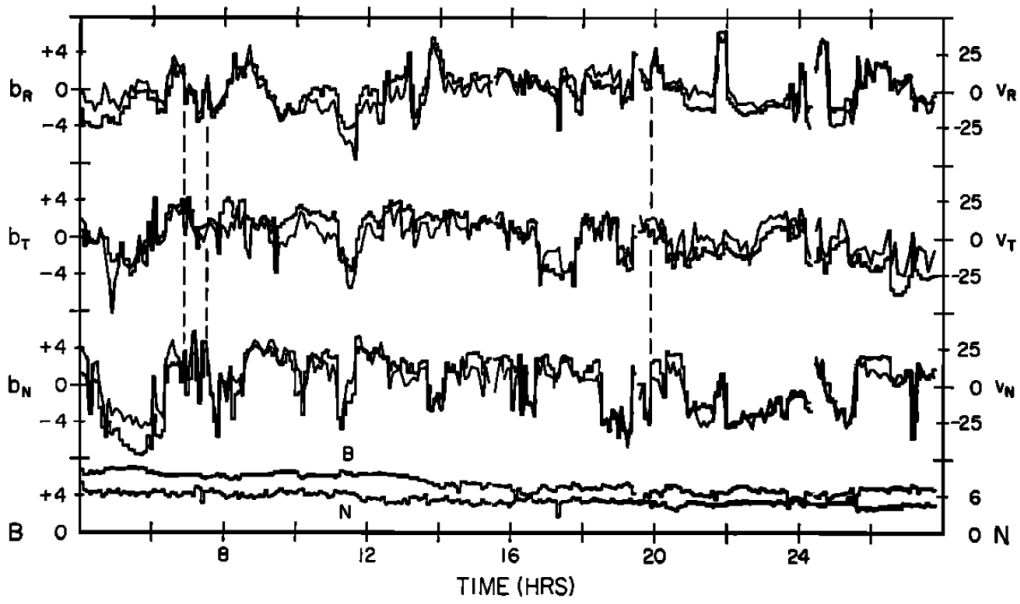

Figure 7.6: Thirtytwo hours of data showing the presence of Alfvén waves in a high-speed stream. The upper six curves show 5.04-minute bulk velocity (diagonal lines) and magnetic field components (step lines). Units are km/s for velocity averages and gammas (1 nT). From *Belcher* and *Davis Jr.* (1971).

suggested that the Alfvén waves were mainly remnants of waves generated at or near the Sun. They were postulated to be remnants of the heating of solar wind streams by wave damping. The highest level of wave activity was observed in compression regions at the leading edges of high-speed streams. This was interpreted as due to amplification of the waves as they were swept into those regions as well as freshly generated waves at those locations. The variation of wave activity across a range of solar wind conditions is shown in Fig. 7.7.

The difficulty with both isolated views - turbulence generated by shear motions and solar-origin Alfvén waves - is that most waves were found to be propagating outward, but with an inward-propagating population of waves

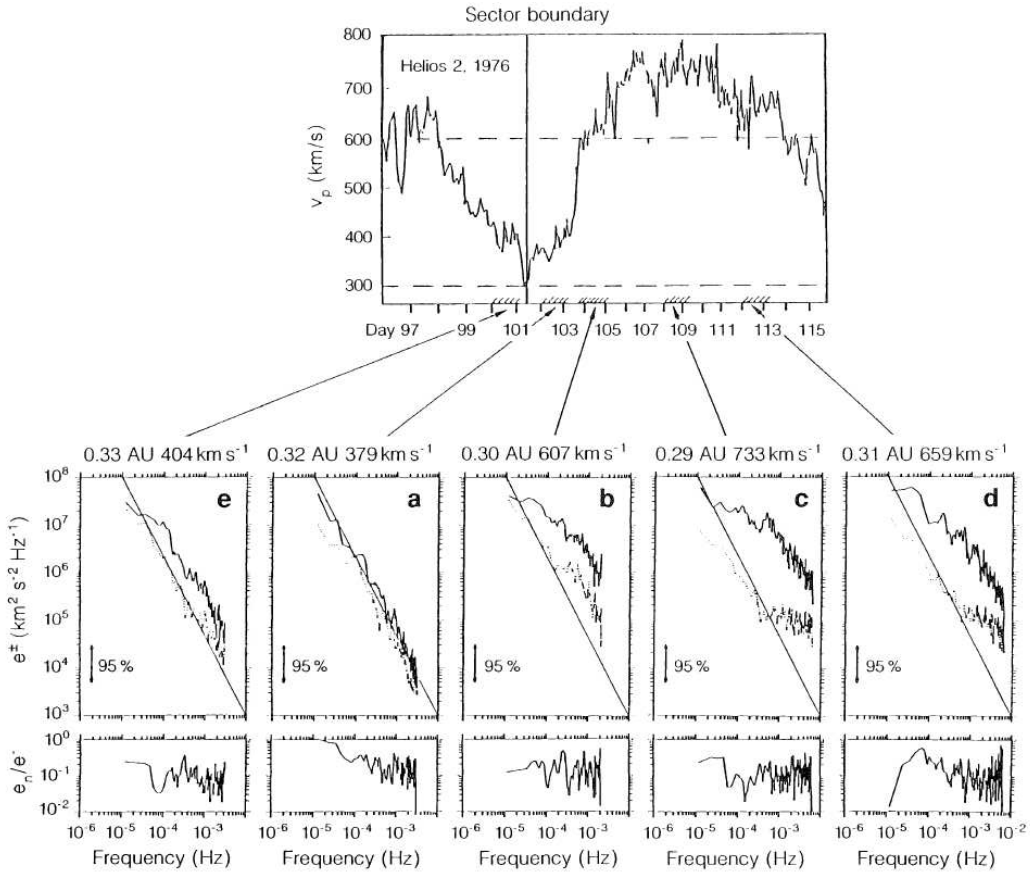

Figure 7.7: Sequence of e^+ and e^- spectra across the transition from slow wind to a high-speed stream. From *Tu* and *Marsch* (1995).

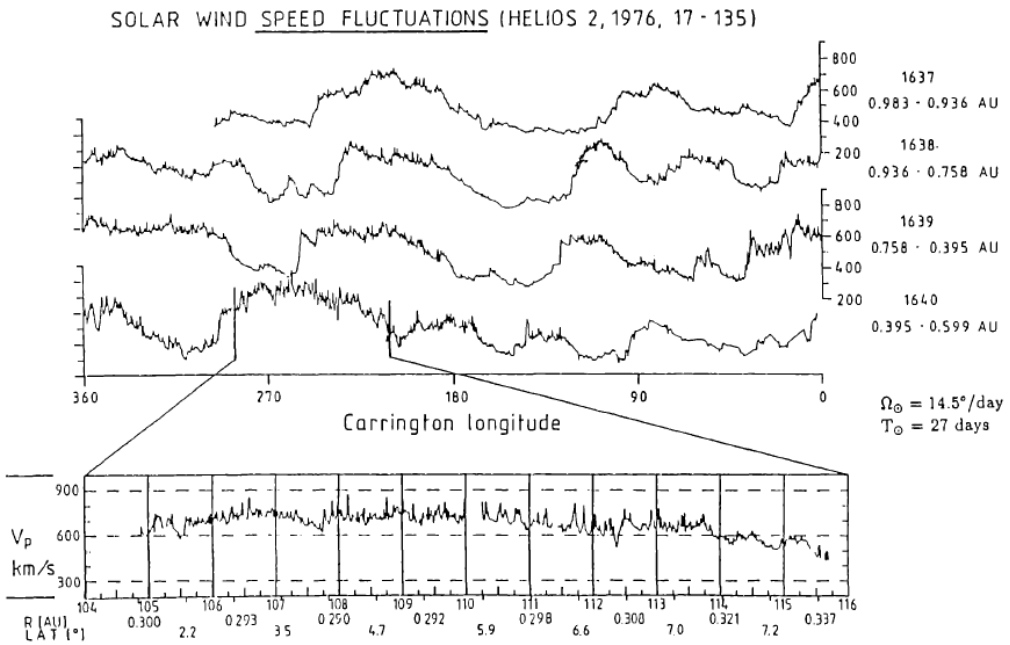

Figure 7.8: Solar wind streams and speed variations observed by Helios 2 in 1976 between 1 AU and 0.29 AU (perihelion). Four subsequent solar rotations are shown with speed displayed vs. Carrington longitude. The blow-up shows the detailed structure of the large corotating high-speed stream and clearly exhibits Alfvénic fluctuations. From *Marsch* (1991*b*).

which was also present in various proportions. The first view could not explain the predominance of outward-propagating waves while the second could not explain the inward-propagating ones.

Today, we understand the ubiquitous presence of Alfvén waves in the solar wind as a consequence of outward-propagating Alfvén waves driven by photospheric motions at the Sun as well as Alfvén waves produced by shear between differentially-streaming solar wind streams. The latter waves are equally distributed into outward and inward-propagating waves. Figure 7.8 shows observations of the solar wind by Helios 2 in 1976, when the spacecraft encountered a corotating high-speed stream four successive times on its way from aphelion to perihelion. The lowest panel shows the perihelion observations of twelve days as a blow-up. Alfvénic fluctuations are easily seen.

However, this view still fails to fully explain the turbulent phenomena in the solar wind. How much of it is due to outward-convected structures which flow by the observer? What is the spectrum of such structures? How, if at all, can they be discerned from propagating waves? The difficulty with all these studies lies in the limitation to single-point measurements which are all that

is possible with single spacecraft.

Table 7.2 gives an overview of the timescales acting in the heliospere and their relation to turbulence.

Phenomenon	Frequency [s^{-1}]	Time [days]	Speed [km/s]	Turbulence
Solar rotation	$\Omega_\odot = 2.7 \times 10^{-6}$ $\nu_\odot = 4.3 \times 10^{-7}$	27	$\omega_\odot R_\odot \approx 2$	Generation
Solar wind expansion	$\nu_{\rm exp} \sim$ $5.9 - 1.9 \times 10^{-6}$	2 – 6	$V_{\rm sw} \approx$ 300 - 900	Generation
Alfvén waves ($\lambda_A \approx 10^{-3}$ AU)	$\nu_A \approx 2.8 \times 10^{-4}$	1/24	$V_A \approx 50$ (at 1 AU)	inertial range
Ion-cyclotron waves ≈ 50 km	$\Omega_p \approx 6.3$ $\nu_p \approx 1$	1.2×10^{-5} 1 s	$V_a \approx 50$ at 1 AU	dissipation

Table 7.2: Typical timescales in the solar wind plasma at 1 AU. From *Marsch* (1991*b*).

That Alfvén waves are indeed present in the solar wind was shown by **?** again using Helios data. Fig. 7.9 shows their results of in-situ solar wind measurements of differential streaming between protons and alpha particles. The top panel shows proton (solid line) and alpha-particle (dots) mean speeds. Obviously, the alpha particles stream faster than the protons. The next panel relates this differential velocity to the Alfvén speed. The two are nearly equal and certainly of comparable magnitude. The following panels shows the dot product $\vec{B} \cdot \Delta\vec{V}_{\alpha p}$ which is close to unity most of the time. This means that $\Delta\vec{V}_{\alpha p}$ and $\vec{B}$ are nearly co-aligned. The lower panels show flow angles of protons and alpha particles as well as the magnetic field angles. Obviously the alpa particles closely follow the magnetic field fluctuations, but not the protons. This was interpreted as alpha particles "surfing" the Alfvén waves in the solar wind.

In the following, we will show how convected structures can be discerned from propagating waves and how waves can be identified in the solar wind. Basically, this boils down to understanding the two components of turbulence observed in the solar wind - so-called 2-d turbulence and so-called slab turbulence. 2-d turbulence is associated with convected structures and slab turbulence with wave activity. We will closely follow the review by *Tu* and *Marsch* (1995) and references therein.

Insert beams on bulk here, i.e., Marsch et al. results

7.3.1 Tools for Describing Turbulence

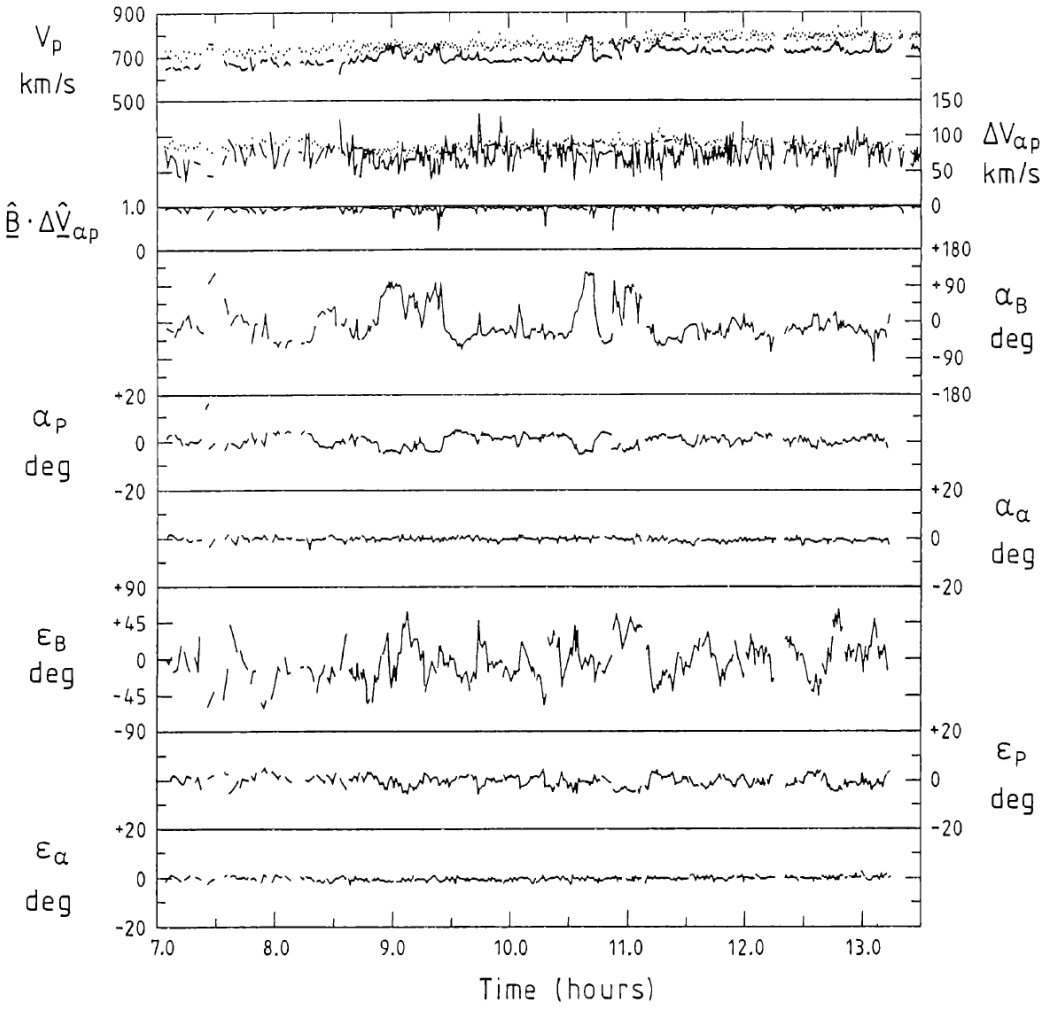

Figure 7.9: Alpha-particle-proton differential streaming in the solar wind as observed by Helios 2 at 0.75 AU in 1976. From top: proton (solid) and alpha (dots) mean speeds, differential speed, $\Delta V_{\alpha p}$, (solid line) and Alfvén speed (dots). The next lower panel shows the dot product, $\vec{B}\dot{\Delta}\vec{V}_{\alpha p}$. The lower panels show the flow angles of protons and alpha particles, as well as magnetic field angles. From *Marsch* (1991*a*).

need to define two-point correlation function here.

The mathematical description of turbulence relies on some tools which we prepare in this subsection. The basic idea is to divide up quantities into a slowly or systematically varying and a more rapidly fluctuating part. The systematic variation may be slow in time or in space, it does not matter according to **Talyor's hypothesis**. This states that **for fully developed turbulence, averages taken over a large region in space around one point or over a long period of time at the same point will lead to the same average** (as long as the spatial extent and time period are chosen long enough but not too long, i.e., appropriately). Thus, assume that we separate the velocity field into a mean (average in the above sense) and a fluctuating part

$$v_i(\vec{x}) = U_i(\vec{x}) + u_i(\vec{x}), \tag{7.23}$$

where

$$\langle v_i(\vec{x})\rangle = U_i(\vec{x}); \quad \langle u_i(\vec{x})\rangle = 0; \quad \left\langle u_i^2(\vec{x})\right\rangle \neq 0. \tag{7.24}$$

Next we define the two-point correlation tensor, $R_{ij}(\vec{r})$, which is the statistical average over two (velocity) components i and j,

$$\langle v_i(\vec{x}) v_j\ (\vec{x}')\rangle = U_i(\vec{x}) U_j(\vec{x}') + R_{ij}(\vec{r}), \tag{7.25}$$

where $\vec{r} = \pm(\vec{x}' - \vec{x})$. $R_{ij}(\vec{r})$ is a crucial quantity in the study of turbulence. It is related to the specific energy density (energy density per mass) of the turbulent velocity field and also describes transport processes in turbulent media.

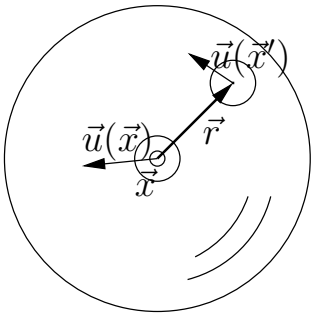

Figure 7.10: The two-point correlation function averages over the volumes of the small spheres with radius δ.

Consider the sketch in Fig. 7.10 which helps visualize the two-point correlation function. A point $\vec{x}$ is surrounded by a sphere with radius $\vec{r}$. If we average over the product of all velocity vectors $\vec{u}(\vec{x}')$ with $\vec{u}(\vec{x})$ we have the two-point correlation function. The larger $|\vec{r}|$, the more we expect that every combination of $\vec{u}(\vec{x}) \cdot \vec{u}(\vec{x}')$ will average out with another $\vec{u}(\vec{x}) \cdot \vec{u}(\vec{x}'')$ at some

other location $\vec{x}''$. On the other hand, if we stay close to $\vec{x}$, we expect less cancellation because there may be more similarities in the velocity field. If we go to infinity with the surface, we expect the velocity fluctuations there to be totally uncorrelated with the velocity fluctuation at $\vec{x}$, and hence, we expect $R_{ij}(r \to \infty)$ to vanish. At the point $\vec{x}$ itself, we expect maximum correlation. The crucial point here is that the correlation tensor in fully developed (isotropic) turbulence only depends on $|\vec{r}|$, but not on position, $\vec{x}$.

From these considerations, we can see that we expect $R(r)$ to be an even function in r and hence, $R(r)$ will have only even powers of r in any analytic expression for it. Moreover, at $r = 0$ we expect a maximum, and hence, there the first derivative will vanish. Its second derivative will be negative.

If we further assume that the correlation tensor $R_{ij}(\vec{r})$ is normalizable we can define its Fourier transform,

$$\Phi_{ij}(\vec{k}) \doteq \frac{1}{(2\pi)^3} \int R_{ij}(\vec{r}) e^{-i\vec{k}\cdot\vec{r}} \mathrm{d}\vec{r}. \tag{7.26}$$

7.3.2 Tools for Data Analysis

According to Taylor's hypothesis, time averages of measurements in the solar wind are equivalent to spatial averages and thus to ensemble averages. Thus, they are insensitive to the local origin in time. Therefore, the mean of a time series $B(t)$,

$$B_0 \doteq \langle B(t) \rangle \tag{7.27}$$

is independent of time. We define the two-point correlation function by

$$R(\tau) \doteq \langle \delta B(t) \delta B(t+\tau) \rangle \tag{7.28}$$

where

$$\delta B \doteq B - B_0.$$

The angled parenthesis ("bra and ket") are used to denote ensemble averaging. In data analysis, it is calculated by time averaging over a time interval

$$\langle A \rangle \doteq \frac{1}{T} \int_0^T A(t) \mathrm{d}t \tag{7.29}$$

where $A(t)$ stands for some solar wind quantity, e.g., $B(t)$ or $\delta B(t)$ or $\delta B(t+\tau)$. We make one important assumption, namely that if we average over long enough periods, then the values of B_0 and $R(\tau)$ will not vary strongly anymore. Obviously, if the averaging period T is too short, this can not be true, if it is too long, then solar wind structure may begin to influence the values. This assumption has been tested, the result is that one needs to average over roughly 5-10 T_c, where T_c is the correlation time defined by

$$T_c \doteq \int_0^\infty \mathrm{d}\tau R(\tau)/R_0 \tag{7.30}$$

where $R(0)$ is the two-point correlation function for zero time lag. If according time averages are used, the values obtained for B_0 and $R(\tau)$ are believed to be accurate with ony small errors.

Taylor's hypothesis (see page 141) in the MHD-case is given by

$$\langle B(\vec{x},t)B(\vec{x}+\vec{r},t)\rangle = \langle B(\vec{x},t)B(\vec{x},t+\tau)\rangle\,, \tag{7.31}$$

where $\vec{r} = -V_{\rm sw}\tau\vec{e}_{\rm w}$. $V_{\rm sw}$ is mean solar wind speed and $\vec{e}_{\rm sw}$ is the unit vector in the direction of the solar wind which is approximately in the radial direction from the Sun. The negative sign is needed because at later times ($\tau > 0$) plasma is seen which was closer to the Sun a time τ earlier. Under this assumption the frequency ω in the spacecraft frame and the wave number k are related by

$$k = \omega/V_{\rm sw}.$$

This is only valid if the separation r is less than the large-scale L over which the solar wind changes its nature, i.e., r has to be less than, e.g., the extent of a high-speed stream. Moreover, r also has to be small enough so that any fluctuation which may have developed has not had much time to change and it is simply convected by the spacecraft. This requires that the transit time of fluctuations is considerably smaller than the characteristic dynamical evolution time for fluctuations. For Alfvén waves, this means

$$V_{\rm sw} \gg V_A. \tag{7.32}$$

This is usually guaranteed in the super-Alfvénic solar wind. However, this is by no means always the case. Let us consider fully developed turbulence. Then the evoltion time can be estimated by the eddy turnover time

$$\tau_k = \frac{1}{b_k k} \tag{7.33}$$

where b_k is the Fourier amplitude at wave number k of the magnetic field measured in units of speed,

$$b_k = \frac{\delta B}{\sqrt{\mu_0\rho}} \tag{7.34}$$

Then this condition can be writen more precisely as

$$\frac{V_{\rm sw}}{V_A} \gg 2\pi\left(\frac{\delta B}{B_0}\right) \tag{7.35}$$

where V_A is the Alfvén speed based on the mean field, B_0, and δB represents the rms magnetic field contribution of the eddy in question. At 1 AU $V_{\rm sw}/V_A \approx 10$ and $\delta B/B_0$ is generally lower than 0.5, so the assumption above is valid. However, for low-Mach-number situations which do occur in the solar wind,

or in the heliosheath, this assumption is not necessarily satisfied anymore and the phase speed of the Alfvén waves needs to be taken into account.

The procedures outlined above needs to be applied to the measured data. The fundamental measurement and their derived quantities are thus,

$$\vec{V} = \left\langle \vec{V} \right\rangle + \delta\vec{V}, \tag{7.36}$$

$$\vec{B} = \left\langle \vec{B} \right\rangle + \delta\vec{B}. \tag{7.37}$$

From these quantities their correlation functions, correlation times and the corresponding frequency spectra can be calculated.

One normally uses the rugged invariants of MHD,

$$E = \frac{1}{2}\left(V^2 + V_A^2\right), \quad \text{energy} \tag{7.38}$$

$$H_c = \left\langle \vec{V} \cdot \vec{B} \right\rangle, \quad \text{cross helicity} \tag{7.39}$$

$$H_m = \left\langle \vec{A} \cdot \vec{B} \right\rangle, \quad \text{magnetic helicity} \tag{7.40}$$

where $\vec{A}$ is the magnetic vector potential $\vec{\nabla} \times \vec{A} = \vec{B}$. The integrals of these quantities over the plasma-containing region are the invariants of the ideal MHD equations, i.e., they are conserved for vanishing magnetic diffusivity (infinite conductivity) and for vanishing kinematic viscosity, $\nu = 0$. Often it is more convenient to use the normalized cross helicity,

$$\sigma_c = 2H_c/E \tag{7.41}$$

which more properly describes the correlation between $\vec{V}$ and $\vec{B}$ and is physically more relevant as a ratio of two rugged invariants.

7.4 Elsässer Variables

The observation that Alfvén waves are mainly outward propagating in the solar wind, especially in high-speed streams, can be seen with the normalized cross-helicity. It describes the ratio of inward and outward-propagating Alfvén waves. However, as we believe that these waves have different sources, measuring only their relative importance is not sufficient. An appropriate way to measure both waves separately was introduced by *Elsässer* (1950). Following *Tu* and *Marsch* (1995) we define the **Elsässer-variables** as

$$\vec{Z}^{\pm} \doteq \vec{V}' \pm \vec{V}_A', \tag{7.42}$$

where $\vec{V}'$ is the proton velocity in the inertial frame of reference, $\vec{V}_A' = \vec{B}'/\sqrt{\mu_0\rho'}$ is the Alfvén velocity and $\vec{B}'$ is the magnetic field vector, ρ' the proton density. The primed symbols $\vec{V}'$, $\vec{B}'$, and ρ' denote the instantaneous measured

values and are obtained directly from the high-resolution data. The Elsässer variables measure outward propagating waves (the '+' component) and inward propagating waves (the '−' component). Time averaging eq. 7.42 we obtain the decomposition

$$\vec{Z}^{\pm} = \vec{Z}_0^{\pm} \pm \delta\vec{Z}^{\pm} \tag{7.43}$$

where

$$\vec{Z}_0^{\pm} = \left\langle \vec{Z}^{\pm} \right\rangle = \vec{V} \pm \vec{V}_A, \tag{7.44}$$

$$\vec{V} = \left\langle \vec{V}' \right\rangle, \tag{7.45}$$

$$\vec{V}_A = \langle V_A' \rangle, \quad \text{and} \tag{7.46}$$

$$\delta\vec{Z}^{\pm} = \delta\vec{V} \pm \delta\vec{V}_A. \tag{7.47}$$

The mean field is $\vec{B}_0 = \left\langle \vec{B}' \right\rangle$. To simplify data analysis, the following convention is used. If the radial component of $\vec{B}_0$ is positive (pointing away from the Sun), one uses $-\vec{B}'$ instead of $\vec{B}'$ to ensure that the sense of propagation of $\vec{Z}^{\pm}$ does not change in dependence of the magnetic field polarity, i.e., across magnetic sector boundaries.

7.4.1 Power Spectra

The spectral properties of solar wind turblence or waves in the solar wind can be obtained by the usual spectral methods, i.e., using (Fast) Fourier transforms of the variables introduced above. Defining

$$\delta Z_{j,k}^{\pm} \doteq \frac{1}{2\pi} \int \mathrm{d}x \delta Z_j^{\pm} e^{-ikx} \tag{7.48}$$

where $\delta Z_j^{\pm}$ is the j component of $\delta\vec{Z}^{\pm}$ and $j = x, y, z$. With this definition we can now find the power spectra of the $\delta\vec{Z}^{\pm}$ fluctuations (outward- and inward-propagating Alfven waves),

$$e_j^{\pm}(f_k) = \frac{2\Delta T}{n} \delta Z_{j,k}^{\pm} \cdot \left(\delta_{j,k}^{\pm}\right)^* . \tag{7.49}$$

n is the number of data points, ΔT the time interval between samples, and f_k is the frequency determined by

$$f_k = \frac{k}{n\Delta T}, \quad \text{for } k = 0,1,2,3,\ldots n/2. \tag{7.50}$$

Furthermore, the "coincident spectrum" and the "quadrature spectrum" need to be calculated,

$$C_j(f_k) - iQ_j(f_k) \doteq \frac{2\Delta T}{n} \left(\delta Z_{j,k}^{+}\right)^* \ \delta Z_{j,k}^{-}. \tag{7.51}$$

All relevant spectra can now be calculated with $e_j^{\pm}(f_k)$, $C_j(f_k)$, and $Q_j(f_k)$. The specific energy spectrum of $\delta\vec{Z}^{\pm}$ is

$$e^{\pm}(f_k) \doteq \frac{1}{2}\sum_{j=x,y,z} e_j^{\pm}(f_k). \tag{7.52}$$

The total energy spectrum and the cross-helicity spectrum are

$$e(f_k) = \frac{1}{2}\left(e^{+}(f_k) + e^{-}(f_k)\right), \tag{7.53}$$

$$e^{c}(f_k) = \frac{1}{2}\left(e^{+}(f_k) - e^{-}(f_k)\right). \tag{7.54}$$

The normalized cross-helicity spectrum is just the above divided by the total energy spectrum,

$$\sigma_c(f_k) \doteq \frac{e^c(f_k)}{e(f_k)} \tag{7.55}$$

and the "Elsässer ratio"

$$r_E(f_k) \doteq \frac{e^{-}(f_k)}{e^{+}(f_k)}. \tag{7.56}$$

The residual energy or the symmetric part of the cross-correlatoion spectrum is given by

$$e^{R}(f_k) \doteq \frac{1}{2}\sum_j C_j(f_k) \tag{7.57}$$

and the corresponding anti-symmetric part is given by the imaginary part (quadrature spectrum),

$$e^{S}(f_k) \doteq \frac{1}{2}\sum_j Q_j(f_k). \tag{7.58}$$

The corresponding normalized spectra are

$$\sigma_R(f_k) \doteq \frac{e^R(f_k)}{e(f_k)} \quad \text{and} \quad \sigma_C(f_k) \doteq \frac{e^C(f_k)}{e(f_k)}. \tag{7.59}$$

The Alfvén ratio spectrum is given by

$$r_A(f_k) \doteq \frac{1+\sigma_R(f_k)}{1-\sigma_R(f_k)} \tag{7.60}$$

and for the components it can be given as

$$r_{A,j}(f_k) \doteq \frac{\frac{1}{2}\left(e_j^{+}(f_k) + e_j^{-}(f_k)\right) + C_j}{\frac{1}{2}\left(e_j^{+}(f_k) + e_j^{-}(f_k)\right) - C_j} \tag{7.61}$$

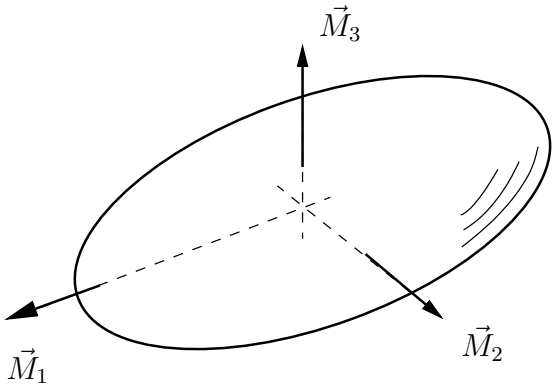

Figure 7.11: The variance ellipsoid is spanned by the eigenvectors, $\vec{M}_1$, $\vec{M}_2$, and $\vec{M}_3$ of the fluctuation tensor T_{ij}. The corresponding eigenvalues, $\lambda_1 \geq \lambda_2 \geq \lambda_3$, quantify the anisotropy of the fluctuations.

This gives the ratios between kinetic energy and magnetic energy in the three components, $j = x, y, z$.

Information about the anisotropy of fluctuations is easily obtained by considering the minimum-variance directions (eigenvectors) of the real symmetric fluctuation tensor

$$T_{ij} \doteq \langle \delta B_i \delta B_j \rangle \,. \tag{7.62}$$

Again, $i,\ j = x, y, z$. The tensor T_{ij} has eigenvalues $\lambda_1 \geq \lambda_2 \geq \lambda_3$ and the corresponding eigenvectors $\vec{M}_1$, $\vec{M}_2$, and $\vec{M}_3$ define the principal axes of the variance ellipsoid. Figure 7.11 shows such an ellipsoid. The eigenvector $\vec{M}_1$ points along the direction with maximum variability, $\vec{M}_3$ along the direction with minimum variability, and $\vec{M}_2$ completes the right-hand system. If $\lambda_3/\lambda_2 \ll 1$, and $\lambda_2 \sim \lambda_1$, the variations (fluctuations) lie mainly in a plane perpendicular to $\vec{M}_3$. If $\lambda_3 \gg \lambda_2$ and λ_1, the fluctuations are oriented primarily along the direction of $\vec{M}_3$. If $\lambda_3 = \lambda_2 = \lambda_1$, the ellipsoid is a sphere, i.e., the fluctuations are equally probable in all directions, in her words, they are isotropic.

7.5 Radial Evolution of Fluctuations

Do WKB...

The fluctuations in the solar wind evolve with time or heliocentric distance. This can be seen already in Fig. 7.8, which shows that the largest fluctuations are seen close to the Sun. It can be seen better in Fig. 7.5 which shows e^+ (solid line) and e^- (dotted line) spectra for a high-speed stream (right panel) and slow wind (left panel) at three heliocentric distances. Outward-propagating fluctuations dominate in high-speed streams. However, they appear to be

damped with increasing distance from the Sun. Fluctuations appear to grow the closer Helios approached the Sun. This can be understood in the picture of evolving turbulence. The Alfvén waves generated at the Sun evolve through a turbulent cascade until they dissipate. Th takes some time which is mapped to heliocentric distance by the radial motion of the solar wind away from the Sun. This is also borne out by the results presented in Table 7.3 and Fig. 7.5 which shows the radial evolution of the Alfvéncity ratio for high-speed streams (right panel) and slow wind (left panel).

		0.3 AU	1 AU	2 AU	>8 AU
$\delta\vec{B}$	Small scale	Dissip.	Intermed.	"WKB"	"WBK"
	Large scale	"WKB"	Intermed.	Intermed.	Saturated
r_A	small scale	≈ 1	0.5	0.5	0.5
	large scale	5	3	2	0.5
	large scale transverse	≈ 1	0.6	0.5	0.5
σ_c	small scale	0.8	0.4	0.3	≈ 0
	large scale	0.5	≈ 0	≈ 0	≈ 0
$\frac{\lambda_2+\lambda_3}{\lambda_1}$	$\delta\vec{B}$ small scale	5:1	4:1	3:1	3:1
	$\delta\vec{V}$	3:1	3:1	3:1	3:1
$\delta\rho/\rho$	small scale	0.1	0.1	0.1	0.1

Table 7.3: Radial evolution of turbulence parameters between 0.3 AU and beyond 8 AU. After *Tu* and *Marsch* (1995) who cite *Roberts* (1992).

The data presentedin Tab. 7.3 are a mixture of data from the Helios and Voyager missions and, therefore, need to interpreted carefully. For instance, the time difference between the 0.3 AU studies with Helios and the 20 AU studies (beyond 8 AU) with Voyager is seven years. While it is widely believed that solar activity does not strongly influence the basi behavior of the probabilitiy distribution functions of the various turbulence parameters presented in Table 7.3, this is by no means certain. As we only have single-point measurements available at different times, it is impossible to discern between temporal and spatial variations. For instance, it could well be that we are over-interpreting data acquired at different locations and different instruments at different times. However, both Helios and Voyager were two-spacecraft missions. The Helios data has been investigated for such effects and the probybility distributions functions of the measurements by the two spacecraft are very similar. Therefore, we believe that the results presented in Table 7.3 are indeed valid and representative of turbulence in the heliosphere. The data presented here are based on our-averaged data and the relevant quantities have been averaged over 30 to 100 days to average out the solar rotation period. The term "small"

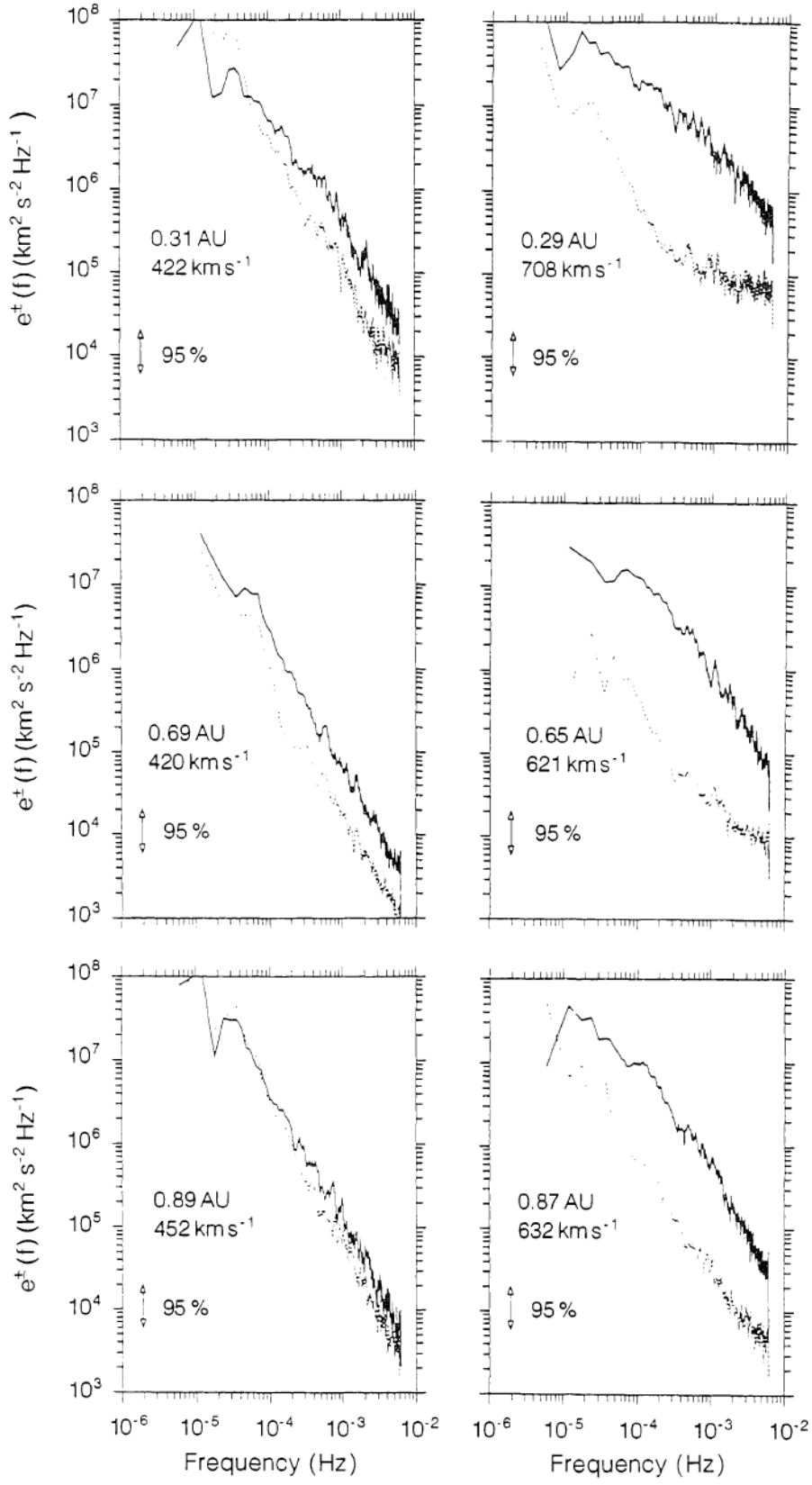

Figure 7.12: Power spectra of e^+ (solid line) and e^- (dotted line) for slow wind (left-hand panel) and high-speed streams (right-hand panel) for various distances. From *Tu* and *Marsch* (1995).

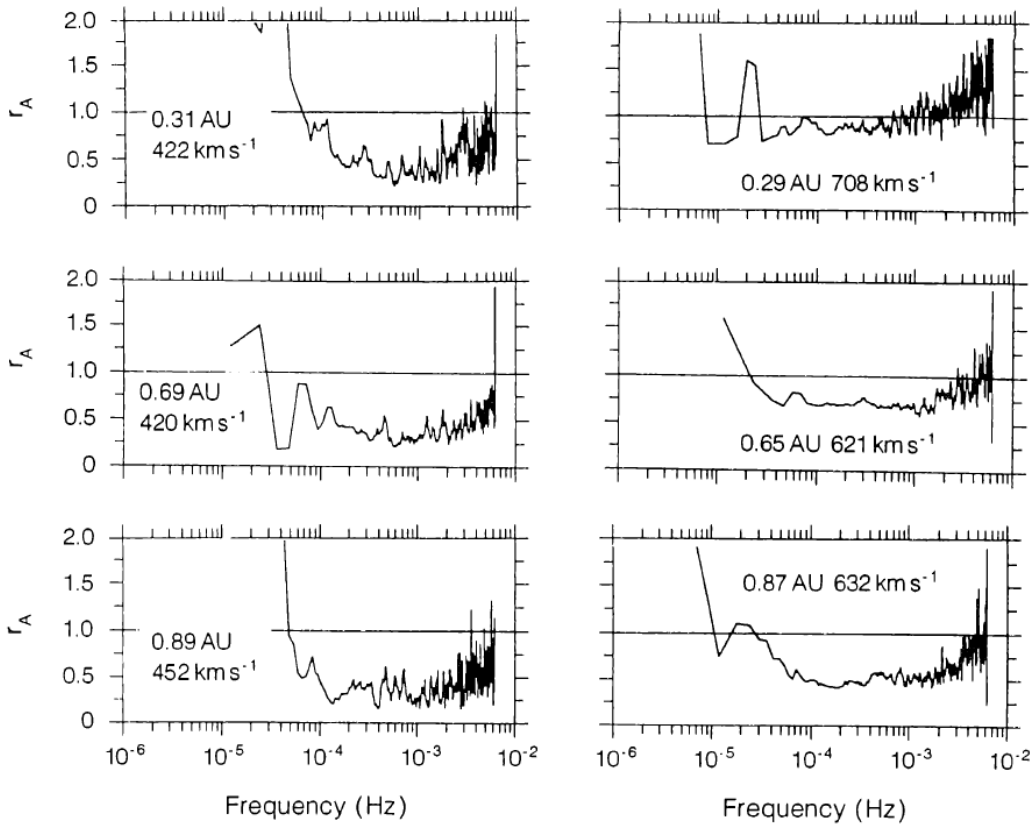

Figure 7.13: Radial dependence of the Alfvénicity ratio, r_A for slow wind (left-hand panels) and high-speed streams (right-hand panels). From *Tu* and *Marsch* (1995).

is used for scales of 0.1 AU or less, implying a period of 10 hours or less in the spacecraft frame. "Large" scales implies scales above 0.1 AU to about 1 AU. "WKB" *define!* means $\delta B \approx r^{-3/2}$, saturated $\delta B \approx B_0$, and "intermed" refers to a scale intermediate between these two.

7.6 Nature and Origin of Incompressible MHD Fluctuations

The radial evolution of r_A shown in Tab. 7.3 is somewhat puzzling. It can be shown that the Alfvén ratio spectrum is given by

$$r_A(f_k) = \frac{e_V(f_k)}{e_{V_A}(f_k)}, \tag{7.63}$$

were $e_V(f_k)$ and $e_{V_A}(f_k)$ are the spectra of the trace of the correlation tensors of the velocity and magnetic field vectors. If all turbulence were Alfvénic, we would expect r_A to remain constant at unity. So observations show that there must be some non-Alfvénic contribution to turbulence in the solar wind. Nevertheless, the radial decline of r_A remains a puzzle. Simply adding other, non-Alfvénic wave modes does not decrease the predominance of magnetic energy, as there is an equipartition between kinetic and potenital energy in all other wave modes. There potential energy is magnetic energy plus something else. So the decrease of r_A implies that the magnetic contribution increases or the kinetic contribution decreases. But the ratio of the kinetic contribution to magnetic can't decrease if there's an equipartition between kinetic and potential energy. Thus, adding other wave modes can't solve the puzzle.

The observed dominance of magnetic energy can't be understood with MHD turbulence theory either (*Tu* and *Marsch*, 1995).

Adding compressive effects does not help either. Compression will tend to enhance the magnetic fluctuation energy. Moreover, the radial dependence of r_A is most prominent in high-speed streams which have only low levels of compressible fluctuations.

A first hint to the origin of the radial dependence of r_A came from Helios observations of incompressible structures which are convected by past the observer. Figures 7.14 and 7.15 show such data. Density fluctuations were very small as was r_A and σ_C. The power spectra of e^+, e^-, and e_V and e_B have slopes close to -5/3. At the same time there is no noteable compression during this time period. The small compressible fluctuations are pressure balanced. The magnetic field was nearly perpendicular to $\vec{e}_r$ which is normally the case at large heliocentric distances. The bottom panels of Fig. 7.15 shows that both σ_C and r_A were close to zero for this time period. Fluctuations with zero σ_C and r_A it can be considered a special kind of magnetic structure which is composed of directional changes of the magnetic field vector. These directional

changes need to fulfill $\delta\vec{B} \cdot \vec{B} = 0$, i.e., they need to be perpendicular to the ambient magnetic field. $\vec{V}$ needs to be constant, as are B, n_p, and T. This kind of fluctuation obeys the MHD equations and is called **Magnetic Field Directional Turning** (MFDT). If such structures are convected by the solar wind the result in magnetic fluctuations with $\delta V = 0$ and hence $\sigma_C = 0$ and $r_A = 0$. This is, of course, an idealized picture of such fluctations. In reality, $\delta\vec{V}$ and r_A may not be exactly zero. A more general situation is the case where $\vec{B} \cdot \delta\vec{B} = 0$ and $\vec{B} \cdot \delta\vec{V} = 0$ and with total pressure balance, i.e., $\delta P_T = 0$. This kind of structures are called **Tangential Turnings** (TTs) which support perpendicular fluctuations of $\delta\vec{B}$, $\delta\vec{V}$, δn, δB, and δT. Such incompressible fluctuations are actually convective structures which are non propagating. They are quasi-static or evolve slowly in the plasma frame of reference.

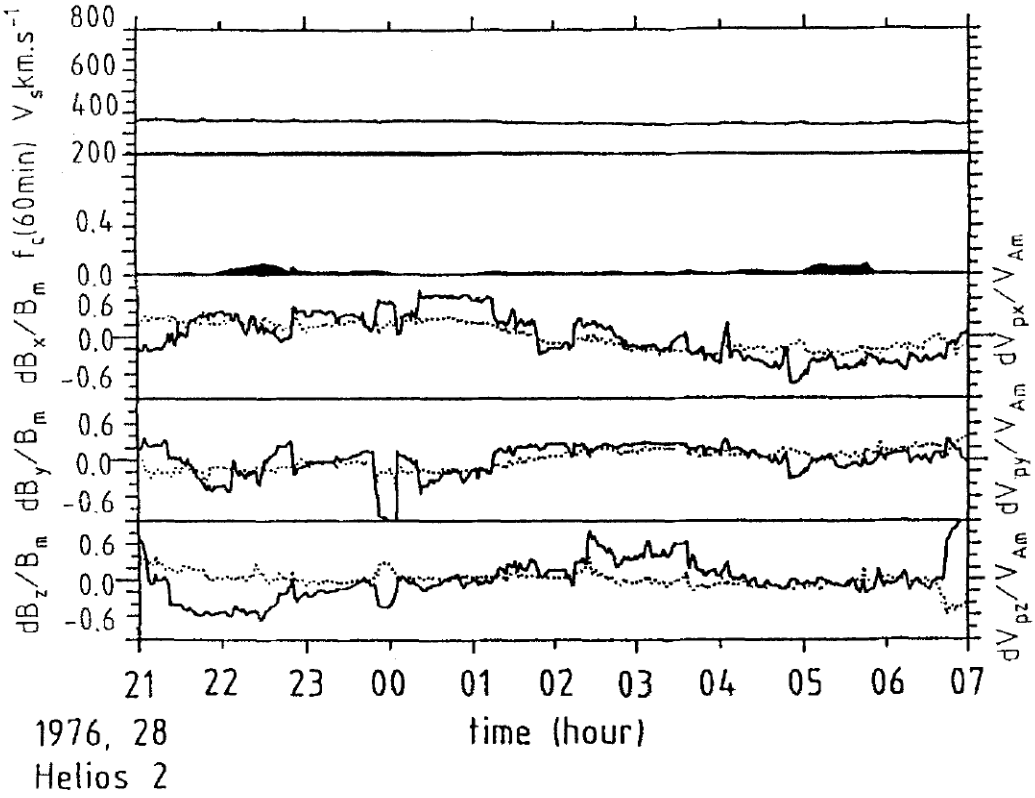

Figure 7.14: Ten hours of Helios 2 data showing nearly incompressible fluctuations in $\vec{B}$ (solid lines in bottom three panels) and $\vec{V}$ (dotted lines in bottom three panels) components. The bulk speed did not vary much (top panel) and the plasma exhibited very little compression regions as seen from the compressibility factor, f_C (second panel from top). From *Tu* and *Marsch* (1995).

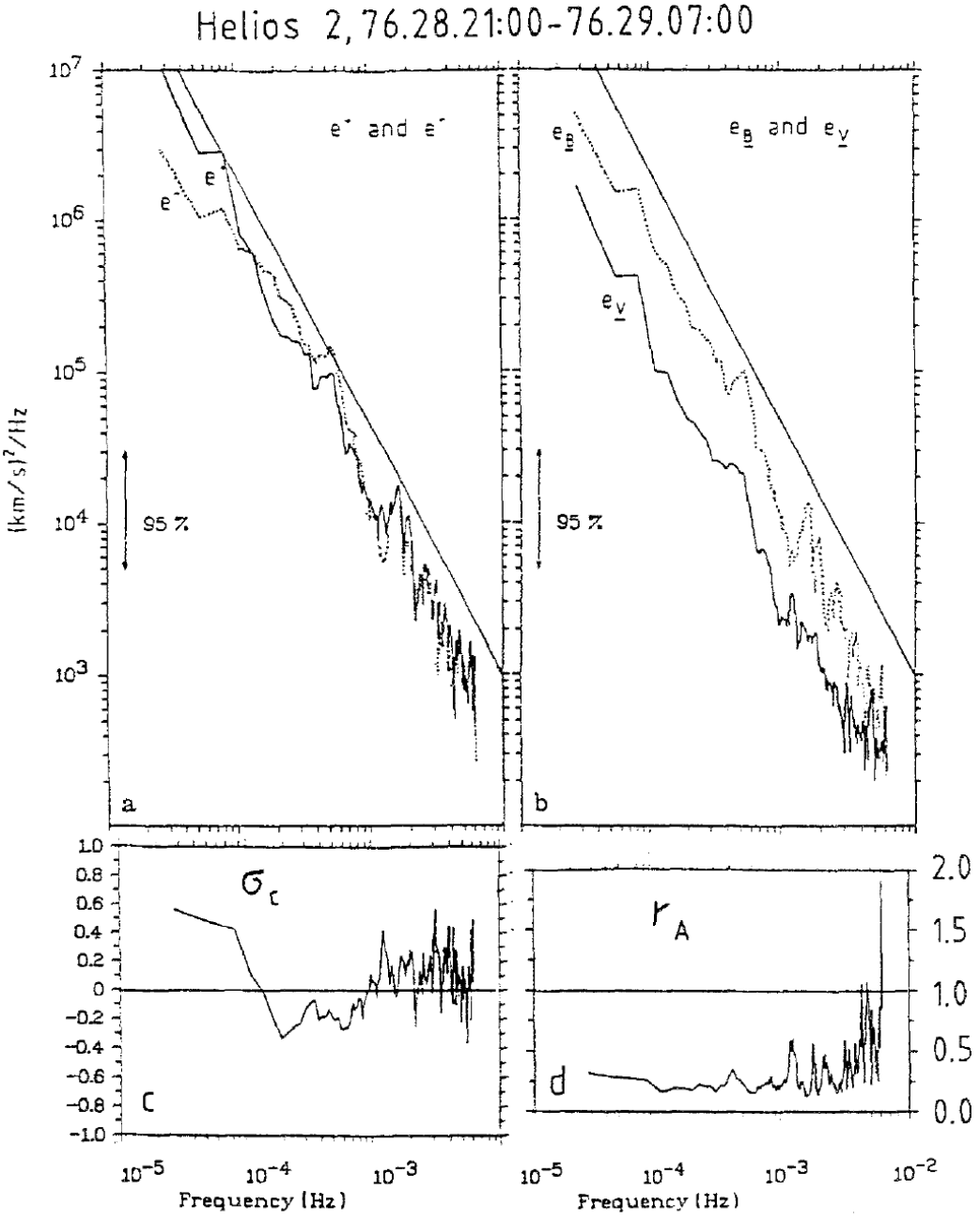

Figure 7.15: top left panel: Spectra of e^+ (solid) and e^- (dotted). Top right panel: spectra of the trace of the correlation tensor of $\delta\vec{V}_A$, $e_{\vec{B}}$ (dotted) and of the correlation tensor of $\delta\vec{V}$, $e_{\vec{V}}$ (solid line) for the time period studied in Fig. 7.14. The bottom panels show the spectra of the normalized cross helicity σ_C and the Alfvén ratio, r_A. From *Tu* and *Marsch* (1995).

The planar magnetic structures (PMS) found by *Nakagawa et al.* (1989) and *Nakagawa* (1993) are special TTs in which the magnetic field vecors all lie in parallel planes but a re highly variable in direction and magnitude within those planes. Such incompressible structures are ubiquitous in the solar wind and are an important source of turbulence in the spacecraft frame of reference. This **2-d turbulence** is quasi-static or evolves only slowly in the plasma frame of reference.

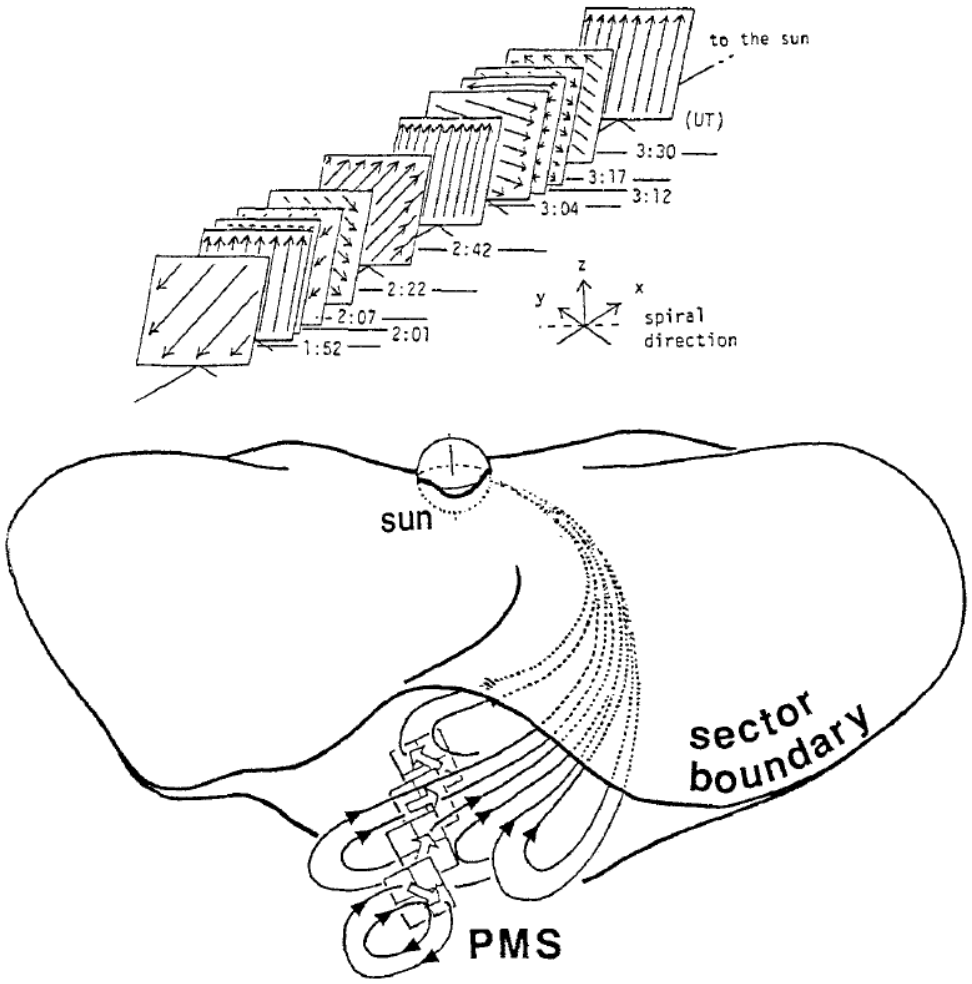

Figure 7.16: Illustration of Magnetic Field Directional Turnings (MFDTs) or Planar Magnetic Structures (PMS). From *Nakagawa et al.* (1989) and *Nakagawa* (1993).

Thus, it appears that incompressible structures need to be included in the description of solar wind fluctuations. They allow us to understand the radial evolution of σ_C and r_A. Since MFDTs are incompressible structures, they are likely to coexist with Alfvénic fluctuations in high-speed streams. *Tu*

and *Marsch* (1991) suggested that solar wind fluctuations consist of mainly two components, Alvén waves of coronal origin, and inompressible structures convected by the observer. In addition, there can be some locally generated Alfvén waves (in- and outward propagating), e.g., by the Kelvin-Helmholtz instability. Now the Alfvén waves damp and dissipate in a turbulent cascade, while the convected, quasi-static incompressible fluctuations do not. Together, this results in a decrease of r_A and σ_C with increasing heliocentric distance.

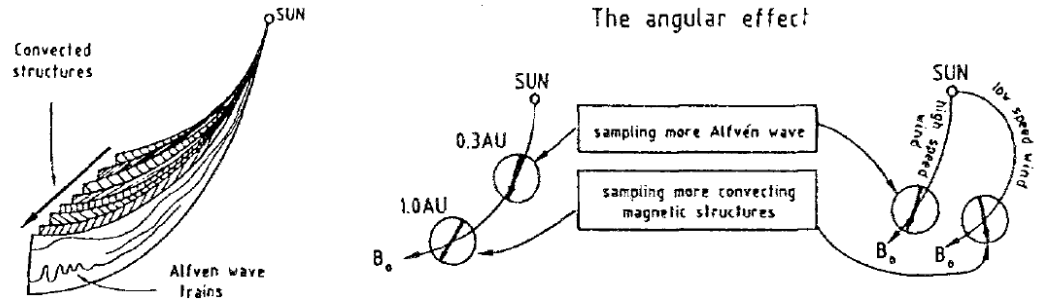

Figure 7.17: Explanation for the radial dependence of r_A and σ_C, from *Tu* and *Marsch* (1992).

Figure 7.17 shows a sketch of the model by *Tu* and *Marsch* (1995). Each sheet in the left-hand panel shows a family of correlated field lines, e.g., with a common solar source. There may be large-scale fluctuations along these fields. However, the magnetic stress tensor is too small to drive the fluid to move with considerable speed during the expansion time, so the different sheets don't mingle and remain as incompressible structures which are convected by the spacecraft. Thus, if one were to sample along one of these structures, one would measure $r_A \sim 1$ and $\sigma_C \sim 1$, if one were to measure only across such structures (perpendicular to them), one would sample only the variations from the convected structures, and hence observe $r_A \sim 0$ and $\sigma_C \sim 0$. The right-hand panel shows how this situation varies with helioscentric distance and solar wind speed. As we move further out, the average Parker spiral angle inreases and we tend to measure more across incompressible structures. This effect is stronger for slow wind than for high-speed streams because the latter have smaller average Parker angles.

A beautiful way to visualize this mixture of 2-d turbulence with "normal" or "slab" turbulence, was first shown by **?** with their "Maltese cross". Figure 7.18 shows 15-minute observations with the ISEE-3 magnetometer. For every one of the 463 observions used here, the correlation function was determined under the assumption of rotational symmetry with respect to $\vec{B}_0$. Then the two-point

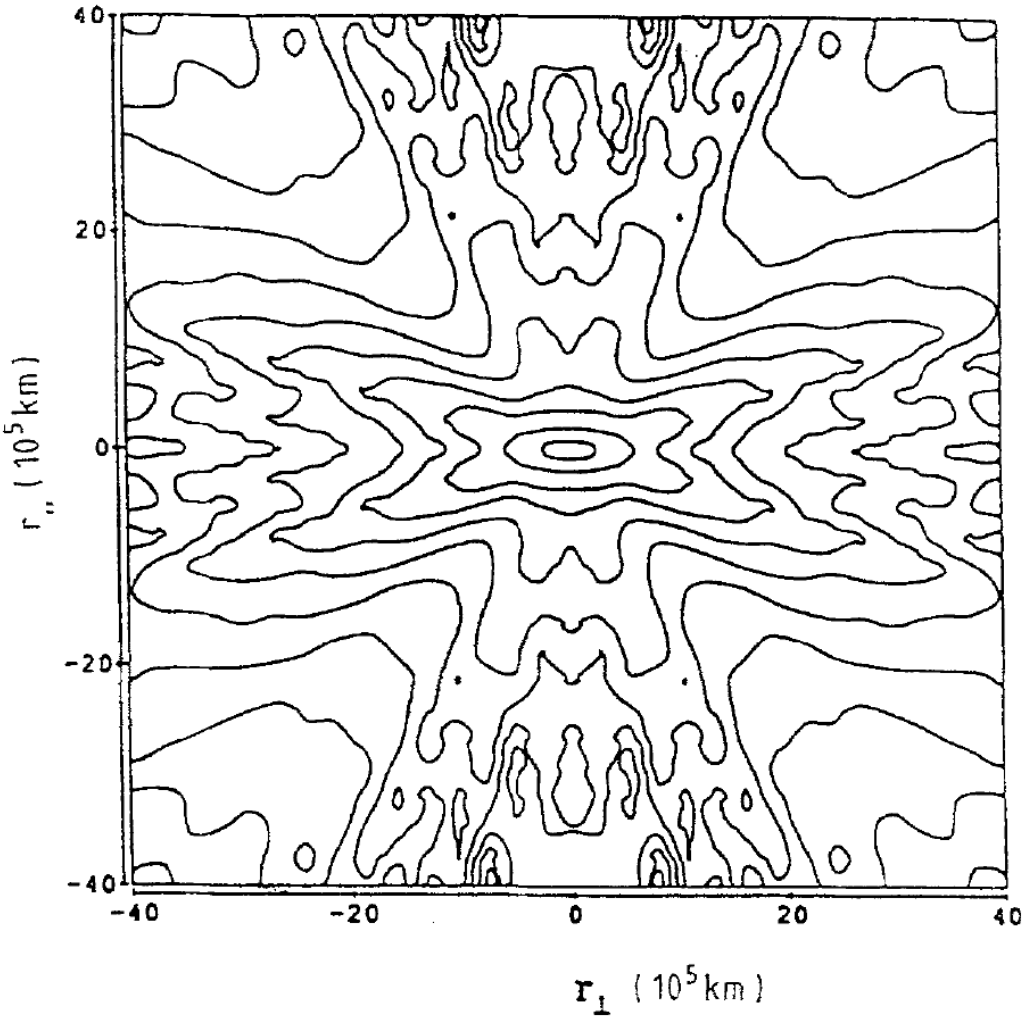

Figure 7.18: Maltese cross described by the mixture of 2-d turbulence and Alfvén waves. From ?.

correlation function,

$$R(r_\perp, r_\parallel) \tag{7.64}$$

can be computed using the frozen in approximation (or Taylor's hypothesis for MHD) and the convection of fluctuations across the spacecraft. Plotting the strength of R on a rectangular grid spanned by $r_\perp$ and $r_\parallel$ and mirroring across the two axes gives the "Maltese cross" of solar wind turbulence. It can be interpreted in the following way. Alfvén waves with $\vec{k} \parallel \vec{B}_0$ contribute to contours elongated parallel to $r_\perp$ while fluctuations of the 2-d turbulence type appear as contours elongated parallel to $r_\parallel$. Thus, this data set is not described b pure Alvénic turbulence, nor by pure isotropic turbulence. Two populations are needed - fluctuations with large correlation lengths transverse to $\vec{B}$ (Alfvénic) and fluctuations in a plane parallel to $\vec{B}$ (quasi-2-d). At small ($r_\perp < 5 \cdot 10^5$ km) separations, Alfvénic fluctuations dominate, but at $r_\parallel > 15\dot{1}0^5$km quasi-2-d fluctuations become important.

7.7 A Worked Example

solar wind

Use ACE data for exercise

Prepare python script

Chapter 8

The Fokker-Planck Formalism

In this chapter, we will consider the consequences of collisions in a plasma. We will begin with a brief repetition of some aspects of kinetic physics and the Boltzmann and Vlassov equations. We will then investigate various kinds of collisions and their treatment. Finally, we will derive the Fokker-Planck equation and consider two applications - equilibration and the slowing down of a beam in a plasma. We will closely follow the excellent text book by *Rossi* and *Olbert* (1970).

8.1 A Brief Repetition of Kinetic Physics

A plasma as well as a gas can be considered as a collection of individual particles. The exact mathematical treatment of such a collection is difficult if not impossible and, therefore, these collections of particles are treated in a statistical manner.

In the simplest case of point particles, a single particle is completely characterized by its mass, position, $\vec{x}$, and momentum, $\vec{p}$. The total energy of the particle is

$$U = \sqrt{p^2c^2 + m^2c^4} = m\gamma c^2, \tag{8.1}$$

where c is the speed of light, $\gamma = (1 - v^2/c^2)^{-1/2}$ is the Lorentz factor, $p = |\vec{p}|$, and m is the particle's rest mass. The velocity of the particle, i.e., the rate of change of its spatial position, is found by inverting eq. 8.1 to be

$$\vec{v} = \dot{\vec{x}} = \frac{c^2\vec{p}}{U}, \text{ where } \vec{p} = m\gamma\vec{v}. \tag{8.2}$$

The instantaneous condition of the particle is determined by its position and momentum vectors and may be represented by a point in the six-dimensional phase space, $(\vec{x}, \vec{p}) = (x_1, x_2, x_3, p_1, p_2, p_3)$ where $\vec{x} = (x_1, x_2, x_3)$ is the position in "ordinary" space and $\vec{p} = (p_1, p_2, p_3)$ is the position in momentum space.

As the particle moves through phase space, it describes a curve through it. The velocity of the movement is given by the six-dimensional vector $(\dot{x_1}, \dot{x_2}, \dot{x_3}, \dot{p_1}, \dot{p_2}, \dot{p_3})$. According to Newton's second law,

$$\dot{\vec{p}} = \vec{F}, \tag{8.3}$$

where $\vec{F}$ is the force acting on the particle.

The system under consideration normally consists of many particles and we make the assumption that we can divide phase space into small volumes which all still contain enough particles to make averaging over them a sensible operation. These small volumes are small compared to the characteristic scales of the system. Then we can study the properties of the bulk of all particles in a statistical manner. For this purpose, we introduce the **distribution function** $f(x_1, x_2, x_3, p_1, p_2, p_3, t) = f(\vec{x}, \vec{p}, t)$ such that

$$f(x_1, x_2, x_3, p_1, p_2, p_3, t)\ \mathrm{d}x_1\ \mathrm{d}x_2\ \mathrm{d}x_3\ \mathrm{d}p_1\ \mathrm{d}p_2\ \mathrm{d}p_3\ = f(\vec{x}, \vec{p}, t)\ \mathrm{d}^3x\ \mathrm{d}^3p \tag{8.4}$$

gives the number of particles that lie in the phase space volume $\mathrm{d}^3x\ \mathrm{d}^3p$ at time t. The integral of the distribution function, f, with respect to d^3p gives the number density of particles in the volume element, d^3x, in ordinary space,

$$n(x_1, x_2, x_3, t) = \int_\infty^\infty \mathrm{d}p_1 \int_\infty^\infty \mathrm{d}p_2 \int_\infty^\infty \mathrm{d}p_3\ f(x_1, x_2, x_3, p_1, p_2, p_3, t). \tag{8.5}$$

The distribution function f is invariant under Lorentz transformations.

Many detectors measure the so-called **differential directional intensity** of particles. This quantity is defined as a function $J(x_1, x_2, x_3, U, \vartheta, \varphi, t)$ with which $J\ \mathrm{d}A\ \mathrm{d}\omega\ \mathrm{d}U\ \mathrm{d}t$ gives the number of particles with energy between U and $U + \mathrm{d}U$ measured during a time interval $\mathrm{d}t$ to traverse the cross-sectional area $\mathrm{d}A$ from a direction within solid angle $\mathrm{d}\omega$ around the normal to $\mathrm{d}A$, see Fig. 8.1.

Next, we relate this quantity to the distribution function f. The particles incident on the detector from direction (ϑ, φ) from within solid angle $\mathrm{d}\omega$ and with energy in $U,\ U + \mathrm{d}U$ occupy a volume $p^2\ \mathrm{d}p\ \mathrm{d}\omega$ in momentum space. Here, p is the magnitude of the momentum corresponding to total energy U according to eq. 8.1. The number of particles which pass through the surface element $\mathrm{d}A$ in a time interval $\mathrm{d}t$ is just the number density in ordinary space times the space volume spanned by $\mathrm{d}A\ v\ \mathrm{d}t$, which is just $\mathrm{d}A\ v\ \mathrm{d}t\ f\ p^2\ \mathrm{d}p\ \mathrm{d}\omega$. From conservation of the number of particles, it follows that

$$J\ \mathrm{d}A\ \mathrm{d}\omega\ \mathrm{d}U\ \mathrm{d}t = f\ \mathrm{d}A\ p^2\ \mathrm{d}p\ \mathrm{d}\omega\ v\ \mathrm{d}t. \tag{8.6}$$

Differentiation of eq. 8.1 with respect to momentum p gives

$$\frac{\mathrm{d}U}{\mathrm{d}p} = \frac{c^2\ p}{U}. \tag{8.7}$$

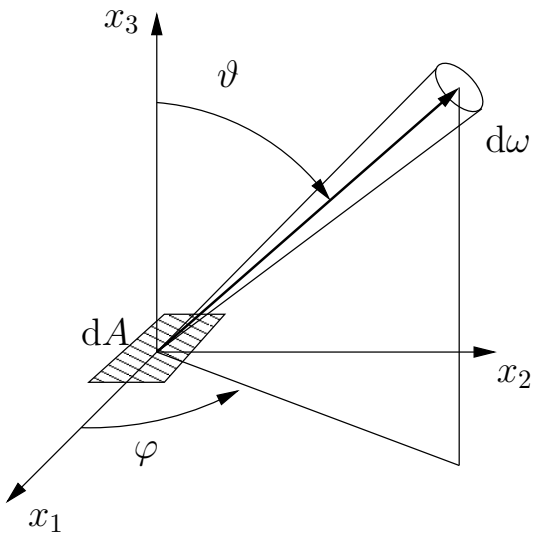

Figure 8.1: The differential directional intensity is measured by a detector with area $\mathrm{d}A$ from a direction (ϑ, φ) from the normal to $\mathrm{d}A$ and from within solid angle $\mathrm{d}\omega$. The number of particles in the energy interval between U and $U + \mathrm{d}U$ is the differential directional intensity, $J(\vec{x}, U, \vartheta, \varphi, t)$.

Replacing the velocity term by the expression given in eq. 8.2 and cancelling common factors, we have

$$J = p^2 f. \tag{8.8}$$

Thus, measurement of the differential directional intensity, J, by a sensor is equivalent to measuring the distribution function, f. This is an important finding, by measuring J and U (or p^2), you have also measured the particle distribution function, f.

8.1.1 Continuity Equation in Phase Space

If we allow processes to gradually change the momentum (vector) and position (vector) of individual particles, e.g., by external forces which result in acceleration, the distribution function is altered in a way which we we need to be able to describe quantitatively. Because of the conservation of particles, there must be a continuity equation in phase space which allows us to describe these changes under certain assumptions,

$$-\frac{\partial f}{\partial t} = \frac{\partial}{\partial x_i}\left(\dot{x}_i f\right) + \frac{\partial}{\partial p_i}\left(\dot{p}_i f\right). \tag{8.9}$$

Here, we have applied Einstein's summation convention,

$$\vec{x} \cdot \vec{y} = x_i y_i \doteq \sum_{i=1}^{3} x_i y_i.$$

We can also write the continuity equation as

$$-\frac{\partial f}{\partial t} = \vec{\nabla} \cdot (f\vec{v}) + \vec{\nabla}_p \left(f\dot{\vec{p}} \right), \tag{8.10}$$

where

$$\vec{\nabla}_p \doteq \vec{e}_1 \frac{\partial}{\partial p_1} + \vec{e}_2 \frac{\partial}{\partial p_2} + \vec{e}_3 \frac{\partial}{\partial p_3}$$

and $\vec{\nabla}$ in ordinary space is defined accordingly. Because $\vec{v}$ is only a function of $\vec{p}$, but not of $\vec{x}$, the divergence of $\vec{v}$ vanishes, $\vec{\nabla} \cdot \vec{v} = 0$. This argument is not really watertight. For instance, in a compressible gas, speed can depend on position, and the argument breaks down. But we will remedy this situation in a short while, so bear with me. Thus,

$$\vec{\nabla} \cdot (f\vec{v}) = \vec{v} \cdot \vec{\nabla} f. \tag{8.11}$$

Because of $\dot{\vec{p}} = \vec{F}$, we can write the momentum divergence as

$$\vec{\nabla}_p \cdot (f\dot{\vec{p}}) = \vec{\nabla} \cdot (f\vec{F}) = \vec{F} \cdot \vec{\nabla} f \ + \ f \ \vec{\nabla}_p \vec{F}. \tag{8.12}$$

The force acting on the particles can consist of gravitation and electromagnetic forces. We will neglect nuclear forces as they are very short ranged and because their inclusion could lead to a violation of the assumpton of particle conservation via nuclear reactions. Gravitation is often negligible in heliospheric physics, but we can, nevertheless, include it in our considerations.

$$\vec{F} = m\vec{g} + q(\vec{E} + \vec{v} \times \vec{B}) \tag{8.13}$$

The vectors $\vec{g}$ and $\vec{E}$ are independent of momentum, $\vec{p}$, and, therefore the only term to survive in eq. 8.12 is

$$\nabla_p \cdot (\vec{v} \times \vec{B}) = \vec{B} \cdot (\vec{\nabla}_p \times \vec{v}) - \vec{v} \cdot (\vec{\nabla}_p \times \vec{B}), \tag{8.14}$$

where $\vec{\nabla}_p \times$ is the curl operator in momentum space. The second term vanishes again, because $\vec{B}$ is independent of $\vec{p}$. The first term vanishes as well. According to eq. 8.2, the velocity vector is given by the gradient of total energy, U, in momentum space,

$$\vec{v} = \vec{\nabla}_p \sqrt{c^2 p^2 \ + \ m^2 c^4}.$$

Because the curl of a gradient vanishes, the first term in eq. 8.14 vanishes as well. Hence, eq. 8.12 becomes

$$\vec{\nabla} \cdot (f\dot{\vec{p}}) = \vec{F} \cdot \vec{\nabla}_p f. \tag{8.15}$$

Using eqs. 8.11 and 8.15, we can rewrite the continuity equation (eq. 8.9) in simplified form,

$$-\frac{\partial f_a}{\partial t} = \vec{v} \cdot \vec{\nabla} f_a \; + \; \vec{F}_a \cdot \vec{\nabla}_p f_a. \tag{8.16}$$

If there are several different particle species in the system, this equation needs to be replaced by a set of equations, one each for each particle species. We have indicated this by adding an index a to mark different particle species.

In fact, the independence of $\vec{v}$ on $\vec{x}$ and of $\vec{F}$ on $\vec{p}$ is not required separately. Consider the following generalized argument. From Hamiltonian mechanics we know that

$$\dot{x}_i = \frac{\partial H}{\partial p_i}, \quad \text{and} \quad \dot{p}_i = -\frac{\partial H}{\partial x_i}. \tag{8.17}$$

Hence, differentiating the left-hand equation with respect to x_i and the right-hand equation and with respect to p_i, we have an identity,

$$\frac{\partial \dot{x}_1}{\partial x_i} = \frac{\partial^2 H}{\partial x_i \partial_i} = -\frac{\partial \dot{p}_1}{\partial p_i}. \tag{8.18}$$

However, this entails that the first and third term in the continuity equation (eq. 8.9) cancel,

$$\begin{aligned} -\frac{\partial f}{\partial t} &= \frac{\partial}{\partial x_i}\left(\dot{x}_i f\right) + \frac{\partial}{\partial p_i}\left(\dot{p}_i f\right), \\ &= \frac{\partial \dot{x}_i}{\partial x_i} \; f \; + \dot{x}_i \frac{\partial f}{\partial x_i} \; + \; \frac{\partial \dot{p}_i}{\partial p_i} \; f \; + \; \dot{p}_i \frac{\partial f}{\partial p_i}, \quad \text{i.e.,} \\ -\frac{\partial f}{\partial t} &= \dot{x}_i \frac{\partial f}{\partial x_i} \; + \; \dot{p}_i \frac{\partial f}{\partial p_i} \; = \; \vec{v} \cdot \vec{\nabla} f_a \; + \; \vec{F}_a \cdot \vec{\nabla}_p f_a. \end{aligned} \tag{8.19}$$

Thus, we have just found a more general derivation of the continuity equation and remedied the situation on page 162. We found the same final result as in eq. 8.16, but without taking recourse to hand-waving arguments.

As long as the forces are entirely determined by external agents, e.g., by the Earth's gravitational and magnetic field in the case of the magnetosphere, this equation, together with the prescriptions for the external fields, fully describes the system. However, if the electromagnetic field is determined by the charge and current distributions of the particles, as is the case in highly ionized plasmas such as the interplanetary plasma, a self-consistent set of equations must be found. This is the subject of plasma physics or the statistical or kinetic description of that subject and will not be treated here.

8.1.2 The Vlasov Equation

Equations 8.16 and 8.19 are often called the **Vlasov equations**. It describes systems of particles for which collisions are unimportant. This set of equations looks innocent, deceitfully simple. In fact, it is not. As soon as electric

charge and current densities in the plasma and maybe even self-gravitation play an appreciable role in the net forces acting on the particles, these forces, $\vec{F}_a$, depend on the distribution functions f_a. Mathematically speaking, the components $F_{a,i}$ of the forces become functionals of the distribution functions f_a (often of many particle species), and, hence, the Vlasov equations turn into a set of non-linear integro-diffrential equations. No general methods exist for solving such problems and, therefore, only solutions for special cases have been found.

8.1.3 The Boltzmann Equation

The solution of the Vlasov equations becomes even more complex when collisions are play an important role in the physics of the system, such as when particles can be scattered on temporal and spatial scales which are small compared with the dimensions of the system. Such collisions can change the momentum by a large amount, or, in other words, the forces acting on the particles can change considerably on scales smaller than the volume elements over which we average the particles. In ordinary space, this could be, e.g., the Debye-radius. In this case, we can no longer average over all particles in that phase-space volume and the fluid description ought to break down. However, we can resort to the following prescription when collisions are important but still rare. In addition to the underlying flow of particles through phase space, we need to add the possibility of occasional large changes in the momentum of particles.

Formally, these changes can be represented by a collision term in the continuity equation which serves as a "source term". We then obtain the so-called **Boltzmann equations**,

$$\frac{\partial f_a}{\partial t} + \vec{v} \cdot \vec{\nabla} f_a \; + \; \vec{F}_a \cdot \vec{\nabla}_p f_a = \left(\frac{\delta f_a}{\delta t} \right)_{\text{coll}} . \tag{8.20}$$

A similar equation was first investigated by Boltzmann when he studied ordinary gases and Brownian motion.

It is sometimes difficult to keep apart the physics that contributes to the collision term and that contributes to the global average forces $\vec{F}_a$. A simple case is that of an ordinary gas in a gravitational field. Then the average force is well described by gravitation and the collision term is entirely due to the forces acting during the interaction of gas molecules when they approach to scatter or interact. Gravitational forces between the molecules are entirely negligible. A complicated case is that of a plasma where both microscopic and macroscopic forces have the same origin in the charge and current densities of the particles. In this case, one needs to somehow separate the electromagnetic field into a regular, average background field, $\vec{F}$ and a stochastic field that is the basis of the collision term. However, how this separation is to be performed is again often strongly dependent on the problem and no standard method exists.

In some cases, e.g., when particle energies are so large as to exceed the rest mass of some of the particle species, particles can also be created and destroyed, in some cases, energy is lost due to radiation (e.g., bremsstrahlung). Particles may also decay, leading to destruction of particles, but also to creation of new particles. In this case the Boltzmann equation must be generalized to include these effects as well, which is done by adding additional "collision terms",

$$\frac{\partial f_a}{\partial t}+\vec{v}\cdot\vec{\nabla} f_a + \vec{F}_a\cdot\vec{\nabla}_p f_a = \left(\frac{\delta f_a}{\delta t}\right)_{\text{coll}}+\left(\frac{\delta f_a}{\delta t}\right)_{\text{creation}}+\left(\frac{\delta f_a}{\delta t}\right)_{\text{destruction}}+\left(\frac{\delta f_a}{\delta t}\right)_{\text{radiation}} \tag{8.21}$$

In section 8.2 we will derive a method how to compute collision terms in some special cases, the so-called Fokker-Planck method.

8.1.4 Liouville's Theorem

In the special case where collisions and other losses or scattering mechanisms are unimportant, the Vlasov equation holds. It can be rewritten in the following form

$$\frac{\partial f_a}{\partial t} + \vec{v}\cdot\vec{\nabla} f_a \;+\; \vec{F}_a\cdot\vec{\nabla}_p f_a \doteq \frac{\mathrm{d}f_a}{\mathrm{d}t} = 0, \tag{8.22}$$

where $\frac{\mathrm{d}}{\mathrm{d}t}$ is the total derivative with respect to time. The total derivative with respect to time of f_a vanishes, i.e., f_a is conserved. In other words, as we move along through phase space with a particle, the distribution function, f_a, of neighboring particles remains constant. In again other word, this tells us that, in phase space, the gas formed by the particles is incompressible. This is known as **Liouville's theorem**. Basically, what it tells us is the following. Imagine a surface in phase space that encloses a number of particles. As the particles move through phase space according to the respective momentum equations the shape of the surface is constantly being changed in such a way that 1.) the number of particles inside the surface remains conserved, and 2.) the volume enclosed by the surface is constant in time. In other words, phase space is incompressible. In fact, that is also exactly what eqs. 8.18 are telling us, as we can see by considering the following analogy from ordinary fluid dynamics.

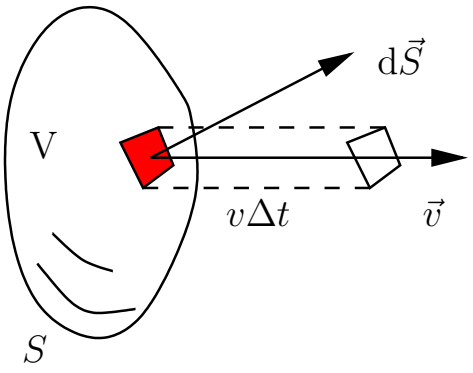

Figure 8.2: Analogy with a compressible comoving fluid control volume.

Consider a control volume comoving with the fluid. It will always contain the same number of particles (ignoring diffusion), and so its mass is conserved in time, $\mathrm{d}m/\mathrm{d}t = 0$. However, it can be compressed, and then the total volume is not conerved, $\mathrm{d}V/\mathrm{d}t \neq 0$, and hence mass density is also not conserved, $\mathrm{d}\rho/\mathrm{d}t \neq 0$. Fig. 8.1.4 shows an example.

Let us consider the change of its volume, V, which is due to the motion of $\mathrm{d}\vec{S}$ with velocity $\vec{v}$. Then the change of volume will be

$$\Delta V = (\vec{v}\Delta t) \cdot \mathrm{d}\vec{S}.$$

Using Gauss's law and dividing by Δt, we obtain

$$\frac{\Delta V}{\Delta t} = \int\int\int_V \vec{\nabla} \cdot \vec{v} \mathrm{d}V.$$

Next we assume that V is very small, $V \to \delta V$, in fact so small, that $\vec{\nabla} \cdot \vec{v} =$ const. over δV. Then we have

$$\frac{\Delta \delta V}{\Delta t} = \int\int\int_{\delta V} \vec{\nabla} \cdot \vec{v} \mathrm{d}V = \left(\vec{\nabla} \cdot \vec{v}\right) \delta V,$$

exactly because $\vec{\nabla} \cdot \vec{v} =$ const. over δV. Taking the left- and right-most terms, we find that

$$\vec{\nabla} \cdot \vec{v} = \frac{1}{\delta V} \cdot \frac{\Delta \delta V}{\Delta t}, \tag{8.23}$$

in other words, the divergence of the velocity vector field equals the relative temporal change of the volume. In yet other words, if the volume changes with time, the divergence of the velocity field must be non-zero, or if $\vec{\nabla} \cdot \vec{v} = 0$, we have an incompressible fluid.

Now inspect equation 8.18. What it tells us is nothing else, than that the phase space volume is incompressible.

Of course, Liouville's theorem also maps to the differential directional intensity, $J = p^2 f$. From Liouville's theorem, it follows that the quantity J/p^2 must also be conserved along a trajectory in phase space. Consider a particles with momentum $\vec{p}$ and corresponding energy U in ordinary space. If we measure $J(U)$ in the direction of $\vec{p}$, i.e., tangentially to the particle trajectory, then Liouvilles theorem states that J/p^2 has the same value at all points along the trajectory. If the particles momentum changes, then so will $J(U)$, but in such a manner as to conserve J/p^2 (eq. 8.8).

8.2 The Fokker-Planck Method

In this section we will derive the Fokker-Planck equation and introduce the Fokker-Planck Formalism for deriving collision terms for some special cases. For this we need to consider the random-walk problem and binary collisions in a plasma. We will then derive the Fokker-Planck equation and give some applications.

8.2.1 Random Walk in one Dimension

We will follow *Chandrasekhar* (1943) in his derivation of the problem of a random walk in one dimension. Such a problem was first studied by *Pearson* (1905) who formulated the problem as we will here. A more general fomulation of the problem was given by *Rayleigh* (1880). See the bibliographic notes in *Chandrasekhar* (1943) for more information about the history of the problem. While the problem will need to be applied in three dimensions, its properties are more clearly seen in just one dimension and, therefore, we consider it in only one dimension.

Consider a particle (or a drunken sailor) which takes a series of steps of equal length, l, in either forward or backward direction with equal probability, $p = 1/2$. After taking N steps, it could be at any of the points

$$-Nl, (-N+1)l, \ldots, -1, 0, 1, \ldots, (N-1)l, Nl.$$

The situation is shown in Fig. 8.3. Obviously, there are different paths that can lead to a position ml after N steps. Therefore, we need to ask the question what is the probability $W(m, N)$ that the particle be at location m after N steps?

The probability of any one given sequence of N steps is

$$p_N = \left(\frac{1}{2}\right)^N$$

because the probability of moving forward or backward is always 1/2. In order to arrive at position ml, more steps must be taken in the positive direction (for positive m), to be more precise, n_p steps must be taken in the positive, and n_n steps in the negative direction. The sum $n_p + n_n$ must equal N, the difference, $n_p - n_n = m$. Hence, $n_p = (N+m)/2$ and $n_n = (N-m)/2$. If N is odd, then m is always odd as well, so we have no difficulties with non-integer numbers n_p or n_n. The number of distinct sequences (n_p, n_n) is given by

$$W(m, N) = \frac{N!}{\left(\frac{1}{2}(N+m)!\right)\left(\frac{1}{2}(N-m)!\right)}\left(\frac{1}{2}\right)^N, \tag{8.24}$$

which is the Bernoulli distribution. The expectation value for m, $\langle m \rangle$ vanishes, $\langle m \rangle = 0$, as expected. The expectation value for m^2 is given by $\langle m^2 \rangle = N$. These are properties of the Bernoulli distribution.

We now make an important assumption. In the case that N is large and $m \ll N$ we can simplify the Bernoulli distribution by applying Stirlings approximation for the factorial,

$$\log n! = (n + \frac{1}{2}) \log n \; - \; n \; + \frac{1}{2} \log 2\pi \; + \; O(n^{-1}), \quad \text{for} \;\; n \longrightarrow \infty.$$

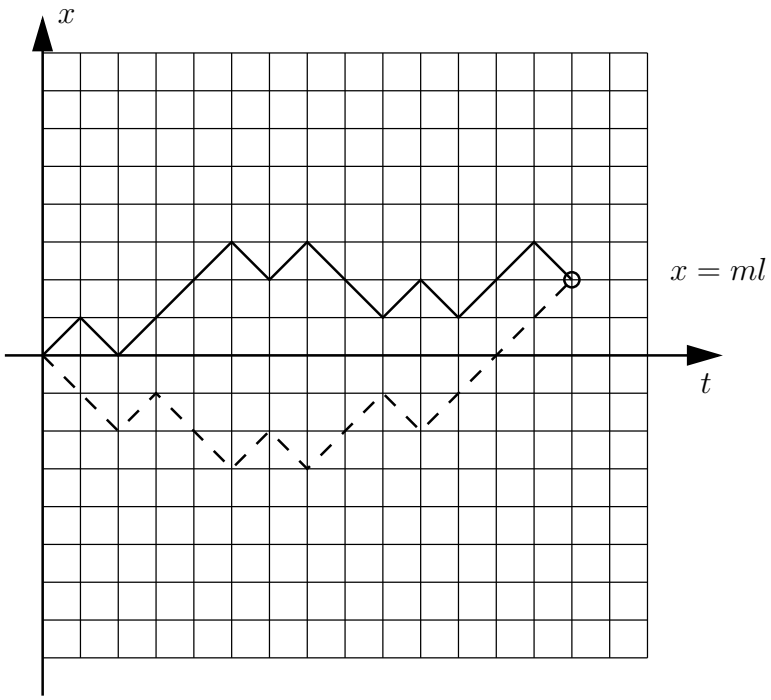

Figure 8.3: Random walk in one dimension. Several paths lead to location m. The probability distribution is given by eq. 8.24.

We then have

$$\begin{aligned}\log W(m,N) &\approx (N+\frac{1}{2})\log N \\ &\quad -\frac{1}{2}(N+m+1)\log\left(\frac{N}{2}\left(1+\frac{m}{N}\right)\right) \\ &\quad -\frac{1}{2}(N-m+1)\log\left(\frac{N}{2}\left(1-\frac{m}{N}\right)\right) \\ &\quad -\frac{1}{2}\log 2\pi \ -N\log 2, \end{aligned} \tag{8.25}$$

where the last term comes from the $(1/2)^N$ term. Because $m \ll N$ we can also expand the logarithm

$$\log\left(1\pm\frac{m}{N}\right) = \pm\frac{m}{N} - \frac{m^2}{2N^2} + O\left(\frac{m^3}{N^3}\right).$$

With this approximation eq. 8.25 becomes

$$\begin{aligned}\log W(m,N) &\approx (N+\frac{1}{2})\log N - \frac{1}{2}\log 2\pi \ -N\log 2 \\ &\quad -\frac{1}{2}(N+m+1)\left(\log N \ -\log 2 \ +\frac{m}{N} \ - \ \frac{m^2}{2N^2}\right) \\ &\quad -\frac{1}{2}(N-m+1)\left(\log N \ -\log 2 \ -\frac{m}{N} \ - \ \frac{m^2}{2N^2}\right) \end{aligned} \tag{8.26}$$

We can further simplify this equation and obtain

$$\log W(m,N) \approx -\frac{1}{2}\log N \ + \ \log 2 - \frac{1}{2}\log 2\pi \ - \frac{m^2}{2N}. \tag{8.27}$$

Exponentiating, we finally find the expression for $W(m,N)$ in the limit of large N and $m \ll N$,

$$W(m,N) = \left(\frac{2}{\pi N}\right)^{1/2}\exp\left(-\frac{m^2}{2N}\right). \tag{8.28}$$

Clearly, for large N, we will be more interested in measuring the displacement, $x = ml$, from the original position of the particle. If we further consider intervals, Δx, which are large compared with a single step, l, we can ask for the probability, $W(x)\Delta x$, that the particle is likely to be in interval $[x, x+\Delta x]$ after$N$ steps (or a time $t = N\tau$, where τ is the time between steps.). This is given by

$$W(x,N)\Delta x = W(m,N)\left(\frac{\Delta x}{2l}\right), \tag{8.29}$$

because m must be even or odd, depending on whether N is even or odd. In other words, because Δm has to be $\Delta m = 0, \pm 2, \pm 4, \ldots$. Inserting $m = x/l$ and eq. 8.28 in this result, we obtain

$$W(x, N) = \frac{1}{\sqrt{2\pi N l^2}} \exp\left(-\frac{x^2}{2Nl^2}\right). \tag{8.30}$$

In the final step, we will now consider what happens to the particle in time. Suppose the particle undergoes $\nu = 1/\tau$ scatterings or displacemnts per unit time, then we can write the probability $W(x,t)\Delta x$ that the particle be in the interval $[x, x + \Delta x]$ after a time t as

$$W(x,t)\Delta x = \frac{1}{2\sqrt{\pi D t}} \exp\left(-\frac{x^2}{4Dt}\right) \Delta x, \tag{8.31}$$

where we have written the diffusion constant

$$D = \frac{1}{2}\nu l^2.$$

Eq. 8.31 is the general solution to the problem of random walks. It is also the solution to diffusion problems and many other problems.

We have not discussed what is the cause of the scattering or displacement events discussed in the previous paragraphs. In this chapter we will assume that displacements are due to binary collisions between particles. Therefore, we will briefly repeat the physics of such collisions in a plasma as it is more complicated in a plasma than for simple binary collisions of isolated particles.

8.2.2 A Brief Repetition of Binary Collisions

Consider an elastic collision between two particles of masses m_1 and m_2 and charges q_1 and q_2 as shown in Fig. 8.4. The asymptotic angle is given by (see, e.g., volume I of *Landau* and *Lifschitz* (1981)) $\theta = \pi - 2\alpha$ and can be written as

$$\tan\frac{\theta}{2} = \frac{q_1 q_2}{\mu v_0^2 b}, \tag{8.32}$$

where $\mu = m_1 m_2/(m_1 + m_2)$ is the reduced mass. Next we consider the flux of particles which flows through the circular rings in Fig. 8.4. All particles with a given impact parameter $(b, b+\mathrm{d}b)$ are deflected into the angular interval $(\theta, \theta + \mathrm{d}\theta)$. They first cross the area $A_1 = 2\pi b\ \mathrm{d}b$, then through $A_2 = \sigma(\theta) 2\pi \sin\theta\ \mathrm{d}\theta$. The flux through these two cross-sectional areas must be conserved, every particle that enters A_1 is scattered into angle θ. This defines the scattering cross section, $\sigma(\theta)$

$$\sigma(\theta) \doteq \frac{b}{\sin\theta}\frac{\mathrm{d}b}{\mathrm{d}\theta}. \tag{8.33}$$

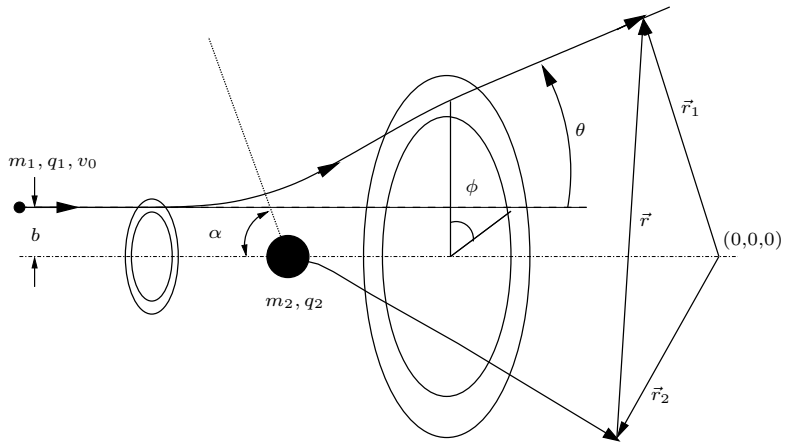

Figure 8.4: Geometry for two-body collisions between particles of masses m_1 and m_2 and charges q_1 and q_2.

After some calculation one obtains the expected expression for the scattering cross section of Coulomb collisions, the well-known Rutherford cross section,

$$\sigma(\theta) = \left(\frac{q_1 q_2}{2\mu v_0^2 \ \sin^2(\theta/2)} \right)^2 . \tag{8.34}$$

Armed with this expression we can now calculate scattering properties in a plasma. This is more complicated than it sounds because of the long range of the Coulomb force. In classical scattering situations such as those described by the Boltzmann equation, the interaction between two particles is considered to be instantaneous. This is certainly not the case for interactions governed by the long-ranged Coulomb force. On the other hand, in a plasma a positive charge is shielded by electrons (Debye-shielding) and vice versa. Therefore, the Coulomb force acting between two particles a and b will not extend to infinity as it would in empty space, but will be limited to a volume largely determined by the Debye length,

$$\lambda_D = \sqrt{\frac{\varepsilon_0 k_B T_e}{n_e e^2}}. \tag{8.35}$$

In interplanetary space the Debye length is on the order of several meters. Normal flow speeds are hundreds of km per second, and so a typical interaction time is given by $\Delta t = \lambda_D / v \approx 10^{-5}$ seconds which is short compared with typical time scales of the plasma, such as relaxation time, growth time of instabilities, etc. Thus, Debye shielding allows us to use the same formalisms as used for classical scattering theory. Nevertheless, we should not feel too comfortable with this situation. There are typically some 10^6 particles within a Debye sphere and these particles are definitely not statistically independent.

Thus, we are now faced with the problem of correlated many-particle ensembles which is not described by the classical Ansatz of one-particle distribution functions, f_a, as we used it in the introduction to this chapter.

There is a further complication that we need to mention. Although we can treat scattering as an instantaneous process, as we just saw in the previous paragraph, one other important assumption of classical scattering theory is not fulfilled. There one normally assumes that the collision process results in a discontinuous velocity change $|\Delta\vec{v}|$ which is of the order of the particles velocity before the scattering, $|\vec{v}'|$. In the Fokker-Planck formalism to be derived below, we will make the opposite assumption, namely that the change in velocity is small enough to make certain Taylor expansions good approximations that can be truncated after the second-order terms in Δv. Obviously, this approach will not be able to correctly describe the large-angle scattering of close Coulomb collisions. However, as we will see shortly, such large-angle scatterings are much rarer than small-angle scatters. In fact, the average time needed for a deflection by 90 degrees is shorter for a succession of multiple small-angle scatterings than for a single large scatter. It is because of this property, which we will derive shortly, that we can apply the Fokker-Planck formalism to a plasma. This makes life a lot easier because it leads to a second-order partial differential equation governing the distribution function, f_a, and we do not need to consider the much more complicated integro-differential equations which we would have to consider if we allowed large deflections.

We are now ready to compute the scattering of a particle in a plasma. We begin by investigating the scattering cross section for scattering by 90 degrees. The impact parameter that leads to a 90-degree scatter is

$$b_{\pi/2} = \frac{q_1 q_2}{\mu v_0^2}, \tag{8.36}$$

(see eq. 8.32) and the corresponding cross section for scattering by at least 90 degrees is

$$\sigma_{\pi/2} = \pi\ b_{\pi/2}^2 = \pi \left(\frac{q_1 q_2}{\mu v_0^2}\right)^2. \tag{8.37}$$

Next we compare the cross sections for small-angle scattering and one single 90-degree scatter. We will see that the probability of multiple scatters leading to a 90-degree deflection is much larger than that of one single collision to lead to such a deflection.

In order to investigate multiple scattering by a small angle we consider a particle moving along the z axis. When it collides with another particle, it will experience a change in its transverse velocity. For simplicity, we only consider one component of that change, e.g., the x component. After N such collisions the total change of velocity in x direction is given by

$$\Delta v_x = \sum_{i=1}^{N} (\Delta v_x)_i. \tag{8.38}$$

For small-angle scattering the change in momentum is small compared to the total momentum and the directional change for small angles can be approximated by

$$\Delta\theta = \frac{2q_1q_2}{\mu v_0^2 b}. \tag{8.39}$$

Obviously, this is only possible for large impact parameters. As a particle moves through a plasma with n scattering centers per unit volume the average change of its direction will cancel out, a similar number of scatters will lead to positive and negative changes because scattering has equal probabilities in all directions. However, the mean square displacement from the original direction will not vanish. The particle will appear to diffuse in direction space. The expectation value of the squared deviation from the original direction is given by

$$\left\langle (\Delta\theta)^2 \right\rangle = \int_{\Delta\theta_{\min}}^{\Delta\theta_{\max}} \mathrm{d}(\Delta\theta)\ (\Delta\theta)^2 F(\Delta\theta), \tag{8.40}$$

where $F(\Delta\theta)$ is the number of collisions which result in a change of direction into the interval $(\Delta\theta, \Delta\theta + \mathrm{d}(\Delta\theta))$. The integral has a lower and an upper integration limit which requires further discussion. Let us consider the corresponding impact parameters $b_{\min} = 2q_1q_2/(\mu v_0^2 \Delta\theta_{\min})$ and $b_{\max} = 2q_1q_2/(\mu v_0^2 \Delta\theta_{\max})$. The number of collisions in an angular interval $(\Delta\theta, \Delta\theta + \mathrm{d}(\Delta\theta))$ is given by

$$F(\Delta\theta)\mathrm{d}(\Delta\theta) = nL2\pi\ b\ \mathrm{d}b, \tag{8.41}$$

as the particle moves along a stretch of length L. Using this expression we can express the square of the directional change by an integral over a range of impact parameters

$$\begin{aligned} \left\langle (\Delta\theta)^2 \right\rangle &= \frac{8\pi n L q_1^2 q_2^2}{\mu^2 v_0^4} \int_{b_{\min}}^{b_{\max}} \frac{\mathrm{d}b}{b}, \\ &= \frac{8\pi n L q_1^2 q_2^2}{\mu^2 v_0^4} \ln \frac{b_{\max}}{b_{\min}}. \end{aligned} \tag{8.42}$$

This is where we can appreciate the technical motivation of the integration limits. The integral is logarithmically divergent for $b_{\min} \longrightarrow 0$ or $b_{\max} \longrightarrow \infty$. This divergence is a consequence of the long range of the Coulomb force. However, as already mentioned, this long range is not justified in a plasma where a charge is screened on a length scale given by the Debye length, λ_D. Then the effective potential is not the ordinary Coulomb potential, $\Phi = -q_1q_2/(4\pi\varepsilon_0 r)$, but is given by $\Phi = -(q_1q_2/(4\pi\varepsilon_0 r))\exp(-r/\lambda_D)$. But then the result that was just derived is not truly valid but only a good approximation for impact pameters which are smaller than the Debye length, λ_D. The deflection of the particle is very small for larger impact parameters. Thus we can use the Debye length as a good approximation for the upper integration limit,

$$b_{\max} = \lambda_D = \sqrt{\frac{\varepsilon_0 kT}{ne^2}}. \tag{8.43}$$

Of course, this is a very coarse approximation, such a sudden cut off of the integration at $b_{\max}$ hardly does justice to the Debye screening in the plasma. However, this imprecise treatment does not affect the final result in a major way because the upper integration limit only enters into the final result logarithmically. The advantage of this treatment is that we do not need to treat scattering in a full Yukawa potential, $\Phi = -(q_1 q_2/(4\pi\varepsilon_0 r))\exp(-r/\lambda_D)$.

The lower integration limit must fulfill two goals. On the one hand, it needs to get rid of the logarithmic divergence of the integral, on the other hand, it needs to recover our approximation of small angle scattering. As soon as the impact parameter gets too small, the approximation of eq. 8.39 is no longer valid (the tangent no longer equals the argument). This approximation is only valid for $\Delta\theta \ll 1$ and so we set $(\Delta\theta_{\max}/2) = 1$ and write for the kinetic energy, $mv_0^2/2 = 3kT/2$, to obtain an expression for $b_{\min}$,

$$b_{\min} \approx \frac{q_1 q_2}{\mu v_0^2} \approx \frac{q_1 q_2}{3kT}. \tag{8.44}$$

Here too, the very coarse approximation is somewhat softened by the logarithmic dependence of the result on $b_{\min}$. With these two limits, we can now give the mean squared deflection,

$$\left\langle (\Delta\theta)^2 \right\rangle = \left(\frac{8\pi n (q_1 q_2)^2}{\mu^2 v_0^4} \ln\Lambda \right) L, \tag{8.45}$$

where

$$\Lambda \doteq \frac{b_{\max}}{b_{\min}} = \frac{3}{q_1 q_2 e} \left(\frac{\varepsilon_0 k^3 T^3}{n} \right)^{1/2} \tag{8.46}$$

is the argument of the so-called **Coulomb-logarithm** and L is the path length which the particle moves through the plasma.

We can now finally determine the path length which leads to a deflection by 90 degrees by multiple scattering by setting $\langle \Delta\theta^2 \rangle = 1$ and solving for L. Again, this result is not very precise because the quadratic addition of the angular deflections $\langle \Delta\theta^2 \rangle = 1$ in x and y direcion do not quite add up to 90 degrees - but nearly.

$$L_{\pi/2} = \left\{ 8\pi n \left(\frac{q_1 q_2}{\mu v_0^2} \right)^2 \ln\Lambda \right\}^{-1}. \tag{8.47}$$

Thus, the cross section for multiple scattering to 90 degrees is given by

$$\sigma_{\pi/2} \doteq \frac{1}{n L_{\pi/2}} = 8\pi \left(\frac{q_1 q_2}{\mu v_0^2} \right)^2 \ln\Lambda. \tag{8.48}$$

We can now compare this result with the cross section for scattering by 90 degrees in a single scatter, eq. 8.37,

$$\frac{\sigma_{\pi/2\mathrm{m}}}{\sigma_{\pi/2\mathrm{s}}} = 8 \ln\Lambda. \tag{8.49}$$

Because the Coulomb logarithm lies between 15 and 30 for most plasmas (and, hence, also for heliospheric plasmas) it is clear that multiple scattering is the dominant process and that scattering by 90 degrees is mainly achieved by a succession of scatterings by small angles.

8.2.3 Derivation of the Fokker-Planck Equation

Next, we want to describe the random (stochastic) motion of a collection of particles, $f(\vec{v}, t)$, with a partial differential equation, the so-called Fokker-Planck equation. This is not as straightforward as it may sound for the following reasons.

Sofar we have assumed that all quantitites in the plasma change slowly. This means that the plasma was always in thermodynamic equilibrium, an assumption which is not always met. For example, in interplanetary space, the electron temperature is quite different from the temperature of the ions, and these are proportional to mass, at least in the high-speed solar wind. We have interpreted this as a consequence of only very rare collisions between ions and electrons and ions and ions and that the coupling between the particles constituting the plasma occurs predominantly via waves. So what happens in regions of the heliosphere in which collisions occur on a time scale which is too slow to allow the plasma to equilibrate? In other words, how can we describe a plasma which changes faster than it can reach equilibrium, i.e., faster that the relaxation time? An example is a beam of energetic particles entering a slow plasma, or also the behavior of a plasma in the vicinity of a heliospheric shock. In this latter example, the collision time between two particles is very long. Phenomena which are related to collisions between particles are often called transport phenomena, examples include electric conductivity of a plasma, or the behavior of a plasma with given initial and end conditions.

To investigate such situations we begin by considering binary collisions[1] and the resulting deflection of the particles. Based on these considerations, we will derive he so-called Fokker-Planck formalism with which one can describe the various phenomena touched upon above. We will only consider a fully ionized plasma. If collisions with neutral particles play an important role, then this problem must be treated differently, e.g., with a so-called Lorentz model. Of course we will not be able to consider every single collision between two particles in the heliospheric plasma, but we will pick out the relevant ones and treat them in a statistical manner. On page 174 we showed that many scatters by small angles are faster at producing a large deflection than waiting for one single scattering event that leads to a large deflection (eq. 8.49). This observation allows us to develop models for diffusion, electric conductivity and other transport phenomena in a plasma. They can be developed using the

[1] If binary collisions are replaced by instabilities and associated similar phenomena, then these are called 'anomalous' transport phenomena.

Fokker-Planck equation which we are going to derive here. Going to higher orders in the expansion parameter $l/(n\lambda_D)$ leads to the so-called Balescu-Lenard equations which need to be derived from the primitive kinetic equations. However, they do not change the end result appreciably, so we will not do so, but consider only the change of the velocity distribution function (VDF), $f(\vec{v},t)$ with time in a plasma in which the electrons and ions are distributed with just this VDF. Let the probability that a particle changes ist velocity $\vec{v}$ by $\Delta\vec{v}$ in a time Δt be given by $F(\vec{v},\Delta\vec{v})$. Then the VDF $f(\vec{v},t)$ at a time t is given by

$$f(\vec{v},t) = \int \mathrm{d}(\Delta\vec{v}) f(\vec{v}-\Delta\vec{v},t-\Delta t)F(\vec{v},\Delta\vec{v}). \tag{8.50}$$

if $f(\vec{v},t)$ changes only due to collisions. Under the assumptions, which we detailed in the discussion leading up to eq. 8.49, i.e., that scattering occurs by multiple small scatters, the change of velocity during a short interval Δt, $\Delta\vec{v}$, must also be small. This allows us to expand the VDF $f(\vec{v})$ into a power series in $\Delta\vec{v}$.

$$\begin{aligned} f(\vec{v},t) &= \int \mathrm{d}(\Delta\vec{v}) \Big\{ \qquad f(\vec{v},t-\Delta t)F(\vec{v},\Delta\vec{v}) \\ &\quad -\Delta\vec{v}\frac{\partial}{\partial\vec{v}}\left[f(\vec{v},t-\Delta t)F(\vec{v},\Delta\vec{v})\right] \\ &\quad +\frac{1}{2}\sum_i\sum_k \Delta v_i\Delta v_k \frac{\partial^2}{\partial v_i\partial v_k}\left[f(\vec{v},t-\Delta t)F(\vec{v},\Delta\vec{v})\right] + o(\Delta\vec{v}^3)\Big\} \end{aligned} \tag{8.51}$$

The term in the first line can be integrated easily, $f(\vec{v},t-\delta t)$ contains no velocity difference, $\Delta\vec{v}$ and can be moved infront of the integral. The probability, $F(\vec{v},\Delta\vec{v})$ is normalized, i.e.,$\int \mathrm{d}\vec{v}F(\vec{v},\Delta\vec{v}) = 1$, allowing us to isolate the first term and move it to the left-hand side of the equation. We now have the numerator of the definition of the partial derivative of f with respect to time, so dividing by Δt we have

$$\begin{aligned} \left(\frac{\partial f(\vec{v},t)}{\partial t}\right)_{\text{coll}} &= \frac{1}{\Delta t}\int \mathrm{d}(\Delta\vec{v})\Big\{-\Delta\vec{v}\frac{\partial}{\partial\vec{v}}\left[f(\vec{v},t)F(\vec{v},\Delta\vec{v})\right] \\ &\quad +\frac{1}{2}\sum_i\sum_k \Delta v_i\Delta v_k\frac{\partial^2}{\partial v_i\partial v_k}\left[f(\vec{v},t)F(\vec{v},\Delta\vec{v})\right] + o(\Delta\vec{v}^3)\Big\}. \end{aligned} \tag{8.52}$$

We have taken the limit $\Delta t \longrightarrow 0$, in which $f(t-\Delta t) \longrightarrow f(t)$. Next we determine the expectation values of the moments of velocity,

$$\left\langle\frac{\Delta\vec{v}}{\Delta t}\right\rangle = \frac{1}{\Delta t}\int \mathrm{d}(\Delta\vec{v})\Delta\vec{v}F(\vec{v},\Delta\vec{v}) \tag{8.53}$$

and

$$\left\langle\frac{\Delta v_i\Delta v_k}{\Delta t}\right\rangle = \frac{1}{\Delta t}\int \mathrm{d}(\Delta\vec{v})\Delta v_i\Delta v_k F(\vec{v},\Delta\vec{v}) \tag{8.54}$$

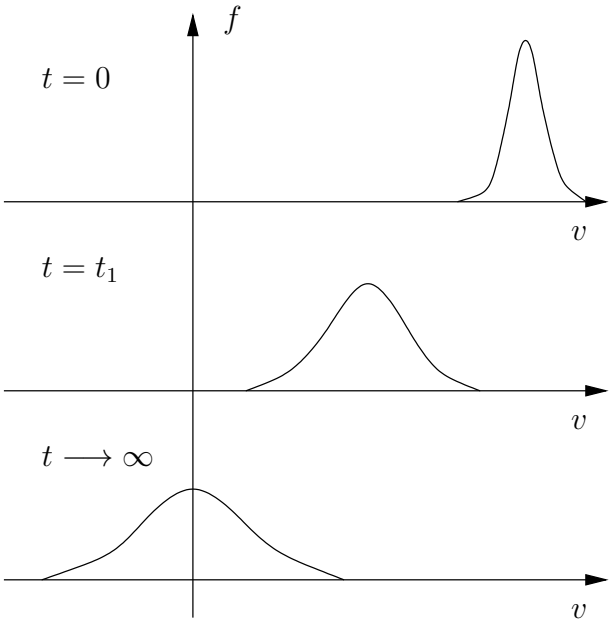

Figure 8.5: The change of a velocity distribution function (VDF) of a beam of energetic particles in a plasma due to Coulomb collisions. The VDF experiences a systematic slowing down which can be envisaged as due to friction, and a broadening which can be viewed as diffusion in velocity space.

with which we can write the change in the VDF due to collisions in the plasma up to terms to order $\Delta\vec{v}^3$ as

$$\left(\frac{\partial f(\vec{v},t)}{\partial t}\right)_{\text{coll}} = -\frac{\partial}{\partial \vec{v}}\left\langle\frac{\Delta\vec{v}}{\Delta t}\right\rangle f(\vec{v},t) + \frac{1}{2}\sum_{i,k}\frac{\partial^2}{\partial v_i \partial v_k}\left[\left\langle\frac{\Delta v_i \Delta v_k}{\Delta t}\right\rangle f(\vec{v},t)\right]. \tag{8.55}$$

This equation is called the **Fokker-Planck** equation. For a plasma in thermodynamic equilibrium both sides vanish, in other cases, this equation describes the collision-induced change of the VDF in a plasma. This change can occur by two processes. The first term describes a systematic change of the velocity which is proportional to velocity itself. The term can be considered as a friction term allowing the velocity of the particles to increase or decrease. The second term describes the other possibility to change $f(\vec{v})$. The VDF can broaden, which can be considered as a diffusion in velocity space. Figure 8.5 illustrates these processes. Had we included higher orders in $\Delta\vec{v}$ in our expansion, we would have found additional processes which are able to change the VDF. However, they would not have changed this picture significantly. The Fokker-Planck equation is limited in validity to plasmas in which collisions tend to result in small changes of the velocity vector, $\vec{v}$ and in which large changes in velocity are predominantly due to multiple small changes or small

scattering processes. Terefore, the higher-order terms beginning with $(\Delta v/v)^3$ which are smaller than the quadratic terms, are unimportant.

In order to apply the Fokker-Planck equation to a plasma, we need to determine the expectation values for the changes of the moments of the velocity (eqs. 8.53 and 8.54) on the basis of the properties of collisions in the plasma. We have already prepared this for a plasma which relaxes via Coulomb collisions when we determined the corresponding scattering cross sections. Let us now consider the interaction of a test particle with velocity $\vec{v}_T$ with a plasma. To do so we need to determine two expectation values, one over all possible impact parameters, b, and a weighted one over all possible velocities, $\vec{v}$, of the background particles. The averaging is best performed in the center of mass frame of reference, but the result must be transformed back into the laboratory system thereafter. This results in lengthy calculations which are given, e.g., in *Krall* and *Trivelpiece* (1986). The end result is a system of auxiliary functions $g_\alpha(\vec{v})$ and $h_\alpha(\vec{v})$,

$$g_\alpha(\vec{v}) = \int \mathrm{d}\vec{v}' f_\alpha(\vec{v})|\vec{v}-\vec{v}'|, \tag{8.56}$$

$$h_\alpha(\vec{v}) = \frac{m_T}{\mu_\alpha}\int \mathrm{d}\vec{v}' \frac{f_\alpha(\vec{v}')}{|\vec{v}-\vec{v}'|}, \quad \text{where} \tag{8.57}$$

$$\mu_\alpha = \frac{m_T\, m_\alpha}{m_T + m_\alpha}, \tag{8.58}$$

with which the Fokker-Planck equation turns into

$$\left(\frac{\partial f(\vec{v},t)}{\partial t}\right)_{\text{coll}} = \sum_\alpha \left[-\partial_{v_i}(f_T \partial_{v_i} h_\alpha) + \frac{1}{2}\frac{\partial^2}{\partial v_i \partial v_k}\left(f_T \frac{\partial^2 g_\alpha}{\partial v_i \partial v_k}\right)\right] \frac{4\pi n_\alpha q_T^2 q_\alpha^2}{m_T^2}\ln\Lambda, \tag{8.59}$$

where the index α runs over all possible particle species in the plasma.

With this form of the Fokker-Planck equation we are now in the position to determine transport properties of the plasma. In the coming paragraphs we will consider the slowing down of a beam of energetic particles in a plasma at rest, the plasma's electric conductivity, and diffusion perpendicular to a magnetic field.

8.3 Slowing Down of a Beam

Let us now investigate the slowing down of a beam of energetic particles (electrons or ions). To do so we need to recall the situation sketched in Fig. 8.5. The beam has a narrow distribution f_T around a velocity $\vec{u}$ which differs substantially from that of the plasma. In the following we will approximate it by a delta function, $\delta(\vec{v}-\vec{u})$, at time $t = 0$, and we will consider the plasma VDF

to be equilibrium, i.e., Maxwell distributions,

$$f_T(\vec{v}) = \delta(\vec{v}-\vec{u}), \tag{8.60}$$

$$f_\alpha(\vec{v}) = \left(\frac{m_\alpha}{2\pi k T_\alpha}\right)^{3/2} e^{-\frac{m_\alpha v^2}{2kT_\alpha}}. \tag{8.61}$$

As we have shown in appendix A in the previous lecture, 'Introduction to Extraterrestrial Physics', the expectation values for certain quantities can be determined by taking moments of the kinetic equations. The expectation value for the change of the velocity of the beam is given by the first moment of the Fokker-Planck equation.

$$\int \mathrm{d}\vec{v}\dot{f}_T\vec{v} = \sum_\alpha \frac{4\pi n_\alpha q_T^2 q_\alpha^2}{m_T^2}\ln\Lambda \int \mathrm{d}\vec{v}\left[-\partial_{v_i}(f_T\partial_{v_i}h_\alpha) + \frac{1}{2}\frac{\partial^2}{\partial v_i \partial v_k}\left(f_T\frac{\partial^2 g_\alpha}{\partial v_i \partial v_k}\right)\right]\vec{v}. \tag{8.62}$$

The left-hand side is easily derived because the time derivative can be moved infront of the integral. What is left over is the expectation for the velocity, $\vec{u}$. With this we have, as expected, the time derivative of the expectation value of the beam's velocity on the left-hand side of the equation. Thus, equation 8.62 indeed describes the change of the beam velocity in time due to collisions with other particles. The right-hand side is not so straightforward to evaluate. Remembering the property of generalized functions (see, e.g., *Gel'fand* and *Shilov* (1967)) that

$$\int \mathrm{d}\vec{v}(\partial_{v_i} f_T(\vec{v}))\varphi(\vec{v}) = -\int \mathrm{d}\vec{v} f_T(\vec{v})(\partial_{v_i}\varphi(\vec{v})). \tag{8.63}$$

for test functions, φ, which tend to zero faster than any power of x (or rather v in our case), we are now equiped to perform the moment calculation. We apply the differential operator ∂_{v_i} from the left to the individual factors in the first term of the right-hand side of the Fokker-Planck equation.

$$\begin{aligned}
&\int \mathrm{d}\vec{v}\partial_{v_i}\left(f_T\left\{\partial_{v_i}h_\alpha\right\}\vec{v}\right) = \\
&= \int \mathrm{d}\vec{v}\left\{\left(\partial_{v_i}f_T\right)\left\{\partial_{v_i}h_\alpha\vec{v}\right\} + f_T\left\{\partial_{v_i}\partial_{v_i}h_\alpha\right\}\vec{v} + f_T\left\{\partial_{v_i}h_\alpha\right\}\left(\partial_{v_i}\vec{v}\right)\right\}, \\
&= \int \mathrm{d}\vec{v}\left\{-f_T\left\{\partial_{v_i}\partial_{v_i}h_\alpha\right\} + f_T\left\{\partial_{v_i}\partial_{v_i}h_\alpha\right\}\vec{v} + f_T\left\{\partial_{v_i}h_\alpha\right\}\left(\partial_{v_i}\vec{v}\right)\right\}, \\
&= \int \mathrm{d}\vec{v}\left\{f_T\left\{\partial_{v_i}h_\alpha\right\}\right\}, \\
&= \frac{\partial}{\partial\vec{u}}h_\alpha(\vec{u}).
\end{aligned} \tag{8.64}$$

Next we perform the same operations to the second term on the right-hand side of eq. 8.62.

$$\begin{aligned}
&\int \mathrm{d}\vec{v}\frac{\partial^2}{\partial_{v_i}\partial_{v_j}}\left(f_T\left\{\frac{\partial^2}{\partial_{v_i}\partial_{v_j}}g_\alpha\right\}\vec{v}\right) = \\
&= \int \mathrm{d}\vec{v}\partial_{v_i}\left[\left(\partial_{v_j}f_T\right)\left\{\frac{\partial^2 g_\alpha}{\partial_{v_i}\partial_{v_j}}\right\}\vec{v} + f_T\left\{\partial_{v_j}\frac{\partial^2 g_\alpha}{\partial_{v_i}\partial_{v_j}}\right\}\vec{v} + f_T\left\{\left(\frac{\partial^2 g_\alpha}{\partial_{v_i}\partial_{v_j}}\partial_{v_j}\vec{v}\right)\right\}\right], \\
&= \int \mathrm{d}\vec{v}\partial_{v_i}\left[-f_T\left\{\partial_{v_j}\frac{\partial^2 g_\alpha}{\partial_{v_i}\partial_{v_j}}\right\}\vec{v} + f_T\left\{\partial_{v_j}\frac{\partial^2 g_\alpha}{\partial_{v_i}\partial_{v_j}}\right\}\vec{v} + f_T\left\{\frac{\partial^2 g_\alpha}{\partial_{v_i}\partial_{v_j}}\left(\partial_{v_j}\vec{v}\right)\right\}\right], \\
&= \int \mathrm{d}\vec{v}\partial_{v_i}\left[f_T\left\{\frac{\partial^2 g_\alpha}{\partial_{v_i}\partial_{v_j}}\left(\partial_{v_j}\vec{v}\right)\right\}\right], \qquad (8.65) \\
&= \int \mathrm{d}\vec{v}\left[\left(\partial_{v_i}f_T\right)\left\{\frac{\partial^2 g_\alpha}{\partial_{v_i}\partial_{v_j}}\right\}\left(\partial_{v_j}\vec{v}\right) + f_T\left\{\partial_{v_i}\frac{\partial^2 g_\alpha}{\partial_{v_i}\partial_{v_j}}\right\}\left(\partial_{v_i}\vec{v}\right) + f_T\left\{\frac{\partial^2 g_\alpha}{\partial_{v_i}\partial_{v_j}}\right\}\left(\frac{\partial^2\vec{v}}{\partial_{v_i}\partial_{v_j}}\right)\right], \\
&= \int \mathrm{d}\vec{v}\left[-f_T\left\{\partial_{v_i}\frac{\partial^2 g_\alpha}{\partial_{v_i}\partial_{v_j}}\right\}\left(\partial_{v_i}\vec{v}\right) + f_T\left\{\partial_{v_i}\frac{\partial^2 g_\alpha}{\partial_{v_i}\partial_{v_j}}\right\}\left(\partial_{v_i}\vec{v}\right) + f_T\left\{\frac{\partial^2 g_\alpha}{\partial_{v_i}\partial_{v_j}}\right\}\left(\frac{\partial^2\vec{v}}{\partial_{v_i}\partial_{v_j}}\right)\right], \\
&= \int \mathrm{d}\vec{v}\left[f_T\left\{\frac{\partial^2 g_\alpha}{\partial_{v_i}\partial_{v_j}}\right\}\left(\frac{\partial^2\vec{v}}{\partial_{v_i}\partial_{v_j}}\right)\right]. \qquad (8.66)
\end{aligned}$$

The last term vanishes, as one can easily see, because

$$\frac{\partial^2\vec{v}}{\partial_{v_i}\partial_{v_j}} = \frac{v\delta_{ij} - v_i v_j/v}{v^2}. \qquad (8.67)$$

Obviously, it vanishes for $i = j$. To show this for $i \neq j$, we move to a frame of reference in which $\vec{v}$ is parallel to the z axis. Then at most one of the factors v_i or v_j is different from zero, and the expression must also vanish in this case.

All that is left to be done now is to determine the left-hand side of the Fokker-Planck equation. This should now be easy. We obtain the preliminary result

$$\frac{\partial\vec{u}}{\partial t} = \frac{4\pi q_T^2}{m_T^2}\ln\Lambda\sum_\alpha n_\alpha q_\alpha^2\int \mathrm{d}\vec{v}\left(\frac{\partial h_\alpha}{\partial\vec{v}}\right)f_T. \qquad (8.68)$$

To obtain the slowing down of the beam we now need to insert the initial distribution, $f_T = \delta(\vec{v} - \vec{u})$ and the explicit expression for h_α for a Maxwellian background plasma, f_α.

$$h_\alpha = \frac{m_T}{\mu_\alpha}\left(\frac{m_\alpha}{2\pi k T_\alpha}\right)^{3/2}\int \mathrm{d}\vec{v}'\frac{e^{-\frac{m_\alpha v'^2}{2kT_\alpha}}}{|\vec{v} - \vec{v}'|}. \qquad (8.69)$$

In further preparation, we substitute $x^2 = (m_\alpha/(2kT_\alpha))v^2$ and use

$$\int \mathrm{d}\vec{x}\frac{e^{-x^2}}{|\vec{x} - \vec{y}|} = \frac{\pi^{3/2}}{|\vec{y}|}\Phi(|\vec{y}|), \qquad (8.70)$$

where $\Phi(y)$ is the error function,

$$\Phi(y) \doteq \frac{2}{\sqrt{\pi}} \int_0^y \mathrm{d}x \; e^{-x^2}. \tag{8.71}$$

Thus we obtain for eq. 8.68

$$\begin{aligned} \frac{\partial \vec{u}}{\partial t} &= \frac{4\pi q_T^2}{m_T^2} \ln\Lambda \sum_\alpha \frac{m_T}{\mu_\alpha} n_\alpha q_\alpha^2 \int \mathrm{d}\vec{v} \left(\frac{\partial}{\partial \vec{v}} \frac{\Phi\left(\sqrt{\frac{m_\alpha}{2kT_\alpha}}|\vec{v}|\right)}{|\vec{v}|} \right) f_T, \\ &= \frac{4\pi q_T^2}{m_T^2} \ln\Lambda \frac{\partial}{\partial \vec{u}} \left\{ \sum_\alpha \frac{m_T}{\mu_\alpha} n_\alpha q_\alpha^2 \frac{\Phi\left(\sqrt{\frac{m_\alpha}{2kT_\alpha}}|\vec{u}|\right)}{|\vec{u}|} \right\}. \end{aligned} \tag{8.72}$$

As the beam with velocity $\vec{u}$ enters a plasma of electrons (index e) and ions (index i) and temperatures T_e and T_i, its slowing down can be written as

$$\begin{aligned} \frac{\partial \vec{u}}{\partial t} = \frac{4\pi q_T^2}{m_T^2} \ln\Lambda \frac{\partial}{\partial \vec{u}} \quad \cdot \quad & \left\{ n_i q_i^2 \left(1 + \frac{m_T}{m_i}\right) \frac{\Phi\left(\sqrt{\frac{m_i}{2kT_i}}|\vec{u}|\right)}{|\vec{u}|} \right. \\ & \left. n_e q_e^2 \left(1 + \frac{m_T}{m_e}\right) \frac{\Phi\left(\sqrt{\frac{m_e}{2kT_e}}|\vec{u}|\right)}{|\vec{u}|} \right\}. \end{aligned} \tag{8.73}$$

The second of the two terms is generally the dominant one because m_T/m_e is always considerably larger (well, by a factor $A \times 1836$) than m_T/m_i. This is a consequence of the dependence of the Rutherford scattering cross section on the reduced mass, μ. Electrons have a considerably larger scattering cross section than ions and, therefore, are better at slowing down other particles than ions. This is true in a plasma, but also in solids, where this is also observed. The energy loss of particles entering a solid is nearly entirely due to electrons. Moreover, the slowing down is not as efficient for all beam velocities. Figure 8.6 shows the behavior of the function $\Phi(u)/u$ and the ensuing slowing down of the beam. Because the error function tends rapidly to unity for large arguments, the quotient, $\Phi(u)/u$, tends hyperbolically to zero and the derivative decreases. A fast beam only experiences a small slowing down, while a beam with a velocity in the vicinity of the thermal speed of the plasma will be slowed down very efficiently. The inefficient slowing down of a fast beam[2] is again a direct consequence of the functional dependence of the Rutherford scattering cross section, $\sigma \sim v^{-4}$.

[2]This is no different than the slowing down in a solid. Particles loose most of their energy towards the end of their trajectory, resulting in the Bragg peak.

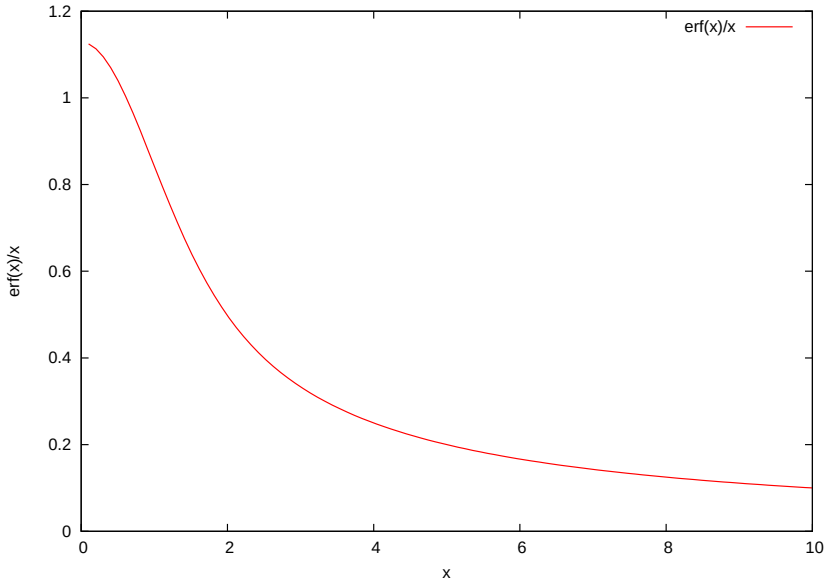

Figure 8.6: Behavior of the function $\Phi(x)/x$ and time derivative of the velocity change by friction in a plasma. Obviously, the slowing down of an energetic beam is small.

8.4 Equilibration or Electric Conductivity of a Plasma

With these considerations we are now well equipped to calculate the electric conductivity of a (thermal) plasma. For that we consider a plasma in a weak electric field. Ions will drift relative to the electrons with a velocity, $\vec{u}$, and we will transform into the rest frame of the electrons which shall also have a higher temperature, as depicted in Fig. 8.7. The ions will be accelerated to higher velocities by the field. If the field is weak and the ions do not reach a high velocity in short time, the slowing down by collisions will tend to counterbalance the acceleration of the ions, and an equilibrium will be established between acceleration by the weak field and slowing down by collisions. Then the equation of motion for the ions can be written according to eq. 8.73

$$q_i E = -\frac{\partial \vec{u}}{\partial t} m_i = -\frac{4\pi n e^2 q_i^2}{m_i^2} \ln\Lambda \frac{\partial}{\partial \vec{u}} \left[\frac{1}{u} \Phi\left(\sqrt{\frac{m_i}{2kT_i}} |\vec{u}| \right) \left(1 + \frac{m_T}{m_i} \right) \right] . \quad (8.74)$$

In this approximation of a small beam velocity in comparison to the thermal speed of the electrons, the error function can be approximated as

$$\Phi(x) \approx \frac{2}{\sqrt{\pi}} \left(x - \frac{x^3}{3} \right) . \quad (8.75)$$

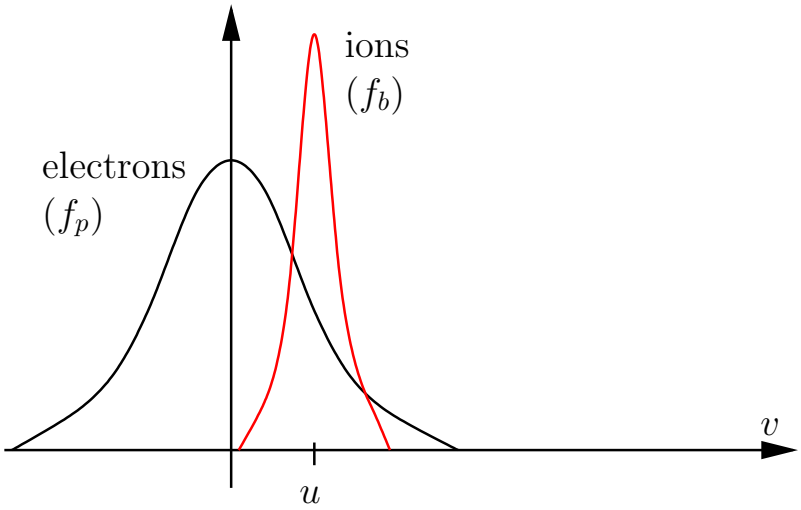

Figure 8.7: A cold ion beam (f_b) in a hot electron plasma (f_p) drifting relative to the electrons which are at rest in this figure.

Inserting gives us an equation for the electric field E. The right-hand side of that equation is proportional to a current density, J,

$$\begin{aligned} E &= \frac{4\pi e^2}{m_i} \ln\Lambda \; n q_i \frac{\partial}{\partial \vec{u}} \left[\frac{2}{\sqrt{\pi}} \left(\sqrt{\frac{m_e}{2kT_e}} - \left(\frac{m_e}{2kT_e}\right)^{3/2} \frac{u^2}{3} \right) \left(1 + \frac{m_i}{m_e}\right) \right], \\ &= \frac{16\sqrt{\pi} e^2}{3 m_e} \ln\Lambda \left(\frac{m_e}{2kT_e}\right)^{3/2} n q_i u, \\ &= \frac{n q_i u}{\sigma} = \frac{J}{\sigma}, \end{aligned} \tag{8.76}$$

where we have approximated $1 + m_i/m_e \approx m_i/m_e$. Invoking the generalized Ohm's law, the constant of proportionality, $1/\sigma$, gives the electric conductivity of the plasma,

$$\sigma = \frac{3 m_e}{16\sqrt{\pi} e^2 \ln\Lambda} \left(\frac{2kT_e}{m_e}\right)^{3/2}. \tag{8.77}$$

8.4.1 Diffusion in a Magnetic Field

As a final application of the Fokker-Planck equation we consider the diffusion perpendicular to a magnetic field. To do so, we consider the equation of motion of MHD, which is given in eqs. B8 and B12 in the appendix of the lecture 'Introduction to extraterrestrial physics',

$$n_i m_i \frac{\partial \vec{u}_i}{\partial t} + n_e m_e \frac{\partial \vec{u}_e}{\partial t} = -\vec{\nabla} P + e \left(n_i \vec{u}_i - n_e \vec{u}_e \right) \times \vec{B}. \tag{8.78}$$

For a vanishing electric field, $E = 0$, and in equilibrium, this equation can be written as

$$\vec{J} \times \vec{B} = \vec{\nabla} P. \tag{8.79}$$

The pressure gradient, $\vec{\nabla} P$, is perpendicular to the current and the magnetic field. If the plasma is isothermal, then the density gradient is parallel to the pressure gradient and, hence, also perpendicular to the current and magnetic field. Therefore, the only systematic motion in the plasma (i.e., the current) has to be perpendicular to the density gradient and can not compensate for it. Such a compensation could only occur if there could be a motion which were also perpendicular to the magnetic field. Thus, eq. 8.79 tells us that there is no diffusion across the magnetic field in a collisionless plasma.

However, this may change as soon as there are collisions in the plasma. Consider Fig. 8.8 which shows a density gradient in a magnetized plasma. In a volume element ΔV at position x_0 there are more particles moving from left to right, than from right to left because there are different numbers of particles gyrating around the field lines at locations $x_0 + a_i$ and $x_0 - a_i$. The number of particles which moves to the left at x_0 is given by

$$n_1 = n_0 + a_i \frac{\mathrm{d}n_{i0}}{\mathrm{d}x} \tag{8.80}$$

and the number of particles moving from left to right is given by

$$n_2 = n_0 - a_i \frac{\mathrm{d}n_{i0}}{\mathrm{d}x}. \tag{8.81}$$

Thus we have a non-vanishing average velocity at position x_0,

$$\langle \vec{v}_0 \rangle = \frac{n_1 |\vec{v}| - n_2 |\vec{v}|}{n_0} = 2 a_i \frac{\mathrm{d}n_{i0}}{\mathrm{d}x} \frac{v_0}{n_{i0}} \hat{\vec{y}}, \tag{8.82}$$

where $\hat{\vec{y}}$ is the unit vector in the $\vec{y}$ direction. Following the previous considerations leading up to eq. 8.76, the particles experience a decelerating force in the y direction,

$$\vec{F}_D = -\frac{16\sqrt{\pi} e^2}{3 m_e} \ln \Lambda \left(\frac{m_e}{2 k T_e} \right)^{3/2} n q_i^2 \langle |\vec{v}_0| \rangle \hat{\vec{y}}, \tag{8.83}$$

where v_0 is the thermal velocity of the ions. According to the general formula for drifts, this force leads to a drift

$$U_D = \frac{1}{q} \frac{\vec{F}_D \times \vec{B}}{B^2} = n q_i \frac{\left(\langle |\vec{v}_0| \rangle \hat{\vec{y}} \right) \times \vec{B}}{\sigma B^2}, \tag{8.84}$$

which is anti-parallel to the density gradient. This means that there is a particle flux, φ,

$$\varphi = -D \vec{\nabla} n, \tag{8.85}$$

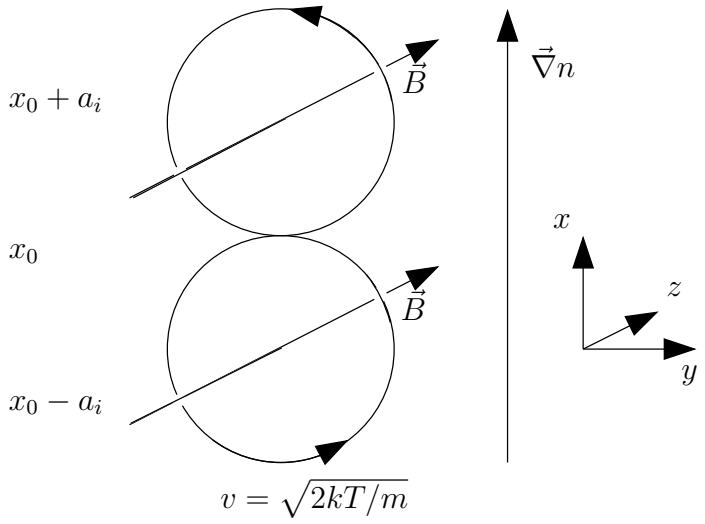

Figure 8.8: A density gradient leads to a drift of ions in the y direction. This in turn leads to a slowing down and thus a force F_D acting in the y direction. This force results in a drift which opposes the density gradient.

where $D \sim \sigma^{-1} B^{-2}$ is a diffusion constant. In other words, collisions lead to a diffusion perpendicular to the magnetic field, but it is weak in a stronlgy magnetized plasma or a highly conductive one.

(8.86)

Chapter 9

Reconnection

9.1 Introduction

flares on Sun and other stars, interplanetary, magnetospheric,

In order to understand the properties of the plasma and magnetic field in interplanetary space one often uses the so-called magneto-hydro-dynamic (MHD) approximation. It approximates a plasma as a globally electrically neutral but magnetized fluid in which temporal and spatial disturbances are slow or large-scaled, respectively, when compared to the characteristic properties of the plasma such as plasma and cyclotron frequencies and Debye radius. The equations of MHD consist of an equation of continuity for both the mass density and the current density, an equation of motion, Ohm's law, as well as Maxwell's equations. Often the displacement current $\dot{\vec{E}}/c^2$ can be neglected.

We combine Ampéres and Ohms laws to obtain

$$\vec{J} = \frac{1}{\mu_0}\vec{\nabla} \times \vec{B} = \sigma \left(\vec{E} + \vec{v} \times \vec{B} \right), \tag{9.1}$$

where σ is the electrical conductivity,

$$\sigma \doteq \frac{ne^2}{m_e}\tau_c, \tag{9.2}$$

where τ_c is the average collision time in the plasma. We take the curl of eq. 9.1 and use Faradays law

$$\dot{\vec{B}} = -\vec{\nabla} \times \vec{E} \tag{9.3}$$

to obtain,

$$\dot{\vec{B}} = \vec{\nabla} \times \vec{u} \times \vec{B} + \frac{1}{\mu_0 \sigma}\Delta\vec{B}, \tag{9.4}$$

where we have used $\nabla \times \nabla \times B = \nabla(\nabla \cdot B) - \Delta B = -\Delta B$. Equation 9.4 is the induction equation of MHD. Understanding its structure helps us understand the properties of the interplanetary medium. Depending on the electric

conductivity of the plasma, either one of the two terms on the right-hand side will dominate. For small conductivity, or for slow movements in the plasma, the induction equation turns into a diffusion equation,

$$\dot{\vec{B}} = \frac{1}{\mu_0 \sigma} \Delta \vec{B}, \tag{9.5}$$

because this term dominates the other term in this case. The quantity $1/\mu_0\sigma$ is called magnetic diffusivity. We can use eq. 9.5 to derive a diffusion time,

$$\left[\frac{\partial \vec{B}}{\partial t}\right] = \left[\frac{1}{\mu_0 \sigma} \frac{\partial^2 \vec{B}}{\partial r^2}\right] \Longrightarrow \tau_{\text{diff}} = \mu_0 \sigma L^2, \tag{9.6}$$

where L is a typical scale of length.

In the case where conductivity is very large, or movements are very fast, the diffusive term can be neglected,

$$\dot{\vec{B}} = \vec{\nabla} \times \vec{u} \times \vec{B}. \tag{9.7}$$

As we will see in the following few paragraphs, this equation implies that the magnetic flux through the surface S spanned by a closed curve C comoving with the plasma is conserved. Figure 9.1 shows a sketch of the situation. The

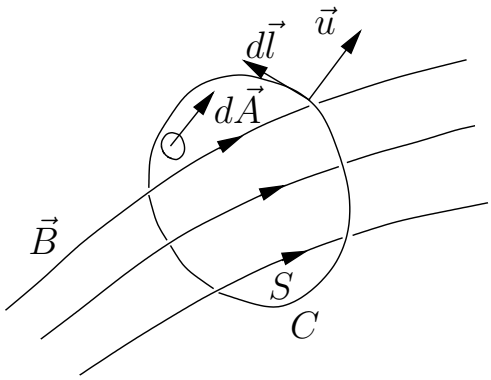

Figure 9.1: Magnetic flux through the surface S spanned by the closed curve C.

magnetic flux passing through S can change in two ways. On the one hand, the field strength $\vec{B}$ within the curve C can change. On the other hand, the curve C can move with respect to the field $\vec{B}$. In the first possibility, the change of flux in a surface element $d\vec{A}$ is given by

$$\dot{\vec{B}} \cdot d\vec{A} \tag{9.8}$$

and the total change is just the integral over the entire surface S. In the second possibility an infinitesimal line element $d\vec{l}$ of the curve moves relative to $\vec{B}$. The change in the enclosed field is then given by

$$\vec{B} \cdot \left(\vec{u} \times d\vec{l} \right) \tag{9.9}$$

and the total change is the contour integral along C. Using the vector identity $A \cdot (B \times C) = (A \times B) \cdot C$ we can rewrite eq. 9.9 and write the entire change in the flux through the surface S spanned by C as

$$\frac{d}{dt} \int_S d\vec{A} \cdot \vec{B} = \int_S d\vec{A} \cdot \frac{\partial \vec{B}}{\partial t} - \oint_C d\vec{l} \cdot \left(\vec{u} \times \vec{B} \right). \tag{9.10}$$

We rewrite the contour integral as a surface integral using Stokes' theorem

$$\oint_C d\vec{l} \cdot \left(\vec{u} \times \vec{B} \right) = \int_S d\vec{A} \vec{\nabla} \times \left(\vec{u} \times \vec{B} \right). \tag{9.11}$$

Now the integrand is exactly the right-hand side of the induction equation for the case of infinite conductivity. This implies that

$$\frac{d}{dt} \int_S d\vec{A} \cdot \vec{B} = \int_S d\vec{A} \cdot \left(\frac{\partial \vec{B}}{\partial t} - \vec{\nabla} \times \left(\vec{u} \times \vec{B} \right) \right) = 0, \tag{9.12}$$

proving that the flux through the curve C remains unchanged. The physical meaning of this is that the magnetic field co-moves with the plasma, this is often called the "frozen-in magnetic field" , or ideal MHD. The transition from a diffusion dominated to a frozen in situation can be parameterized by the ratio of diffusion time τ_d to convection time τ_u, where

$$\tau_d = \mu_0 \sigma L^2, \qquad \text{and} \qquad \tau_u = \frac{L}{u}. \tag{9.13}$$

We can now define the magnetic Reynolds number R_M,

$$R_M \doteq \frac{\tau_d}{\tau_u} = \frac{\mu_0 \sigma L^2 u}{L} = \mu_0 \sigma L u. \tag{9.14}$$

For large R_M the field is frozen in, for small R_M it diffuses. In general, R_M is large in the interplanetary medium, as well as in the chromosphere and corona.

The lesson from this paragraph is that magnetic field can diffuse, if conditions are appropriate. From what we have learned so far, field lines will remain connected ("frozen in") if conductivity is large enough, when diffusion dominates, we can envisage field lines swapping their identity in localized regions of low conductivity or where R_M is not much larger than unity. This can happen, when field is brought into a region where it needs to change on a very

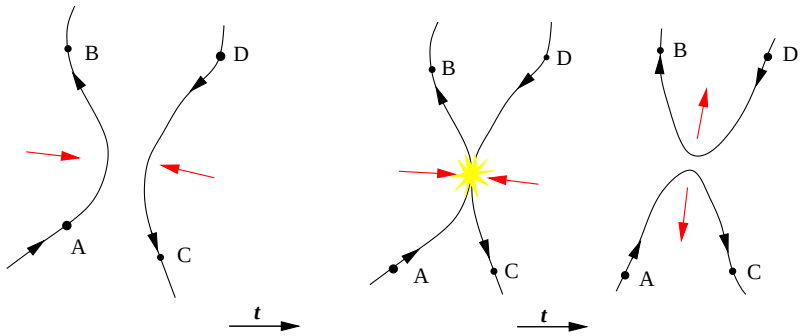

Figure 9.2: Reconnection separates fluid elements that were originally connected and connects them with new ones. This can lead to changes in magnetic topology. In such regions (sketched with a flash here) scale lengths are short, e. g. because the polarity of the magnetic field changes on a small scale.

small scale, e. g. near a current sheet. Then the diffusion time can be short compared to the convection time and the "frozen in" approximation breaks down. A field line can then *dis*connect from its original footpoint and then *re*connect with another field line, as sketched in Figure 9.2. While the "frozen in" approximation is still valid in the global context, it can be broken locally which allows for changes in magnetic topology, as is shown in Fig. 9.2. To summarize, reconnection can occur when there is a global configuration that brings magnetic field together at a rate and on a scale sufficient for breakdown of the "frozen in" approximation. We will now consider the original model of Parker and Sweet, consider its difficulties and improve the situation by introducing Petscheks model for reconnection. A very primitive sketch of the two models is shown in Figure 9.3. where magnetic field of opposite polarity can be transformed into energy by diffusive annihilation. The corresponding diffusion equation

$$\frac{\partial \vec{B}}{\partial t} = \frac{1}{\mu_0 \sigma} \Delta \vec{B},$$

has the one-dimensional solution

$$B = \sqrt{\frac{\mu_0 \sigma}{4t}} e^{-\frac{y^2 \mu_0 \sigma}{4t}}. \tag{9.15}$$

The field diffuses and locations of field strength $1/e$ move away from the current sheet at a speed $v_{1/e} = \sqrt{4/\mu_0 \sigma t}$, as sketched in Fig. 9.4. The field strength in the current sheet diminishes, the difference to the original field strength going into the energy liberated by reconnection. This can be a substantial amount of energy, visualized here by a dramatic change in field strength. However, we can do better than that, and derive an estimate of the reconnection rate, the speed at which magnetic field can be brought into the reconnection region.

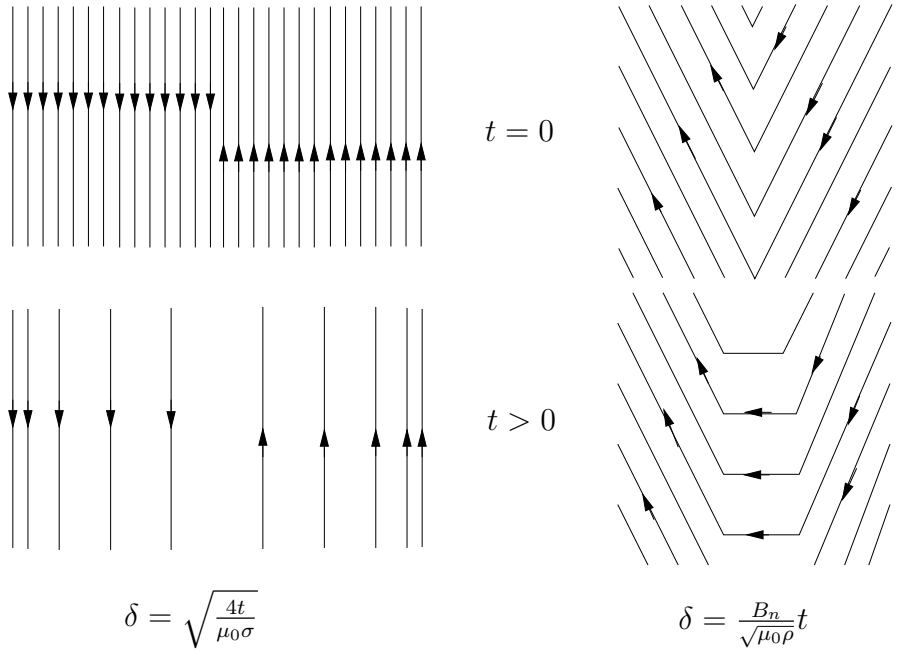

Figure 9.3: Reconnection in the model of Parker and Sweet (left) and Petschek (right).

9.2 The Parker-Sweet Model

Consider a situation as sketched in Fig. 9.3a)

For this, we consider the very much simplified geometry sketched in Fig. 9.5. Plasma flows in from the top and the bottom at a speed u_{y_0} over a width $2L$ and needs to exit the reconnection region (the gray shaded area in Fig. 9.5) of width 2δ at a speed v which can be determined from the equation of continuity,

$$u_{y_0} L = v\delta, \tag{9.16}$$

This speed v can also be estimated from the Bernoulli equation

$$\frac{\rho v^2}{2} = p - p_0, \tag{9.17}$$

where ρ is the plasma density, p the pressure in the center of the reconnection region, and p_0 the pressure in the undisturbed region far away. Of course, we're neglecting magnetic pressure here, in general this is of the same magnitude as the plasma pressure ($\beta \approx 1$), so we're introducing an error of the order of a factor of two. It too, will push the plasma outwards along the current sheet. In order for the reconnection region to remain in hydrostatic equilibrium with the surrounding plasma, the pressure at the boundary needs to be determined

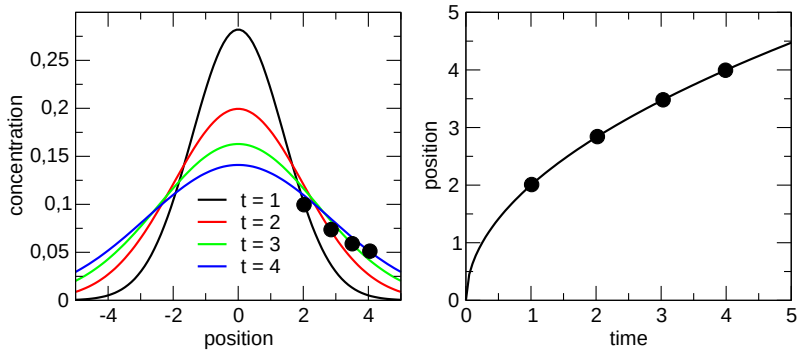

Figure 9.4: Diffusion

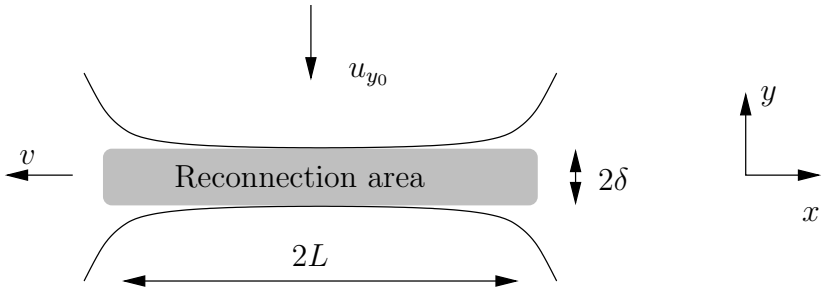

Figure 9.5: Geometry of reconnections and the equation of continuity.

by

$$p - p_0 = \frac{B_{x_0}^2}{2\mu_0}, \tag{9.18}$$

where B_{x_0} is the field strength in the undisturbed region.

Next, we derive an expression relating the inflow speed u_{y_0} to the diffusion speed in the reconnection region. We compute the time is takes diffusion to traverse a layer of thickness δ. From

$$\delta = \int_0^T \mathrm{d}t \sqrt{\frac{1}{4\mu_0 \sigma t}}$$

we obtain the diffusion speed v_{diff}

$$v_{\mathrm{diff}} = \frac{\delta}{T} = \frac{1}{\mu_0 \sigma \delta}. \tag{9.19}$$

The inflow speed u_{y_0} can be estimated in the following way. Inside the reconnection region there must be an X-point because of symmetry considerations. There, B, as well as flow speeds must be very small and hence Ohms law can be written as

$$J_z = \sigma E_z,$$

where J_z is the current density and E_z the electric field. Because σ is a scalar, E_z needs to be along J_z and point along the z-axis. For a stationary flow $\dot{B} = 0$ implies than $\nabla \times E = 0$ and hence E_z is constant. Hence the field can be estimated using quantities valid outside the reconnection region, where Ohms law tells us that

$$E_z = -u_{y_0} B_{x_0}.$$

Because the entire change of the magnetic field over the reconnection region must amount to $2B_{x_0}$, the magnitude of the total current carried by the current sheet can be estimated

$$\mu_0 J_Z = \frac{2B_{x_0}}{2\delta}.$$

Combining the last three equations, we obtain an estimate for the inflow speed u_{y_0},

$$u_{y_0} = \frac{1}{\mu_0 \sigma \delta}, \tag{9.20}$$

i. e. the inflow speed is just the diffusion speed! All we need to do now to estimate whether this is fast or slow, is to compare this with the outflow speed v and relate that to the overall geometry. Inserting eq. 9.18 in eq. 9.17 we find that it is just the Alfvén speed, $v_A \doteq B_{x_0}/\sqrt{\mu_0 \rho}$, (as we could easily have guessed). We estimate the unknown width of the reconnection region, δ, using our knowledge of the diffusion speed (eq. 9.20)

$$\delta = \frac{1}{\mu_0 \sigma u_{y_0}},$$

which we insert in the continuity equation, eq. 9.16, and solve for the inflow speed u_{y_0}

$$u_{y_0} = \left(\frac{B_{x_0}}{\sqrt{\mu_0 \rho}} \frac{1}{\mu_0 \sigma L} \right)^{1/2}. \tag{9.21}$$

This can also be written as

$$u_{y_0} = v_A \left(\frac{1}{v_A} \frac{1}{\mu_0 \sigma L} \right)^{1/2}, \tag{9.22}$$

where the expression in parenthesis is just the inverse of the magnetic Reynolds number, and hence

$$u_{y_0} = v_A \, R_M^{-1/2}.$$

In other words, reconnection is a slow process in the Parker and Sweet configuration because the magnetic Reynolds number is a large number in general.

9.3 Petschek Reconnection

Comparison of light curves of flares on the Sun and on other astrophysical objects with the time scale expected from a Parker and Sweet-like reconnection configuration showed that this is too slow by at least two orders of magnitude. *Petschek* (1964) solved this difficulty by allowing for standing Alfvén waves which deflect the magnetic field far away from the actual reconnection region, as sketched in Figs. 9.3 and 9.6. These waves allow for a much smaller

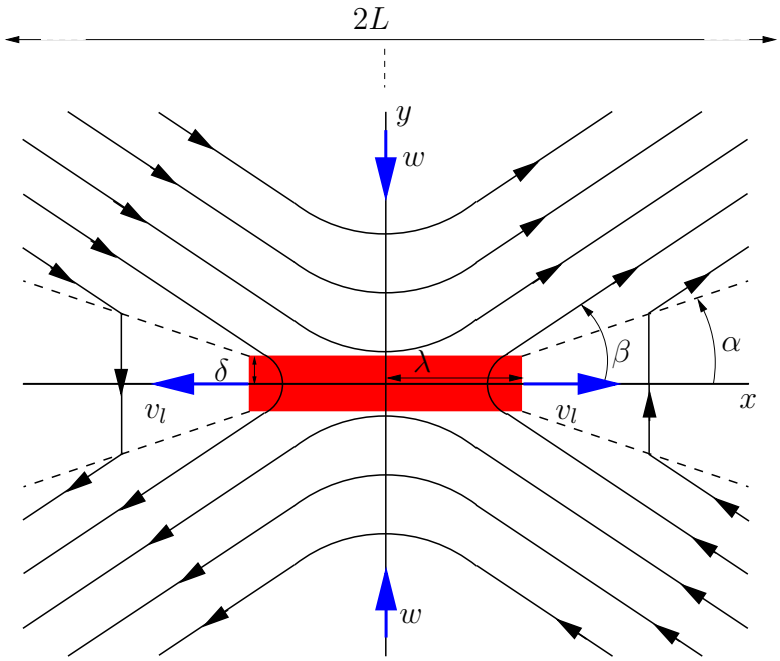

Figure 9.6: The geometry of reconnection according to Petschek. Reconnection takes place in the rectangle $2\lambda \times 2\delta$. The field is transported into the reconnection area with a speed w and over a width $2L$. This leads to a formation of standing Alfvén waves (dashed lines) at an angle α to the x axis. The field is parallel to the x axis far away from the reconnection area but is bent to an angle β with respect to the x axis.

reconnection region than the width of the inflow region, resulting in a much higher inflow velocity. We denote by 2λ the total width of the reconnection region, and by 2δ its total thickness. Inside the reconnection region, continuity requires

$$w = v_A \frac{\delta}{\lambda},$$

however, the situation is quite different outside the reconnection region proper, where the standing Alfvén waves deflect the inflowing plasma. There continuity

only requires

$$w = v_A \tan\alpha$$

which can be a substantial fraction of the Alfvén speed, depending on the unspecified angle α. Continuity of the flow across the boundary of the reconnection region requires that

$$\frac{w}{v_A} = \frac{\delta}{\lambda} = \tan\alpha.$$

This angle α can't be very large, because otherwise the tension force (determined largely by the angle β in Fig. 9.6) on the inflowing magnetic field would prevent it from reaching the reconnection region. Hence there must be an optimal value for λ at which the inflow speed is maximized (but still smaller than v_A). Petschek found a way of estimating this λ as a combination of the angles α and β, as well as of other plasma quantities. As the derivation is somewhat lengthy and involved, we only give the final result for the inflow speed, or reconnection speed, which is possible in a Petschek-type configuration,

$$\frac{w}{v_A} =\approx \frac{\pi}{4\,e\,\ln R_m}. \tag{9.23}$$

The reconnection speed only decreases with the logarithm of the magnetic Reynolds number. As is illustrated in Fig. 9.7, this makes a great difference when we consider astrophysical plasmas, for which R_M is generally large.

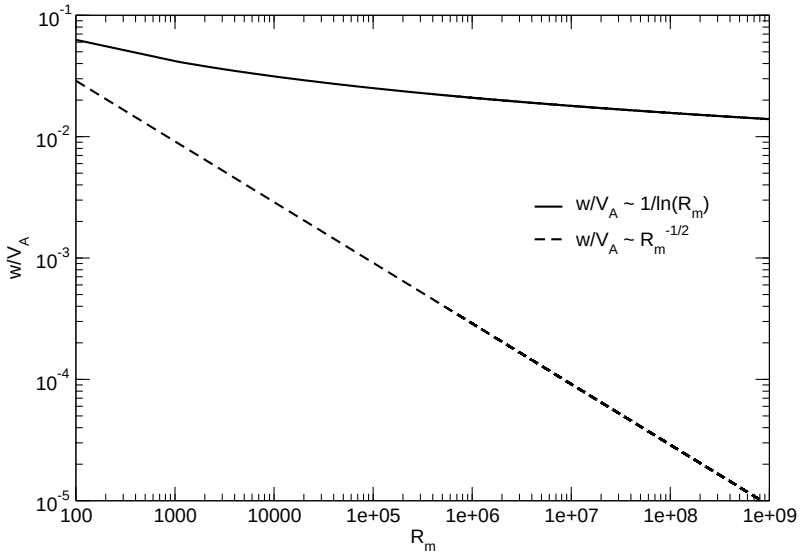

Figure 9.7: Comparison of the reconnection speeds in the model of Petschek (solid line) and the model of Parker and Sweet (dashed line).

The reconnected field lines are not only expelled from the reconnection region by the outflowing plasma, they also feel a tension force acting on them which is due to the force

$$\vec{F} = q\left(\vec{E} + \vec{v} \times \vec{B}\right). \tag{9.24}$$

acting on the particles constituting the plasma. This microscopic force is better replaced by a macroscopic quantity, the force $\mathcal{F}$ acting on a unit volume of plasma. This can be written as

$$\mathcal{F} = \nabla \cdot \mathcal{M} - \epsilon_0 \frac{\partial(\vec{E} \times \vec{B})}{\partial t}, \tag{9.25}$$

where the second term is just the temporal change in the Poynting flux and $\mathcal{M}_{ij}$ is the Maxwell stress tensor,

$$\mathcal{M}_{ij} = -\delta_{ij}\left(\frac{\epsilon_0}{2}E^2 + \frac{1}{2\mu_0}B^2\right) + \epsilon_0 E_i E_j + \frac{1}{\mu_0}B_i B_j \tag{9.26}$$

The first term describes the isotropic pressure exerted on the plasma by the magnetic field. Because the electric field vanishes under normal circumstances in the heliosphere, we neglect it in the following considerations of the remaining part of $\mathcal{M}$, $(1/\mu_0)\, B_i B_j$. It describes a tension. Consider a small surface $\mathrm{d}\vec{S}$ in Fig. 9.8 whose normal vector points along the tangent to the magnetic field. Obviously, the i component of the surface normal $\vec{n}$ is then $n_i = B_i/B$. The tension acting on $\mathrm{d}S_i$ (and hence along B_i) is

$$\mathrm{d}S\, n_j\, B_i B_j/\mu_0 = \mathrm{d}S\, B_j\, B_i\, B_j/(\mu_0 B) = n_i\, \mathrm{d}S\, B^2/\mu_0. \tag{9.27}$$

The sign in the tension term is opposite of that in the pressure term which shows us that the two are indeed something else. $\mathcal{M}_{ij}$ is the force per unit area in the i direction exerted by the j component of the field. The force on the field within the flux tube depicted in Fig. 9.8 is exerted on it by the j component of the field coming from above $\vec{B}$ over the positive side of the surface $\mathrm{d}S_j$ onto the field on the negative side of the surface (inside the flux tube). Hence we may envisage bent field lines as rubber bands under tension. When the holding force disappears (as it does after the field lines leave the diffusion dominated reconnection region), they try to straighten out thus acquiring an energetically more favorable state. Reconnected field lines will thus tend to move away from the reconnection region and pull the plasma with them.

The process of reconnection, of outflowing plasma and contracting field lines probably generates a very turbulent medium in the vicinity of the reconnection site. It will tend to generate this on a large spatial scale (small wave number k) and the enormous amount of turbulent energy will cascade in a Kolmogorov-type cascade to higher and higher wave numbers k where it is absorbed by ions with a low Q/A ratio. The energy that is not absorbed is available to ions with a higher Q/A. Figure 7.4 shows a cartoon of the cascade process.

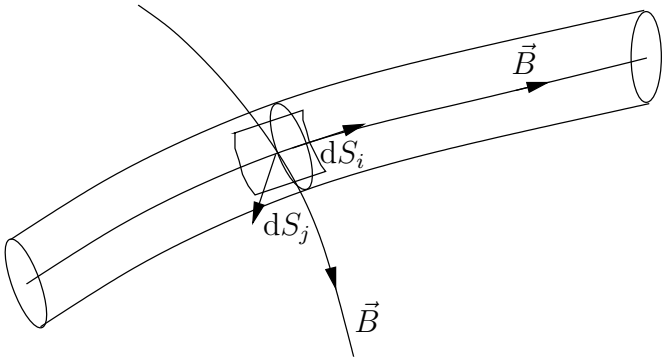

Figure 9.8: The Maxwell stress tensor $\mathcal{M}_{ij}$ describes the tension which the electromagnetic field in the j direction exerts on the field in the i direction.

9.4 Consequences of Reconnection

9.5 Observations of Reconnection

Add interplanetary observations here (**?**)

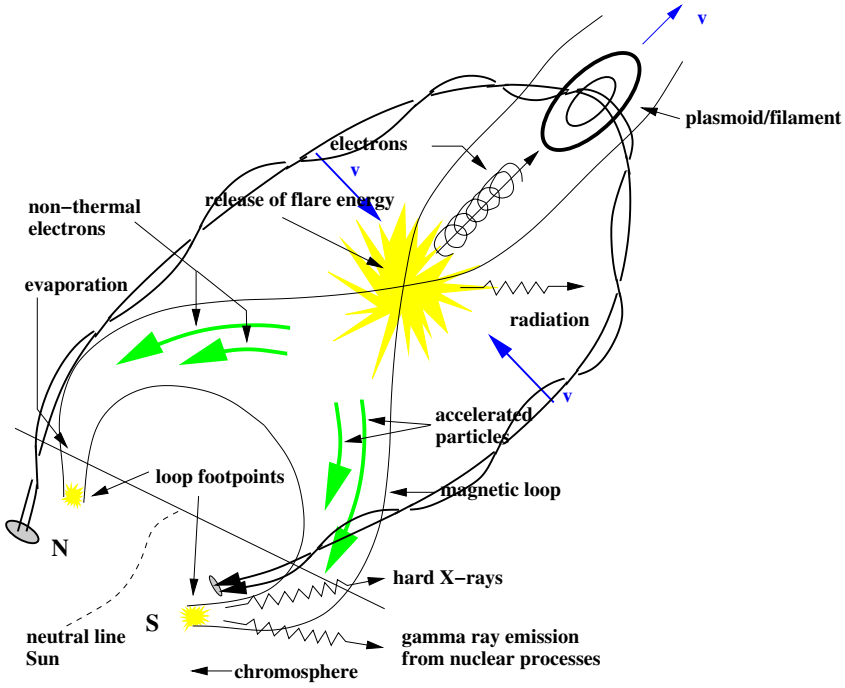

Figure 9.9: Model of a flare on the Sun, after *Lang* (2000) with modifications. *Add discussion of high outflow velocities as consequence of ongoing reconnection, SDO results, Shibata.*

Chapter 10

Sources of Particles in the Heliosphere

Chapter 11

Suprathermal Particles

Chapter 12

Particle Acceleration

Chapter 13

Particle Transport

2014-04-09: corrections not done yet

In this Chapter, we will consider various transport effects on particles, namely the Compton-Getting effect, adiabatic cooling or deceleration, and drifts. Following the logics of a review by *Fisk* (1999), we will then assemble all these processes into one equation, the so-called transport equation found by *Parker* in 1965 and now called Parker's equation.

13.1 The Compton-Getting Effect

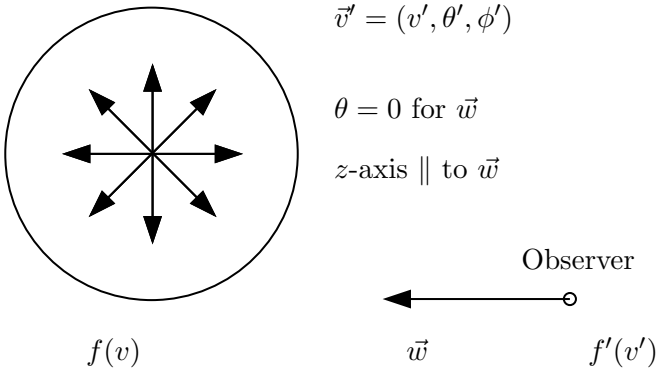

Figure 13.1: The Compton-Getting effect can be viewed as a relativistic aberration problem. See text for discussion.

Consider the situation sketched to the left in which an observer is moving at a velocity $\vec{w}$ through a background distribution of particles with a distribution function $f(\vec{v})$. The velocities of the particles appear red- or blue-shifted to the observer, depending on their relative motion,

$$\vec{v}' = \vec{v} - \vec{w}, \qquad (13.1)$$

the observer sees a distribution function

$$f'(\vec{v}') = f(\vec{v}) = f(\vec{v}' + \vec{w}). \qquad (13.2)$$

The question we want to ask and answer in this section is what kind of effects does the observer see which are only due to his motion relative to the distribution's rest frame. To put it more mathematically, how does the distribution

function $f(v)$ transform into the observer's frame of reference? Following *Gleeson* and *Axford* (1967, 1968), let us begin by assuming that the observer moves much more slowly than the particles, i.e., $|w| \ll |v|$, as is the case, e. g., with an observer in the solar wind, in SEPs or GCRs. We will begin with this non-relativistic case and give the relativistically correct results at the end. This allows us to concentrate on the underlying ideas and circumvent the more complex mathematical derivation. Because of the smallness of w compared to v, we may use a Taylor expansion of $f'(v')$,

$$\begin{aligned} f'(v') &= f(v'+w) = f(v') + \vec{w}\cdot\frac{\partial f(v')}{\partial \vec{v}'} + O\left((w\frac{\partial}{\partial v})^2 f\right) \\ &= f(v') + w\cos\theta'\frac{\partial f(v')}{\partial v'} + O\left(w^2\frac{\partial^2 f}{\partial v'^2}\right) \end{aligned} \tag{13.3}$$

This is a good approximation if $f(v)$ is sufficiently smooth, e. g., if $(v\partial_v)^n f = O(f)$.

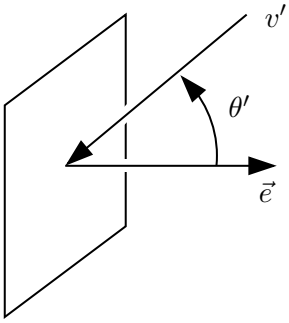

Figure 13.2: Geometry for $\vec{S}(v,\vec{e})$. See text for discussion.

Now it turns out that is is advantageous to consider the differential flux $\overline{S}(v,\vec{e})dv$ which is just the number of particles with speeds between v and $v+\mathrm{d}v$ which cross an unit area perpendicular to $\vec{e}$ per unit time. Then we can define the differential current density, $\vec{S}_v(\vec{v})$, by

$$\vec{S}_v(v) = \overline{S}(v,\vec{e}_{max})\vec{e}_{max}, \tag{13.4}$$

where $\vec{e}_{max}$ is the unit vector pointing in the direction in which $\overline{S}(v,\vec{e})$ has its greatest value.

Let us assume that $\vec{e}_{max}$ is parallel to $\vec{w}$. Then we can obtain $\vec{S}'_v$ by summing all particles crossing the unit area in the velocity range $(v', v+dv')$. The crossing is proportional to $v'\cos\theta'$ which takes the projection into account. Therefore, we have

$$S'_v(v')\mathrm{d}v' = \int_0^{2\pi}\mathrm{d}\phi' \int_0^{\pi}\mathrm{d}\theta'\left[f(v') + w\cos\theta'\frac{\partial f(v')}{\partial v'}\right](v')^3\cos\theta'\sin\theta'\mathrm{d}v' \tag{13.5}$$

Now we know that the following relation holds (see eq. ??? in **?**),

$$\int_0^{\pi}\mathrm{d}\theta'\ \cos^n\theta'\ \sin\theta' \ = \ -\frac{1}{3}\frac{1}{1+n}\cos^{n+1}\theta'\Big|_0^{\pi}$$

and yields $2/3$ for $n=2$, and, hence

$$\vec{S}'_v(v') = \frac{4\pi}{3}(v')^3\frac{\partial f(v')}{\partial v'}\vec{w}. \tag{13.6}$$

So where ha $f(v')$ gone? This is an isotropic distribution, and hence its contribution to S vanishes.

Let $U_v(v)$ be the differential density with respect to velocity, i. e. , there are $U_v dv$ particles per unit volume with speeds in the interval $[v, v+dv]$. Summing over all particles in $[v, v+dv]$ gives

$$U_v(v)\mathrm{d}v = \int_0^\pi \mathrm{d}\theta \int_0^{2\pi} \mathrm{d}\phi \; f(v)v^2 \sin\theta \mathrm{d}v \;=\; 4\pi v^2 f(v)\mathrm{d}v. \tag{13.7}$$

Next, we need to write $U_v(v)$ in the moving frame of reference, i.e., by using the primed quantities and eq. 13.2,

$$U'_{v'}(v')\mathrm{d}v' = \int_0^\pi \int_0^{2\pi} \mathrm{d}\theta' \; \mathrm{d}\phi' \; \left[f(v') + w\cos\theta' \frac{\partial f(v')}{\partial v'} \right] (v')^2 \sin\theta' \mathrm{d}v' \tag{13.8}$$

up to terms of order $w^2 \frac{\partial^2 f}{\partial v'^2}$. The integral over $w\cos\theta'$ vanishes, and we are left with

$$U'_{v'}(v') = 4\pi (v')^2 f(v') \tag{13.9}$$

Thus, we have found how the number of particles in a velocity interval in one frame, $U_v(v)$ transforms into the frame moving at speed w relative to it,

$$U_v(v) = U'_v(v'). \tag{13.10}$$

This is a remarkable finding, to first order in w/v the mean density at a speed v is unaltered by the motion $\vec{w}$!

Now differential densities and current densities are normally written as functions of kinetic energy T in terms of energy intervals $\mathrm{d}T$. For non-relativistic particles with rest mass m_0 we have

$$\mathrm{d}T = m_0 v dv \tag{13.11}$$

because $T = \frac{1}{2} m_0 v^2$ which, taking the derivative, transforms to $\frac{\mathrm{d}T}{\mathrm{d}v} = m_0 v$. We can transform to $U(T)$ and $S(T)$ by equating particle numbers

$$U(T)\mathrm{d}T = U_v(v)\mathrm{d}v \qquad ; \qquad S\mathrm{d}T = S_v \mathrm{d}v. \tag{13.12}$$

Thus, to summarize our results so far, we have with eqs. 13.6, 13.7, 13.9, 13.11, and 13.12

$$U(T) = U'(T') = \frac{4\pi v'}{m_0} f(v') \tag{13.13}$$

and

$$\vec{S}'(T') = \frac{4\pi}{3} \frac{v'^2}{m_0} \frac{\partial f'(v')}{\partial v'} \vec{w} \tag{13.14}$$

Next, we will express the current density $\vec{S}(T)$ in terms of T and differential intensity $U(T)$. We prepare

$$f = \frac{m_0}{4\pi v} U \qquad \text{and} \qquad v = \sqrt{\frac{2T}{m_0}},$$

and throw everything together

$$\begin{aligned}
S &= \frac{4\pi}{3}\frac{v^2}{m_0}\frac{\partial f}{\partial v} w \;=\; \frac{4\pi}{3}\frac{2T}{m_0^2}\frac{\partial f}{\partial v} w, \\
&= \frac{4\pi}{3}\frac{2T}{m_0^2}\frac{m_0}{4\pi}\frac{\partial\left(\frac{U}{v}\right)}{\partial v} w, \\
&= \frac{1}{3}\frac{2T}{m_0}\frac{\partial}{\partial T}\left(\frac{U}{v}\right)\frac{\partial T}{\partial v_0} w, \\
&= \frac{1}{3}\frac{2T}{m_0}\frac{\partial}{\partial T}\left(\frac{U}{v}\right) m_0 v w, \\
&= \frac{1}{3} 2T\sqrt{\frac{2T}{m_0}}\frac{\partial}{\partial T}\left(U\left(\frac{2T}{m_0}\right)^{-1/2}\right) w, \\
&= \frac{1}{3} 2T\sqrt{T}\frac{\partial}{\partial T}\left(UT^{-1/2}\right) w, \\
&= \frac{1}{3} 2T\sqrt{T}\left(\frac{\partial U}{\partial T}T^{-1/2} - \frac{1}{2}T^{-3/2}U\right) w, \\
&= \frac{1}{3} 2T\left(\frac{\partial U}{\partial T} - \frac{1}{2}\frac{U}{T}\right) w, \\
&= \frac{1}{3}\left(2\frac{\partial U}{\partial T}T - U\right) w, \\
&= -\left(U - \frac{1}{3}\frac{\partial}{\partial T}\left(2TU\right)\right) w,
\end{aligned}$$

where the last step was only done to obtain a result which looks similar to what one obtains in the relativistic case. Thus, we now have the expression for the transformation of the differential current density, $\vec{S}$,

$$\vec{S}'(T') = -\left[U' - \frac{1}{3}\frac{\partial}{\partial T'}(2T'U')\right]\vec{\omega}. \tag{13.15}$$

At relativistic speeds, the transformation given in eq. 13.2 must be replaced by the more complicated one,

$$f(v,\theta) = \gamma^5(1 + v'w'\cos\theta'/c^2)^5 f'(v',\theta') \tag{13.16}$$

where $\gamma = (1 - w^2/c^2)^{1/2}$, c is the speed of light, and (v,θ) and $(v'\theta')$ are related by the usual relativistic velocity transformation.

One can now go through the same steps as we did in the non-relativistic case to obtain the transformation properties of U and S for the relativistic case and finds:

$$U'(T') = U(T') \tag{13.17}$$

$$\vec{S}(T') = -\left[U' - \frac{1}{3}\frac{\partial}{\partial T'} \cdot (\alpha T' U')\right]\vec{\omega} \tag{13.18}$$

where

$$\alpha(T') \doteq \frac{T' + 2m_0c^2}{T' + m_0c^2} \tag{13.19}$$

In the non-relativistic case we have $T' \ll m_0c^2$, so the non-relativistic transformation, eq. 13.15, follows from eq. 13.18 with $T' \ll m_0c^2$ and $\alpha(T') = 2$. Eq. 13.18 is often rewritten in more compact form

$$\vec{S}(T') = -C(T')U'\vec{\omega}, \tag{13.20}$$

where

$$C(T') = \left(1 - \frac{1}{3}\frac{1}{U'}\frac{\partial}{\partial T'}(\alpha T' U')\right). \tag{13.21}$$

The quantitiy $\vec{S}$ is also called **streaming**. It is connected with the differential anisotropy ξ

$$\begin{aligned}\xi'(T') &= \frac{f'_{max} - f'_{min}}{f'_{max} + f'_{min}}\vec{e}_{max} = \left(\frac{\partial f'(v')/\partial v'}{f(v')}\right) \cdot w\vec{e}_{max} \\ &= \frac{3\vec{S}}{v'U'} = -\frac{3C(T')}{v'}\vec{w}\end{aligned} \tag{13.22}$$

For relativistic speeds $T' \to \infty$ and for a power-law distribution $U'(T') \propto (T')^{-\mu}$ we have

$$\begin{aligned}\xi' &= -\frac{3\vec{w}}{v'}\left(1 - \frac{1}{3}T^{\mu}\left(\frac{\partial}{\partial T}\right)\left(T^{1-\mu}\right)\right) \\ &= -\frac{3\vec{w}}{v'}\left(1 - \frac{1}{3}T^{\mu}(1-\mu)T^{-\mu}\right) \\ &= -\frac{3\vec{w}}{v'}\left(1 - \frac{1}{3}(1-\mu)\right) \\ &= -\frac{\vec{w}}{v'}(2+\mu)\end{aligned} \tag{13.23}$$

which is the result obtained by *Compton* and *Getting* (1935).

13.2 Adiabatic Cooling or Deceleration

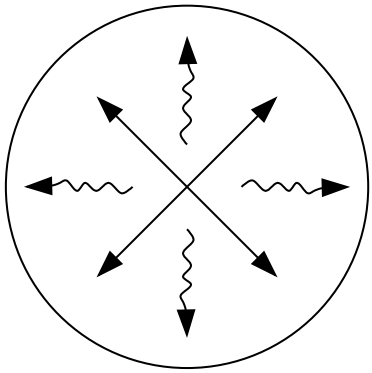

Figure 13.3: Scattering centers for particles are carried outwards by the expanding solar wind.

As energetic particles encounter the solar wind, they experience adiabatic cooling or deceleration which is due to the expansion of the solar wind. Scattering centers are convected out by the expanding solar wind. The inner energy, U, in a relativistic gas is determined by

$$\mathrm{d}U = \mathrm{d}W = -p\mathrm{d}V, \tag{13.24}$$

where the pressure, p, in such a gas is given by

$$p = \frac{1}{3}n\frac{T(T+2T_0)}{T+T_0} \tag{13.25}$$

where n is number density and T is kinetic energy and T_0 rest energy. With the usual definition of the Lorentz factor we have

$$p = \frac{1}{3}nT\frac{\gamma+1}{\gamma} \qquad \text{where} \qquad \gamma = \frac{1}{\sqrt{1-v^2/c^2}}. \tag{13.26}$$

We now want to investigate how the kinetic energy, T, changes as the gas expands (as it is doing work). With the above results we have

$$\mathrm{d}U = -\frac{1}{3}nT\frac{\gamma+1}{\gamma}\cdot\mathrm{d}V = \frac{-1}{3}nT\frac{T+2T_0}{T+T_0}\cdot\mathrm{d}V$$
$$\mathrm{d}U = n\cdot V\cdot\mathrm{d}\langle E\rangle = -\frac{1}{3}nT\frac{T+2T_0}{T+T_0}\mathrm{d}V$$
$$\frac{\mathrm{d}T}{T} = -\frac{1}{3}\frac{T+2T_0}{T+T_0}\frac{\mathrm{d}V}{V}$$

where the last line follows from the observation that a change in energy can only occur by chaning the kinetic energy, the rest energy remains unchanged. Inserting the volume change $\mathrm{d}V$

$$\begin{aligned}
\mathrm{d}V &= (r+\mathrm{d}r)^3\frac{4\pi}{3} - \frac{4\pi}{3}r^3 \\
&= \left[r^3 + 2r^2\mathrm{d}r + 0(\mathrm{d}r^2)\right]\frac{4\pi}{3} - \frac{4\pi}{3}r^3 \\
&= \frac{8\pi}{3}r^2\mathrm{d}r + 0(\mathrm{d}r^2) \\
\frac{\mathrm{d}V}{V} &= \frac{8\pi}{3}\frac{3}{4\pi}\frac{r^2\mathrm{d}r}{r^3} = 2\frac{\mathrm{d}r}{r},
\end{aligned}$$

we thus obtain

$$\begin{aligned}
\frac{1}{T}\frac{\mathrm{d}T}{\mathrm{d}t} &= -\frac{1}{3}\frac{T+2T_0}{T+T_0}\frac{2}{r}\frac{\mathrm{d}r}{\mathrm{d}t} \\
&= -\frac{1}{3}\frac{T+2T_0}{T+T_0}\frac{2v}{r}.
\end{aligned}$$

But $\frac{2v}{r}$ is actually $\vec{\nabla}\vec{v}$ in an isotropic (radially) expanding wind. Thus,

$$\frac{1}{T}\frac{\mathrm{d}T}{\mathrm{d}t} = -\frac{1}{3}\frac{T+2T_0}{T+T_0}\vec{\nabla}\cdot\vec{v} \tag{13.27}$$

This is actually due to the scattering of particles off the irregularities in the fields frozen into the solar wind. We will investigate this in more detail later on.

13.3 Drifts or Streaming

We follow Isenberg and Jokipii(1979) and will show that, for a magnetic field of arbitrary spatial variation, a nearly isotropic distribution of charged particles drifts with a velocity $\langle\vec{v}_D\rangle$.

To begin, consider a situation in which the particle gyroradius

$$R_g = \frac{1}{q}\frac{\vec{B}\times\vec{p}}{B^2} \tag{13.28}$$

is much smaller than any scale of variation of the magnetic field,

$$R_g \ll L \hat{=} \left|\frac{1}{B}\frac{\partial B_i}{\partial x_j}\right|^{-1} \tag{13.29}$$

We will relax this requirement shortly, so just bear with it for the time being. The drift of the particle is given by the general expression

$$\langle\vec{v}_D\rangle = \frac{pv}{3qB^4}\left(B^2(\vec{\nabla}\times\vec{B}) + \vec{B}\times\vec{\nabla}B^2\right) \tag{13.30}$$

This result is obtained for an isotropic pitch-angle distribution.

Now consider a 'nearly isotropic' distribution function. A perfectly isotropic particle distribution must be homogeneous in space. In our case, in which we are investigating the transport of particles in interplanetary space, this space is permeated by a magnetic field. Now a static magnetic field can not produce any observable effect on such a particle population because a magnetic field performs no work. This means that any observable drift requires the presence of some level of anisotropy or spatial inhomogeneity in the plasma.

So let us assume a particle distribution, n, with a small anisotropy, δn,

$$\begin{aligned} n &= n_0 + \delta n(\Omega), \quad \text{where} \\ n_0 &= \frac{1}{4\pi}\int n\mathrm{d}\Omega \gg \delta n(\Omega) \propto \nabla n_0, \end{aligned}$$

where n_0 is the isotropic part of the distribution. Moreover, let's assume that temporal changes of the system are smaller than other time scales

$$\left|\frac{\partial A}{\partial t}\right| \ll \left|\frac{A}{\tau}\right| \ll |\omega A|, \tag{13.31}$$

where $\omega_i = \frac{qB_i}{\gamma mc}$ is the gyrofrequency and A some macroscopic parameter.

The distribution function for these particles then satisfies the Boltzmann eq.

$$\dot{n} + \vec{v}\cdot\vec{\nabla}n + \frac{q}{\gamma mc}(\vec{v}\times\vec{B})\frac{\partial n}{\partial \vec{v}} = -\frac{n-n_0}{\tau}, \tag{13.32}$$

where the right-hand side is the collision term which forces the system toward equilibrium or isotropy in a typical time τ.

Next we multiply eq. 13.32 by v and average over all directions,

$$\dot{F}_i + \int v_i v_j \frac{\partial n}{\partial x_j}\mathrm{d}\Omega + \frac{q}{\gamma mc}\int v_i(\vec{v}\times\vec{B})_j\frac{\partial n}{\partial v_j}\mathrm{d}\Omega = -\frac{F_i}{\tau}, \tag{13.33}$$

where $F_i = \int v_i n \mathrm{d}\Omega$. Now with $n_0 = \frac{1}{4\tau}\int n\mathrm{d}\Omega \ll \delta n$ we have

$$\int v_i v_j \frac{\partial}{\partial x_j}(n+\delta n)\mathrm{d}\Omega \approx \int v_i v_j \frac{\partial n_0}{\partial x_j}\mathrm{d}\Omega = \frac{v^2}{3}\frac{\partial n_0}{\partial x_i} \tag{13.34}$$

The third term is more complicated. First we note that

$$\frac{\partial}{\partial v_j}\left(v_i(\vec{v}\times\vec{B})_j n\right) = \delta_{ij}\cdot(\vec{v}\times\vec{B})_j + v_i\frac{\partial}{\partial v_j}(\vec{v}\times\vec{B})_j n + v_i(\vec{v}\times\vec{B})_j\frac{\partial n}{\partial v_j}. \tag{13.35}$$

Now $(\vec{v}\times\vec{B})_j$ is independent of v_j, and hence

$$\frac{\partial}{\partial v_j}(\vec{v}\times\vec{B})_j = 0. \tag{13.36}$$

Thus,

$$\frac{\partial}{\partial v_j}\left(v_i(\vec{v}\times\vec{B})_j n\right) = \delta_{ij}(\vec{v}\times\vec{B})_j n + v_i(\vec{v}+\vec{B})_j\frac{\partial n}{\partial v_j} \tag{13.37}$$

Integrating this expression over all directions must vanish because every contribution from one combination of components is cancelled by another,

$$\int \frac{\partial}{\partial v_j}\left(v_i(\vec{v}\times\vec{B})n\right)\mathrm{d}\Omega = 0. \tag{13.38}$$

Thus we have

$$\dot{\vec{F}} + \frac{v^2}{3}\vec{\nabla}n_0 - \frac{q}{\gamma mc}(\vec{F}\times\vec{B}) = \frac{\vec{F}}{\tau}. \tag{13.39}$$

Now $\dot{F}$ can be neglected because of the assumption given in eq. 13.31. We want to solve this for $\vec{F}$ to derive the distribution function. This can be done

by writing the cross product with the fully anti-symmetric Levi-Civita tensor, ε_{ijh},

$$(\vec{F} \times \vec{B})_i = \varepsilon_{ijh} F_j B_k. \tag{13.40}$$

With this we can solve for F_i,

$$F_i = -\frac{v^2\tau}{3}\frac{\partial n_0}{\partial x_j} \cdot (\delta_{ij} - \varepsilon_{ijh}\omega_k\tau)^{-1}. \tag{13.41}$$

This expression is still a little unwieldy and we use the following approximation

$$(\delta_{ij} - \varepsilon_{ijh}\omega_k\tau)^{-1} \approx \frac{\delta_{ij} + \varepsilon_{ijh}w_k\tau + w_i w_j\tau^2}{1 + w^2\tau^2} \tag{13.42}$$

to obtain an approximate solution,

$$F_i = -\frac{v^2\tau}{3} \cdot \frac{\delta_{ij} + \varepsilon_{ijh}\omega_k\tau + \omega_i\omega_j\tau^2}{1 + \omega^2\tau^2}\frac{\partial n_0}{\partial x_j}. \tag{13.43}$$

The coefficient of $-\vec{\nabla}n_0$ can be thought of as a diffusion tensor. The symmetric part,

$$\kappa^s_{ij} = \frac{v^2\tau}{3}(1 + \omega^2\tau^2)^{-1}(\delta_{ij} + \omega_i\omega_j\tau^2), \tag{13.44}$$

produces the anisotropic scattering or diffusion. The antisymmetric part contains the drift effects. In the limit $\omega\tau \ll 1$, i. e. for very efficient scattering, we have an isotropic diffusion tensor

$$\kappa_{ij} \overset{\omega\tau\ll 1}{\longrightarrow} \frac{v^2\tau}{3}\delta_{ij} \tag{13.45}$$

On the other hand, for weak scattering, as we assumed in eq. 13.31, we have $\omega\tau \gg 1$ and thus,

$$-\frac{v^2}{3}\frac{\varepsilon_{ijh}\omega_k\tau}{\omega^2\tau^2} \cdot \tau\frac{\partial n_0}{\partial x_j} \tag{13.46}$$

is the antisymmetric part. With $\omega = \frac{qB}{\gamma mc}$ we then obtain

$$-\frac{pvc}{3q}\varepsilon_{ijh}\frac{B_k}{B^2}\frac{\partial n_0}{\partial x_j}. \tag{13.47}$$

Adding both symmetric and antisymmetric parts, we obtain

$$F_i = -\kappa^{(s)}_{ij}\frac{\partial n_0}{\partial x_j} - \frac{pvc}{3p}\varepsilon_{ijh}\frac{B_k}{B^2}\frac{\partial n_0}{\partial x_j} \tag{13.48}$$

We have now finally found the quantity F_i which is called 'streaming' and is related to drifts.

Let us now investigate what it means and how it can be used. Consider an isotropic distribution, $n = n_0$, and insert it into the Boltzmann eq., eq. 13.32

$$\dot{n} + \vec{v}\vec{\nabla}n + \frac{q}{\gamma mc}(\vec{v} \times \vec{B})\frac{\partial n}{\partial \vec{v}} = -\frac{n - n_0}{\tau}, \tag{13.49}$$

which we will now average over directions, i. e. perform the integration $\int \mathrm{d}\Omega$. The right-hand side vanishes by definition. The last term on the left-hand side vanishes as well because the velocity distribution is assumed to be isotropic and hence $\int \langle \frac{\partial n}{\partial v} \rangle \mathrm{d}\Omega = 0$. Thus, only the following survives this directional averaging,

$$\dot{n}_0 + \frac{\partial F_i}{\partial x_i} = 0. \qquad \text{Why?} \tag{13.50}$$

We can now insert the streaming from above (eq. 13.48) to obtain

$$\dot{n}_0 = \frac{\partial}{\partial x_i}\left(\kappa_{ij}^{(s)}\frac{\partial n_0}{\partial x_j}\right) + \frac{pvc}{3q}\varepsilon_{ijh}\left(\frac{\partial B_j}{\partial x_i B^2}\right)\frac{\partial n_0}{\partial x_n} = 0 \tag{13.51}$$

This is simply an equation which describes particles differing according to $\kappa_{ij}^{(s)}$ and convecting with a convection speed

$$\langle v_D \rangle_k = \frac{pvc}{3q}\varepsilon_{ijh}\frac{\partial}{\partial x_i}\frac{B_j}{B^2} \tag{13.52}$$

This can be rewritten in the form

$$\langle \vec{v}_D \rangle = \frac{pvc}{3q}\left(\frac{1}{B^2}\vec{\nabla} \times \vec{B} + \frac{1}{B^4}\vec{B} \times \vec{\nabla}B^2\right) \tag{13.53}$$

which is identical to the first drift speed which is derived under entirely different assumptions! The reason for this is intuitively clear. Imagine a 'local gyro-orbit' - the trajectory a particle would take in a uniform field. The isotropic distribution guarantees that, at any point, there will be a particle moving along any given portion of that 'local gyro-orbit'.

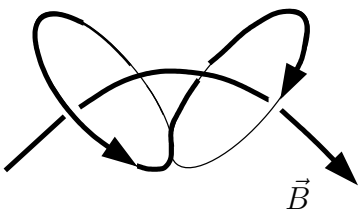

Figure 13.4: A particle can leave its local gyro-orbit.

In a spatially varying field, the particle will leave its local gyro-orbit after a short time (see Fig. 13.3 to the left). It will always be replaced by another particle for the next portion of its original local gyro-orbit. In addition, the ensemble averaging will smooth any sharp changes in the field over a spatial scale of 2 gyro-radii. Thus, the ensemble averaging over an isotropic distribution and the first-order approximation produce the same result.

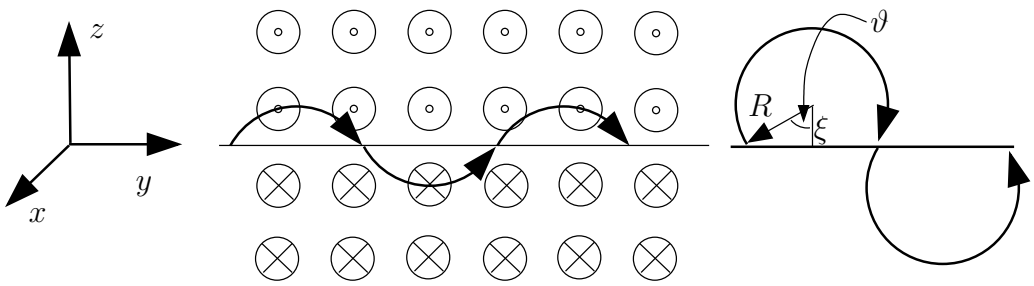

Figure 13.5: Particle drift at the heliospheric current sheet.

13.4 An Example of Drifts with a discontinuous $\vec{B}$-field configuration

Following *Isenberg* and *Jokipii* (1979), let us consider an extended thin neutral (current) sheet such as an interplanetary sector boundary. Its extent is certainly much smaller than the gyroradius of a cosmic ray.

Consider

$$\vec{B} = B_0(2\theta(z) - 1)\vec{e}_x, \tag{13.54}$$

where $\theta(z)$ is the Heaviside step function. The motion of the guiding center is not continuous or smooth, it moves in steps along the y-direction, as shown in Fig. 13.5, where the quantities used in the following discussion are also defined. Nevertheless, we can compute the particle drift velocity. Consider a particle in the region $z \geq 0$ with a temporary guiding center at position $z = \xi \geq -R$. As long as $|\xi| < R$ it will drift a distance $R\sin\vartheta$ in the y-direction while it moves a distance $R(\pi - \vartheta)$ along its gyro-orbit or rather it moves by $2R\sin\vartheta$ along the y-direction while it moves $2R(\pi - \vartheta)$ along its gyro-orbit. So the drift velocity of its particle is

$$\begin{aligned} \vec{V}_0 &= v \cdot \sin\alpha \frac{\sin\vartheta}{\pi - \vartheta} \cdot \vec{e}y \qquad \text{for} \quad |\xi| < R \\ &= 0 \qquad \text{for} \quad |\xi| \geq R, \end{aligned}$$

where α is the particle pitch angle and $\theta = \arccos(\xi/R)$ as defined in Fig. 13.5.

Now consider an isotropic distribution of particles in this field. We sum over all the individual particle velocities and average over pitch angle to obtain the total flux of particles.

$$\vec{F} = \frac{N}{4\pi} \int \mathrm{d}\Omega \int \mathrm{d}\xi f(\xi) \vec{V}_D(\xi, \Omega). \tag{13.55}$$

Here, N is the local (uniform) particle number density and $f(\xi)$ is the distribution function which gives the number of particles with guiding centers at $z = \xi$.

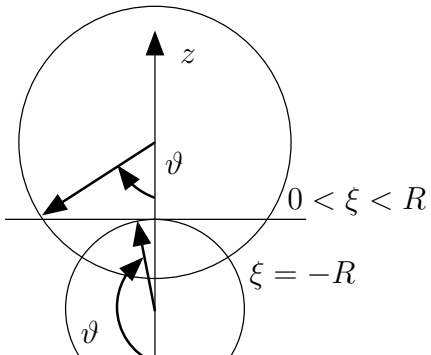

The guiding centers will be uniformly distributed along the z direction, se Fig. 13.4. In the region $|z| \leq R$ they can be described by $\xi = R \cdot \cos\vartheta$ where θ varies from 0 to π for $\xi = +R$ to $\xi = -R$. In this region we have

$$f(\xi) = \frac{\pi - \vartheta}{\pi} \quad \text{for} \quad z > 0 \tag{13.56}$$

and we have the same contribution for $z < 0$ because particles in $z > 0$ have their guiding centers in $z > 0$ or in $z < 0$. Thus,

$$\begin{aligned}
\vec{F} &= \frac{N}{2\pi}\int_0^{2\pi} \mathrm{d}\phi \int_0^{\pi} \mathrm{d}\alpha \sin\alpha \int_{-R}^{R} \mathrm{d}\xi \frac{\pi - \vartheta}{\pi} v \sin\alpha \frac{\sin\vartheta}{\pi - \vartheta}\vec{e}_y \\
&= \frac{Nv}{\pi}\int_0^{\pi} \mathrm{d}\alpha \sin^2\alpha \int_{-R}^{R} \mathrm{d}(R\cos\vartheta)\sin\vartheta\vec{e}_y \\
&= (-1)^2\frac{Nv}{\pi}\frac{p}{qB}\int_0^{\pi} \mathrm{d}\alpha \sin^3\alpha \int_0^{\pi} \mathrm{d}\vartheta \sin^2\vartheta\vec{e}_y \\
&= \frac{Nv}{\pi}\frac{p}{qB}\frac{2\pi}{3}\vec{e}_y = \frac{2}{3}\frac{Nvp}{qB}\vec{e}_y,
\end{aligned}$$

where we have used

$$\int_{-R}^{R} \mathrm{d}\xi \rightarrow -\int_{\pi}^{0} \mathrm{d}\theta \sin\theta \rightarrow \int_0^{\pi} \mathrm{d}\theta \sin\theta \tag{13.57}$$

in the step between line 2 and 3 as well as the integral identities

$$\begin{aligned}
A: \qquad \int_0^{\pi} \mathrm{d}x \sin^2 x &= \left[-\frac{1}{2}\left(x - \sin x \ \cos x\right)\right]_0^{\pi} = \left[-\frac{1}{2}x\right]_0^{\pi} = -\frac{\pi}{2}, \\
B: \qquad \int_0^{\pi} \mathrm{d}x \sin^3 x &= \left[-\frac{1}{3}\left(sin^2 x \ \cos x \ + 2\cos x\right)\right]_0^{\pi} = \left[-\frac{2}{3}\cos x\right]_0^{\pi} = \frac{4}{3}, \\
&\text{and thus} \quad A \cdot B = -\frac{2\pi}{3}.
\end{aligned}$$

With the general definition of a flux

$$\vec{F} = N \cdot \vec{v}_D, \tag{13.58}$$

we now have the expression for the drift velocity of an isotropic distribution of particles along the current sheet described by eq. 13.54,

$$\vec{v}_D = \frac{2}{3} v \frac{p}{qB}\vec{e}_y \tag{13.59}$$

Obviously, the requirement $|R| \ll |\frac{1}{B}\frac{\partial B_i}{\partial x_j}|^{-1}$ is not satisfied, but the result for the drift velocity is still valid. This can be seen by inserting this field configuration into the general expression for the drift velocity.

The requirement that the spatial scale of field changes be small compared to the gyro-radius is replaced by the ensemble average over the isotropic distribution. The same holds true for the requirement that $|\frac{\partial A}{\partial t}| \ll |\frac{A}{\tau}| \ll |\omega A|$. In an isotropic distribution, there will always be a particle which takes the place of a particle which leaves its local gyro-radius, as discussed at the end of the previous subsection.

13.5 Putting Everything Together

So far, we found two expressions for the streaming of particles. From the considerations of the Compton-Getting effect we found

$$\vec{S}(T) = -C(T)U\vec{\omega}, \qquad \text{where} \qquad C(T) = \left(1 - \frac{1}{3U}\frac{\partial}{\partial t}(\alpha T U)\right). \tag{13.60}$$

We also found a contribution which is due to drifts which is given by

$$F_i = -\kappa^s_{ij}\frac{\partial n_0}{\partial x_j} + \frac{pvc}{3q}\xi_{ijh}\frac{B_j}{B^2}\frac{\partial n_0}{\partial x_k} \tag{13.61}$$

The two derivations did not use the same nomenclature. n_0 is defined as the isotropic part of a particle distribution function n such that $n = n_0 + \delta n(\Omega)$ where

$$n_0 = \frac{1}{4\pi}\int \mathrm{d}\Omega u \gg \delta n(\Omega) \tag{13.62}$$

On the other hand, U was defined as the differential density with respect to velocity

$$\begin{aligned} U_v(v) &= \int_0^{2\pi}\mathrm{d}\varphi\int_0^{\pi}\mathrm{d}\vartheta\sin\vartheta f(v)v^2 \\ U_v(v) &= \int \mathrm{d}\Omega v^2 f(v) \\ &= \int \mathrm{d}\Omega f(\vec{v}) \end{aligned}$$

Thus, n_0 and U are the same up to a normalization factor 4π. However, no mention of the normalization of U and u_0 was ever made and so, without loss of generality, we will equate U and n_0 and use U from now on.
The relative velocity, $\vec{w}$, between the two frames of reference in the Compton-Getting derivation of the streaming was

$$\vec{w} = -\vec{V}_{s\omega} \tag{13.63}$$

as the cosmic rays were assumed to be isotropic in a stationary frame of reference.
Now consider again the direction-averaged Boltzmann-equation (eq. 13.50) in our new nomenclature

$$\dot{U} + \vec{\nabla} \cdot \vec{S} = 0. \tag{13.64}$$

In a stationary state we have

$$\vec{\nabla} \cdot \vec{S} = 0. \tag{13.65}$$

All we need to do now is to insert all the terms of $\vec{S}$ to find the general transport equation for cosmic rays. We also need to remember the definition of the drift velocity which we derived from the Boltzmann equation. Then we can put everything together to obtain

$$\begin{aligned} \vec{\nabla} \cdot S = & -\vec{\nabla} \cdot \kappa^{(s)} \cdot \vec{\nabla} U && \text{diffusion} \\ & + \langle \vec{v}_D \rangle \vec{\nabla} U && \text{drifts,} \\ & + \vec{\nabla} \cdot \vec{V}_{s\omega} U && \text{convection,} \\ & - \frac{1}{3} \vec{\nabla} \cdot \vec{V} \frac{\partial}{\partial T} (\alpha T U) = 0 && \text{adiabatic cooling.} \end{aligned}$$

This is the general equation for U, the differential number of galactic cosmic rays, i. e., the number of particles per unit volume and energy. This equation was first derived by *Parker* (1965).

Let us discuss the cosmic ray transport equation. It describes galactic cosmic rays which diffuse among the irregularities and turbulence of the magnetized solar wind. This diffusion is governed by the diffusion term which is determined by the diffusion tensor. This was defined as the symmetric part $\kappa^{(s)}$ of a more general 'diffusion tensor'. Because of the gradient of cosmic rays (there are more cosmic rays outside the heliosphere than inside) this diffusion amounts to an inward flux of particles. This inward diffusion is balanced by the outward convection at the speed of the solar wind. If we only consider these two terms, we have a classical diffusion-convection equation such as, for example, that of heat conduction through running water. In one dimension and for a spatially homogeneous diffusion tensor, we would have

$$\kappa \partial_x^2 u = v_D \partial_x u. \tag{13.66}$$

This can be rewritten

$$\left(\partial_x - \frac{v - \partial_x \kappa_x}{\kappa} \right) (\partial_x - 0) U = 0 \tag{13.67}$$

which has the solution

$$U(x) = C_1 + C_2 e^{\frac{v - \partial_x \kappa}{\kappa} x}. \tag{13.68}$$

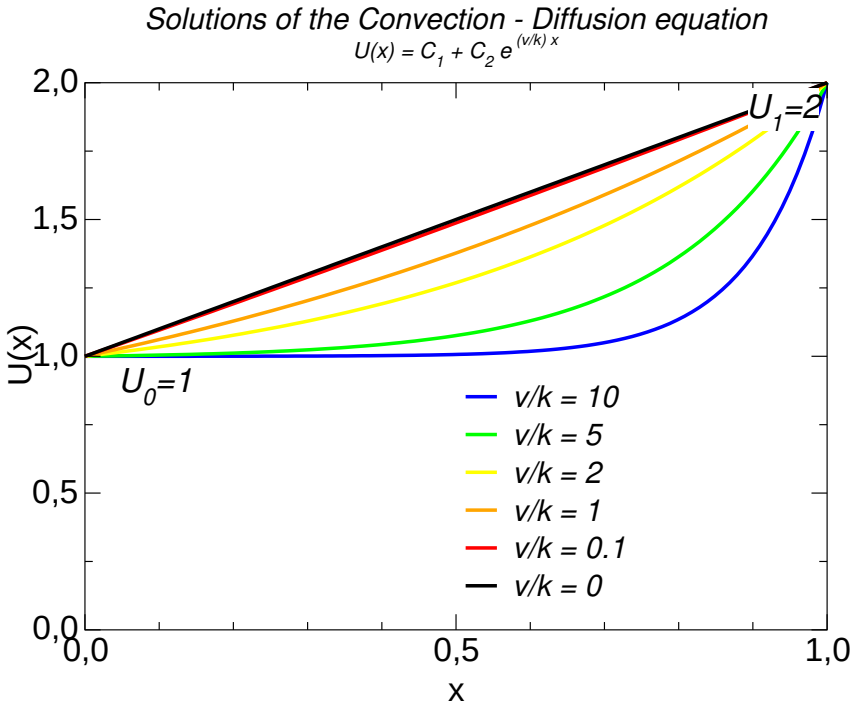

Figure 13.7: Solutions of the convective diffusion equation.

For $\partial_x \kappa = 0$ (as assumed above), we have

$$U(x) = C_1 + C_2 e^{\frac{v}{\kappa} \cdot x} \tag{13.69}$$

For small values of v/κ, this reduces to the ordinary diffusion solution. For non-zero v/κ, there is an exponential increase with growing x, as illustrated in Fig. 13.7. This results in a radial gradient of typically a few percent per AU in the intensity of cosmic rays (*Teegarden et al.*, 1974).

$$\frac{\partial_r U}{U} \approx \text{few percent/AU} \tag{13.70}$$

However, we aren't yet through our discussion of Parker's equation. As the cosmic rays bounce off the irregularities in the expanding wind they are adiabatically cooled. This happens because they are isotropic (nearly) in the frame of reference that is convected out by the solar wind and expands with it. This cooling is given by the adiabatic cooling term.
Finally, the particles experience drifts which are due to gradients and curvatures of the mean magnetic field. These ensemble-averaged drifts can also be expressed as a convection at drift speed

$$\vec{v}_D = \frac{pvc}{3q} \left(\vec{\nabla} \times \frac{\vec{B}}{B^2} + \frac{1}{B^4} \vec{B} \times \vec{\nabla} B^2 \right) \tag{13.71}$$

In the vicinity of the current sheet the first term dominates. The effect of drifts can be expressed as a 'streaming' of particle distributions mormal to the magnetic field

$$\vec{S'} = \frac{pvc}{3q}\frac{\vec{B}}{B^2} \times \vec{\nabla} U. \tag{13.72}$$

This is a cross product and was found to be the off-diagonal component of the diffusion tensor. We found that

$$\vec{\nabla} \cdot \vec{S'} = \frac{pvc}{3q}\vec{\nabla} \times \frac{\vec{B}}{B^2} \cdot \vec{\nabla} U = \vec{v}_D \cdot \vec{\nabla} U. \tag{13.73}$$

This is a divergenceless convection at the drift speed. Interestingly each of the four terms in Parker's transport equation turns out to be of comparable magnitude (*Jokipii et al.*, 1977).

We can treat the diffusion-convection equation a little more generally than before. Including adiabatic deceleration, we have

$$-\kappa \partial_r^2 U + \partial_r (CU\vec{V}) = 0 \tag{13.74}$$

where C is now the Compton-Getting factor. We assume $\partial_r \vec{V} = 0$ and $\partial_r C = 0$. Then we again obtain a radial gradient in U

$$\begin{aligned}
\partial_r^2 U &= \frac{C|\vec{V}|}{\kappa}\partial_r U \\
\frac{\partial_r U}{U} &= \frac{CV}{\kappa} \qquad\qquad C_1 = 0 \text{ because } U(0) = 0 \\
\frac{\partial U}{U} &= \frac{CV}{\kappa} dr \\
\ln U &= \frac{CV}{\kappa} \int \mathrm{d}r
\end{aligned}$$

where we have performed an integration in the steps between lines 1 and 2 and lines 2 and 3. With this we can obtain a 'modulation factor' M

$$M = \frac{U(r = r_{\rm obs})}{U(r = r_{\rm out})} \tag{13.75}$$

by integrating from an inner boundary at the observer, e. g. , at Earth, out to $r = r_{\rm obs}$, the source of galactic cosmic rays outside the heliosphere at $r = r_{\rm out}$

$$M = \frac{U(r = r_{\rm obs})}{U(r = r_{\rm out})} = \exp\left(-\frac{CV}{\kappa}\int_{r_{\rm obs}}^{r_{\rm out}} \mathrm{d}r\right).$$

For a diffusion coefficient which depends on the particle rigidity $P = \frac{\gamma m v}{q}$ via

$$\kappa \alpha P \cdot v, \tag{13.76}$$

we obtain

$$M = \exp\left(-\text{const.} \cdot \frac{3CV}{v} \int_{r_{\rm obs}}^{r_{\rm out}} \frac{\mathrm{d}r}{\lambda_{\rm mfp}}\right) \tag{13.77}$$

where the integral counts the number of scatters or mean free paths (mfps) of the particle. $\lambda_{\rm mfp}$ is the particle's mean free path. The quantity

$$\phi = \frac{3CV}{v} \int_{r_{\rm obs}}^{r_{\rm out}} \frac{dr}{\lambda(r)} \tag{13.78}$$

is called the modulation parameter and can be interpreted in terms of an effective potential of a conservative force field. It varies from about 350 MeV at solar activity minimum to about 750 MeV at solar activity maximum.

Parker's transport equation

$$\vec{\nabla} \cdot \vec{V}_{s\omega} U - \frac{1}{3} \vec{\nabla} \cdot \vec{V} \frac{\partial}{\partial T}(\alpha t U) + \vec{v}_D \vec{\nabla} U = \vec{\nabla} \cdot \kappa \vec{\nabla} U \tag{13.79}$$

looks deceitfully simple. In fact, no analytic solutions are known for it in the general form shown here. We have investigated some highly simplified versions of it but cannot discuss it in full detail.

Numerical solutions use Parker's equation superimposed on (magneto) hydrodynamic codes that describe heliospheric structure to simulate the transport of galactic cosmic rays throughout the heliosphere. Nevertheless, there are several problems apart from the sheer size of solving the coupled MHD equations that describe the heliosphere in 3-d:

1. The expression for the diffusion tensor κ is uncertain or even controversial. Obviously it has to do with the process of scattering. As we will see in section (next section) we don't even really understand the mean free path of energetic particles, let alone their scattering processes.

2. The magnetic field in the heliosphere is also an important factor in Parker's equation. It enters through the drift term but also through the diffusion tensor. Diffusion along $\vec{B}$ is much easier than perpendicular to $\vec{B}$.

So it turns out that we need to understand better the scattering process and the magnetic field. The latter was believed to be well modeled by an Archimedian spiral (Parker spiral), but observations by Ulysses have cast doubt on this. Low-energy particles ($\sim$50 MeV electrons and sub-MeV protons) are accelerated at shocks driven by co-rotating interaction regions. These regions extend in heliospheric latitude about up to the heliographic extent of the streamer belt. However, Ulysses saw accelerated particles occuring like a clock every solar rotation at heliospheric latitudes which greatly exceed those of the streamer belt and also of the locations where CIRs were observed, always

below 40 degrees. Ulysses saw these reoccuring particle increases up to the highest latitudes observed, above 80 degrees.

If the magnetic field follows the Parker Archimedian spiral, then there would have to be strongly enhanced cross-field diffusion to transport these particles up to those high latitudes. However, this seems highly unlikely.

The problem could be addressed by a process called footpoint motion. A systematic motion of footpoints across all latitudes is suggested by *Fisk* (1996). This model is based on the observation that coronal holes exhibit nearly rigid rotation with the Sun whereas the photosphere rotates differentially with a pronounced latitude dependence of the rotation rate. This systematic motion of footpoints would connect low and high latitudes and allow efficient transport of particles along field lines.

A random footpoint motion had already been put forward by Jokipii and Parker (1969). In their picture, random photospheric motions let the footpoints of magnetic field lines diffuse across the photosphere. This process too allows to connect low and high latitude regions in the heliosphere.

Consider for a moment the implications of such footpoint motion – be it systematic or random does not really matter. It will dramatically alter the heliospheric magnetic structure. While old models predicted nearly radial magnetic fields over the solar poles this would no longer be the case. For cosmic rays this would mean that they would no longer have easy access over the poles – an observation indeed made by Ulysses. On the other hand, such configurations would have a highly complicating consequence on the drift terms in the transport equation. Would they even conspire to average out to a diffusion-like behavior? Then they would have to be included in the diffusion tensor.

And this is where we encounter the next problem. There is no reliable and independent way to calculate the diffusion tensor. Inspite of the fact that we should be able to neglect higher-order terms in a power-series expansion of magnetic field fluctuations (so-called quasi-linear theory), the mean free paths calculated with such approximations strongly disagree with observations. Therefore, many modelers fit the diffusion tensor to the observations which can hardly be called a satisfactory state. If we consider diffusion along the magnetic field, we find far less scattering than we expect, while we find far more scattering across field lines than we can explain.

This is why footpoint motion may be a key to solving the problem. It mimicks cross field diffusion.

13.6 The Focused Transport Equation

We begin our considerations with the Liouville equation

$$\frac{\mathrm{D}f}{\mathrm{d}t} = 0 = \partial_t f + \vec{v}\partial_{\vec{r}} f + \vec{F}\partial_{\vec{p}} f = 0, \tag{13.80}$$

where

$$\begin{aligned} f(\vec{r},\vec{p},t) &= \frac{\mathrm{d}^6 n}{\mathrm{d}r^3\ p^2\mathrm{d}p\sin\vartheta\mathrm{d}\vartheta\mathrm{d}\varphi}, \\ &= \frac{\mathrm{d}^6 n}{\mathrm{d}r^3 p^2\mathrm{d}p\mathrm{d}\Omega} \doteq \frac{1}{p^2}\hat{f}(\vec{r},\vec{p},t) \end{aligned} \tag{13.81}$$

We can write this with the differential directional intensity, $I(\vec{r},E,\vec{\Omega},t)$, using $\mathrm{d}E/\mathrm{d}p = v$. Then

$$f = \frac{\mathrm{d}^6 n}{\mathrm{d}r^3 p^2\mathrm{d}p\mathrm{d}\Omega} = \frac{v}{p^2}\frac{\mathrm{d}^6 n}{\mathrm{d}r^3\mathrm{d}E\mathrm{d}\Omega} \doteq \frac{1}{p^2} I(\vec{r},E,\vec{\Omega},t). \tag{13.82}$$

The units of $I(\vec{r},E,\vec{\Omega},t)$ are

$$\left[I(\vec{r},E,\vec{\Omega}mt)\right] = \left(\mathrm{cm}^2\ \mathrm{sr\ s\ MeV}\right)^{-1}.$$

The differential flux, $J(\vec{r},E,t)$, is given by

$$J(\vec{r},E,t) = \frac{1}{4\pi}\int \mathrm{d}\Omega\ I(\vec{r},E,\vec{\Omega},t) \tag{13.83}$$

and particle number density by

$$\frac{\mathrm{d}^4 n}{\mathrm{d}r^3\mathrm{d}E} = \frac{1}{v}\int \mathrm{d}\Omega I(\vec{r},E,\vec{\Omega}t) = \frac{4\pi}{v} J(\vec{r},E,t) = N(\vec{r},E,T)$$

where the second last step is valid for an isotropic differential directional intensity, I.

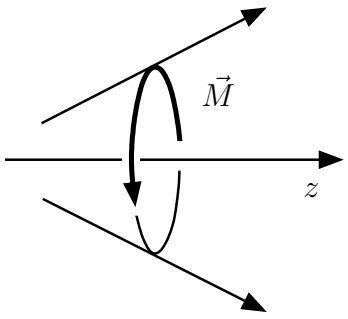

Figure 13.8: Mirror force

Next, we consider gyrotropic distributions in which the phase angle, φ, of the gyration is irrelevant. Then only the pitch angle of the particle is important and the particle can only move along the magnetic field. Thus, we have a reduced phase space density

$$f = f(z,\mu,t),$$

where z is the length along the magnetic field and $\mu = \cos\alpha$ is the cosine of the pitch angle. Thus,

$v_\parallel = v_z = |v|\cdot\mu$, and $\vec{p} = \begin{pmatrix} p_\parallel \\ \vec{p}_\perp \end{pmatrix} = \begin{pmatrix} \mu p \\ \vec{p}_\perp \end{pmatrix}$

The force acting on a particle with magnetic moment $\vec{M}$ is the magnetic mirror force (Fig. 13.6)

$$F_z = -\vec{M}\frac{\partial B}{\partial z} = -\frac{p_\perp^2}{2\gamma m B}\frac{\partial B}{\partial z}$$

Because of gyrotropy we have

$$\frac{\partial f}{\partial \vec{p}} = \frac{\partial f}{\partial p_\parallel} = \begin{pmatrix} \frac{\partial f}{\partial p_\parallel} \\ 0 \\ 0 \end{pmatrix}, \text{ i.e., } \frac{\partial f}{\partial p_\perp} = 0.$$

Thus we can take only the derivative in the parallel direction,

$$\begin{aligned} \frac{\partial f}{\partial p_\parallel} &= -\frac{p^2(1-\mu^2)}{2\gamma m B}\frac{\partial B}{\partial z}\frac{1}{p}\frac{\partial f}{\partial \mu} \\ &= \frac{1-\mu^2}{2B}\frac{\partial B}{\partial z} v \frac{\partial f}{\partial \mu}, \end{aligned} \tag{13.84}$$

because $p = m\gamma v$. Thus, we can write the force term in Liouville's equation in the following way:

$$\vec{F}\cdot\frac{\partial f}{\partial \vec{p}} = -\frac{p_\perp^2}{2\gamma m B}\frac{\partial B}{\partial z}$$

and

$$\vec{F}\cdot\frac{\partial f}{\partial \vec{p}_\parallel} = -\frac{p^2(1-\mu^2)}{2\gamma m B}\frac{\partial B}{\partial z}\frac{1}{p}\frac{\partial f}{\partial \mu} = \frac{1-\mu^2}{2B}\frac{\partial B}{\partial z} v \frac{\partial f}{\partial \mu}, \tag{13.85}$$

because $p = \gamma m v$. Defining a characteristic focusing length

$$L(z) \doteq \frac{B(z)}{\partial B/\partial z}, \tag{13.86}$$

we have now

$$\frac{\partial f}{\partial t} + \mu v\frac{\partial f}{\partial z} - \frac{1-\mu^2}{2L(z)}\, v\, \frac{\partial f}{\partial \mu} = 0.$$

This is Liouville's equation without any scattering processes taken into account. These can be included in the equation as stochastic processes via a diffusive term

$$-\partial_\mu\left(D_{\mu\mu}(\mu)\frac{\partial f}{\partial \mu}\right),$$

or, equivalently, a Fokker-Planck term

$$-\frac{1}{2}\partial_\mu\left(\frac{\langle\Delta\mu^2\rangle}{\Delta t}\cdot\frac{\partial f}{\partial \mu}\right).$$

We can also add a source term $S(z,\mu,t)$, e. g., an isotropic distribution of energetic particles at the Sun.

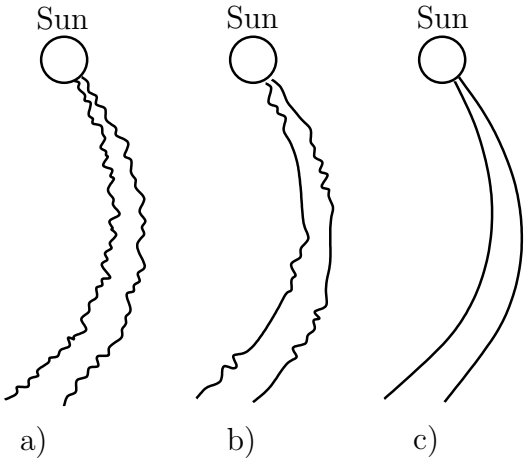

Figure 13.9: Three possible situations described by transport equations. a) efficient scattering, or. equivalently, a short mean free path is described by ordinary diffusion. b) some scattering, or intermediate mean free path is described by focused transport. c) inefficient scattering, or long mean free path is descrbed by "scatter-free" propagation. After **?**.

Thus, we have derived the so-called 'focused transport equation', (*Roelof*, 1969)

$$\partial_t f + \mu v \partial_z f - \frac{1-\mu^2}{2L(z)} v \partial_\mu f - \partial_\mu D_{\mu\mu}(\mu) \partial_\mu f = S(z,\mu,t) \tag{13.87}$$

Here, $D_{\mu\mu}(\mu)$, is the pitch-angle diffusion coefficient or tensor.

There are two extreme solutions to this equation. They are shown in Fig. 13.9.

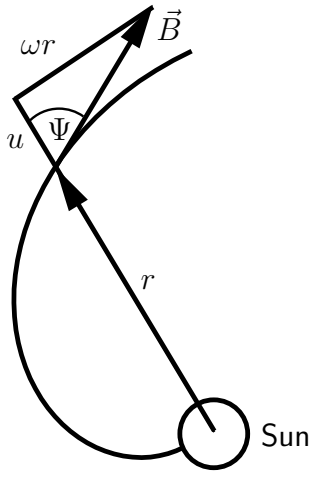

Figure 13.10: The Parker magnetic field spiral.

Let us first consider the scatter-free propagation. The angle subtended by the magnetic field, $\vec{B}$, and solar wind velocity, $\vec{v}_{\rm sw}$ is Ψ, the so-called Parker-spiral angle (see Fig. 13.6). With solar rotation rate Ω and the radial solar wind speed, $v_{\rm sw}$, we have

$$\cos\Psi = \frac{1}{\sqrt{1+(r/(v_{\rm sw}/\Omega))^2}} = \frac{1}{\sqrt{1+(r\Omega/v_{\rm sw})^2}}.$$

As the solar wind plasma moves by an observer, he senses an electric field which is due to the convection of the frozen-in magnetic field,

$$\vec{E} = \vec{v}_{\rm sw} \times \vec{B} = |\vec{v}_{\rm sw}| \cdot |\vec{B}| \cdot \sin\Psi.$$

In the frame of the observer, energetic particles streaming by him experience a drift force leading

to a drift velocity,

$$\vec{v}_D = -\frac{\vec{B} \times \vec{v}_{\rm sw} \times \vec{B}}{B^2} = |\vec{v}_{\rm sw}| \sin \Psi.$$

This drift velocity leads to a co-rotation of energetic particles. In other words, they follow the magnetic field lines. They remain stuck to their field lines. This means that particles injected at the Sun fill the field line which they were injected on. A pulse injected onto one field line at the Sun propagates outward along the same field line.

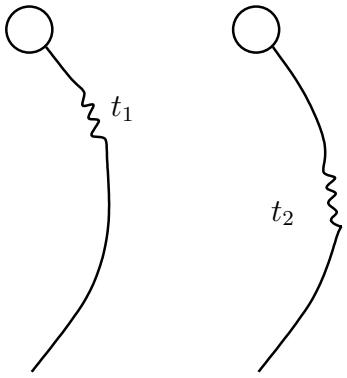

Figure 13.11: Particles remain bound to their original magnetic field line.

Particles remain attached to their original field line (Fig. 13.6). This is important when considering time series of solar particle events. They necessarily consist of a time-dependent injection profile and a convection time profile. *Add swoosh plot for discussion.*

Next, consider the next case with strong diffusion in pitch angle, i.e., where the particle distribution function can be written as a sum of an isotropic part and a small anisotropic contribution,

$$f(\mu, z, t) = f_0(z, t) + f_1(\mu, z, t),$$

where $f_1 \ll f_0$ and $\partial_t f_1 \ll 1/\tau_\mu$ and $\partial_z f_1 v_{\rm sw} \ll 1/\tau_\mu$, where τ_μ is a typical time scale for pitch-angle diffusion. In other words, we assume that all temporal changes are slow compared to pitch-angle diffusion (second assumption). This is also to be the case for changes which are due to the convection of a flux tube by the observer (third assumption). In this assumption of strong pitch-angle scattering focusing is unimportant, i.e., the times between scattering events are short. In this limit of infinite focussing length, $L(z) \longrightarrow \infty$, we have

$$\partial_t f + \mu v \partial z f - \partial_\mu \left(D_{\mu\mu}(\mu) \partial_\mu f \right) = 0. \tag{13.88}$$

We now make the assumption that $D_{\mu\mu} \sim 1/\tau_\mu$ and that the assumptions mentioned above are valid. Then we can try to convert eq. 13.88 into a spatial diffusion equation. This can't always be done. Diffusion can't be faster than the particles and if one uses spatial diffusion indiscriminantly, such nonphysical effects could occur. In addition to the assumptions mentioned above, we assume that the anisotropy, $f_1(\mu, t, t)$, describes only that, i. e. , that

$$\int_{-1}^{+1} {\rm d}\mu f_1(\mu) = 0.$$

Then we can rewrite eq. 13.88 as

$$\partial_t f_0 + \partial_t f_1 + \mu v \partial z f_0 + \mu v \partial z f_1 - \partial_\mu \left(D_{\mu\mu}(\mu) \partial_\mu f_1 \right) = 0. \tag{13.89}$$

We now average over pitch angle μ, and use

$$\langle f(\mu)\rangle \doteq \frac{1}{2}\int_{-1}^{+1} \mathrm{d}\mu f(\mu) \quad \text{and} \quad \langle f_0\rangle = f_0$$

Then we have, by averaging eq. 13.89,

$$\frac{1}{2}\left\{\int \mathrm{d}\mu \partial_t f_0 + \int \mathrm{d}\mu \partial_t f_1 + \int \mathrm{d}\mu\mu v \partial_z f_0 + \int \mathrm{d}\mu\mu v \partial_z f_1 - \int \mathrm{d}\mu \partial_\mu \left(D_{\mu\mu}(\mu)\partial_\mu f_1\right)\right\} = 0.$$

The second term vanishes by definition and the third term does so too because the integrand is an odd function of μ. The last term vanishes as well because there is no flux at $\mu = \pm 1$. Thus, we are left with

$$\partial_t f_0 + \frac{1}{2}\int_{-1}^{+1} \mathrm{d}\mu\ \mu v \partial_z f_1 = 0 \tag{13.90}$$

or, in other words,

$$\partial_t f_0 = -\frac{1}{2}\int \mathrm{d}\mu\ \mu v \partial_z f_1.$$

We insert this in eq. 13.89 and obtain

$$-\frac{1}{2}\int_{-1}^{+1} \mathrm{d}\mu\ \mu v \partial_z f_1 + \partial_t f_1 + \mu v \partial_z f_1 - \partial_\mu (D_{\mu\mu}(\mu)\partial_\mu f_1) = -\mu v \partial_z f_0,$$

where we have retained all terms involving f_1 on the left hand side. Now according to our assumptions, the first three terms are negligible compared to $1/\tau_\mu$, and hence, we are left with

$$\partial_\mu \left(D_{\mu\mu}(\mu)\partial_\mu f_1\right) = +\mu v \partial_z f_0.$$

Next, we integrate over pitch angle,

$$\int \mathrm{d}\mu \partial_\mu \left(D_{\mu\mu}(\mu)\partial_\mu f_1\right) = +\int \mathrm{d}\mu\mu v \partial_z f_0, \tag{13.91}$$

$$D_{\mu\mu}(\mu)\partial_\mu f_1 = +\frac{\mu^2}{2} v \partial_z f_0 + C1. \tag{13.92}$$

We can determine the integration constant, C_1, by considering that the flux at $\mu = \pm 1$ vanishes, and, hence

$$D_{\mu\mu}(\mu)\partial_\mu f_1|_{\pm 1} = 0.$$

Thus, at $\mu = \pm 1$

$$C_1 = -\frac{v}{2}\partial_z f_0$$

and, hence, eq. 13.92 evaluates to

$$\partial_\mu f_1 = -\partial_z f_0 \frac{v}{2} \frac{1-\mu^2}{D_{\mu\mu}}.$$

Integrating once more we have

$$f_1 = -\partial_z f_0 \frac{v}{2} \left[\int \mathrm{d}\mu' \frac{1-(\mu')^2}{D_{\mu'\mu'}}(\mu') \right] + C_2$$

where the exact positioning of the square brackets does not matter, as we are only considering an integration constant. We now insert this into eq. 13.90

$$\begin{aligned}
\partial_t f_0 &= -\frac{v}{2} \int_{-1}^{+1} \mathrm{d}\mu \; \mu \frac{\partial f_1}{\partial z}, \\
&= \frac{v^2}{4} \partial_z \int_{-1}^{+1} \mathrm{d}\mu \; \mu \left(\left[\int \mathrm{d}\mu' \frac{1-(\mu')^2}{D_{\mu'\mu'}} \right] + C_2 \right) \partial_z f_0, \\
&= \frac{v^2}{4} \partial_z \left[\int_{-1}^{+1} \mathrm{d}\mu \; \mu \int \mathrm{d}\mu' \frac{1-(\mu')^2}{D_{\mu'\mu'}} + \int_{-1}^{+1} \mathrm{d}\mu\mu C_2 \right] \partial_z f_0.
\end{aligned}$$

The term involving the integration constant, C_2, vanishes because it is an odd function of μ. Hence, we are left with

$$\partial_t f_0 = \frac{v^2}{4} \partial_z \left[\int_{-1}^{+1} \mathrm{d}\mu \; \mu \int \mathrm{d}\mu' \frac{1-(\mu')^2}{D_{\mu'\mu'}} \right] \partial_z f_0 \;=\; \partial_z \left(\kappa(z) \partial_z f_0 \right), \qquad (13.93)$$

where

$$\kappa(z) = \frac{v^2}{4} \int_{-1}^{+1} \mathrm{d}\mu \; \mu \int \mathrm{d}\mu' \frac{1-(\mu')^2}{D_{\mu'\mu'}}, \qquad (13.94)$$

i. e. we have found a diffusion equation with diffusion coefficient $\kappa(z)$ which is given entirely by the pitch-angle diffusion coefficient, $D_{\mu\mu}$.

In other words, we have found that pitch-angle diffusion translates to spatial diffusion via the diffusion coefficient given in eq. 13.94.

In fact, the result we found is more general than the assumptions appear to imply. The diffusion coefficient has the same functional form for finite scattering length, $L(z)$.

The diffusion coefficient $\kappa(z)$ parallel to the magnetic field is <u>not</u> the radial diffusion coefficient in the heliosphere. As long as cross-field diffusion (or footpoint motion) does not dominate, we can write

$$\kappa_r = \kappa(z) \cdot \cos\psi \qquad (13.95)$$

where ψ is the spiral angle between the radial and magnetic field directions.

The mean free path is given by

$$\lambda_\parallel = \frac{3\kappa(z)}{v}$$

as is usual in diffusive problems.

13.7 Pitch-Angle Scattering II

We have modeled the transport of cosmic rays (solar or galactic) with the two transport equations (Parker's and focussed) in which pitch-angle scattering was an important physical process. But how does it work and how does it depend on the magnetic field and fluctuations in it?

We have already inroduced pitch-angle scattering as an example of wave-particle interactions in section 2.6 and considered wave-particle interactions as a mechanism for solar wind acceleration in Sec. 4.3.1 and 4.3.3. Let us now take another look at it by considering the interaction of cosmic rays with Alfvén waves. For simplicity's sake we will consider linearly polarized Alfvén waves, we will see that this is not really a restriction on the result.

Consider the wave packet depicted in figure 13.12. It has a length $L \sim \lambda$ and we assume that it is linearly polarized in the x-direction.

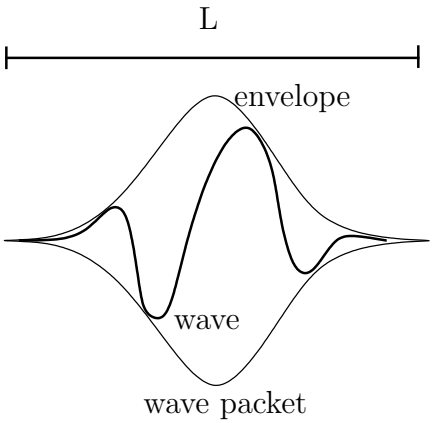

Figure 13.12: An archetypical wave packet consists of wave and evelope.

Now consider a cosmic ray encountering the wave packet from the left. We will choose a frame of reference in which the wave is at rest. We write the perturbation in the magnetic field (the wave) as

$$\delta B_\perp = \delta B \sin(kz - \omega t)\vec{e}_x$$

superimposed on an average background field B_0. The cosmic ray gyrates around B_0 with gyrofrequency Ω and, hence, the y-component of its velocity also has this frequency

$$v_y = v_\perp \sin(\Omega t + \Phi), \quad \text{where} \quad \Omega = \frac{qB}{m\gamma},$$

where Φ is the random phase between the cosmic ray and the wave packet. The z component of the Lorentz force acting on the cosmic ray (along the magnetic field $\vec{B}_0$) is given by

$$q\left(\vec{v} \times \vec{B}\right)_z = -qv_y\delta B_\perp$$

because we assumed that δB is linearly polarized in the x-direction. Then

$$-q(v_y\delta B_\perp) = -qv_\perp\delta B \sin(kz_0 + kv_z t - \omega t)\ \sin(\Omega t + \Phi)$$

where $z = z_0 + v_z \cdot t$ is the position of the cosmic rays guiding center. Using the relation

$$\sin\alpha \sin\beta = \cos(\alpha + \beta) - \cos(\alpha - \beta)$$

we rewrite the product of the sines as

$$\begin{aligned} -q\left(\vec{v}\times\vec{B}\right)_z &= \frac{1}{2}qv_\perp\delta B * \\ &\quad * \left[\cos\left((kv_z-\omega+\Omega)\cdot t+(kz_0+\Phi)\right)\right. \\ &\quad \left.-\cos\left((kv_z-\omega-\Omega)\cdot t+(kz_0-\Phi)\right)\right]. \end{aligned}$$

As the cosmic ray moves across the wave at velocity $v_z > 0$ the first term will have a high frequency and will average out. However, the second term has lower frequency and if $\kappa v_z - \omega - \Omega \approx 0$ it will not average out. This is, of course, nothing else but resonance condition, eq. 4.3. If the particle moves with $v_z < 0$ the rates of the two cos-terms are reversed. If there is resonance, we can compute the change of the particle's momentum in z-direction,

$$\begin{aligned} \Delta p_z &= q\int \mathrm{d}t\left(\vec{v}\times\vec{B}\right)_z, \\ &= \frac{1}{2}qv_\perp\delta B\cos(kz_0-\Phi)\cdot\frac{2\pi}{kv_z}, \end{aligned}$$

where we have inserted the interaction time

$$\tau = \frac{2\pi}{k}\cdot\frac{1}{v_z} = \frac{\lambda}{v_z} \approx \frac{L}{v_z}$$

The interaction time τ is also approximately the wave period

$$\tau \approx \frac{2\pi}{kv_z-\omega} = \frac{2\pi}{k(v_z-v_A)} \approx \frac{2\pi}{kv_z},$$

because $v_z \gg v_A$. Because of the resonance condition, this is also about the time it takes the cosmic ray to complete a gyroorbit, Ω^{-1}. Thus,

$$\begin{aligned} \delta p_z &= \pi q\frac{v_\perp\delta B}{\Omega}\cos(kz_0-\Phi) \\ &\approx \pi\frac{qv_\perp\delta B}{qB}m\gamma\cos(kz_0-\Phi) \\ &= \pi p_\perp\frac{\delta B}{B}\cos(kz_0-\Phi) \\ &= \pi p\sin\vartheta\frac{\delta B}{B}\cos(kz_0-\Phi). \end{aligned}$$

Because the electric field vanished in the frame of reference of the wave, the energy of the cosmic ray is conserved, but its pitch angle is changed in the wave frame of reference.

Because of $p_z = p\cos\vartheta$ we have

$$\delta(p\cos\vartheta) = -p\sin\vartheta\delta\vartheta = \pi p\sin\vartheta\left(\frac{\delta B}{B}\right)\cos(kz_0-\Phi),$$

or

$$\delta\vartheta = -\pi \left(\frac{\delta B}{B}\right) \cos(kz_0 - \Phi).$$

Now cosmic rays do not encounter isolated waves but rather see many of them. So let's consider the effect of a train of Alfvén wave packets with random phases. During a time t there will be t/τ interactions. Because of the random phases, the $\cos(kz_0 - \Phi)$ will average out to zero. However, the square of δB will not, because $\langle \cos^2 \Phi \rangle = 1/2$. Thus, in the case of resonance,

$$\left\langle (\Delta\vartheta)^2 \right\rangle = \sum \left\langle (\delta\vartheta)^2 \right\rangle = \frac{t}{\tau}\frac{\pi^2}{2} \left\langle \left(\frac{\delta B}{B}\right)^2 \right\rangle,$$

or

$$\frac{\left\langle (\Delta\vartheta)^2 \right\rangle}{t} = \frac{\pi}{4}\Omega \left\langle \left(\frac{\delta B}{B}\right)^2 \right\rangle.$$

This is an important finding, the pitch angle diffuses at a rate which is proportional to the particle's gyrofrequency and the square of the fluctuations in the magnetic field.

Thus, cosmic rays interact with Alfvén waves for which

$$kv \approx \Omega$$

or, equivalently (with $k = 2\pi/\lambda$) whose wave length is approximately

$$\frac{1}{k} = \frac{\lambda}{2\pi} \approx \frac{v}{\Omega} \approx \frac{v}{qB} m\gamma = r_g,$$

the size of the particle's gyroradius.

If the wave has much shorter wave length, its effect averages out, if it is much longer, the particle will adiabatically follow the field line and nothing will change.

Note also, that our assumption that the wave packet is about one wavelength long is no restriction of the result. Consider what would happen if it were n wavelengths long. Then the change in $\langle (\delta\vartheta)^2 \rangle$ would be larger by $n^2 t/\tau$. But τ would also be longer by n and so we would have

$$\frac{\left\langle (\Delta\vartheta)^2 \right\rangle}{t} = n\frac{\pi}{4}\Omega \left\langle \left(\frac{\delta B}{B}\right)^2 \right\rangle.$$

Now the fluctuations are part of a spectrum

$$\left(\frac{\delta B}{B}\right)^2 = \Delta k \cdot I(k).$$

How well can we know Δk? Obviously, the more wave periods we observe, the better we know Δk. In other words,

$$\Delta k = \frac{k}{n} = \frac{1}{nr_g}$$

for a wave train of n wave lengths, the resonance narrows! Thus,

$$\begin{aligned} \frac{\langle(\Delta\vartheta)^2\rangle}{t} &= \frac{n\pi}{4}\left\langle\left(\frac{\delta B}{B}\right)^2\right\rangle, \\ &= \frac{n\pi}{4}\Delta k I(k), \\ &= \frac{\pi}{4}\Omega k I(k). \end{aligned} \tag{13.96}$$

The pitch angle diffusion coefficient is proportional to Ω and the wave intensity at the resonant wave number.

13.8 The 90-degree pitch-angle scattering problem

Consider again the resonance condition

$$\begin{aligned} kv_z - \omega &= \Omega, \\ kv\cos\vartheta - \omega &= \Omega. \end{aligned} \tag{13.97}$$

For most cosmic rays the first term on the left is much larger than the second, i.e., $kv_z \ll \omega$, and thus

$$kv\cos\vartheta \approx \Omega \tag{13.98}$$

is the appropriate resonance condition. Taking the inverse of eq. 13.98 we have

$$\frac{\lambda}{2\pi} = \frac{v}{\Omega}\cos\vartheta = r_g\cos\vartheta. \tag{13.99}$$

As the particle's pitch angle, ϑ, approaches 90 degrees, the resonant wave length approaches zero. Because of the turbulence spectrum of the wave power spectral density there are only few waves with such very short wave lengths available to scatter the particle's pitch angle through 90 degrees. This is called the 90-degree pitch-angle scattering problem. It is solved by reflection at magnetic mirrors. One might also say that for $\cos\vartheta \sim 0$ the neglect of ω is not warranted.

Appendix A

Some Useful Concepts

A.1 Python Scripts used for this Course

A.2 Useful Relations

A.3

A.4 Vector Operators in Various Coordinate Systems

A.4.1 Cartesian Coordinates: (x, y, z)

$$\vec{\nabla}\Psi = \frac{\partial\Psi}{\partial x}\hat{x} + \frac{\partial\Psi}{\partial y}\hat{y} + \frac{\partial\Psi}{\partial z}\hat{z} \tag{A.1}$$

$$\vec{\nabla}\cdot\vec{A} = \frac{\partial A_x}{\partial x} + \frac{\partial A_y}{\partial y} + \frac{\partial A_z}{\partial z} \tag{A.2}$$

$$\vec{\nabla}\times\vec{A} = \left(\frac{\partial A_z}{\partial y} - \frac{\partial A_y}{\partial z}\right)\hat{x} + \left(\frac{\partial A_x}{\partial z} - \frac{\partial A_z}{\partial x}\right)\hat{y} + + \left(\frac{\partial A_y}{\partial x} - \frac{\partial A_x}{\partial y}\right)\hat{z} \tag{A.3}$$

$$\vec{\nabla}^2\Psi = \Delta\Psi = \frac{\partial^2\Psi}{\partial x^2} + \frac{\partial^2\Psi}{\partial y^2} + \frac{\partial^2\Psi}{\partial z^2} \tag{A.4}$$

A.4.2 Cylindrical Coordinates: (ρ, θ, z)

$$\vec{\nabla}\Psi = \frac{\partial\Psi}{\partial\rho}\hat{\rho} + \frac{1}{\rho}\frac{\partial\Psi}{\partial\theta}\hat{\theta} + \frac{\partial\Psi}{\partial z}\hat{z} \tag{A.5}$$

$$\vec{\nabla}\cdot\vec{A} = \frac{1}{\rho}\frac{\partial\left(\rho A_\rho\right)}{\partial\rho} + \frac{1}{\rho}\frac{\partial A_\theta}{\partial\theta} + \frac{\partial A_z}{\partial z} \tag{A.6}$$

$$\begin{aligned}\vec{\nabla}\times\vec{A} &= \left(\frac{1}{\rho}\frac{\partial A_z}{\partial\theta} - \frac{\partial A_\theta}{\partial z}\right)\hat{\rho} + \left(\frac{\partial A_\rho}{\partial z} - \frac{\partial A_z}{\partial\rho}\right)\hat{\theta} + \\ &+\frac{1}{\rho}\left(\frac{\partial}{\partial\rho}\left(\rho A_\theta\right) - \frac{\partial A_\rho}{\partial\theta}\right)\hat{z}\end{aligned} \tag{A.7}$$

$$\vec{\nabla}^2\Psi = \Delta\Psi = \frac{1}{\rho}\frac{\partial}{\partial\rho}\left(\rho\frac{\partial\Psi}{\partial\rho}\right) + \frac{1}{\rho^2}\frac{\partial^2\Psi}{\partial\theta^2} + \frac{\partial^2\Psi}{\partial z^2} \tag{A.8}$$

A.4.3 Spherical Coordinates: (r, θ, ϕ)

$$\vec{\nabla}\Psi = \frac{\partial\Psi}{\partial r}\hat{r} + \frac{1}{r}\frac{\partial\Psi}{\partial\theta}\hat{\theta} + \frac{1}{r\sin\theta}\frac{\partial\Psi}{\partial\phi}\hat{\phi} \tag{A.9}$$

$$\vec{\nabla}\cdot\vec{A} = \frac{1}{r^2}\frac{\partial}{\partial r}\left(r^2 A_r\right) + \frac{1}{r\sin\theta}\frac{\partial}{\partial\theta}\left(\sin\theta A_\theta\right) + \frac{1}{r\sin\theta}\frac{\partial A_\phi}{\partial\phi} \tag{A.10}$$

$$\begin{aligned}\vec{\nabla}\times\vec{A} &= \frac{1}{r\sin\theta}\left(\frac{\partial}{\partial\theta}\left(\sin\theta A_\phi\right) - \frac{\partial A_\theta}{\partial\phi}\right)\hat{r} + \left(\frac{1}{r\sin\theta}\frac{\partial A_r}{\partial\phi} - \frac{1}{r}\frac{\partial}{\partial r}\left(rA_\phi\right)\right)\hat{\theta} + \\ &+\frac{1}{r}\left(\frac{\partial}{\partial r}\left(rA_\theta\right) - \frac{\partial A_r}{\partial\theta}\right)\hat{\phi}\end{aligned} \tag{A.11}$$

$$\vec{\nabla}^2\Psi = \Delta\Psi = \frac{1}{r}\frac{\partial}{\partial r}\left(r^2\frac{\partial\Psi}{\partial r}\right) + \frac{1}{r^2\sin\theta}\frac{\partial}{\partial\theta}\left(\sin\theta\frac{\partial\Psi}{\partial\theta}\right) + \frac{1}{r^2\sin\theta}\frac{\partial^2\Psi}{\partial\phi^2} \tag{A.12}$$

Appendix B

An Introduction to Stochastic Differential Equations

B.1 The Concept of Stochastic Differetial Equations

B.2 SDEs in Transport Problems

B.3

Bibliography

Antiochos, S. K., Z. Mikić, V. S. Titov, R. Lionello, and J. A. Linker: "A Model for the Sources of the Slow Solar Wind". *Astrophys. J. Lett.*, **731**, (2011), 112–+.

Aschwanden, M.: *Physics of the Solar Corona*. Springer (2005).

Audard, M., M. Güdel, A. Sres, A. J. J. Raassen, and R. Mewe: "A study of coronal abundances in RS CVn binaries%". *Astron. Astrophys.*, **398**, (2003), 1137–1149.

Auer, S.: "Instrumentation". In "Interplanetary Dust", edited by E. Grün, S. G. B. Å S. F. Dermott, and H. Fechtig. Springer (2001). 385 – 444.

Bame, S. J., J. R. Asbridge, W. C. Feldman, and J. T. Gosling: "Evidence for a structure-free state at high solar wind speeds". *J. Geophys. Res.*, **82**, (1977), 1487 – 1492.

Bartels, J.: "Geomagnetic and solar data". *J. Geophys. Res.*, **54**, (1949), 296 – 297.

Baumjohann, W. and R. A. Treumann: *Basic Space Plasma Physics*. Imperial college Press (1997).

Belcher, J. W. and L. Davis Jr.: "Large-amplitude Alfvén waves in the interplanetary medium, 2". *J. Geophys. Res.*, **76**, (1971), 3534 – 3563.

Biermann, L.: "Kometenschweife und solare Korpuskularstrahlung". *Z. Astrophys.*, **29**, (1951), 274 – 286.

Biermann, L.: "Physical processes in comet tails and their relation to solar activity". *Extrait des Mem. Soc. Roy. Sci. Liege Quatr. Ser.*, **13**, (1953), 291 – 302.

Biermann, L.: "Solar corpuscular radiation and the interplanetary gas". *Observatory*, **77**, (1957), 109 – 110.

Birkeland, K.: "Sur les rayons cathodiques sons l'action de force magnétiques intenses". *Arch. des sci. naturelles*, **1**, (1896), 497 – 512.

Birkeland, K.: *The Norwegian Aurora Polaris Expedition 1902–1903, vol. 1, On the Cause of Magnetic Storms and the Origin of Terrestrial Magnetism, first section*. H. Aschehoug and Co, Christiania (1908).

Birkeland, K.: *The Norwegian Aurora Polaris Expedition 1902–1903, vol. 1, On the Cause of Magnetic Storms and the Origin of Terrestrial Magnetism, second section*. H. Aschehoug and Co, Christiania (1913).

Blum, P. W. and H. J. Fahr: "Interaction between interstellar hydrogen and the solar wind". *Astron. Astrophys.*, **4**, (1970), 280 – 290.

Bohren, C. F. and D. R. Huffman: *Absorption and Scattering of Light by Small Particles*. John Wiley & Sons, New York, USA (1983).

Bonetti, A., H. S. Bridge, A. J. Lazarus, E. F. Rossi, and F. Scherb: "Explorer 10 plasma measurements". *J. Geophys. Res.*, **68**, (1963), 4017 – 4063.

Borg, J., J. Chaumont, C. jouret, Y. Langevin, and M. Maurette: "Solar wind radiation damage in lunar dust grains and the characteristics of the ancient solar wind". In "The Ancient Sun", edited by R. O. Pepin, J. A. Eddy, and R. B. Merrill, Geochim. Cosmochim. Acta Suppl. 13 (1980). 431 – 461.

Borrini, G., J. M. Wilcox, J. T. Gosling, S. J. Bame, and W. C. Feldman: "Solar wind helium and hydrogen structure near the heliospheric current sheet: A signal of coronal streamers at 1 AU". *J. Geophys. Res.*, **86**, (1981), 4565 – 4573.

Breneman, H. H. and E. C. Stone: "Solar coronal and photospheric abundances from solar energetic particle measurements". *Astrophys. J.*, **299**, (1985), L57 – L61.

Brinkman, A. C., E. Behar, M. Güdel, M. Audard, A. J. F. den Boggende, G. Branduardi-Raymont, J. Cottam, C. Erd, J. W. den Herder, F. Jansen, *et al.*: "First light measurements with the XMM-Newton reflection grating spectrometers: Evidence for an inverse first ionisation potential effect and anomalous Ne abundance in the Coronae of HR 1099". *Astron. Astrophys.*, **365**, (2001), L324–L328.

Brooks, D. H. and H. P. Warren: "Establishing a Connection Between Active Region Outflows and the Solar Wind: Abundance Measurements with EIS/Hinode". *Astrophys. J. Lett.*, **727**, (2011), L13+.

Bürgi, A. and J. Geiss: "Helium and minor ions in the corona and solar wind: dynamics and charge states". *Sol. Phys.*, **103**, (1986), 347 – 383.

Burlaga, L. F., N. F. Ness, J. W. Belcher, A. Szabo, P. A. Isenberg, and M. A. Lee: "Pickup protons and pressure-balanced structures: Voyager 2 observations in merged interaction regions near 35 AU". *J. Geophys. Res.*, **99**, (1994), 21511 – 21524.

Burns, J. A., P. H. Lamy, and S. Soter: "Radiation forces on small particles in the solar system". *Icarus*, **40**, (1979), 1 – 48.

Burton, M. E., M. Neugebauer, N. U. Crooker, R. von Steiger, and E. J. Smith: "Identification of trailing edge solar wind stream interfaces: A comparison of Ulysses plasma and composition measurements". *J. Geophys. Ses.*, **104**, (1999), 9925 – 9932.

Chandrasekhar, S.: "Stochastic Problems in Physics and Astronomy". *Rev. Mod. Phys.*, **15**, (1943), 1 – 89.

Chapman, S.: "The energy of magnetic storms". *Monthly Notices Roy. Astron. Soc.*, **79**, (1918), 70 – 83.

Chapman, S.: "Solar streams of corpuscules: Their geometry, absorption of light, and penetration". *Proc. Roy. Soc. London*, **A, 95**, (1919), 61 – 83.

Chen, F. F.: *Plasma Physics and Controlled Fusion*. Plenum Press, New York (1984). Fourth printing.

Compton, A. H. and I. A. Getting: "An apparent effect of galactic rotation on the intensity of cmic rays". *Phys. Rev.*, **47**, (1935), 817 – 821.

Cook, W. R., E. C. Stone, and R. E. Vogt: "Elemental composition of solar energetic particles". *Astrophys. J.*, **279**, (1984), 827 – 838.

Cranmer, S. R.: "Self-Consistent Models of the Solar Wind". *Space Sci. Rev.*, 160–+.

Cranmer, S. R., J. L. Kohl, G. Noci, E. Antonucci, G. Tondello, M. C. E. Huber, L.Strachan, A. V. Panasyuk, L. D.Gardner, M. Romoli, *et al.*: "An empirical model of a polar coronal hole at solar minimum". *Astrophys. J.*, **511**, (1999), 481 – 501.

Cranmer, S. R., A. V. Panasyuk, and J. L. Kohl: "Improved constraints on the preferential heating and acceleration of oxygen ions in the extended solar corona". *Astrophys. J.*, **678**, (2008), 1480 – 1497.

Cranmer, S. R., A. A. van Ballegooijen, and R. J. Edgar: "Self-consistent Coronal Heating and Solar Wind Acceleration from Anisotropic Magnetohydrodynamic Turbulence". *Astrophys. J. Suppl.*, **171**, (2007), 520–551.

Cummings, A. C. and E. C. Stone: "Composition of anomalous cosmic rays and implications for the heliosphere". *Space. Sci. Rev.*, **78**, (1996), 117 – 128.

De Pontieu, B., S. W. McIntosh, M. Carlsson, V. H. Hansteen, T. D. Tarbell, C. J. Schrijver, A. M. Title, R. A. Shine, S. Tsuneta, Y. Katsukawa, *et al.*: "Chromospheric Alfvénic Waves Strong Enough to Power the Solar Wind". *Science*, **318**, (2007), 1574–.

Dessler, A. J.: "Solar wind and interplanetary magnetic field". *Rev. Geophys.*, **5**, (1967), 1 – 41.

Draine, B. T.: "Tabulated optical properties of graphite and silicate grains". *Astrophys. J. Suppl. Ser.*, **57**, (1985), 587 – 594.

Drake, J. J., N. S. Brickhouse, V. Kashyap, J. M. Laming, D. P. Huenemoerder, R. Smith, and B. J. Wargelin: "Enhanced Noble Gases in the Coronae of Active Stars". *Astrophys. J. Lett.*, **548**, (2001), L81–L85.

Elsässer, W. M.: "The Hydromagnetic Equations". *Physical Review*, **79**, (1950), 183–183.

Eyles, C. J., R. A. Harrison, C. J. Davis, N. R. Waltham, B. M. Shaughnessy, H. C. A. Mapson-Menard, D. Bewsher, S. R. Crothers, J. A. Davies, G. M. Simnett, *et al.*: "The Heliospheric Imagers Onboard the STEREO Mission". *Sol. Phys.*, **254**, (2009), 387–445.

Fahr, H. J.: "On the influence of neutral interstellar matter on the upper atmosphere". *Astrophys. & Space Sci.*, **2**, (1968), 474 – 495.

Fechtig, H., C. Leinert, and O. E. Berg: "Historical perspectives". In "Interplanetary Dust", edited by E. Grün, S. G. B. Å S. F. Dermott, and H. Fechtig. Springer (2001). 1 – 55.

Feldman, W. C., J. R. Asbridge, S. Bame, E. E. Fenimore, and J. T. Gosling: "The solar origin of solar wind interstream flows: Near equatorial coronal streamers". *J. Geophys. Res.*, **86**, (1981), 5408 – 5416.

Fisk, L. A.: "Motion of the footpoints of heliospheric magnetic field lines at the Sun: Implications for recurrent energetic particle events at high heliographic latitudes". *J. Geophys. Res.*, **101**, (1996), 547 – 553.

Fisk, L. A.: "An overview of the transport of galactic and anomalous cosmic rays in the heliosphere: Theory". *Adv. Space Sci.*, **23**, (1999), (3)415 – (3)423.

Fitzgerald, G. F.: "Sunspots and magnetic storms". *The Electrician*, **30**, (1892), 48.

Fitzgerald, G. F.: "Sunspots, magnetic storms, comet tails, atmospheric electricity, and aurorae". *The Electrician*, **46**, (1900), 287 – 288.

Forsyth, R. J., A. Balogh, E. J. Smith, G. Erdös, and D. J. McComas: "The underlying Parker spiral structure in the Ulysses magnetic field observations, 1990-1994". *J. Geophys. Res.*, **101**, (1996), 395–404.

Gazis, P.: "Limits on deceleration and asymmetry of solar wind speed". *Geophys. Res. Lett.*, **22**, (1995), 2441 – 2444.

Geiss, J. and P. Bochsler: *Rapports isotopiques dans le systeme solaire.* Cepadues-Editions, Paris (1985) 213.

Geiss, J., G. Gloeckler, U. Mall, R. von Steiger, A. B. Galvin, and K. W. Ogilvie: "Interstellar oxygen, nitrogen and neon in the heliosphere". *Astron. Astrophys.*, **282**, (1994), 924 – 933.

Geiss, J., G. Gloeckler, and R. von Steiger: "Origin of the solar wind from composition measurements". *Space Sci. Rev.*, **72**, (1995*a*), 49 – 60.

Geiss, J., G. Gloeckler, R. von Steiger, H. Balsiger, L. A. Fisk, A. B. Galvin, F. M. Ipavich, S. Livi, J. F. Mackenzie, K. W. Ogilvie, *et al.*: "The southern high-speed stream: Results from the SWICS instrument on Ulysses". *Science*, **268**, (1995*b*), 1033 –1036.

Gel'fand and Shilov: *Verallgemeinerte Funktionen (Distributionen).* VEB, Berlin (1967).

Gleeson, L. J. and W. I. Axford: "Cosmic rays in the interplanetary medium". *Astrophys. J. Lett.*, **149**, (1967), L115 – L118.

Gleeson, L. J. and W. I. Axford: "The Compton-Getting effect". *Astrophys.&Space Sci.*, **2**, (1968), 431 – 437.

Gloeckler, G., L. A. Fisk, J. Geiss, N. A. Schwadron, and T. H. Zurbuchen: "Elemental composition of the inner source pickup ions". *J. Geophys. Res.*, **105**, (2000), 7459 – 7463.

Gloeckler, G., N. A. S. L. A. Fisk, and J. Geiss: "Weak pitch angle scattering of few MV rigidity ions from measurements of anisotropies in the distribution function of interstellar H^+". *Geophys. Res. Lett.*, **22**, (1995), 2665 – 2668.

Gloeckler, G., J. Geiss, H. Balsiger, L. A. Fisk, A. B. Galvin, F. M. Ipavich, K. W. Ogilvie, R. von Steiger, and B. Wilken: "Detection of interstellar pick-up hydrogen in the solar system". *Science*, **261**, (1993), 70 – 73.

Gloeckler, G., J. Geiss, E. C. Roelof, L. A. Fisk, F. M. Ipavich, K. W. Ogilvie, L. J. Lanzerotti, R. von Steiger, and B. Wilken: "Acceleration of interstellar pickup ions in the disturbed solar wind observed on ULYSSES". *J. Geophys. Res.*, **99**, (1994), 17637 – 17643.

Goedbloed, H. and S. Poedts: *Principles of Magnetohydrodynamics, with Applications to Laboratory and Astrophysical Plasma*. Cambridge University Press (2004).

Gosling, J. T., G. Borrini, J. R. Asbridge, S. J. Bame, W. C. Feldman, and R. F. Hansen: "Coronal streamers in the solar wind at 1 AU". *J. Geophys. Res.*, **86**, (1981), 5438 – 5448.

Gradshteyn, I. S. and I. M. Ryzhik (eds.): *Table of Integrals, Series, and Products*. Academic Press, Orlando, Florida (1980). Corrected and enlarged edition.

Gringauz, K. I.: "Some results of experiments in interplanetary space by means of charged particle traps on Soviet space probes". *Space Res.*, **2**, (1961), 539 – 553.

Gringauz, K. I., V. V. Bezrikikh, and L. S. Musatov: "Solar wind observations with the Venus 3 probe". *Cosmic Research*, **5**, (1967), 216 – 222.

Gringauz, K. I., V. V. Bezrukikh, V. D. Ozerov, and R. E. Rybchinskyi: "Study of the interplanetary ionized gas, high energy electrons, and solar corpuscular radiation by means of three electrode traps for charged particles on the second Soviet cosmic rocket". *Soviet Physics Doklady*, **5**, (1960), 361 – 364.

Gurnett, D. A., W. S. Kurth, S. C. Allendorf, and R. L. Poynter: "Radio emission from the heliopause triggered by an interplanetary schock". *Science*, **262**, (1993), 199 – 203.

Harra, L. K., T. Sakao, C. H. Mandrini, H. Hara, S. Imada, P. R. Young, L. van Driel-Gesztelyi, and D. Baker: "Outflows at the Edges of Active Regions: Contribution to Solar Wind Formation?" *Astrophys. J. Lett.*, **676**, (2008), L147–L150.

Hénoux, J.-C.: "FIP fractionation: Theory". *Space Sci. Rev.*, **85**, (1998), 215 – 226.

Hovestadt, D., O. Vollmer, G. Gloeckler, and C. Y. Fan: "Measurement of elemental abundance of very low energy solar cosmic rays". In "13th Int. Conf. Cosmic Rays", Denver (1973). 1498.

Isenberg, P. A. and J. R. Jokipii: "Gradient and curvature drifts in magnetic fields with arbitrary spatial variation". *Astrophys. J.*, **234**, (1979), 746 – 752.

Jackson, J. D.: *Classical Electrodynamics* (1962).

Jokipii, J. R., E. H. Levy, and W. B. Hubbard: "Effects of particle drift on cosmic-ray transport. I - General properties, application to solar modulation". *Astrophys. J.*, **213**, (1977), 861–868.

Klecker, B., V. Bothmer, A. C. Cummings, J. S. George, J. Keller, E. Salerno, U. J. Sofia, E. C. Stone, F.-K. Thielemann, M. E. Wiedenbeck, *et al.*: "Galactic abundances: Report of working group 3". In "Solar and Galactic Composition", edited by R. F. Wimmer-Schweingruber. AIP conference proceedings, Melville, NY (2001). 207 – 220.

Ko, Y.-K., J. C. Raymond, T. H. Zurbuchen, P. Riley, J. M. Raines, and L. Strachan: "Abundance Variation at the Vicinity of an Active Region and the Coronal Origin of the Slow Solar Wind". *Astrophys. J.*, **646**, (2006*a*), 1275 – 1287.

Ko, Y.-K., J. C. Raymond, T. H. Zurbuchen, P. Riley, J. M. Raines, and L. Strachan: "Abundance Variation at the Vicinity of an Active Region and the Coronal Origin of the Slow Solar Wind". *Astrophys. J. Lett.*, **646**, (2006*b*), 1275–1287.

Kolmogorov, A. N.: "The local structure of turbulence in incompressible viscous fluid for very large Reynolds numbers". *Proceedings of the USSR Academy of Sciences*, **30**, (1941), 299–303. In Russian.

Krall, N. A. and A. W. Trivelpiece: *Principles of Plasma Physics*. San Francisco Press, Ltd. (1986).

Krieger, A. S., A. F. Timothy, and E. C. Roelof: "A coronal hole and its identification as the source of a high velocity solar wind stream". *Sol. Phys.*, **29**, (1973), 505 – 525.

Krüger, H., M. Landgraf, N. Altobelli, and E. Grün: "Interstellar Dust in the Solar System". *Space Science Reviews*, **130**, (2007), 401–408.

Kulsrud, R. M. (ed.): *Plasma Physics for Astrophysicists*. Princeton Univ. Press, Princeton (2005).

Kurth, W. S., D. A. Gurnett, F. L. Scarf, and R. L. Poynter: "Detection of a radio emission at 3 kHz in the outer heliosphere". *Nature*, **312**, (1984), 27 – 31.

Laming, J. M.: "A Unified Picture of the First Ionization Potential and Inverse First Ionization Potential Effects". *Astrophys. J. Lett.*, **614**, (2004), 1063–1072.

Landau, L. D. and E. M. Lifschitz: *Lehrbuch der theoretischen Physik*. Akademie Verlag Berlin (1981).

Lang, K. R.: *The Sun from Space*. Springer, Berlin (2000).

Lodge, O.: "Sunspots, magnetic storms, comet tails, atmospheric electricity, and aurorae". *The Electrician*, **46**, (1900), 249 – 250.

Madjarska, M. S., J. G. Doyle, and L. van Driel-Gesztelyi: "Evidence of Magnetic Reconnection along Coronal Hole Boundaries". *Astrophys. J. Lett.*, **603**, (2004), L57 – L59.

Marsch, E.: *Kinetic physics of the solar wind*. Springer (1991*a*) 45 –133.

Marsch, E.: *MHD turbulence in the solar wind*. Springer (1991*b*) 159 – 241.

Marsch, E., H. Tan, J. Sun, and T. Wiegelmann: "Plasma flows guided by strong magnetic fids in the solar corona". *Astrophys. J.*, **685**, (2008), 1262 – 1269.

McComas, D. J., R. W. Ebert, H. A. Elliott, B. E. Goldstein, J. T. Gosling, N. A. Schwadron, and R. M. Skoug: "Weaker solar wind from the polar coronal holes and the whole Sun". *Geophys. Res. Lett.*, **35**, (2008), 18103–+.

Meyer, J.-P.: "Element fractionation at work in the solar atmosphere". In "Symposium on the "Origin and Evolution of the Elements"", edited by N. Prantzos, E. Vagioni-Flam, and M. Cassé. Cambridge University Press (1993). 26.

Möbius, E., D. Hovestadt, B. Klecker, M. Scholer, G. Gloeckler, and F. M. Ipavich: "Direct observation of He^+ pick-up ions of interstellar origin in the solar wind". *Nature*, **318**, (1985), 426 – 429.

Mukai, T., J. Blum, A. M. Nakamura, R. J. Johnson, and O. Havnes: "Physical processes on interplanetary dust". In "Interplanetary Dust", edited by E. Grün, S. G. B. Å S. F. Dermott, and H. Fechtig. Springer (2001). 445 – 507.

Nakagawa, T.: "Solar source of the interplanetary planar magnetic structures". *Solar Phys.*, **147**, (1993), 169–197.

Nakagawa, T., A. Nishida, and T. Saito: "Planar magnetic structures in the solar wind". *J. Geophys. Res.*, **94**, (1989), 11761–11775.

Ness, N. F., C. S. Scearce, and J. B. Seek: "Initial results of the Imp 1 magnetic field experiment". *J. Geophys. Res.*, **69**, (1964), 3531 – 3569.

Neugebauer, M., R. J. Forsyth, A. B. Galvin, K. L. Harvey, J. T. Hoeksema, A. J. Lazarus, R. P. Lepping, J. A. Linker, Z. Mikic, J. T. Steinberg, *et al.*: "The spatial structure of the solar wind and comparisons with solar data and models". *J. Geophys. Res.*, **103**, (1998), 14587 – 14599.

Neugebauer, M. and C. W. Snyder: "Mariner 2 observations of the solar wind, 1, average properties". *J. Geophys. Res.*, **71**, (1966), 4469 – 4484.

Neugebauer, M. and C. W. Snyder: "Relation of plasma properties to the magnetic field". *J. Geophys. Res.*, **72**, (1967), 1823 – 1828.

Nolte, J. T., A. S. Krieger, A. F. Timothy, R. E. Gold, E. C. Roelof, G. Vaiana, A. J. Lazarus, J. D. Sullivan, and P. S. McIntosh: "Coronal holes as sources of solar wind". *Sol. Phys.*, **46**, (1976), 303 – 322.

Parker, E. N.: "Dynamics of the Interplanetary Gas and Magnetic Fields." *Astrophys. J*, **128**, (1958), 664 – 676.

Parker, E. N.: *Interplanetary Dynamical processes.* John Wiley & Sons, New York, USA (1963).

Parker, E. N.: "The passage of energetic charged particles through interplanetary space". *Planetary and Space Sci.*, **13**, (1965), 9 – 49.

Pearson, K.: "". *Nature*, **77**, (1905), 294.

Petschek, H. E.: "Magnetic field annihilation". In "The Physics of Solar Flares", edited by W. N. Ness. NASA SP-50 (1964). 425 – 439.

Posner, A., T. H. Zurbuchen, N. A. Schwadron, L. A. Fisk, G. Gloeckler, J. A. Linker, Z. Mikić, and P. Riley: "Nature of the boundary between open and closed magnetic field line regions at the Sun revealed by composition data and numerical models". *J. Geophys. Res.*, **106**, (2001), 15869 – 15880.

Rayleigh, L.: "". *Phil. Mag.*, **10**, (1880), 73.

Richardson, J. D., K. I. Paularena, A. J. Lazarus, and J. W. Belcher: "Evidence for a solar wind slowdown in the outer heliosphere". *Geophys. Res. Lett.*, **22**, (1995), 1469–1472.

Roberts, D. A.: "Observation and simulation of the radial evolution and stream structure of solar wind turbulence". In "Solar Wind Seven", edited by E. Marsch and R. Schwenn (1992). 533. Cospar Colloquia Series, vol. 3.

Roelof, E. C.: "Propagation of Solar Cosmic Rays in the Interplanetary Magnetic Field". In "Lectures in High-Energy Astrophysics", edited by H. Ögelman & J. R. Wayland (1969). 111–+.

Rossi, B. and S. Olbert: *Introduction to the Physics of Space*. Intl. Series in Pure and Applied Physics. McGraw-Hill (1970).

Sakao, T., R. Kano, N. Narukage, J. Kotoku, T. Bando, E. E. DeLuca, L. L. Lundquist, S. Tsuneta, L. K. Harra, Y. Katsukawa, *et al.*: "Continuous Plasma Outflows from the Edge of a Solar Active Region as a Possible Source of Solar Wind". *Science*, **318**, (2007*a*), 1585–.

Sakao, T., R. Kano, N. Narukage, J. Kotoku, T. Bando, E. E. DeLuca, L. L. Lundquist, S. Tsuneta, L. K. Harra, Y. Katsukawa, *et al.*: "Continuous Plasma Outflows from the Edge of a Solar Active Region as a Possible Source of Solar Wind". *Science*, **318**, (2007*b*), 1585–.

Scherb, F.: "Velocity distributions of the interplanetary plasma detected by Explorer 10". *Space Res.*, **4**, (1964), 797 – 818.

Schwadron, N. A., L. A. Fisk, and G. Gloeckler: "Statistical acceleration of interstellar pick-up ions in co-rotating interaction regions". *Geophys. Res. Lett.*, **23**, (1996), 2871 – 2874.

Schwadron, N. A. and J. Geiss: "On the processing and transport of inner source hydrogen". *J. Geophys. Res.*, **105**, (2000), 7473 – 7481.

Schwadron, N. A., J. Geiss, L. A. Fisk, G. Gloeckler, T. H. Zurbuchen, and R. v. Steiger: "Inner source distributions: Theoretical interpretation, implications, and evidence for inner source protons". *J. Geophys. Res.*, **105**, (2000), 7465 – 7472.

Schwadron, N. A. and D. J. McComas: "Solar wind scaling law". *Astrophys. J.*, **599(2)**, (2003), 1395–1403. 10.1086/379541.

Sekanina, Z.: "Solar and heliospheric observatory sungrazing comets with prominent tails: Evidence on dust-production peculiarities". *Astrophys. J.*, **545**, (2000), L69 – L72.

Semar, C. L.: "Effect of interstellar neutral hydrogen on the termination of the solar wind". *J. Geophys. Res.*, **75**, (1970), 6892 – 6898.

Slavin, J. D. and P. C. Frisch: "The boundary conditions of the heliosphere: photoionization models constrained by interstellar and in situ data". *Astron. Astrophys.*, **491**, (2008), 53–68.

Snyder, C. W. and M. Neugebauer: "Interplanetary solar wind measurements by Mariner 2". *Space Res.*, **4**, (1964), 89 – 113.

Suess, S. T.: "The heliopause". *Rev. Geophys.*, **28**, (1990), 97 – 115.

Teegarden, B. J., F. B. McDonald, J. H. Trainor, W. R. Webber, and E. C. Roelof: "Interplanetary MeV electrons of jovian origin". *J. Geophys. Res.*, **79**, (1974), 3615.

Title, A. M. and C. J. Schrijver: "The Sun's Magnetic Carpet". In "Cool Stars, Stellar Systems, and the Sun", edited by R. A. Donahue & J. A. Bookbinder, volume 154 of *Astronomical Society of the Pacific Conference Series* (1998). 345–+.

Tsurutani, B. T. and G. . Lakhina: "Some basic concepts of wave-particle interactions in collisionless plasmas". *Rev. Geophys.*, **35**, (1997), 491 – 502.

Tu, C.-Y. and E. Marsch: "A case study of very low cross-helicity fluctuations in the solar wind". *Annales Geophysicae*, **9**, (1991), 319–332.

Tu, C. Y. and E. Marsch: "The evolution of MHD turbulence in the solar wind". In "Solar Wind Seven Colloquium", edited by E. Marsch and R. Schwenn (1992). 549–554.

Tu, C.-Y. and E. Marsch: "MHD structures, waves and turbulence in the solar wind: Observations and theories". *Space Sci. Rev.*, **73**, (1995), 1 – 210.

Vauclair, S. and J.-P. Meyer: "Diffusion in the chromosphere, and the composition of the solar corona and energetic particles". In "19th Int. Conf. Cosmic Rays", volume 4. La Jolla (1985). 233.

von Steiger, R., N. A. Schwadron, L. A. Fisk, J. Geiss, G. Gloeckler, S. Hefti, B. Wilken, R. F. Wimmer-Schweingruber, and T. H. Zurbuchen: "Composition of quasi-stationary solar wind flows from Ulysses/Solar Wind Ion Composition Spectrometer". *J. Geophys. Res.*, **105**, (2000), 27217–27238.

Wang, C., J. D. Richardson, and J. T. Gosling: "Slowdown of the solar wind in the outer heliosphere and the interstellar neutral hydrogen density". *Geophys. Res. Lett.*, **27**, (2000), 2429 – 2432.

Wang, Y.-M. and N. R. Sheeley, Jr.: "Sources of the Solar Wind at Ulysses during 1990-2006". *Astrophys. J.*, **653**, (2006), 708 – 718.

Wang, Y.-M., N. R. Sheeley, Jr., J. H. Walters, G. E. Brueckner, R. A. Howard, D. J. Michels, P. L. Lamy, R. Schwenn, and G. M. Simnett: "Origin of Streamer Material in the Outer Corona". *Astrophys. J. Lett.*, **498**, (1998), L165 – L168 & plates L8 – L12.

Wimmer-Schweingruber, R. F., R. v. Steiger, and R. Paerli: "Solar wind stream interfaces in corotating interaction regions: New SWICS/Ulysses results". *J. Geophys. Res.*, **104**, (1999), 9933 – 9945.

Wimmer-Schweingruber, R. F., R. von Steiger, and R. Paerli: "Solar wind stream interfaces in corotating interaction regions: SWICS/Ulysses results". *J. Geophys. Res.*, **102**, (1997), 17407 – 17417.